Aspects of strong correlations in low dimensions

Dissertation
zu Erlangung des Doktorgrades
der Naturwissenschaften

vorgelegt beim Fachbereich Physik
der Johann Wolfgang Goethe-Universität
in Frankfurt am Main

von
Florian Schütz
aus Göttingen

Frankfurt (2005)
(D F 1)

vom Fachbereich Physik der

Johann Wolfgang Goethe-Universität

als Dissertation angenommen.

Dekan:	Prof. Dr. W. Aßmus
Gutachter:	Prof. Dr. P. Kopietz, Prof. Dr. M.-R. Valenti
Datum der Disputation:	7. September, 2005

Abstract of the thesis

The challenging intricacies of strongly correlated electronic systems necessitate the use of a variety of complementary theoretical approaches. In this thesis, we analyze two distinct aspects of strong correlations and develop further or adapt suitable techniques.

First, we discuss magnetization transport in insulating one-dimensional spin rings described by a Heisenberg model in an inhomogeneous magnetic field. Due to quantum mechanical interference of magnon wave functions, persistent magnetization currents are shown to exist in such a geometry in analogy to persistent charge currents in mesoscopic normal metal rings.

The second, longer part is dedicated to a new aspect of the functional renormalization group technique for fermions. By decoupling the interaction via a Hubbard-Stratonovich transformation, we introduce collective bosonic variables from the beginning and analyze the hierarchy of flow equations for the coupled field theory. The possibility of a cutoff in the momentum transfer of the interaction leads to a new flow scheme, which we will refer to as the interaction cutoff scheme. Within this approach, Ward identities for forward scattering problems are conserved at every instant of the flow leading to an exact solution of a whole hierarchy of flow equations. This way the known exact result for the single-particle Green's function of the Tomonaga-Luttinger model is recovered.

Contents

Chapter 1:

Overview

1.1 Persistent spin currents

The first part of this work is dedicated to transport of magnetization in mesoscopic magnetic insulators subject to spatially inhomogeneous magnetic fields. We develop a formulation of spin-wave theory adapted to this situation and clarify the proper definition of the spin current operator in Heisenberg magnets. We argue that only the components of the naive "current operator" $J_{ij}\boldsymbol{S}_i \times \boldsymbol{S}_j$ in the plane spanned by the local order parameters $\langle \boldsymbol{S}_i \rangle$ and $\langle \boldsymbol{S}_j \rangle$ are related to transport of magnetization. Spin currents are then a direct manifestation of quantum correlations and vanish within a mean field approximation or in the classical ground state. The electric dipole fields generated by a stationary flow of magnetic dipoles are discussed and a Biot-Savart type law is derived.

We then specialize to mesoscopic Heisenberg rings in inhomogeneous magnetic fields that span a finite solid angle Ω as one moves around the ring. We show that in analogy to the magnetic flux for persistent charge currents, the solid angle Ω can act as a geometric flux and drive persistent magnetization currents. For a mesoscopic ferromagnetic ring at low temperatures T in an inhomogeneous magnetic field with magnitude B we calculate the spin current in leading-order spin-wave theory. Under optimal conditions it can be as large as $g\mu_{\mathrm{B}}(T/\hbar)\exp[-2\pi(g\mu_{\mathrm{B}}B/\Delta)^{1/2}]$, where g is the gyromagnetic factor, μ_{B} is the Bohr magneton, and Δ is the energy gap between the ground state and the first spin-wave excitation. A rough estimate shows that a measurement of a potential drop on the order of nanovolts across the size of the mesoscopic ring would be required for an experimental detection of the generated electric dipole field.

Antiferromagnetic rings can also exhibit persistent circulating spin currents. We show this for integer-spin Haldane-gap systems by using a modified spin-wave approach. Due to quantum fluctuations the current has a finite limit on the order of $(-g\mu_{\mathrm{B}})c/L$ at zero temperature, provided the staggered correlation length ξ exceeds the circumference L of the ring, in close analogy to ballistic charge currents in mesoscopic normal-metal rings. Here c is the spin-wave velocity, g is the gyromagnetic ratio, and μ_{B} is the Bohr magneton. For $\xi \ll L$ the current is exponentially suppressed.

1.2 Functional renormalization group with collective fields

In the second part, we develop a new formulation of the functional renormalization group (RG) for interacting fermions. Our approach unifies the purely fermionic formulation based on the Grassmannian functional integral, which has been used in recent years by many authors, with the traditional Wilsonian RG approach to quantum systems pioneered by Hertz [Hertz, 1976], which attempts to describe the infrared behavior in terms of an effective bosonic theory associated with the soft modes of the underlying fermionic problem. In our approach, we decouple the interaction by means of a suitable Hubbard-Stratonovich transformation (following the Hertz approach), but do not eliminate the fermions; instead, we derive an exact hierarchy of RG flow equations for the irreducible vertices of the resulting coupled field theory involving both fermionic and bosonic fields. The freedom of choosing a momentum transfer cutoff for the bosonic soft modes in addition to the usual band cutoff for the fermions opens the possibility of new RG schemes. In particular, we show how the exact solution of the Tomonaga-Luttinger model (i.e., one-dimensional fermions with linear energy dispersion and interactions involving only small momentum transfers) emerges from the functional RG if one works with a momentum transfer cutoff. Then the Ward identities associated with the local particle conservation at each Fermi point are valid at every stage of the RG flow and provide a solution of an infinite hierarchy of flow equations for the irreducible vertices. The RG flow equation for the irreducible single-particle self-energy can then be closed and can be reduced to a linear integro-differential equation, the solution of which yields the result familiar from bosonization. We suggest new truncation schemes of the exact hierarchy of flow equations, which might be useful even outside the weak coupling regime.

Part I

Persistent spin currents

Chapter 2:

Introduction

With the rapid pace of miniaturization in microelectronics, device dimensions will reach a fundamental limit in the near future. Moore's empirical "law" [Moore, 1965] predicting the doubling of the number of transistors on an integrated circuit about every two to three years has guided the development for the last forty years. Yet, atomic length scales are a natural limit to this exponential trend and by simple extrapolation should be reached in commercial chip fabrication in only about one or two decades. Advances in fabrication technology can keep up the "law" for the time being, but conventional design will eventually not suffice.

Looking beyond these difficulties, the quantum-mechanical coherence that becomes important at these length scales also offers possibilities for new computational schemes [Feynman, 1982]. The ultimate goal is a quantum computer which would exploit the coherent quantum-mechanical time evolution of a large number of coupled quantum bits (qubits). To date, experimental realizations provide a proof of principle, but are far from any scalable physical realization of quantum computation. Nevertheless, the goal furnishes a strong motivation for research in the field, since quantum algorithms [Shor, 1994] promise an exponential speed-up in computation time for certain classes of problems.

On the way towards a quantum computer, a catalog of extremely challenging experimental problems has to be resolved [DiVincenzo, 2000]. Among a multitude of proposals, solid state realizations offer the best potential for scalability [Cerletti *et al.*, 2005]. Yet, decoherence is a problem due to inevitable coupling to a huge number of extraneous degrees of freedom such as phonons, nuclear spins, etc. Decoherence times are generally larger for spin than for charge degrees of freedom. Therefore, electron spins on quantum dots have been proposed as a good realization for qubits [Loss and DiVincenzo, 1998]. In this context, the spin states of molecular magnets are also being considered as candidates for qubits [Meier *et al.*, 2003, Leuenberger and Loss, 2001].

For more conventional electronic devices, the use of spin degrees of freedom in addition to or as a substitute for the charge of the electron may eventually lead to a great improvement of performance. The activities in this field are subsumed under the name of spintronics (spin-based electronics) [Wolf *et al.*, 2001, Awschalom *et al.*, 2002]. Products that are already commercially available or almost ready for marketing comprise read heads for hard drives based on the giant magnetoresistance (GMR) effect as well as non-volatile magnetic random access memory (MRAM). More ambitious proposals aim at a complete electric control of the creation, the processing and the read-out of spin states and spin currents. A possible approach to achieve this goal exploits the Rashba spin-orbit coupling in semi-conducting inversion layers that can be controlled by an

applied gate voltage. To implement information processing based on spin degrees of freedom, the problem of magnetization transport has generally received a lot of attention [Awschalom *et al.*, 2002]. The focus lays mainly on systems where spin currents are carried by itinerant electrons [Loss *et al.*, 1990, Stern, 1992, Gao and Qian, 1993, König *et al.*, 2001, Tatara and Kohno, 2003, Mal'shukov *et al.*, 2003, Shen and Xie, 2003], but magnetic insulators also show interesting spin transport phenomena [Gorelik *et al.*, 2003, Meier and Loss, 2003]. Recently, Meier and Loss [Meier and Loss, 2003] calculated the mesoscopic spin conductance for Heisenberg-type systems in a two-terminal geometry.

For device dimensions below the strongly temperature dependent coherence length L_ϕ the quantum states have to be described by coherent wave functions extending over the entire system. For currently achievable device sizes of a few tens of nanometers the systems are mesoscopic at low temperatures [Imry, 1997], from the greek 'meso' meaning 'intermediate' or 'in the middle', in the sense that device dimensions are still above atomic length scales, but small enough for quantum-mechanical interference effects to be important. A well known example for mesoscopic phenomena are persistent currents in normal metal rings threaded by a magnetic flux [Imry, 1997]. The experimental detection of this prototypical quantum mechanical interference effect is a clear demonstration of quantum-mechanical coherence.

In this first part of the thesis we present a new mesoscopic interference effect in Heisenberg spin rings subject to inhomogeneous magnetic fields. It is a spin-current analogue of the persistent charge currents in mesoscopic rings, and is driven by a geometric Berry phase associated with the solid angle subtended by the inhomogeneous field.

2.1 Persistent currents in normal metal rings

The phenomenon of persistent currents in normal metal rings is closely related to the Aharonov-Bohm effect [Aharonov and Bohm, 1956] and was theoretically predicted long ago [Hund, 1938, Büttiker *et al.*, 1983]. Yet, the experimental detection of the effect had to await advances in fabrication technology. In the 1990s, the difficulties in measuring persistent currents were overcome and an oscillating magnetization as a function of the magnetic flux was observed under various conditions [Lévy *et al.*, 1990, Chandrasekhar *et al.*, 1991, Mailly *et al.*, 1993, Reulet *et al.*, 1995, Rabaud *et al.*, 2001, Jariwala *et al.*, 2001]. Surprisingly, for metallic rings in the diffusive regime the observed currents were much larger than predicted by theory [Imry, 1997]. Despite a considerable amount of theoretical work, a consistent theoretical description of the experiments in the diffusive regime is still lacking [Eckern and Schwab, 2002]. The interplay of disorder and electron-electron interaction is believed to be responsible for the observed amplitude of the current. But different assumptions about the nature of the dominant

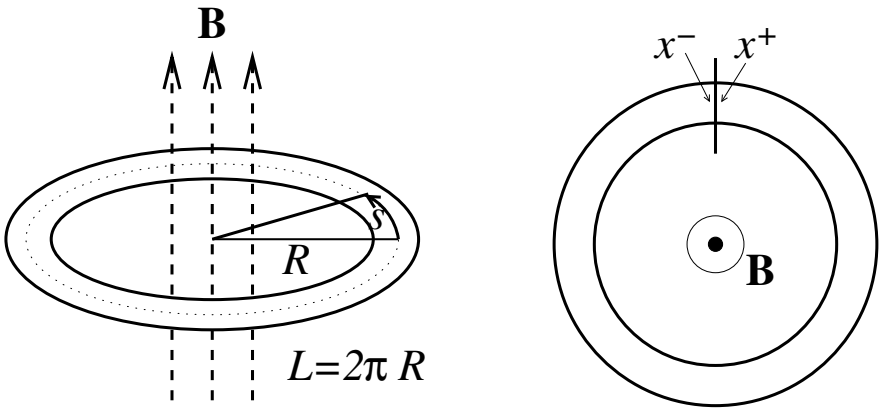

Figure 2.1: Normal metal ring pierced by a magnetic flux.

interaction mechanism lead to incompatible estimates [Ambegaokar and Eckern, 1990, Schechter *et al.*, 2003, Chau and Kopietz, 2004].

In contrast, in the ballistic regime [Mailly *et al.*, 1993] the order of magnitude of the observed current can be explained with a simple model of free fermions moving on a ring pierced by a magnetic flux ϕ, as depicted in Fig. 2.1. In later chapters, we will perform a spin-wave calculation along the same lines. In real space, the Hamiltonian for a single electron reads

$$H(\boldsymbol{x}) = \frac{1}{2m_*}\left[\frac{\hbar}{i}\nabla + \frac{e}{c}\boldsymbol{A}(\boldsymbol{x})\right]^2 , \tag{2.1}$$

where $\boldsymbol{A}(\boldsymbol{x})$ is the vector potential which is assumed to be time independent, and m_* is the effective mass of the electrons. The time-independent Schrödinger equation

$$H(\boldsymbol{x})\psi(\boldsymbol{x}) = E\psi(\boldsymbol{x}) , \tag{2.2}$$

is then invariant under the gauge transformation

$$\boldsymbol{A}(\boldsymbol{x}) \;\rightarrow\; \boldsymbol{A}(\boldsymbol{x}) - \frac{c}{e}\nabla\chi(\boldsymbol{x}) = \boldsymbol{A}'(\boldsymbol{x}) \tag{2.3}$$

$$\psi(\boldsymbol{x}) \;\rightarrow\; e^{i\chi(\boldsymbol{x})/\hbar}\psi(\boldsymbol{x}) = \psi'(\boldsymbol{x}) . \tag{2.4}$$

When the magnetic field $\boldsymbol{B} = \nabla \times \boldsymbol{A}$ vanishes inside the conductor, we can make the vector potential disappear in the Hamiltonian by the choice

$$\chi(\boldsymbol{x}) = \frac{e}{\hbar c}\int_{\boldsymbol{x}_0}^{\boldsymbol{x}} \boldsymbol{A}(\boldsymbol{x}) \cdot d\boldsymbol{x} , \tag{2.5}$$

where the integral is along a path connecting $\boldsymbol{x}$ to a reference point $\boldsymbol{x}_0$. For a singly connected geometry the function χ obtained in this way does not depend on the chosen path, since $\boldsymbol{B} = \nabla \times \boldsymbol{A} = 0$. However, for a doubly-connected ring

geometry, the function χ defined in Eq. (2.5) is not single-valued. We can then still choose a gauge in which the vector potential vanishes, but a new boundary condition has to be introduced at an imaginary plane splitting the ring in a way that a singly connected volume results, see Fig. 2.1. For the jump of χ at the boundary, one obtains

$$[\chi(\boldsymbol{x}^+) - \chi(\boldsymbol{x}^-)]/\hbar = \frac{e}{\hbar c} \oint \boldsymbol{A}(\boldsymbol{x}) \cdot d\boldsymbol{x} = \frac{e}{\hbar c} \int d\boldsymbol{a} \cdot \boldsymbol{B}(\boldsymbol{x}) = \frac{2\pi\phi}{\phi_0}\,, \tag{2.6}$$

where ϕ is the magnetic flux through the ring, and $\phi_0 = hc/e$ is the flux quantum. Stokes' theorem has been used to express the line integral in terms of a surface integral over a surface spanned by the ring. This results in the following boundary condition for the wave function in the new gauge,

$$\psi'(\boldsymbol{x}^+) = e^{i[\chi(\boldsymbol{x}^+)-\chi(\boldsymbol{x}^-)]/\hbar}\psi'(\boldsymbol{x}^-) = e^{2\pi i\phi/\phi_0}\psi'(\boldsymbol{x}^-)\,. \tag{2.7}$$

When the motion of the electrons is restricted to a very narrow ring, it is effectively one-dimensional. The Hamiltonian in the gauge with vanishing vector potential and the boundary condition are given by

$$H(s) = -\frac{\hbar^2}{2m_*}\frac{d^2}{ds^2}\,, \qquad \psi'(L) = e^{2\pi i\phi/\phi_0}\psi'(0)\,, \tag{2.8}$$

where s is the coordinate along the ring, and L is the circumference. The single-particle eigenstates are then plane waves with the energies

$$\epsilon_n = \frac{\hbar^2 k_n^2}{2m_*}\,, \tag{2.9}$$

where the quantized wavevectors are given by

$$k_n = \frac{2\pi}{L}\left(n + \frac{\phi}{\phi_0}\right) \qquad n = 0, \pm1, \pm2, \ldots\,. \tag{2.10}$$

One may then calculate the current at constant chemical potential as a derivative of the flux-dependent part of the grand-canonical potential $\Omega_{\rm gc}(\phi)$ [Cheung *et al.*, 1988],

$$I = -c\frac{\partial\Omega_{\rm gc}(\phi)}{\partial\phi}\,. \tag{2.11}$$

At finite temperature T one obtains for spinless fermions

$$I = \frac{-e}{L}\sum_n \frac{v_n}{e^{(\epsilon_n-\mu)/T}+1}\,, \tag{2.12}$$

where $v_n = \hbar k_n/m_*$. At zero temperature Eq. (2.12) reduces to a sawtooth function. For an even number of electrons at $T = 0$ one obtains

$$I = (-e)\frac{v_F}{L}\left(1 - \frac{2\phi}{\phi_0}\right)\,, \qquad 0 < \frac{\phi}{\phi_0} < 1\,, \tag{2.13}$$

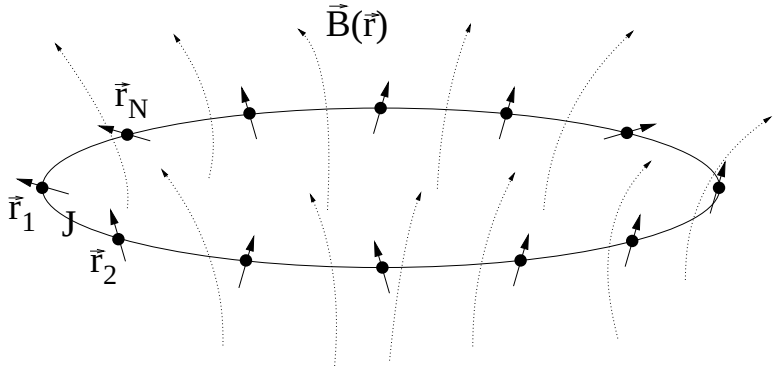

Figure 2.2: Heisenberg spin ring in an inhomogeneous magnetic field.

where v_F is the Fermi velocity. The amplitude $(-e)v_F/L$ of this current is in agreement with the experiments in the ballistic regime [Mailly *et al.*, 1993].

Finite temperature, disorder, and phase-breaking scattering all have a similar effect on the persistent charge current [Cheung *et al.*, 1988]. For a weak perturbation, they smooth the discontinuity around $\phi = 0$ and with increasing strength higher harmonics are exponentially suppressed such that a sinusoidal shape is approached. In the limit of a very strong perturbation the current is exponentially suppressed with the relevant length or energy scale, i.e., the current becomes proportional to $\exp(-T/T^*)$, $\exp(-L/L_\xi)$, or $\exp(-L/L_\phi)$ under the influence of a non-zero temperature, strong disorder or strong inelastic scattering, respectively. Here T^* is the temperature scale associated with the discrete level spacing, L_ξ is the localization length, and L_ϕ is the phase-coherence length. Yet, as mentioned above the interplay of disorder and interaction still needs further investigation.

2.2 Analogue in mesoscopic spin rings

In the following chapters, we will show that Heisenberg spin chains in inhomogeneous magnetic fields can be used to realize a spin-current analogue of the persistent currents in mesoscopic normal metal rings. We treat mesoscopic ferromagnetic rings as well as antiferromagnetic rings with integer spin S using linear spin-wave theory. We find a persistent magnetization current that is carried by magnons and that endows the rings with an *electric* dipole field, which is the counterpart of the magnetic dipole fields associated with the persistent charge current in a normal metal ring. For realistic parameters the spin analogues of the experiments in Refs. [Lévy *et al.*, 1990, Chandrasekhar *et al.*, 1991, Mailly *et al.*, 1993] would require the detection of a potential drop on the order of nanovolts. Furthermore, for the antiferromagnetic ring, we find that the correlation length ξ is the relevant length scale to which the size L of the ring has to be compared. The interference effect is only detectable for $L \lesssim \xi$ and becomes exponentially

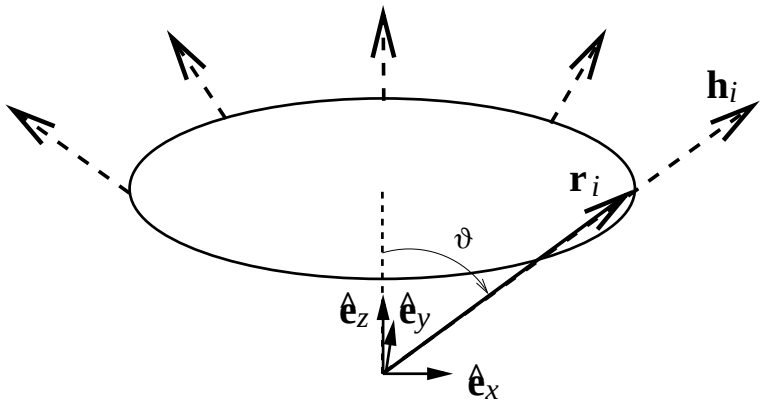

Figure 2.3: Crown-shaped magnetic field geometry.

suppressed for $L \gg \xi$. We also briefly comment on the creation of spin currents by inhomogeneous electric fields [Cao *et al.*, 1997] in the presence of spin-orbit coupling, due to the Aharonov-Casher effect [Aharonov and Casher, 1984].

The systems we have in mind are described by an isotropic Heisenberg Hamiltonian in an inhomogeneous magnetic field

$$\hat{H} = \sum_{i=1}^{N} \left[J \hat{\boldsymbol{S}}_i \cdot \hat{\boldsymbol{S}}_{i+1} - \boldsymbol{h}_i \cdot \hat{\boldsymbol{S}}_i \right] . \tag{2.14}$$

Here, $\hat{\boldsymbol{S}}_i$ are spin-S operators localized on equally spaced sites $\boldsymbol{r}_i$ of a ring as depicted in Fig. 2.2. They are normalized as $\hat{\boldsymbol{S}}_i^2 = S(S+1)$. Periodic boundary conditions $\hat{\boldsymbol{S}}_{N+1} = \hat{\boldsymbol{S}}_1$ are used, and $\boldsymbol{h}_i = g\mu_B \boldsymbol{B}(\boldsymbol{r}_i)$ is the magnetic field at the site i of the ring, where g is the gyromagnetic ratio and μ_B is the Bohr magneton. For a ferromagnetic ring the exchange integral J is negative, whereas for an antiferromagnetic ring J is positive. Furthermore, we will assume a magnetic field that is constant in magnitude $|\boldsymbol{h}_i| = h$, but inhomogeneous in direction. The precise form of the inhomogeneity is irrelevant, since the leading contribution to the persistent magnetization current will only depend on the solid angle spanned by the field as one moves once around the ring. For illustrative purposes, however, we will repeatedly use the crown-shaped field geometry shown in Fig. 2.3. The local direction of the field is then given by

$$\boldsymbol{h}_i = h \left[\cos(\vartheta) \hat{\boldsymbol{e}}_z + \sin(\vartheta) \cos\left(\frac{2\pi}{L} l_i\right) \hat{\boldsymbol{e}}_x + \sin(\vartheta) \sin\left(\frac{2\pi}{L} l_i\right) \hat{\boldsymbol{e}}_y \right] , \tag{2.15}$$

where $i = 1, \ldots, N$, the unit vectors $\hat{\boldsymbol{e}}_{x/y/z}$ point along the coordinate axes, and l_i is the position of site $\boldsymbol{r}_i$ measured along the circumference of the ring. With an appropriately chosen origin of the coordinate system, as shown in Fig. 2.3, the magnetic field is radial, since $\boldsymbol{h}_i = h\boldsymbol{r}_i/|\boldsymbol{r}_i|$.

The rest of part I is organized as follows. In Chap. 3, we derive a formulation of spin-wave theory which is appropriate for the case of a non-collinear classical ground state. We also explain the concept of gauge freedom associated with the choice of the transverse quantization axis. In the following chapter, we then clarify the definition of the spin current operator in such a geometry. Some subtleties are discussed that are not widely appreciated in the literature. The electric dipole fields generated by a current of magnetic moments are also analyzed. Chaps. 5 and 6 are dedicated to the details of the spin-wave calculation for ferromagnetic and antiferromagnetic rings, respectively. In Chap. 7, we briefly comment on the possibility of driving persistent magnetization currents with inhomogeneous electric fields. Finally, we give a summary of part I in Chap. 8.

Most of the results of part I are published in [Schütz *et al.*, 2003, Schütz *et al.*, 2004a, Schütz *et al.*, 2004b].

Chapter 3:

Spin-wave theory

Spin-wave theory, with its long history, has become a standard tool in solid state physics [Auerbach, 1994]. The concept of a spin wave was invented by Bloch [Bloch, 1930] to describe the magnetization of a ferromagnet at low temperatures. In this case, spin waves are nothing but a wave-like superposition of states with a single spin deviation from the fully polarized state. Later on, spin-wave theory was formalized using representations of the spin operators in terms of bosonic creation and annihilation operators [Holstein and Primakoff, 1940,Maleyev, 1957]. Such representations underline the fact that spin waves are bosonic quasi-particles and simplify the study of their interaction. These interactions were rigorously shown to be weak for a three dimensional ferromagnet, such that spin-waves can be used to derive asymptotic low-energy expansions of thermodynamic quantities [Dyson, 1956a, Dyson, 1956b].

For three-dimensional antiferromagnets spin-wave theory was developed in the 1950s [Anderson, 1952, Kubo, 1952, Oguchi, 1960]. Here, the ground state is no longer identical with the classical Néel state and quantum fluctuations occur. Technically, this is manifest in the linear spin-wave Hamiltonian by the appearance of anomalous terms that necessitate a Bogoliubov transformation for its diagonalization. Corrections to the linear spin-wave theory can be systematically calculated by an expansion in the inverse magnitude of the spins $1/S$. Therefore, spin-wave theory has evolved into a powerful computational tool [Harris *et al.*, 1971].

Interest in spin-wave theory was renewed with the discovery of high temperature superconductivity in doped cuprates [Bednorz and Müller, 1986]. Since the undoped parent compounds are layered antiferromagnets, it is essential to understand the elementary excitations of two-dimensional antiferromagnets [Manousakis, 1991]. The nature of the ground state and the low-temperature behavior in two-dimensional antiferromagnets was thoroughly investigated using the renormalization group [Chakravarty *et al.*, 1988a, Chakravarty *et al.*, 1988b]. At zero temperature the square-lattice antiferromagnet is ordered and spin-wave theory is well suited for detailed calculations [Singh and Huse, 1989, Castilla and Chakravarty, 1991, Igarashi, 1992, Canali *et al.*, 1992]. In the renormalized classical regime at finite temperature, spin waves are still well defined at length scales that are short compared to the correlation length [Kopietz, 1990] and spin-wave theory remains a powerful tool. As another example of low-dimensional systems, one-dimensional spin chains were also intensively studied. Here, long-range order does no longer occur even at $T = 0$. Still, a modified spin-wave theory can be used for ferromagnets as well as for antiferromagnets with integer spin S, as will be further discussed in Chap. 6.

Despite the long history of spin-wave theory, there are still open conceptual problems. For example antiferromagnets in a magnetic field lead to instabilities that require further analysis [Zhitomirsky and Nikuni, 1998, Zhitomirsky and Chernyshev, 1999, Maleyev, 2000, Syromyatnikov and Maleyev, 2002]. Recently, we have developed a modified spin-wave theory to discuss the finite temperature properties of a Heisenberg antiferromagnet on a special lattice in the presence of a finite magnetic field [Spremo *et al.*, 2005].

Here, we develop a formulation of spin-wave theory that is suitable for non-collinear spin arrangements. For conceptual clarity, we consider a more general Heisenberg Hamiltonian than in Eq. (2.14). In the presence of an inhomogeneous magnetic field it reads

$$\hat{H} = \frac{1}{2} \sum_{i,j} \hat{\boldsymbol{S}}_i^T \mathbf{J}_{ij} \hat{\boldsymbol{S}}_j - \sum_i \boldsymbol{h}_i \cdot \hat{\boldsymbol{S}}_i \,. \tag{3.1}$$

Here, $\hat{\boldsymbol{S}}_i$ are spin-S operators localized on lattice sites $\boldsymbol{r}_i$ normalized such that $\hat{\boldsymbol{S}}_i^2 = S(S+1)$, and T denotes transposition in coordinate space. The spin operators obey the standard commutation relations of angular momentum operators

$$\left[\hat{S}_i^\alpha, \hat{S}_j^\beta\right] = i\,\delta_{ij}\,\epsilon_{\alpha\beta\gamma}\,\hat{S}_i^\gamma \,. \tag{3.2}$$

For distinct indices i and j, the square matrices $\mathbf{J}_{ij}$ of dimension three represent the exchange coupling between the spins at distinct sites $\boldsymbol{r}_i$ and $\boldsymbol{r}_j$. In principle, $\mathbf{J}_{ii}$ gives the strength of the single ion anisotropy, but such terms will be excluded from now on. Under the summation, we can assume $\mathbf{J}_{ji} = \mathbf{J}_{ij}^T$.

As an example consider the isotropic Heisenberg model with nearest-neighbor exchange coupling J. In this case, we have

$$\mathbf{J}_{ij} = \begin{cases} J\mathbf{1} & \text{for } (i,j) \text{ nearest neighbors} \\ 0 & \text{otherwise} \end{cases} \,. \tag{3.3}$$

The last term in Eq. (3.1) is the Zeeman energy which tends to align the spins with the local magnetic field. The inhomogeneous magnetic field $\boldsymbol{h}_i$ is related to the magnetic induction at the site of the spin by $\boldsymbol{h}_i = g\mu_\mathrm{B}\boldsymbol{B}(\boldsymbol{r}_i)$, where μ_B is the Bohr magneton and g is the gyromagnetic ratio. With the conventions used in Eq. (3.1), the exchange couplings as well as the magnetic fields $\boldsymbol{h}_i$ have units of energy.

3.1 Associated classical problem

Spin-wave theory is an expansion around the classical limit $S \to \infty$. Hence, as a first step, we consider the associated classical problem. The thermodynamics is uniquely specified by the classical energy H which is obtained from the

Hamiltonian in Eq. (3.1) by the replacement

$$\hat{\boldsymbol{S}}_i \longrightarrow \boldsymbol{\Omega}_i \,, \tag{3.4}$$

where $\boldsymbol{\Omega}_i$ are classical vectors of length S, i.e. $|\boldsymbol{\Omega}_i| = S$. At zero temperature, classical spins freeze into the configuration of lowest energy. This classical ground state is obtained by minimizing the energy with respect to the orientation of all vectors $\boldsymbol{\Omega}_i = S\hat{\boldsymbol{m}}_i$. Alternatively, we can minimize with respect to all components of the unit vectors $\hat{\boldsymbol{m}}_i$ and introduce Lagrange multipliers to ensure the constraints $\hat{\boldsymbol{m}}_i^2 = 1$. In this way we obtain a necessary condition for an extremum of the classical energy,

$$\hat{\boldsymbol{m}}_i \times \boldsymbol{h}_i^{\text{eff}} = 0 \,, \qquad \boldsymbol{h}_i^{\text{eff}} := \boldsymbol{h}_i - S\sum_j \mathbf{J}_{ij}\hat{\boldsymbol{m}}_j \,. \tag{3.5}$$

As expected, the magnetization aligns parallel to an effective field defined in the second equality which contains the external field as well as an exchange field. For given $\boldsymbol{h}_i$ and $\mathbf{J}_{ij}$, this is a system of non-linear equations for the spin directions $\hat{\boldsymbol{m}}_i$ in the classical ground state. To ensure that the set of unit vectors $\hat{\boldsymbol{m}}_i$ indeed leads to a *minimum* of the classical energy, we need to analyze the behavior of H for small deviations from the supposed ground state. These deviations are conveniently parameterized as

$$\boldsymbol{\Omega}_i = \Omega_i^{\parallel}\hat{\boldsymbol{m}}_i + \boldsymbol{\Omega}_i^{\perp} \,, \tag{3.6}$$

where $\boldsymbol{\Omega}_i^{\perp}$ is in the plane orthogonal to $\hat{\boldsymbol{m}}_i$, i.e. $\boldsymbol{\Omega}_i^{\perp} \cdot \hat{\boldsymbol{m}}_i = 0$. The length of the vector $\boldsymbol{\Omega}_i$ is fixed by choosing

$$\Omega_i^{\parallel} = \sqrt{S^2 - |\boldsymbol{\Omega}_i^{\perp}|^2} \,. \tag{3.7}$$

The classical Hamiltonian can then be decomposed as

$$H = H^{\parallel} + H^{\perp} + H' \,, \tag{3.8}$$

$$H^{\parallel} = \frac{1}{2}\sum_{ij} \hat{\boldsymbol{m}}_i^T \mathbf{J}_{ij} \hat{\boldsymbol{m}}_j \Omega_i^{\parallel}\Omega_j^{\parallel} - \sum_i \boldsymbol{h}_i \cdot \hat{\boldsymbol{m}}_i \Omega_i^{\parallel} \,, \tag{3.9}$$

$$H^{\perp} = \frac{1}{2}\sum_{ij} (\boldsymbol{\Omega}_i^{\perp})^T \mathbf{J}_{ij} \boldsymbol{\Omega}_j^{\perp} \,, \tag{3.10}$$

$$H' = -\sum_i \boldsymbol{\Omega}_i^{\perp} \cdot (\boldsymbol{h}_i - \sum_j \mathbf{J}_{ij}\hat{\boldsymbol{m}}_j\Omega_j^{\parallel}) \,. \tag{3.11}$$

We now expand the energy H in powers of the transverse vectors $\boldsymbol{\Omega}_i^{\perp}$. The first order terms

$$H^{(1)} = -\sum_i \boldsymbol{h}_i^{\text{eff}} \cdot \boldsymbol{\Omega}_i^{\perp} \tag{3.12}$$

vanish due to the condition (3.5). Second order terms are given by

$$H^{(2)} = \frac{1}{2S}\left[\sum_i (\boldsymbol{h}_i^{\text{eff}} \cdot \hat{\boldsymbol{m}}_i)|\boldsymbol{\Omega}_i^{\perp}|^2 + S\sum_{ij} \boldsymbol{\Omega}_i^{\perp} \cdot \mathbf{J}_{ij}\boldsymbol{\Omega}_j^{\perp}\right] . \tag{3.13}$$

It is now useful to decompose the transverse vectors in a site-dependent basis of unit vectors $\hat{\boldsymbol{e}}_i^1$ and $\hat{\boldsymbol{e}}_i^2$ chosen in a way that $\{\hat{\boldsymbol{e}}_i^1, \hat{\boldsymbol{e}}_i^2, \hat{\boldsymbol{m}}_i\}$ defines a right-handed triad. With the representation

$$\boldsymbol{\Omega}_i^{\perp} = \sum_{\alpha=1,2} X_i^{\alpha}\hat{\boldsymbol{e}}_i^{\alpha} , \tag{3.14}$$

the second-order terms in the classical Hamiltonian can be written as

$$H^{(2)} = \frac{1}{2S}\sum_{i\alpha,j\beta} X_i^{\alpha} H_{i\alpha;j\beta}^{(2)} X_j^{\beta} . \tag{3.15}$$

Here, we have defined the symmetric matrix $\mathbf{H}^{(2)}$ with elements

$$H_{i\alpha;j\beta}^{(2)} = \delta_{ij}\delta_{\alpha\beta}\boldsymbol{h}_i^{\text{eff}} \cdot \hat{\boldsymbol{m}}_i + S\hat{\boldsymbol{e}}_i^{\alpha} \cdot \mathbf{J}_{ij}\hat{\boldsymbol{e}}_j^{\beta} . \tag{3.16}$$

The spin configuration specified by the vectors $\hat{\boldsymbol{m}}_i$ leads to a minimum of the classical energy, if $\mathbf{H}^{(2)}$ is positive definite, i.e., if all eigenvalues are positive. In real situations there are often degenerate ground-state configurations that are related to each other by a continuous global symmetry transformation, as for example a simultaneous rotation of all spins. As a result, the energy matrix $\mathbf{H}^{(2)}$ has an eigenvalue zero. To avoid this situation, one can introduce an additional magnetic field to break the global symmetry and shift all eigenvalues to strictly positive values. At the end of the calculation, this extra field should be taken to zero.

At the classical level, the thermodynamics is specified by the energy alone and the spin dynamics is completely decoupled. Nevertheless, as a preparation to the semi-classical treatment in the next section, it is instructive to consider the dynamics generated by the Poisson brackets

$$\left\{\Omega_i^{\alpha}, \Omega_j^{\beta}\right\} = \delta_{ij}\epsilon_{\alpha\beta\gamma}\Omega_i^{\gamma} . \tag{3.17}$$

One then obtains an equation of motion for the time-dependent classical spin vectors $\boldsymbol{\Omega}_i(t)$,

$$\frac{d\boldsymbol{\Omega}_i}{dt} = \{H, \boldsymbol{\Omega}_i\} = -\boldsymbol{\Omega}_i \times \left[\boldsymbol{h}_i - \sum_j \mathbf{J}_{ij}\boldsymbol{\Omega}_j\right] . \tag{3.18}$$

Note that the ground-state configuration $\boldsymbol{\Omega}_i = S\hat{\boldsymbol{m}}_i$ yields a stationary solution of Eq. (3.18). The dynamics of states that deviate only slightly from the

classical ground state can be studied by using a time-dependent version of the decomposition (3.6) and by expanding Eq. (3.18) to first order in the $\mathbf{\Omega}_i^{\perp}$,

$$\frac{d\mathbf{\Omega}_i^{\perp}}{dt} = \boldsymbol{h}_i^{\mathrm{eff}} \times \mathbf{\Omega}_i^{\perp} + S\hat{\boldsymbol{m}}_i \times \sum_j \mathbf{J}_{ij}\mathbf{\Omega}_j^{\perp} \,. \tag{3.19}$$

If we further use the representation (3.14) in terms of transverse basis vectors, we obtain

$$\frac{d\boldsymbol{X}}{dt} = -\mathbf{M}\mathbf{H}^{(2)}\boldsymbol{X} \,. \tag{3.20}$$

Here, we have defined the skew-symmetric matrix $\mathbf{M}$ as

$$M_{i\alpha;j\beta} = \delta_{ij}\left[\delta_{\alpha,1}\delta_{\beta,2} - \delta_{\alpha,2}\delta_{\beta,1}\right] = i\,\delta_{ij}\sigma^y_{\alpha\beta} \,, \tag{3.21}$$

where σ^y is the usual Pauli matrix. We can also explicitly exhibit the block structure in the (upper) spin index by writing

$$\mathbf{M} = \begin{pmatrix} \mathbf{0} & \mathbf{1} \\ -\mathbf{1} & \mathbf{0} \end{pmatrix} , \tag{3.22}$$

where $\mathbf{1}$ is an N by N unit matrix in the (lower) spatial index. From this representation the following symmetry relations are obvious

$$\mathbf{M}^2 = -\mathbf{1} \,, \qquad \mathbf{M}^T = -\mathbf{M} \,. \tag{3.23}$$

A general solution of the linearized equation of motion (3.20) can be obtained by a transformation to eigenmodes. To achieve this goal, we note that the square root of the matrix $\mathbf{H}^{(2)}$ can be taken, since it was shown to be symmetric and positive definite. Using this, we can rewrite Eq. (3.20) in the form

$$\frac{d\boldsymbol{Y}}{dt} = i\mathbf{Q}\,\boldsymbol{Y} \,, \tag{3.24}$$

where we have defined

$$\mathbf{Q} = i\sqrt{\mathbf{H}^{(2)}}\mathbf{M}\sqrt{\mathbf{H}^{(2)}} \,, \qquad \boldsymbol{Y} = \sqrt{\mathbf{H}^{(2)}}\boldsymbol{X} \,. \tag{3.25}$$

The matrix $\mathbf{Q}^+ = \mathbf{Q}$ is Hermitian and has a complete set of eigenvectors, i.e., a unitary matrix $\mathbf{U}$ exists such that

$$\mathbf{Q}\mathbf{U} = \mathbf{U}\mathbf{W} \,, \qquad \mathbf{U}^+\mathbf{U} = \mathbf{U}\mathbf{U}^+ = \mathbf{1} \,, \tag{3.26}$$

where $\mathbf{W}$ is diagonal and contains the eigenvalues on the diagonal. Since $\mathbf{Q}^* = -\mathbf{Q}$ and the eigenvalues of a Hermitian operator are real, we have

$$\mathbf{Q}\mathbf{U}^* = -\mathbf{U}^*\mathbf{W} \,. \tag{3.27}$$

Thus, the complex conjugate of an eigenvector of $\mathbf{Q}$ with eigenvalue ω yields an eigenvector with eigenvalue $-\omega$. Hence, eigenfrequencies always occur in pairs $(\omega, -\omega)$. Note that $\omega = 0$ does not occur, since this would imply that $\mathbf{H}^{(2)}$ also had a zero eigenvalue which we have excluded above. By arranging eigenvectors with positive eigenvalues in the first N rows of $\mathbf{U}$ and their complex conjugates in the next N rows, we can then write

$$\mathbf{W} = \begin{pmatrix} \boldsymbol{\omega} & \mathbf{0} \\ \mathbf{0} & -\boldsymbol{\omega} \end{pmatrix}, \qquad \boldsymbol{\omega} = \mathrm{diag}(\omega_1, \ldots, \omega_N)\,. \tag{3.28}$$

In this representation, we also have

$$\mathbf{U}^* = \mathbf{U} \begin{pmatrix} \mathbf{0} & \mathbf{1} \\ \mathbf{1} & \mathbf{0} \end{pmatrix}. \tag{3.29}$$

By going to the eigenbasis of $\mathbf{Q}$, we can further simplify Eq. (3.24),

$$\frac{d\boldsymbol{Z}}{dt} = i\mathbf{W}\boldsymbol{Z}\,. \tag{3.30}$$

Here the transformation of variables is given by

$$\boldsymbol{Z} = |\mathbf{W}|^{-\frac{1}{2}}\,\mathbf{U}^{+}\boldsymbol{Y} = \mathbf{R}^{-1}\boldsymbol{X}\,. \tag{3.31}$$

The normalization factor has been introduced for later convenience. It contains the matrix $|\mathbf{W}|$ defined as

$$|\mathbf{W}| = \begin{pmatrix} \boldsymbol{\omega} & \mathbf{0} \\ \mathbf{0} & \boldsymbol{\omega} \end{pmatrix}. \tag{3.32}$$

The complete transformation matrix $\mathbf{R}$ is given by

$$\mathbf{R} = [\mathbf{H}^{(2)}]^{-\frac{1}{2}}\,\mathbf{U}\,|\mathbf{W}|^{\frac{1}{2}}\,. \tag{3.33}$$

Furthermore, from Eq. (3.29), we can deduce the relation

$$\mathbf{R}^* = \mathbf{R} \begin{pmatrix} \mathbf{0} & \mathbf{1} \\ \mathbf{1} & \mathbf{0} \end{pmatrix}. \tag{3.34}$$

This relation, together with the fact that $\boldsymbol{X}$ is real, insures that $\mathbf{Z}$ contains two complex conjugate parts, and we can write

$$\boldsymbol{Z} = \begin{pmatrix} \boldsymbol{\beta} \\ \boldsymbol{\beta}^* \end{pmatrix}, \qquad \frac{d\boldsymbol{\beta}}{dt} = i\boldsymbol{\omega}\boldsymbol{\beta}\,. \tag{3.35}$$

This is the representation of the small-amplitude dynamics in terms of eigenmodes announced above.

3.2 Semi-classical expansion

The quantum nature of the spins can be taken into account in a spin-wave expansion around the classical limit. For this purpose, one formally assumes large S and performs an expansion in powers of S^{-1}. Because statics and dynamics are inextricably linked in the quantum system, the energies of the spin-wave modes in the leading approximation are identical to the eigenfrequencies of the classical small amplitude dynamics, as we will show in detail below. In analogy to the classical case, it is convenient to first decompose the spin operators into a component parallel to the $\hat{\boldsymbol{m}}_i$ in the classical ground state and a transverse part as

$$\hat{\boldsymbol{S}}_i = \hat{S}_i^{\parallel}\hat{\boldsymbol{m}}_i + \hat{\boldsymbol{S}}_i^{\perp}\,, \tag{3.36}$$

where $\hat{\boldsymbol{S}}_i^{\perp}\cdot\hat{\boldsymbol{m}}_i = 0$. Again, the Hamiltonian contains contributions $\hat{H}^{\parallel}$ and $\hat{H}^{\perp}$ for the longitudinal and transverse degrees of freedom as well as a mixing term H':

$$\hat{H} = \hat{H}^{\parallel} + \hat{H}^{\perp} + \hat{H}'\,, \tag{3.37}$$

$$\hat{H}^{\parallel} = \frac{1}{2}\sum_{ij}\hat{\boldsymbol{m}}_i^T\mathbf{J}_{ij}\hat{\boldsymbol{m}}_j\hat{S}_i^{\parallel}\hat{S}_j^{\parallel} - \sum_i \boldsymbol{h}_i\cdot\hat{\boldsymbol{m}}_i\hat{S}_i^{\parallel}\,, \tag{3.38}$$

$$\hat{H}^{\perp} = \frac{1}{2}\sum_{ij}(\hat{\boldsymbol{S}}_i^{\perp})^T\mathbf{J}_{ij}\hat{\boldsymbol{S}}_j^{\perp}\,, \tag{3.39}$$

$$\hat{H}' = -\sum_i \hat{\boldsymbol{S}}_i^{\perp}\cdot(\boldsymbol{h}_i - \sum_j \mathbf{J}_{ij}\hat{\boldsymbol{m}}_j\hat{S}_j^{\parallel})\,. \tag{3.40}$$

We further decompose the transverse spin operators $\hat{\boldsymbol{S}}_i^{\perp}$ using the site dependent transverse basis vectors $\hat{\boldsymbol{e}}_i^1$ and $\hat{\boldsymbol{e}}_i^2$ which are chosen such that $\{\hat{\boldsymbol{e}}_i^1, \hat{\boldsymbol{e}}_i^2, \hat{\boldsymbol{m}}_i\}$ form a local right-handed triad of unit vectors. Defining spherical basis vectors as $\boldsymbol{e}_i^p = \hat{\boldsymbol{e}}_i^1 + ip\hat{\boldsymbol{e}}_i^2$, $p = \pm$, we can express the transverse spin operators as

$$\hat{\boldsymbol{S}}_i^{\perp} = \frac{1}{2}\sum_{p=\pm}\hat{\boldsymbol{e}}_i^p\hat{S}_i^{-p}\,. \tag{3.41}$$

With this decomposition, the transverse Hamiltonian becomes

$$\hat{H}^{\perp} = \frac{1}{8}\sum_{i,j}\sum_{p,p'}J_{ij}^{pp'}\hat{S}_i^{-p}\hat{S}_j^{-p'}\,, \tag{3.42}$$

where we have defined the matrix elements

$$J_{ij}^{pp'} = \hat{\boldsymbol{e}}_i^p\cdot\mathbf{J}_{ij}\hat{\boldsymbol{e}}_j^{p'}\,. \tag{3.43}$$

Technically, small fluctuations around the classical ground state are treated with bosonic transformations, which represent the algebra of the spin operators by

bose operators $\hat{b}_i$ obeying standard commutation relations $[\hat{b}_i, \hat{b}_j^+] = \delta_{ij}$. The most common representations are the Holstein-Primakoff (HP) or the Dyson-Maleyev (DM) transformations. In the DM approach, the spin operators are represented as

$$\hat{S}_i^{\parallel} = S - \hat{b}_i^+ \hat{b}_i \,, \tag{3.44}$$

$$\hat{S}_i^+ = \sqrt{2S}\left(1 - \frac{\hat{n}_i}{2S}\right)\hat{b}_i \,, \tag{3.45}$$

$$\hat{S}_i^- = \sqrt{2S}\,\hat{b}_i^+ \,, \tag{3.46}$$

where the occupation number operators are $\hat{n}_i = \hat{b}_i^+ \hat{b}_i$. Alternatively, a Holstein-Primakoff transformation would read

$$\hat{S}_i^{\parallel} = S - b_i^\dagger b_i \tag{3.47}$$

$$\hat{S}_i^+ = \sqrt{2S - \hat{n}_i}\;\hat{b}_i \tag{3.48}$$

$$\hat{S}_i^- = \hat{b}_i^+ \sqrt{2S - \hat{n}_i} \,. \tag{3.49}$$

The Dyson-Maleyev transformation has the advantage that, as a power series in $\hat{n}_i/S$, the Hamiltonian is finite, whereas it contains an infinite number of terms in the Holstein-Primakoff formalism. Yet, it is not formally hermitian in the DM approach. In later chapters, we will only consider the leading order spin-wave expansion for which both representations coincide. For concreteness, we will from now on assume a DM transformation. After ordering terms with respect to the number of boson operators the transformed Hamiltonian reads:

$$\hat{H}^{(0)} = \frac{1}{2}\sum_{ij} \hat{\boldsymbol{m}}_i^T S^2 \mathbf{J}_{ij} \hat{\boldsymbol{m}}_j - \sum_i S \boldsymbol{h}_i \cdot \hat{\boldsymbol{m}}_i \,, \tag{3.50}$$

$$\hat{H}^{(1)} = -\frac{\sqrt{2S}}{2}\sum_i (\boldsymbol{e}_i^+ \hat{b}_i^+ + \boldsymbol{e}_i^- \hat{b}_i) \cdot \boldsymbol{h}_i^{\text{eff}} \,, \tag{3.51}$$

$$\hat{H}^{(2)} = \sum_i (\boldsymbol{h}_i^{\text{eff}} \cdot \hat{\boldsymbol{m}}_i)\hat{n}_i + \frac{S}{4}\sum_{ij} \Big\{ J_{ij}^{++}\, \hat{b}_i^+ \hat{b}_j^+ + J_{ij}^{--}\, \hat{b}_i \hat{b}_j + J_{ij}^{+-}\, \hat{b}_i^+ \hat{b}_j + J_{ij}^{-+}\, \hat{b}_i \hat{b}_j^+ \Big\} \,, \tag{3.52}$$

$$\hat{H}^{(3)} = -\frac{\sqrt{2S}}{2}\sum_{ij}(\boldsymbol{e}_i^+\hat{b}_i^+ + \boldsymbol{e}_i^-\hat{b}_i)\cdot(\mathbf{J}_{ij}\hat{\boldsymbol{m}}_j)\hat{n}_j + \frac{(2S)^{-\frac{1}{2}}}{2}\sum_i(\hat{\boldsymbol{e}}_i^-\cdot\boldsymbol{h}_i^{\text{eff}})\hat{n}_i\hat{b}_i\,, \tag{3.53}$$

$$\hat{H}^{(4)} = \frac{1}{2}\sum_{ij}(\hat{\boldsymbol{m}}_i^T\mathbf{J}_{ij}\hat{\boldsymbol{m}}_j)\hat{n}_i\hat{n}_j - \frac{1}{8}\sum_{ij}\Big\{J_{ij}^{--}(\hat{n}_i\hat{b}_i\hat{b}_j + \hat{b}_i\hat{n}_j\hat{b}_j) + J_{ij}^{+-}\hat{b}_i^+\hat{n}_i\hat{b}_j + J_{ij}^{-+}\hat{n}_i\hat{b}_i\hat{b}_j^+\Big\} \tag{3.54}$$

$$\hat{H}^{(5)} = \frac{(2S)^{-\frac{1}{2}}}{2}\sum_{ij}(\boldsymbol{e}_i^-\cdot\mathbf{J}_{ij}\hat{\boldsymbol{m}}_j)\hat{n}_i\hat{b}_i\hat{n}_j\,, \tag{3.55}$$

$$\hat{H}^{(6)} = \frac{(2S)^{-1}}{8}\sum_{ij}J_{ij}^{--}\hat{n}_i\hat{b}_i\hat{n}_j\hat{b}_j\,. \tag{3.56}$$

Note, that ordering terms with respect to the number of boson operators automatically leads to an expansion of H in powers of $1/S$. As it stands, the expansion is valid for an arbitrary choice of the unit vectors $\hat{\boldsymbol{m}}_i$. If the $\hat{\boldsymbol{m}}_i$ satisfy the necessary condition (3.5) for a minimum of the classical energy, the linear term $\hat{H}^{(1)}$ in the Hamiltonian vanishes, as well as the second term in $\hat{H}^{(3)}$.

3.3 Linear spin-wave theory

Let us analyze the leading spin-wave Hamiltonian $\hat{H}^{(2)}$ a little further for the general case. Instead of the bosonic operators, we can also define the operators

$$\hat{X}_i^1 = \frac{1}{\sqrt{2}}\left(\hat{b}_i + \hat{b}_i^+\right)\,, \qquad \hat{X}_i^2 = \frac{1}{\sqrt{2}i}\left(\hat{b}_i - \hat{b}_i^+\right)\,, \tag{3.57}$$

which are directly related to fluctuations in the direction of the transverse basis vectors. They fulfill the commutation relations

$$\left[\hat{X}_i^\alpha, \hat{X}_j^\beta\right] = iM_{i\alpha;j\beta}\,, \tag{3.58}$$

with $\mathbf{M}$ given by Eq. (3.21). In particular, $\hat{X}_i^1$ and $\hat{X}_i^2$ have the commutator $[\hat{X}_i^1, \hat{X}_i^2] = i$ and thus play a role similar to position and momentum operators $\hat{X}$ and $\hat{P}$ in canonical quantum mechanics. With these operators, the spin-wave Hamiltonian can be written as

$$\hat{H}^{(2)} = \frac{1}{2}\sum_{i\alpha;j\beta}\hat{X}_i^\alpha H_{i\alpha;j\beta}^{(2)}\hat{X}_j^\beta - \frac{1}{2}\sum_i\boldsymbol{h}_i^{\text{eff}}\cdot\hat{\boldsymbol{m}}_i = \frac{1}{2}\hat{\boldsymbol{X}}^T\mathbf{H}^{(2)}\hat{\boldsymbol{X}} + \tilde{E}_{\text{qc}}\,, \tag{3.59}$$

with $\mathbf{H}^{(2)}$ as in Eq. (3.16). The quasi-particle energies of this Hamiltonian can be obtained from the considerations regarding the small-amplitude classical dynamics in Sec. (3.1). To show this, we derive the Heisenberg equation of motion for the new operators:

$$\frac{d\hat{\boldsymbol{X}}}{dt} = -\mathbf{M}\mathbf{H}^{(2)}\hat{\boldsymbol{X}}\,. \tag{3.60}$$

This is simply an operator version of the classical equation of motion (3.20). We can use the results derived above to write

$$\frac{d\hat{\boldsymbol{Z}}}{dt} = i\mathbf{W}\hat{\boldsymbol{Z}}\,, \tag{3.61}$$

where the transformation of variables is given by

$$\hat{\boldsymbol{X}} = \mathbf{R}\hat{\boldsymbol{Z}}\,, \tag{3.62}$$

and the matrix $\mathbf{R}$ is defined in Eq. (3.33). Since the operators $\hat{X}_i^\alpha$ are Hermitian, the transformed operator contains two Hermitian conjugate parts,

$$\boldsymbol{Z} = \begin{pmatrix} \hat{\boldsymbol{\beta}} \\ \hat{\boldsymbol{\beta}}^+ \end{pmatrix}\,, \qquad \boldsymbol{\beta} = (\beta_1, \ldots, \beta_N)^T\,. \tag{3.63}$$

The operators $\hat{\beta}_i^+$ and $\hat{\beta}_i$ create or annihilate the physical magnons. They obey canonical commutation relations, provided that the transformation matrix $\mathbf{R}$ fulfills the following relation,

$$\mathbf{R}\mathbf{M}\mathbf{R}^T = i\,\mathbf{M}\,. \tag{3.64}$$

It is readily checked that the transformation matrix defined in Eq. (3.33) does indeed satisfy this property. Here, the normalization anticipated in Eq. (3.33) is important. With the matrix properties derived in Sec. 3.1, the spin-wave Hamiltonian can be written in the form

$$\hat{H}^{(2)} = \tilde{E}_{\mathrm{qc}} + \frac{1}{2}\sum_{l=1}^{N}\omega_l(\hat{\beta}_l^+\hat{\beta}_l + \hat{\beta}_l\hat{\beta}_l^+) = E_{\mathrm{qc}} + \sum_{l=1}^{N}\omega_l\hat{\beta}_l^+\hat{\beta}_l\,. \tag{3.65}$$

Here, the correction to the ground-state energy due to quantum fluctuations is given by

$$E_{\mathrm{qc}} = \frac{1}{2}\sum_{l=1}^{N}\left[\omega_l - \boldsymbol{h}_l^{\mathrm{eff}}\cdot\hat{\boldsymbol{m}}_l\right]\,. \tag{3.66}$$

The procedure described in this section constitutes a generalized Bogoliubov transformation. It is always applicable provided that one starts from a ground-state spin configuration $\hat{\boldsymbol{m}}_i$ that leads to a minimum of the classical energy. In summary, we have reduced the derivation of the transformation to two successive

matrix diagonalization. The first diagonalization is required to take the square root of the symmetric positive definite matrix $\mathbf{H}^{(2)}$ defined in Eq. (3.16). In a second step we need to diagonalize the Hermitian matrix $\mathbf{Q}$ defined in Eq. (14.29) and arrange the eigenvalues as specified above Eq. (3.28). The overall transformation matrix $\mathbf{R}$ is then given by Eq. (3.33). For finite systems, this procedure could be implemented numerically using standard diagonalization routines. When the underlying lattice and the applied local magnetic fields have a spatial symmetry, the procedure can be simplified. The energy matrix $\mathbf{H}^{(2)}$ can then be block diagonalized by an orthogonal transformation that acts on spatial indices alone. The (generalized) Bogoliubov transformation can then be applied separately to each block. For system with translational invariance this block diagonalization is performed by a Fourier transformation. In Chaps. 5 and 6, we will treat ferromagnetic and antiferromagnetic spin rings.

3.4 Gauge invariance

While the longitudinal directions of quantization $\hat{\boldsymbol{m}}_i$ in the spin-wave expansion are fixed by the classical ground-state condition in Eq. (3.5), the choice of the transverse basis is not unique. There is a remaining local U(1) gauge freedom associated with the rotation of the vectors $\hat{\boldsymbol{e}}_i^1$ and $\hat{\boldsymbol{e}}_i^2$ around the classical magnetization direction $\hat{\boldsymbol{m}}_i$. Let us rewrite the matrix elements $J_{ij}^{pp'}$ in a way that the local gauge invariance is manifest. For each site i and j of the given link, we fix a transverse reference basis $\{\tilde{\boldsymbol{e}}_i^1, \tilde{\boldsymbol{e}}_i^2\}$ and $\{\tilde{\boldsymbol{e}}_j^1, \tilde{\boldsymbol{e}}_j^2\}$ by demanding that $\tilde{\boldsymbol{e}}_i^2$ and $\tilde{\boldsymbol{e}}_j^2$ be equal. For non-collinear directions $\hat{\boldsymbol{m}}_i$ and $\hat{\boldsymbol{m}}_j$, this can only be achieved if $\tilde{\boldsymbol{e}}_i^2 = \tilde{\boldsymbol{e}}_j^2$ is parallel to $\hat{\boldsymbol{m}}_i \times \hat{\boldsymbol{m}}_j$, i.e., if it points along the intersecting line of the two transverse planes as depicted in Fig. 3.1. The original transverse basis $\{\hat{\boldsymbol{e}}_i^1, \hat{\boldsymbol{e}}_i^2\}$ is then related to the reference basis by a rotation about an angle $\omega_{i\to j}$ around the local normal $\hat{\boldsymbol{m}}_i$. For the spherical basis vectors, this leads to

$$\boldsymbol{e}_i^p = e^{ip\omega_{i\to j}} \tilde{\boldsymbol{e}}_i^p \,. \tag{3.67}$$

Note that the reference basis $\tilde{\boldsymbol{e}}_i^p$ does not only depend on the site i but also on the link (i,j). In general it is therefore not possible to choose $\boldsymbol{e}_i^p = \tilde{\boldsymbol{e}}_i^p$. With the convention for the rotation angle in Eq. (3.67) the matrix elements for the spin-wave Hamiltonian can be written as

$$J_{ij}^{pp'} = \exp[ip\omega_{i\to j} + ip'\omega_{j\to i}] \tilde{J}_{ij}^{pp'} \,, \tag{3.68}$$

where $\tilde{J}_{ij}^{pp'} = \tilde{\boldsymbol{e}}_i^p \cdot \mathbf{J}_{ij} \tilde{\boldsymbol{e}}_j^{p'}$ does not depend on the choice of transverse basis anymore, but is solely determined by the $\hat{\boldsymbol{m}}_i$. E.g., for the isotropic Heisenberg model with $\mathbf{J}_{ij} = J_{ij}\mathbf{1}$, we have

$$\tilde{J}_{ij}^{pp'} = J_{ij}[\hat{\boldsymbol{m}}_i \cdot \hat{\boldsymbol{m}}_j - pp'] \,. \tag{3.69}$$

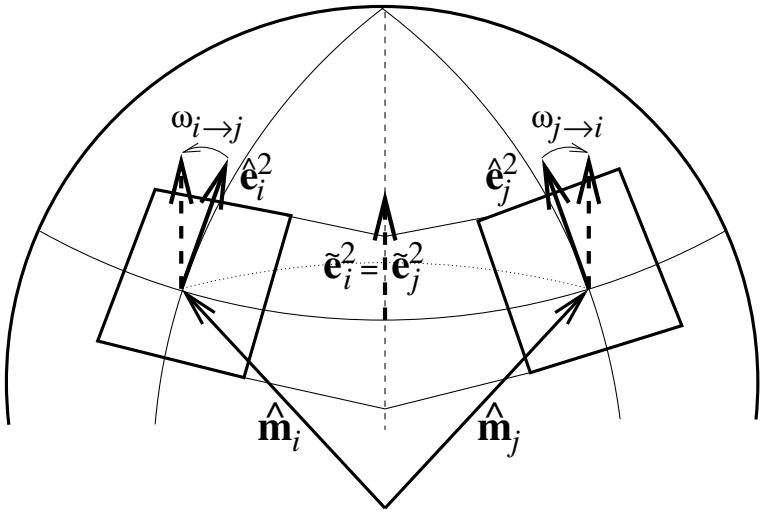

Figure 3.1: Different sets of local transverse basis vectors and gauge fields $\omega_{i\to j}$. For details see text.

The transverse Hamiltonian reads

$$\hat{H}^{\perp} \;=\; \frac{1}{8}\sum_{i,j}\Big[e^{i(\omega_{i\to j}-\omega_{j\to i})}\tilde{J}_{ij}^{+-}S_i^- S_j^+ \;+\; e^{i(\omega_{i\to j}+\omega_{j\to i})}\tilde{J}_{ij}^{++}S_i^- S_j^- \;+\; \text{H.c.}\Big]\,. \quad (3.70)$$

Alternatively, we can consider the leading order spin-wave Hamiltonian

$$\hat{H}^{(2)} \;=\; \sum_i(\boldsymbol{h}_i^{\text{eff}}\cdot\hat{\boldsymbol{m}}_i)\hat{n}_i + \frac{S}{4}\sum_{ij}\Big\{e^{i(\omega_{i\to j}+\omega_{j\to i})}\tilde{J}_{ij}^{++}\,\hat{b}_i^+\hat{b}_j^+ + e^{i(\omega_{i\to j}-\omega_{j\to i})}\tilde{J}_{ij}^{+-}\,\hat{b}_i^+\hat{b}_j + \text{H.c.}\Big\}\,. \quad (3.71)$$

Here it is clearly seen that the angles $\omega_{i\to j}$ act as gauge fields. A specific gauge corresponds to a choice of orientation of the transverse basis and a rotation of the local tranverse basis vectors by an angle α_i around $\hat{\boldsymbol{m}}_i$ is thus a gauge transformation. In the spin-wave language such a transformation reads

$$\omega_{i\to j}\to\omega_{i\to j}+\alpha_i\,,\qquad \hat{b}_i\to e^{i\alpha_i}\,\hat{b}_i\,, \quad (3.72)$$

or alternatively for the spin ladder operators $S_i^{\pm}\to S_i^{\pm}e^{\pm i\alpha_i}$.

In the special case of an isotropic Heisenberg ring in an inhomogeneous magnetic field, we can write the leading order spin-wave Hamiltonian as

$$\hat{H}^{(2)}_{\text{ring}} = \sum_i\Big\{(\boldsymbol{h}_i^{\text{eff}}\cdot\hat{\boldsymbol{m}}_i)\hat{b}_i^+\hat{b}_i + \frac{JS}{2}\Big[(1+\hat{\boldsymbol{m}}_i\cdot\hat{\boldsymbol{m}}_{i+1})e^{i(\omega_{i\to i+1}-\omega_{i+1\to i})}\hat{b}_i^+\hat{b}_{i+1} - (1-\hat{\boldsymbol{m}}_i\cdot\hat{\boldsymbol{m}}_{i+1})e^{i(\omega_{i\to i+1}+\omega_{i+1\to i})}\hat{b}_i^+\hat{b}_{i+1}^+ + \text{H.c.}\Big]\Big\}\,. \quad (3.73)$$

This Hamiltonian will be further analyzed in Chaps. 5 and 6.

A more general gauge-invariant formulation of the Heisenberg model is discussed in [Chandra *et al.*, 1990] (see also [Kopietz and Castilla, 1991]). In these works, an O(3) gauge field $\boldsymbol{A}_{i\to j}$ was introduced in a rather formal manner to write the Heisenberg model in a gauge-invariant way and to obtain the spin stiffness tensor by means of differentiation with respect to the gauge field [Singh and Huse, 1989].

Chapter 4:

Spin currents in inhomogeneous magnetic fields

In this chapter, we discuss the definition of a spin-current operator for Heisenberg magnets with non-collinear spin configurations generated by inhomogeneous magnetic fields. Problems arise in this context which have not been noticed in the literature. They are due to the fact that the magnetization as a vector quantity is not conserved in the presence of an inhomogeneous field. Yet, for smoothly varying fields, the longitudinal component of the magnetization is locally almost conserved. Thus, the intuitive concept of magnetization transport should still be useful in this case. This leads us to define an effective current operator that describes the flow of the longitudinal component. From this point of view it is clear that the concept of a transverse spin current is meaningless.

In more technical terms, we start from the microscopic equation of motion for the spin operators in Sec. 4.1. It contains only the (lattice) divergence of the spin current operator which is not sufficient to fix its rotational part. A mean-field argument is given in Sec. 4.2, before we show generally in Sec. 4.3 that a certain part of the operator $\sum_j \boldsymbol{S}_i \times J_{ij}\boldsymbol{S}_j$ can be incorporated in a renormalization of the effective magnetic field and should therefore not be included into the definition of the spin current operator. Consequently, we argue that only the projection $\tilde{\boldsymbol{I}}_{i\to j}$ of the naive "current operator" $\boldsymbol{I}_{i\to j} = \boldsymbol{S}_i \times J_{ij}\boldsymbol{S}_j$ onto the plane spanned by the local order parameters $\langle \boldsymbol{S}_i \rangle$ and $\langle \boldsymbol{S}_j \rangle$ is related to real transport of magnetization. This physical spin current vanishes within a mean-field approximation or in the classical ground state where only a purely static twist in the spin configuration exists. Thus, finite spin currents are a direct manifestation of quantum correlations in the system.

Similar conceptual problems arise in the definition of the spin-current operator in semi-conducting electronic systems with strong spin-orbit interactions. Recently, Rashba [Rashba, 2003] pointed out that for this case the precise meaning of the spin current is also subtle. In particular, he emphasized that spin currents in thermodynamic equilibrium, predicted with the standard definition of the spin-current operator used in the literature, are unphysical and should be regarded as background currents which do not correspond to real transport of magnetization. Clearly, for the burgeoning field of spintronics an understanding of this concept is essential.

In this context, it is also interesting to note that in effective low-energy models for ferromagnets involving only spin degrees of freedom even the concept of linear momentum is not well defined [Volovik, 1987]. In general, the dynamical equation for the spin degrees of freedom have to be supplemented by kinetic equations for

the underlying fermionic excitations.

For itinerant systems the spin is an intrinsic property of the charge carriers and is transported accordingly. Here, we consider localized spin models, so that charge degrees are not available to transfer magnetization between different sites. Transport of spin is then a consequence of the time evolution of the magnetization. In special cases the transport can be ascribed to the movement of quasi-particles such as magnons or spinons and again a simple physical picture emerges [Meier and Loss, 2003]. With the spin-wave theory developed in the previous chapter, a description of transport in terms of magnons is also possible in the presence of inhomogeneous fields. In Sec. 4.3 we will explain how the gauge symmetry for the leading order spin-wave Hamiltonian then automatically leads to an acceptable definition of the spin-current operator. Within the spin-wave approximation, it is identical to the effective spin-current operator introduced before.

Finally, in Sec. 4.4 we discuss the electric fields generated by a stationary flow of magnetization. We derive a Biot-Savart-type law for the scalar electric potential and evaluate it explicitly for the case of a crown-shaped current loop.

4.1 Naive definition of the spin current operator

The standard definition of the spin-current operator in magnetic insulators does no longer apply in the presence of an inhomogeneous magnetic field. To show this, we consider again the Heisenberg model in Eq. (3.1), but restrict ourselves to the isotropic case $\mathbf{J}_{ij} = J_{ij}\mathbf{1}$. We assume that the magnetic field $\boldsymbol{h}_i$ is strong enough to induce permanent magnetic dipole moments $\boldsymbol{m}_i = g\mu_{\mathrm{B}}\langle\hat{\boldsymbol{S}}_i\rangle$ which are not necessarily parallel to $\boldsymbol{h}_i$. The brackets $\langle\dots\rangle$ denote the usual thermal average. Let us also introduce the associated unit vectors $\hat{\boldsymbol{m}}_i = \boldsymbol{m}_i/|\boldsymbol{m}_i|$. These are generalizations of the directions of the classical ground state introduced in Sec. 3.1 as a starting point for the spin-wave theory, and we will therefore use the same notation. As an illustration one should bear in mind the example of a ferromagnetic ring in a crown-shaped field geometry mentioned in the introduction (see Fig 2.3), but our arguments are not limited to this case. The Hamiltonian (3.1) implies the equation of motion

$$\hbar\frac{\partial \boldsymbol{S}_i}{\partial t} + \boldsymbol{h}_i \times \boldsymbol{S}_i + \sum_j \boldsymbol{I}_{i\to j} = 0\,, \tag{4.1}$$

where we have defined

$$\boldsymbol{I}_{i\to j} = \boldsymbol{S}_i \times J_{ij}\boldsymbol{S}_j\ . \tag{4.2}$$

Eq. (4.1) shows an obvious similarity with the discrete lattice version of the equation of continuity for charge currents. Thus, it is tempting to identify $\boldsymbol{I}_{i\to j}$ with the operator whose expectation value gives the spin current from site i to site j. Here, we argue that this identification is only correct for a *homogeneous*

magnetic field, for which the equilibrium expectation values $\langle \hat{\boldsymbol{S}}_i \rangle$ of the spins are all collinear and aligned to the spatially constant direction of the field, i.e. $\boldsymbol{h}_i \times \langle \boldsymbol{S}_i \rangle = 0$. For this special case, using that equilibrium averages are time independent, $\frac{d}{dt}\langle \boldsymbol{S}_i \rangle = 0$, the average of the equation of motion (4.1) reduces to

$$\sum_j \langle \boldsymbol{I}_{i\to j} \rangle = 0 \; . \tag{4.3}$$

Hence, the lattice divergence of the spin current in the presence of a homogeneous magnetic field vanishes. For a one-dimensional ring with nearest neighbor hopping this implies at an arbitrary site i

$$\langle \boldsymbol{I}_{i\to i+1} \rangle + \langle \boldsymbol{I}_{i\to i-1} \rangle = \langle \boldsymbol{I}_{i\to i+1} \rangle - \langle \boldsymbol{I}_{i-1\to i} \rangle = 0 \; , \tag{4.4}$$

so that the same spin current $\langle \boldsymbol{I} \rangle = \langle \boldsymbol{I}_{i\to i+1} \rangle$ flows through all links of the ring. However, the equation of motion contains only the divergence of the current and does not fix the value of $\langle \boldsymbol{I} \rangle$ itself. This is due to the fact known from elementary vector analysis, that both the divergence and the curl are necessary to uniquely specify a vector field up to an overall constant. Because the equation of motion contains only the divergence, circulating spin currents cannot be calculated with it. In fact, even the definition of the spin current operator in a geometry permitting circulating spin currents cannot be deduced. Of course, for a ring with a collinear spin configuration we know that $\langle \boldsymbol{I} \rangle = 0$, so that there are no circulating currents.

When a non-uniform magnetic field is present, the spin current operator is *not* simply given by Eq. (4.2). In general, the spin configuration in the ground state is then inhomogeneous as well. For the example of the ferromagnetic ring in a crown-shaped field forming an angle ϑ with the central axis, the magnetic moments will also arrange in the form of a crown with a slightly smaller angle ϑ_m as described in more detail in Sec. 5.1 and shown in Fig. 5.1. To illustrate that in this case the expectation value of $\boldsymbol{I}_{i\to j}$ is not the physical spin current, we further specialize to a star-shaped magnetic field, corresponding to $\vartheta_m = \vartheta = \pi/2$ in Fig. 5.1. If we treat the spins as classical vectors and assume a ring with N evenly spaced sites and a nearest neighbor exchange coupling J, Eq. (4.2) yields at zero temperature

$$\boldsymbol{I}_{i\to i+1} = J\boldsymbol{e}_z \sin(2\pi/N) \; . \tag{4.5}$$

Yet, at the classical level the statics and dynamics of a Heisenberg magnet are completely decoupled. Because the classical ground state does not have any intrinsic dynamics, a spin current, corresponding to moving magnetic dipoles, should not exist. Furthermore, if the classical Heisenberg model is provided with Poisson bracket dynamics, as described in Sec. 3.1, the classical ground state yields a stationary solution. Clearly, such a completely stationary state cannot be used to transport magnetization. We conclude that for twisted spin configurations Eq. (4.2) is not a physically meaningful definition of the spin current operator.

4.2 Effective spin currents with correct classical limit

To get our hands on a better definition, let us have a glimpse at a non-equilibrium situation. Thus, we start with a given density matrix at time $t = 0$ and let the system evolve according to the unitary dynamics generated by the Hamiltonian in Eq. (3.1). The equation of motion (4.1) then directly translates to a relation for the local and instantaneous order parameter

$$\partial_t \langle \boldsymbol{S}_i \rangle_t + \boldsymbol{h}_i \times \langle \boldsymbol{S}_i \rangle_t + \sum_j \langle \boldsymbol{I}_{i\to j} \rangle_t = 0 \,. \tag{4.6}$$

Here, $\langle \dots \rangle_t$ denotes an average with respect to the time dependent density matrix. It is then reasonable to demand that a transport current can lead to an accumulation of magnetization, i.e., a change in the magnitude of the local order parameter in time. For this magnitude, we obtain the equation of motion

$$\partial_t |\langle \boldsymbol{S}_i \rangle_t| + \sum_j \hat{\boldsymbol{m}}_i(t) \cdot \langle \boldsymbol{I}_{i\to j} \rangle_t = 0 \,, \tag{4.7}$$

where $\hat{\boldsymbol{m}}_i(t) = \langle \boldsymbol{S}_i \rangle_t / |\langle \boldsymbol{S}_i \rangle_t|$ is the time dependent direction of the order parameter. Note that only the longitudinal component of the naive "current operator" appears in this continuity equation without source terms.

The transverse components lead to a change in the direction of the local order parameter, but they are largely compensated by the magnetic field term that acts as a source and generates a precession. We want to discuss the electric fields generated by the magnetization dynamics. To do so, one either has to take into account both the current $\boldsymbol{I}_{i\to j}$ and the local precessional motion, or devise a way to make the cancellation explicit by including part of the "transverse current" in an effective magnetic field. We will follow the second route here.

A simple approximate calculation can give an indication of how to proceed. In the classical ground state, the magnetization aligns parallel to the sum of the external and the exchange field as shown in Eq. (3.5). Written in terms of classical expectation values, the necessary condition for a minimum of the classical energy reads

$$\boldsymbol{h}_i^{\text{eff}} \times \langle \boldsymbol{S}_i \rangle = 0 \quad , \quad \boldsymbol{h}_i^{\text{eff}} = \boldsymbol{h}_i - \sum_j J_{ij} \langle \boldsymbol{S}_j \rangle \,. \tag{4.8}$$

Note that the effective magnetic field contains a part of the exchange interaction. To avoid double counting, this part should not be included into the definition of the spin current operator. The exact equation of motion (4.1) can be rewritten in terms of the effective magnetic field $\boldsymbol{h}_i^{\text{eff}}$ defined in Eq. (4.8). This yields

$$\hbar \frac{\partial \boldsymbol{S}_i}{\partial t} + \boldsymbol{h}_i^{\text{eff}} \times \boldsymbol{S}_i + \sum_j \boldsymbol{I}_{i\to j}^{\text{eff}} = 0 \,, \tag{4.9}$$

where the effective current operator is defined as

$$\boldsymbol{I}^{\text{eff}}_{i\to j} = J_{ij}\boldsymbol{S}_i \times [\boldsymbol{S}_j - \langle \boldsymbol{S}_j\rangle] \,. \tag{4.10}$$

The expectation value of this effective current operator is given by

$$\langle \boldsymbol{I}^{\text{eff}}_{i\to j}\rangle = J_{ij}\left[\langle \boldsymbol{S}_i \times \boldsymbol{S}_j\rangle - \langle \boldsymbol{S}_i\rangle \times \langle \boldsymbol{S}_j\rangle\right] \,. \tag{4.11}$$

Obviously, it vanishes identically both in the classical ground state and if the spins are treated within the mean-field approximation, where the spin correlator factorizes. Physically, this is due to the fact that within the mean-field approximation the Heisenberg exchange interaction is replaced by an effective magnetic field, so that the different sites are uncorrelated and there are no degrees of freedom to transfer magnetization between them.

4.3 New definition of the spin current operator

The definition of $\boldsymbol{I}^{\text{eff}}_{i\to j}$ in Eq. (4.10) has the disadvantage of not being antisymmetric with respect to the exchange of site labels, although its expectation value is obviously antisymmetric. In order to solve this problem and to generalize the concept of an effective current operator beyond the mean-field description, we propose the following definition,

$$\tilde{\boldsymbol{I}}_{i\to j} = \boldsymbol{I}_{i\to j} - \boldsymbol{\gamma}_{ij}(\boldsymbol{\gamma}_{ij}\cdot \boldsymbol{I}_{i\to j}) \,, \tag{4.12}$$

with the unit vector

$$\boldsymbol{\gamma}_{ij} = \frac{\boldsymbol{m}_i \times \boldsymbol{m}_j}{|\boldsymbol{m}_i \times \boldsymbol{m}_j|} \,. \tag{4.13}$$

Thus, we interpret only the projection of $\boldsymbol{I}_{i\to j}$ onto the plane spanned by the two local order parameters $\boldsymbol{m}_i$ and $\boldsymbol{m}_j$ as a physical transport current. The contribution subtracted in Eq. (4.12) can be incorporated in an effective magnetic field. More precisely, the equilibrium expectation value of the exact equation of motion (4.1) can be rewritten as

$$\boldsymbol{h}^{\text{eff}}_i \times \langle \boldsymbol{S}_i\rangle + \sum_j \langle \tilde{\boldsymbol{I}}_{i\to j}\rangle = 0 \,, \tag{4.14}$$

with the effective magnetic field now defined as

$$\boldsymbol{h}^{\text{eff}}_i = \boldsymbol{h}_i - \sum_j \frac{\langle \boldsymbol{S}_i \times J_{ij}\boldsymbol{S}_j\rangle \cdot \boldsymbol{\gamma}_{ij}}{[\langle \boldsymbol{S}_i\rangle \times \langle \boldsymbol{S}_j\rangle]\cdot \boldsymbol{\gamma}_{ij}} \langle \boldsymbol{S}_j\rangle \,. \tag{4.15}$$

This reduces to Eq. (4.8) for the classical ground state or at the mean-field level, where the correlation function in the numerator is factorized. The spin-current

operator defined in Eq. (4.12) is manifestly antisymmetric under the exchange of the labels, as it should be. It implicitly depends on the spin configuration via the unit vector $\boldsymbol{\gamma}_{ij}$, so that in twisted spin configurations the spin current operator is a rather complicated functional of the exchange couplings. The fact that the current operator of an interacting many body system is a complicated functional of the interaction is well known from the theory of interacting Fermi systems [Pines and Nozières, 1989]. In particular, when the effective interaction does not only involve densities the construction of the current operator is not straightforward [Metzner *et al.*, 1998].

For explicit calculations, we use the decomposition of the spin operators in a site-dependent basis, as explained in Sec. 3.2. With the notation introduced in the previous chapter, we obtain the following representation for the effective spin current operator,

$$\tilde{\boldsymbol{I}}_{i\to j} = \frac{J_{ij}}{2i}\Big[S_i^- S_j^+ e^{i(\omega_{i\to j}-\omega_{j\to i})}\frac{\hat{\boldsymbol{m}}_i+\hat{\boldsymbol{m}}_j}{2} - S_i^- S_j^- e^{i(\omega_{i\to j}+\omega_{j\to i})}\frac{\hat{\boldsymbol{m}}_i-\hat{\boldsymbol{m}}_j}{2} + S_i^{\parallel} S_j^- e^{i\omega_{i\to j}}(\boldsymbol{\gamma}_{ij}\times\hat{\boldsymbol{m}}_i) - S_i^- S_j^{\parallel} e^{i\omega_{j\to i}}(\boldsymbol{\gamma}_{ij}\times\hat{\boldsymbol{m}}_j) - \text{H.c.}\Big] .$$

The third and fourth terms in this expression couple longitudinal and transverse degrees of freedom and therefore do not contribute to leading order in a spin-wave calculation. The first and second terms are dominant for ferromagnetic and antiferromagnetic rings respectively and will be discussed in detail in Chaps. 5 and 6. For a magnetic field that varies smoothly as one moves through the system, the magnetic moments on neighboring lattice sites are almost collinear, so that in both cases the component of the naive "current operator" $\boldsymbol{I}_{i\to j}$ along the local order parameter is the one that corresponds to the transport of magnetization.

Alternatively, an effective current operator can also be derived by making use of the gauge freedom in the choice of the transverse quantization axis discussed in Sec. 3.4. The partition function Z has to be independent of the chosen gauge. By performing a transformation on the gauge fields $\omega_{i\to j}$ as in Eq. (3.72) and expanding in the rotation angles α_i, we obtain the relation

$$Z[\{\omega\}] = Z[\{\omega+\alpha\}] = \operatorname{tr}\left[e^{-\beta H[\{\omega+\alpha\}]}\right] = Z[\{\omega\}]\left(1+\sum_i \alpha_i\left\langle\frac{\partial H}{\partial\alpha_i}\right\rangle + \mathcal{O}(\alpha^2)\right) . \tag{4.16}$$

Because the α_i are arbitrary, the expectation values of the derivatives of the Hamiltonian with respect to α_i have to vanish individually. In the leading spin-wave approximation, the Hamiltonian $\hat{H}'$, which describes the coupling between longitudinal and transverse degrees of freedom, can be neglected. Since $\hat{H}^{\parallel}$ does not depend on the gauge fields, the derivative of the full Hamiltonian is then identical to the derivative of the transverse part alone,

$$\frac{\partial\hat{H}^{\perp}}{\partial\alpha_i} = \sum_j \frac{\partial\hat{H}^{\perp}}{\partial\omega_{i\to j}} = \sum_j I_{i\to j} = -\sum_j J_{ij}\hat{\boldsymbol{m}}_i\cdot\left(\boldsymbol{S}_i^{\perp}\times\boldsymbol{S}_j^{\perp}\right) . \tag{4.17}$$

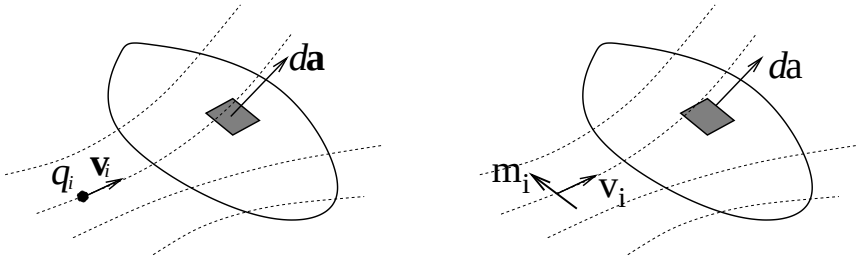

Figure 4.1: Charge versus magnetization currents. For charge currents (left panel), particles with a charge q_i move with a velocity $\boldsymbol{v}_i$. The current density is then a vector and the total current through the surface element $d\boldsymbol{a}$ is a scalar. For magnetization currents (right panel), particles with a magnetic dipole moment $\boldsymbol{m}_i$ move with a velocity $\boldsymbol{v}_i$. The current density is now a tensor and the total current through the surface element $d\boldsymbol{a}$ is still a vector.

This is again the lattice divergence of an effective longitudinal current operator $I_{i\to j}$. The equilibrium expectation value of this divergence vanishes according to Eq. (4.16). Since no magnetic field terms appear, we can directly identify $I_{i\to j}$ as the relevant current operator. Alternatively, we can also derive the equation of motion for the longitudinal components of the spin operators,

$$\hbar\frac{\partial S_i^{\parallel}}{\partial t} = -\sum_j J_{ij}\hat{\boldsymbol{m}}_i\cdot\left(\boldsymbol{S}_i^{\perp}\times\boldsymbol{S}_j^{\perp}\right) - \boldsymbol{S}_i^{\perp}\cdot\left[\hat{\boldsymbol{m}}_i\times(\boldsymbol{h}_i - \sum_j J_{ij}S_j^{\parallel}\hat{\boldsymbol{m}}_j)\right]. \quad (4.18)$$

Due to the condition (3.5) for the classical ground state, the second term vanishes within the leading spin-wave approximation, i.e., when $S_j^{\parallel}$ is replaced by S. Thus, we obtain the same continuity equation for the effective longitudinal current operator. By expanding the transverse spin operators in a spherical basis as in Eq. (3.41), we can show that within linear spin-wave theory, we have

$$\left\langle\frac{\partial\hat{H}^{\perp}}{\partial\omega_{i\to j}}\right\rangle = -\left\langle\hat{\boldsymbol{m}}_i\cdot\tilde{\boldsymbol{I}}_{i\to j}\right\rangle. \quad (4.19)$$

Thus, for a spin configuration with a spatially smoothly varying direction we again arrive at the conclusion that only the longitudinal current operator is relevant for magnetization transport. Hence, in subsequent spin-wave calculations, we will use the scalar current operator $I_{i\to j}$. Eq. (4.19) shows that within linear spin-wave theory this is equivalent to using the effective current operator $\tilde{I}_{i\to j}$.

4.4 Electrodynamics of spin currents

The flow of magnetic moments generates electric dipole fields which possibly allow an experimental detection of magnetization currents. The currents predicted in

this work are due to the collective dynamics of localized spins. Yet, the electric fields are independent of this mechanism. Equivalently, we consider a set of magnetic moments $\hat{\boldsymbol{m}}_i$ at positions $\boldsymbol{r}_i$ that move with velocities $\boldsymbol{v}_i$ and generate the same magnetization current. This situation is compared in Fig. 4.1 with the one for ordinary charge transport. Note that due to the vector character of the magnetization, the magnetization current density is a tensor and the total current through a surface is still a vector. The spatially varying magnetization is given by

$$\boldsymbol{M}(\boldsymbol{r}) = \sum_i \delta(\boldsymbol{r} - \boldsymbol{r}_i)\boldsymbol{m}_i \,. \tag{4.20}$$

It is generated by an effective current density

$$\boldsymbol{j}(\boldsymbol{r}) = c\nabla \times \boldsymbol{M}(\boldsymbol{r}) \,. \tag{4.21}$$

If the magnetization is moving with velocity $\boldsymbol{v}(\boldsymbol{r})$, the current distribution is dragged along. A Lorentz boost from the rest frame of the magnetic dipoles to the laboratory frame then shows that the magnetization current is accompanied by a polarization

$$\boldsymbol{P}(\boldsymbol{r}) = \frac{\boldsymbol{v}(\boldsymbol{r})}{c} \times \boldsymbol{M}(\boldsymbol{r}) \,, \tag{4.22}$$

to leading order in $\boldsymbol{v}(\boldsymbol{r})/c$ [Hirsch, 1999]. The polarization corresponds to a charge density

$$\rho(\boldsymbol{r}) = -\nabla \cdot \boldsymbol{P}(\boldsymbol{r}) \,, \tag{4.23}$$

which in turn generates an electric field

$$\boldsymbol{E}(\boldsymbol{r}) = -\nabla\phi(\boldsymbol{r}) \,. \tag{4.24}$$

Here, the scalar potential is given by

$$\begin{aligned} \phi(\boldsymbol{r}) = \int d^3r' \frac{\rho(\boldsymbol{r}')}{|\boldsymbol{r} - \boldsymbol{r}'|} &= \frac{1}{c}\int d^3r' [\boldsymbol{v}(\boldsymbol{r}') \times \boldsymbol{M}(\boldsymbol{r}')] \cdot \frac{(\boldsymbol{r} - \boldsymbol{r}')}{|\boldsymbol{r} - \boldsymbol{r}'|^3} \\ &= \frac{I_m}{c} \oint [d\boldsymbol{r}' \times \hat{\boldsymbol{m}}(\boldsymbol{r}')] \cdot \frac{\boldsymbol{r} - \boldsymbol{r}'}{|\boldsymbol{r} - \boldsymbol{r}'|^3} \,. \end{aligned} \tag{4.25}$$

The last equality is valid for a current loop, where $\boldsymbol{v}|\boldsymbol{M}|d^3r = I_m d\boldsymbol{r}$. Eq. (4.25) is a generalized Biot-Savart law for magnetization currents. For a current of magnetic dipoles oriented in the z direction and flowing along the infinite x axis, we obtain the following scalar potential,

$$\Phi(\boldsymbol{x}) = -\frac{2I_m}{c} \frac{y}{x^2 + y^2 + z^2} \,. \tag{4.26}$$

This result has already been discussed in [Meier and Loss, 2003].

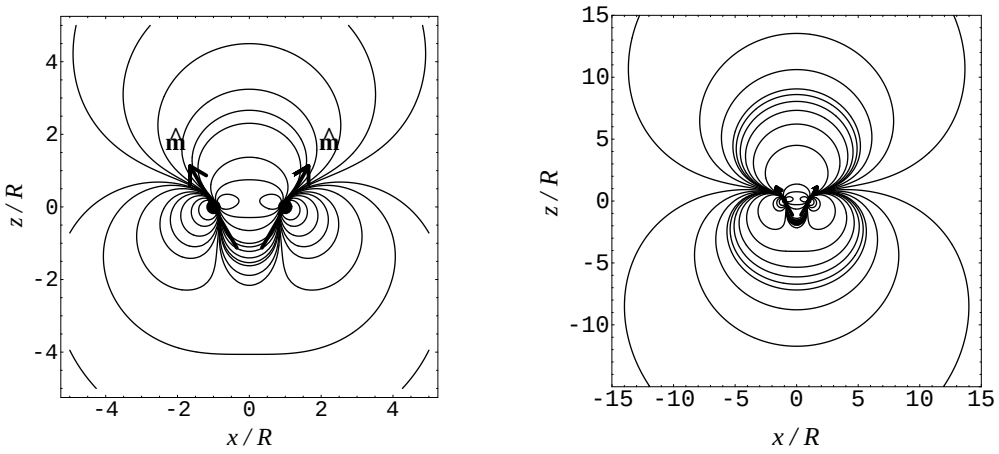

Figure 4.2: Lines of constant electric potential due to a magnetization current circulating around a ring with radius R and an angle $\vartheta_m = 30°$ between the direction of the magnetization an the z axis as in Fig. 2.3. The left graph is on a more expanded scale showing clearly the local dipole character of the field in close vicinity of the ring, whereas the right graph shows the resulting dipole field in the far zone.

Consider now the case of a crown-shaped current loop, which can be imagined as being generated by rotating the magnetization crown shown in Fig. 5.1 at a constant angular velocity around the central axis. The line integral around the ring can be expressed in terms of standard elliptic integrals. For the electric potential we obtain

$$\begin{aligned}\Phi(r,\theta) &= -\frac{I_m}{c}\frac{1}{(r^2+R^2)^{3/2}}\Big\{\left[R\cos(\vartheta_m)+r\cos(\theta)\sin(\vartheta_m)\right]f_1(\lambda)\\ &\qquad -r\sin(\theta)\cos(\vartheta_m)f_2(\lambda)\Big\}\,,\end{aligned} \tag{4.27}$$

where $\lambda = \frac{2rR}{r^2+R^2}\sin(\theta)$, and the elliptic integrals are defined as

$$f_1(\lambda) = \int_0^{2\pi} d\phi\,\frac{1}{[1-\lambda\cos(\phi)]^{3/2}}\,, \qquad f_2(\lambda) = \int_0^{2\pi} d\phi\,\frac{\cos(\phi)}{[1-\lambda\cos(\phi)]^{3/2}}\,. \tag{4.28}$$

The resulting equipotential lines are shown in Fig. 4.2. Close to the ring, the electric field is identical to that of an electric dipole orthogonal to the direction of the magnetization. In the far zone, the electric field approaches again a dipole field with potential

$$\phi(\boldsymbol{r}) = \frac{\boldsymbol{p}\cdot\boldsymbol{r}}{|\boldsymbol{r}|^3}\,, \tag{4.29}$$

and dipole moment

$$\boldsymbol{p} = -\hat{\boldsymbol{e}}_z\frac{I_m}{c}L\sin\theta_m\,. \tag{4.30}$$

This result will be used in the next chapter to estimate the order of magnitude of the electric field generated by the persistent magnetization current in a ferromagnetic ring.

Chapter 5:

Persistent spin currents in ferromagnetic Heisenberg rings

In this chapter, we explicitly calculate the persistent magnetization current for a ferromagnetic Heisenberg ring in an inhomogeneous magnetic field. The Hamiltonian of the ring is given in Eq. (2.14) with an exchange coupling $J < 0$. We assume that the field encloses a solid angle Ω as one moves around the ring. The classical ground state for a crown-shaped field geometry is determined in Sec. 5.1. In Sec. 5.2, we obtain the spin-wave spectrum in the linear approximation. This spectrum will explicitly depend on a magnetic flux Ω whose geometric significance as a defect angle of classical parallel transport is analyzed in more detail in Sec. 5.3. In the following section, we derive an expression for the persistent magnetization current. In Sec. 5.5, we finally estimate the strength of the electric dipole field generated by the persistent magnetization current.

5.1 Classical ground state

The following spin-wave calculation is applicable for any magnetic field that has a constant magnitude h and a smoothly varying spatially inhomogeneous direction. The field then generates a spin configuration in the classical ground state that spans a solid angle Ω as one moves around the ring. For concreteness, we consider again the crown-shaped field arrangement depicted in Fig. 2.3. The classical ground state then exhibits the same rotational symmetry around the z-axis and also forms a crown with a slightly smaller angle ϑ_m, as shown in Fig. 5.1. From the general equation (3.5), we obtain a condition for the angle ϑ_m,

$$\sin(\vartheta - \vartheta_m) = \frac{|J|S}{h}\,[1 - \cos(2\pi/N)]\sin(2\vartheta_m)\,. \tag{5.1}$$

For a sufficiently strong magnetic field h the deviation of ϑ_m from ϑ becomes small and the classical spin configuration approaches the direction of the magnetic field. In contrast, for vanishing h the angle ϑ_m is also zero and all spins align along the z axis. This spin configuration has the same energy as all other ferromagnetically aligned arrangements that can be obtained by rotating all spins simultaneously. Note that for a finite magnetic field h no such degeneracy of the classical ground state exists.

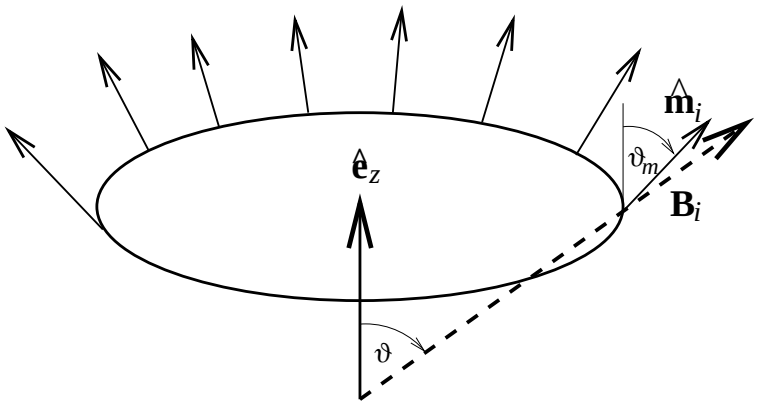

Figure 5.1: Classical ground state of a ferromagnetic Heisenberg ring in a crown-shaped magnetic field.

5.2 Spin-wave spectrum

For a large ferromagnetic ring, i.e. for $N \gg 1$, and for a smooth spatial variation of the magnetic field on the scale of a lattice spacing, neighboring spins are almost parallel in the classical spin configuration. E.g., for the crown-shaped geometry discussed above we easily see that

$$\hat{\boldsymbol{m}}_i \cdot \hat{\boldsymbol{m}}_{i+1} = 1 - \mathcal{O}\left(N^{-2}\right) . \tag{5.2}$$

Therefore, we assume that the anomalous terms in the spin-wave Hamiltonian in Eq. (3.73), i.e., the second term in square brackets and its hermitian conjugate, can be neglected. Thus the dominant influence of the inhomogeneity is captured by the phase factors alone. This is similar to an adiabatic approximation for magnons, since spin deviations now have to follow the local classical directions as they hop from site to site. Furthermore, for a sufficiently strong magnetic field the unit vectors $\hat{\boldsymbol{m}}_i$ are almost parallel to the applied local field. Therefore, we will replace $\boldsymbol{h}_i \cdot \hat{\boldsymbol{m}}_i = h - 2JS$ in Eq. (3.73), independent of the site index i.

With these approximations the spin-wave Hamiltonian in Eq. (3.73) can be written as

$$\hat{H}^{(2)}_{\mathrm{FM}} = \sum_{i=1}^{N} \Big\{ \big[2|J|S + h\big] \hat{b}_i^+ \hat{b}_i - |J|S \big[e^{i(\omega_{i\to i+1} - \omega_{i+1\to i})} \hat{b}_i^+ \hat{b}_{i+1} + \mathrm{H.c.} \big] \Big\} , \tag{5.3}$$

where periodic boundary conditions $\hat{b}_{N+1} = \hat{b}_1$ apply, and the sign of the ferromagnetic exchange interaction $J = -|J|$ is explicitly shown. This spin-wave Hamiltonian is standard for a ferromagnetic ring, except for the appearance of the phase factors in front of the hopping terms $\hat{b}_i^+ \hat{b}_{i\pm1}$. These phases can be eliminated in favor of twisted boundary conditions by a gauge transformation as

described in Eq. (3.72) with the local rotation angles

$$\alpha_j = \sum_{i=1}^{j-1} (\omega_{i\to i+1} - \omega_{i+1\to i})\,. \tag{5.4}$$

This yields the new boundary condition $\hat{b}_{N+1} = e^{i\Omega}\hat{b}_1$ where

$$\Omega = \alpha_{N+1} = \sum_{i=1}^{N} (\omega_{i\to i+1} - \omega_{i+1\to i}). \tag{5.5}$$

Thus, we have shown that within the adiabatic approximation the physics depends on the texture of the magnetic field only via the single parameter Ω, which is manifestly gauge invariant.

In the special gauge where the phase factors have been eliminated, the spin-wave Hamiltonian is readily diagonalized by the Fourier transformation

$$\hat{b}_i = \frac{1}{\sqrt{N}} \sum_k e^{ikl_i}\, \hat{b}_k\,, \qquad \hat{b}_k = \frac{1}{\sqrt{N}} \sum_i e^{-ikl_i}\, \hat{b}_i\,. \tag{5.6}$$

The diagonal Hamiltonian reads

$$H = \sum_k \epsilon_k b_k^\dagger b_k, \tag{5.7}$$

with the standard tight-binding dispersion for the magnons

$$\epsilon_k = 2|J|S[1 - \cos(ka)] + h\,. \tag{5.8}$$

Due to the twisted boundary condition, the quantized wave vectors are shifted by the quantity Ω,

$$k_n = \frac{2\pi}{Na}\left(n + \frac{\Omega}{2\pi}\right), \qquad n = 0, \ldots, N-1. \tag{5.9}$$

The dispersion relation together with the allowed wave vectors is depicted in Fig. 5.2. The close analogy of the derivation in this section to the calculation of persistent charge currents should be evident. A comparison of Eq. (5.9) with Eq. (2.10) in the introductory chapter shows that the geometric quantity Ω is the analog of the magnetic flux.

5.3 Parallel transport and geometric flux

The geometrical significance of the quantity Ω is best understood in the special gauge where the phase factors in Eq. (5.3) vanish, i.e. where

$$\omega_{i\to i+1} - \omega_{i+1\to i} = 0\,. \tag{5.10}$$

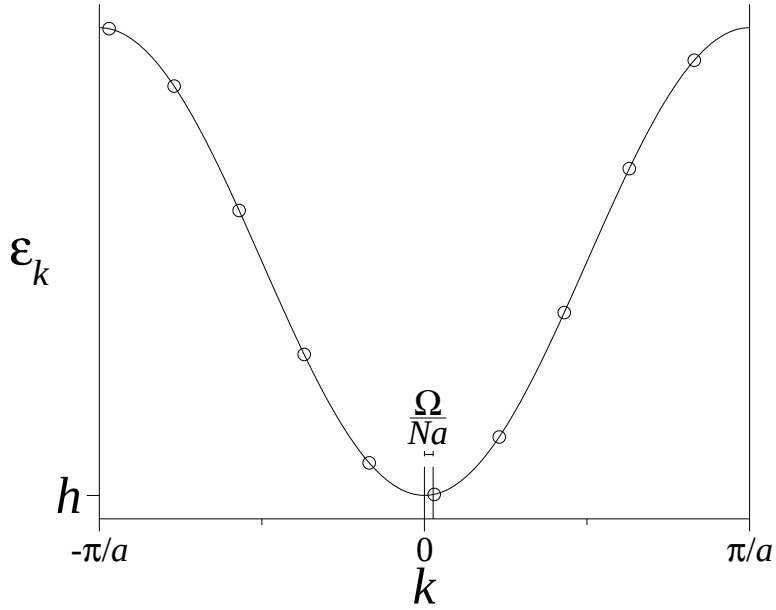

Figure 5.2: Magnon dispersion for a ferromagnetic ring in the presence of an inhomogeneous magnetic field of strength h subtending a solid angle Ω. The quantized wave vectors are shown for a ring with only $N = 10$ sites for better visibility.

This condition implies that the local basis vectors at site $i+1$ are obtained from those at site i by a rotation around $\hat{\boldsymbol{m}}_i \times \hat{\boldsymbol{m}}_{i+1}$ (see Fig. 5.3). If one connects the corresponding transverse unit vectors at the sites i and $i+1$ by geodesics on the unit sphere, then these connections are shortest in the special gauge defined by Eq. (5.10). Thus, the basis at i is rotated in the most direct way into the basis at $i+1$. For other choices of transverse basis vectors an additional twist around $\hat{\boldsymbol{m}}_{i+1}$ needs to be applied. Thus, once the transverse basis vector $\boldsymbol{e}_1^1$ is chosen, the basis at all other sites are fixed by the gauge condition (5.10), yielding the recursion relation

$$\hat{\boldsymbol{e}}_{i+1}^1 = \exp\left(\gamma_{i,i+1} \frac{\hat{\boldsymbol{m}}_i \times \hat{\boldsymbol{m}}_{i+1}}{|\hat{\boldsymbol{m}}_i \times \hat{\boldsymbol{m}}_{i+1}|} \times\right) \hat{\boldsymbol{e}}_i^1 \,, \tag{5.11}$$

and equivalently for $\hat{\boldsymbol{e}}_i^2$. Here, the rotation angles are $\gamma_{i,i+1} = \angle(\hat{\boldsymbol{m}}_i, \hat{\boldsymbol{m}}_{i+1}) = \arcsin|\hat{\boldsymbol{m}}_i \times \hat{\boldsymbol{m}}_{i+1}|$, and the exponential $e^{\boldsymbol{\theta}\times}$ denotes an SO(3) rotation matrix acting on a vector $\boldsymbol{m}$ according to

$$e^{\boldsymbol{\theta}\times}\boldsymbol{m} = \hat{\boldsymbol{\theta}}(\hat{\boldsymbol{\theta}} \cdot \boldsymbol{m}) + (\hat{\boldsymbol{\theta}} \times \boldsymbol{m}) \sin\theta - \hat{\boldsymbol{\theta}} \times (\hat{\boldsymbol{\theta}} \times \boldsymbol{m}) \cos\theta \,, \tag{5.12}$$

with $\boldsymbol{\theta} = \theta\hat{\boldsymbol{\theta}}$. Eq. (5.11) describes a discrete version of parallel transport of a tangential vector on the surface of the unit sphere [Shapere and Wilczek, 1989].

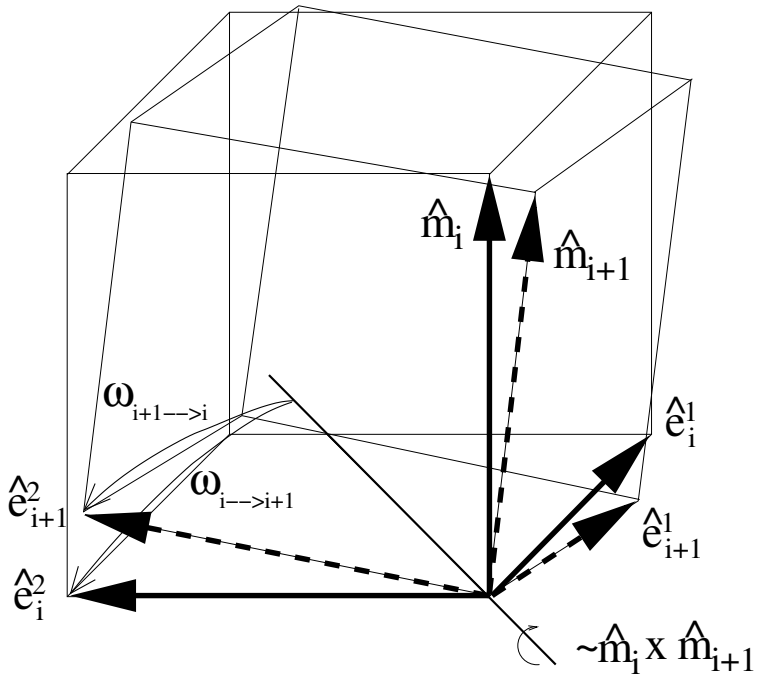

Figure 5.3: Sets of transverse basis vectors at sites i and $i+1$ that are related by discrete parallel transport.

When the basis vectors are transported once around the closed ring by this sequence of finite rotations, they do in general not coincide with the original basis. The quantity Ω defined in Eq. (5.5) is the defect angle between the transported and the original basis,

$$\Omega = \angle(\hat{\boldsymbol{e}}^1_{N+1}, \hat{\boldsymbol{e}}^1_1) = \angle(\hat{\boldsymbol{e}}^2_{N+1}, \hat{\boldsymbol{e}}^2_1). \tag{5.13}$$

To clarify the relation between the recursion relation (5.11) and classical parallel transport, we consider the basis vectors to be continuous functions of the position on the ring,

$$\hat{\boldsymbol{m}}_i = \hat{\boldsymbol{m}}(l_i)\,, \qquad \hat{\boldsymbol{e}}^\alpha_i = \hat{\boldsymbol{e}}^\alpha(l_i)\,, \tag{5.14}$$

where $\alpha = 1, 2$. For a classical ground-state that varies smoothly on the scale of the lattice spacing a, one can use an expansion in powers of a to obtain

$$\hat{\boldsymbol{m}}_i \times \hat{\boldsymbol{m}}_{i+1} = \hat{\boldsymbol{m}}(l_i) \times \hat{\boldsymbol{m}}(l_i + a) \approx a\, \hat{\boldsymbol{m}}(l_i) \times \frac{\partial \hat{\boldsymbol{m}}}{\partial l}(l_i) + \mathcal{O}(a^2). \tag{5.15}$$

In the limit $a \to 0$ the recursion relation (5.11) turns into the differential equations for classical parallel transport [Shapere and Wilczek, 1989],

$$\frac{\partial \hat{\boldsymbol{e}}^\alpha}{\partial l} = \boldsymbol{\omega}(l) \times \hat{\boldsymbol{e}}^\alpha(l)\,, \qquad \boldsymbol{\omega}(l) = \hat{\boldsymbol{m}}(l) \times \frac{\partial \hat{\boldsymbol{m}}}{\partial l}\,. \tag{5.16}$$

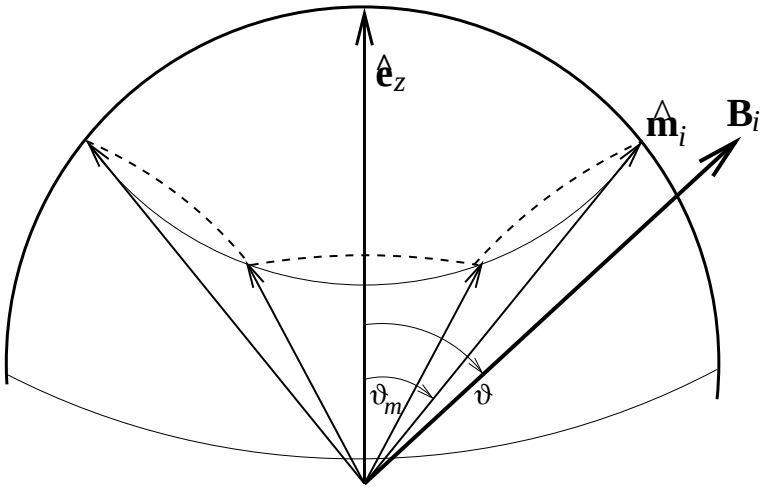

Figure 5.4: Discrete parallel transport for crown-shaped geometry.

This differential transport law exactly reproduces the discrete result (5.11) provided the $\hat{\boldsymbol{m}}(l)$ between the sites i and $i+1$ are chosen along the shortest path connecting $\hat{\boldsymbol{m}}_i$ and $\hat{\boldsymbol{m}}_{i+1}$ on the unit sphere, i.e., along a geodesic. For the crown-shaped geometry, this is shown in Fig. 5.4

The defect angle associated with the parallel transport (5.16) is known to be equal to the solid angle subtended by the closed path of $\hat{\boldsymbol{m}}(l)$ on the unit sphere. In the discrete case, Ω is thus the solid angle subtended by the closed path of geodesics connecting the classical ground-state vectors.

5.4 Evaluation of the persistent magnetization current I_m

As explained in Sec. 4.3, the relevant current operator for the transport of magnetization can be obtained in the spin-wave approximation by a derivative of the Hamiltonian with respect to the gauge field $\omega_{i\to i+1}$. The equilibrium expectation value of the longitudinal spin current can then be written as a gauge invariant derivative with respect to the geometric flux Ω,

$$I_s = -|J|\langle \hat{\boldsymbol{m}}_i \cdot \left(\boldsymbol{S}_i^{\perp} \times \boldsymbol{S}_{i+1}^{\perp}\right)\rangle = -\left\langle \frac{\partial \hat{H}^{\perp}}{\partial \omega_{i\to i+1}} \right\rangle = -\frac{\partial F_s(\Omega)}{\partial \Omega}\,, \tag{5.17}$$

where $F_s(\Omega)$ is the flux dependent part of the free energy. For the gas of free magnons described by the Hamiltonian in Eq. (5.7) it is given by

$$F_s(\Omega) = T\sum_k \ln\left[1 - e^{-\epsilon_k/T}\right]\,. \tag{5.18}$$

The current of magnetic moments around the ring contains contributions from all occupied momentum states,

$$I_m = \frac{g\mu_\mathrm{B}}{\hbar} I_s = -\frac{g\mu_\mathrm{B}}{L} \sum_k v_k \, n_k \,, \tag{5.19}$$

where the magnon velocity v_k and the Bose occupation factor n_k are defined by

$$v_k = \frac{1}{\hbar} \frac{\partial \epsilon_k}{\partial k} \,, \qquad n_k = n_B(\epsilon_k/T) \,, \qquad n_B(x) = \frac{1}{e^x - 1} \,. \tag{5.20}$$

For an analytic evaluation of Eq. (5.19), we note that magnon states are only thermally excited. At low temperatures only low-energy magnons will therefore contribute to the current and it is possible to expand the magnon dispersion around its minimum,

$$\epsilon_n = \epsilon_{k_n} \approx |J| S (k_n a)^2 + h = \Delta \left(n + \frac{\Omega}{2\pi} \right)^2 + h \,, \tag{5.21}$$

where $\Delta = \left(\frac{2\pi}{N}\right)^2 |J| S$ is the level splitting between the lowest-lying magnon states without a geometric flux, i.e. $\Delta = [\epsilon_1 - \epsilon_0]_{\Omega=0}$. With this quadratic dispersion the persistent magnetization current can be written as

$$I_m = \sum_{n=-\infty}^{\infty} \mathcal{I} \left(n + \frac{\Omega}{2\pi} \right) \,, \qquad \mathcal{I}(x) = \frac{g\mu_\mathrm{B}}{\hbar} \frac{\Delta}{\pi} \frac{x}{e^{(x^2+\tilde{h})/t} - 1} \,. \tag{5.22}$$

Here we have introduced a dimensionless magnetic field $\tilde{h} = h/\Delta$ and temperature $t = T/\Delta$. From the structure of the sum, it is clear that I_m is periodic in the flux Ω with period 2π. Therefore, we can decompose it into Fourier components,

$$I_m(\Omega) = \sum_{-\infty}^{\infty} \tilde{I}_l e^{i\Omega l} \,. \tag{5.23}$$

Before performing the integral for the inverse transformation the integration variable can be shifted in each summand and the sum over the integrals can be combined into one integration. This procedure is known under the name of Poisson summation formula [Cheung *et al.*, 1988] and yields

$$\tilde{I}_l = \int_0^{2\pi} \frac{d\Omega}{2\pi} \, I_m(\Omega) e^{-i\Omega l} = \int_{l=-\infty}^{\infty} dx \, \mathcal{I}(x) \, e^{-2\pi i x l} \,. \tag{5.24}$$

To carry out the integration, we further use a representation of the Bose function by a Matsubara sum as

$$n_B(y/t) = \frac{1}{e^{y/t} - 1} = -t \sum_{n=-\infty}^{\infty} \frac{e^{-i\tilde{\omega}_n 0^+}}{i\tilde{\omega}_n - y} \,, \tag{5.25}$$

where $\tilde{\omega}_n = 2\pi t n$ are dimensionless bosonic Matsubara frequencies. This yields

$$\tilde{I}_l = \frac{g\mu_\mathrm{B}}{\hbar}\frac{T}{\pi}\sum_{n=-\infty}^{\infty}\int_{-\infty}^{\infty} dx \frac{x e^{-2\pi i x l}}{x^2 + \tilde{h} - i\tilde{\omega}_n}\,. \tag{5.26}$$

Performing a contour integration, we obtain

$$\tilde{I}_l = -i\mathrm{sgn}(l)\frac{g\mu_\mathrm{B}}{\hbar}T\sum_{n=-\infty}^{\infty} e^{-2\pi|l|z_n}\,, \tag{5.27}$$

where

$$\mathrm{sgn}(l) = \begin{cases} 1 & \text{for } l > 0 \\ 0 & \text{for } l = 0 \\ -1 & \text{for } l < 0 \end{cases}\,, \tag{5.28}$$

and

$$z_n = \sqrt{\tilde{h} - i\tilde{\omega}_n} = \sqrt{\frac{h - 2\pi i T n}{\Delta}}\,. \tag{5.29}$$

Here, the sign of the complex square root is chosen such that its real part is positive. Carrying out the Fourier sums separately for the contribution of each Matsubara frequency, we obtain

$$\begin{aligned} I_m(\Omega) \;=\; & \frac{g\mu_\mathrm{B}T}{\hbar}\Bigg\{\frac{\sin(\Omega)}{\cosh(2\pi\sqrt{h/\Delta}) - \cos(\Omega)} \\ & + \sum_{n=1}^{\infty}\Big[\frac{\sin(\Omega + 2\pi z_n^I)}{\cosh(2\pi z_n^R) - \cos(\Omega + 2\pi z_n^I)} + \frac{\sin(\Omega - 2\pi z_n^I)}{\cosh(2\pi z_n^R) - \cos(\Omega - 2\pi z_n^I)}\Big]\Bigg\}\,, \end{aligned} \tag{5.30}$$

where z_n^R and z_n^I denote the real and imaginary parts of the square root factors in Eq. (5.29).

For the spin-wave theory to be applicable, we must have $T \ll JS$. On the other hand, the temperature has to be well above the level spacing, i.e. $T \gg \Delta$, in order to excite a sizeable number of magnons. From the last condition together with Eq. (5.29), we conclude that terms in the sum in Eq. (5.31) are exponentially suppressed. Hence, we finally obtain

$$I_m = \frac{g\mu_\mathrm{B}T}{\hbar}\frac{\sin\Omega}{\cosh(2\pi\sqrt{h/\Delta}) - \cos\Omega} + O(e^{-2\pi\sqrt{2\pi T/\Delta}})\,. \tag{5.31}$$

From this result, we also conclude that the current is exponentially small for $h \gg \Delta$. A small magnetic field is thus favorable for a large persistent magnetization current. On the contrary, a sufficiently strong magnetic field is necessary to create the inhomogeneous classical ground state as shown in Sec. 5.1. Therefore, a magnetic field h of the order of the level spacing should be applied for a maximal spin current.

5.5 Estimated experimental parameters

Persistent magnetization currents endow the ring with an electric dipole field as discussed in Sec. 4.4. Let us estimate the order of magnitude of the electric field that needs to be measured for an experimental detection of the effect. As reasonable parameters for a mesoscopic $S = 1/2$ Heisenberg ring, we assume $g = 2$, $N = 100$, and $J = 100\text{K}$. Then the condition $g\mu_\text{B}|\boldsymbol{B}| \approx \Delta$ is satisfied for $|\boldsymbol{B}| \approx 0.1\text{T}$. To obtain a sizable Ω one should generate inhomogeneous directions of the magnetic field in the submicron range. In the dipole approximation Eq. (4.29) the potential drop between two points located a distance d above and below the loop on the z-axis is given by

$$U \approx \frac{2g\mu_\text{B}k_B}{\hbar c}\frac{TL}{d^2} \approx 0.5\text{nV} \cdot \frac{TL}{d^2} \cdot \frac{\text{nm}}{\text{K}}\,, \tag{5.32}$$

where we have used the prefactor in Eq. (5.31) to estimate the maximal amplitude of the magnetization current I_m. For $T = 60\text{K}$ and $d = L = 100\text{nm}$ this yields a potential drop of $U \approx 0.3\text{nV}$. The experimental detection of this tiny voltage as well as the creation of the inhomogeneous field are certainly very challenging. Yet, with the rapid development of nanotechnology these tasks might be within experimental reach in the near future.

Chapter 6:

Persistent spin currents in antiferromagnet Heisenberg rings

In this chapter, we consider persistent magnetization currents in antiferromagnetic rings. The results in Eq. (5.19) shows that the persistent magnetization current in a ferromagnetic ring vanishes for $T \to 0$. Physically, this is due to the fact that no quantum fluctuations are present in the ferromagnetic ground state. At $T = 0$ there are thus no magnons to carry the spin current. One may speculate that an antiferromagnetic Heisenberg ring can support a finite persistent spin current even at $T = 0$ due to quantum fluctuations. In this chapter, we show that this is indeed the case and present a quantitative calculation of the spin current using the leading spin-wave approximation. In contrast to the ferromagnetic case, the orientations of the classical ground state of an antiferrmagnet in an inhomogeneous field are orthogonal to the local field direction for small magnetic fields h. Therefore, h no longer leads to a gap in the spin-wave dispersion and the usual spin-wave theory breaks down due to the absence of long-range order in one dimension. Yet, for integer spin S correlation effects lead to a finite spin-correlation length ξ and a Haldane gap of the order of $\hbar c/\xi$ [Haldane, 1983a, Haldane, 1983b, Affleck, 1989], where c is the spin-wave velocity. These features are correctly captured by a modified spin-wave theory [Takahashi, 1986, Takahashi, 1987, Takahashi, 1989, Hirsch and Tang, 1989, Kollar *et al.*, 2003] which we use here for explicit calculations. This approach is only appropriate for integer spin S, where the low-energy excitations can be viewed as renormalized spin waves. In contrast, for half-integer S the spectrum is gapless and spin correlations decay algebraically [Auerbach, 1994]. The elementary excitations are then spinons and the modified spin-wave theory does not correctly reproduce the low energy physics. In this case, the effective low energy theory is the Tomonaga-Luttinger model that will be introduced in Chap. 9. Bosonization is the method of choice in this case and was used recently to analyze persistent spin currents in half-integer antiferromagnetic Heisenberg rings [Schmeltzer *et al.*, 2004]. Meier and Loss [Meier and Loss, 2003] also used such a model to discuss spin currents in $S = \frac{1}{2}$ antiferromagnetic spins chains for a two-terminal geometry.

Similar to the case of a ferromagnet, we find a persistent magnetization current that is carried by magnons. They are subject to mesoscopic interference due to the geometric phase associated with the inhomogeneous nature of the classical ground state. Our result in Eq. (6.26) for the ground-state current in rings with a circumference L smaller that the correlation length ξ shows a remarkable similarity with the saw-tooth shaped persistent charge current of ballistic noninteracting electrons. More precisely, Eq. (2.13) in the introduction is identical

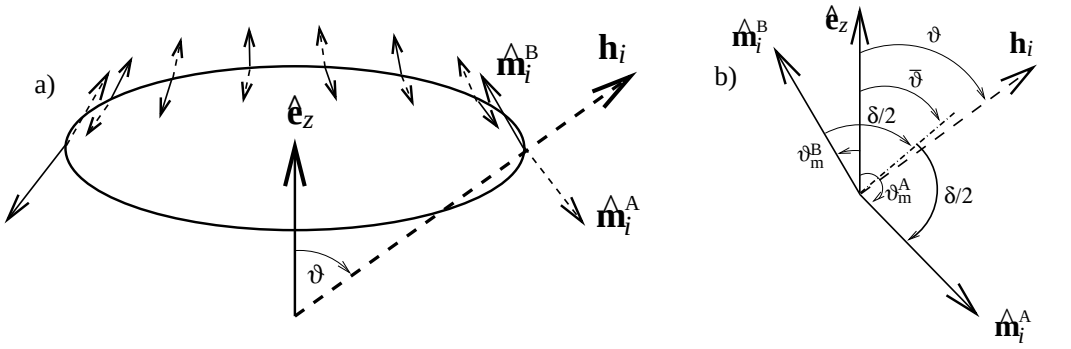

Figure 6.1: Classical ground state of an antiferromagnetic Heisenberg ring in a crown-shaped magnetic field; $\hat{\boldsymbol{m}}_i^A$ and $\hat{\boldsymbol{m}}_i^B$ are the directions of the spins on sublattices A and B.

to our results in Eq. (6.26) when we carry out the replacements $e \to g\mu_{\mathrm{B}}$, $v_F \to c$ and $\phi/\phi_0 \to \Omega/2\pi$ for the charge, the velocity and the magnetic flux, respectively. Here, Ω is the solid angle spanned by the inhomogeneous local Néel vector as one moves once around the ring.

6.1 Classical ground state

We start again from the Hamiltonian of a Heisenberg spin ring in Eq. (2.14), now with an antiferromagnetic exchange coupling $J > 0$. We further assume that the number of sites N is even. For a smoothly varying magnetic field that is weak compared to the exchange interaction, the spins in the classical ground state will be almost antiparallel on neighboring sites and orthogonal to the local direction of the magnetic field. This state will locally resemble a Néel state that changes its direction smoothly with the direction of the inhomogeneous field.

To see this more explicitly we consider again the crown-shaped field geometry in Eq. (2.15) shown in Fig. 6.1 for the antiferromagnet. For very strong fields h the classical unit vectors $\hat{\boldsymbol{m}}_i$ will be aligned parallel to the field and the ground state will have the full rotational symmetry of the applied field. Below a critical spin-flip field $h_c(\vartheta)$ it will be energetically favorable to form two sublattices with different angles $\vartheta_m^{A/B}$ to the z-axis (see Fig. 6.1). Introducing the relative and average angles

$$\delta = \frac{1}{2}(\vartheta_m^A - \vartheta_m^B) \qquad \bar{\vartheta} = \frac{1}{2}(\vartheta_m^A + \vartheta_m^B)\,, \tag{6.1}$$

a minimum of the classical energy is reached for

$$\sin(\vartheta - \bar{\vartheta})\cos(\delta) = -\frac{JS}{h}\,\epsilon_-\sin(2\bar{\vartheta}) \tag{6.2}$$

$$\cos(\vartheta - \bar{\vartheta})\sin(\delta) = +\frac{JS}{h}\,\epsilon_+\sin(2\delta)\,, \tag{6.3}$$

where we have defined $\epsilon_\pm = 1 \pm \cos(2\pi/N)$. For very strong magnetic fields $h > h_c$, we have $\delta = 0$ and Eq. (6.2) reduces to its ferromagnetic analogue (see Eq. (14) in I). For $\delta \neq 0$ the two equations can be combined to give

$$\sin(2(\vartheta - \bar{\vartheta})) = -\left(\frac{2JS}{h}\right)^2 \sin^2(2\pi/N)\sin(2\bar{\vartheta})\,. \tag{6.4}$$

Thus for large rings the magnetic field $h \sim JS/N$ necessary to produce an inhomogeneous classical ground state is well below the spin-flip field $h_c \sim JS$. For $h \sim JS/N \ll JS$ we have $\delta \sim \pi/2$ and the classical ground state locally resembles a Néel state as conjectured above.

6.2 Spin-wave spectrum

For such a classical ground state, the local Néel vector $\hat{\boldsymbol{n}}_i = (-1)^{i+1}\hat{\boldsymbol{m}}_i$ varies smoothly as a function of position on the lattice and is oriented almost orthogonal to the local direction of the magnetic field. We thus have

$$\hat{\boldsymbol{m}}_i \cdot \hat{\boldsymbol{m}}_{i+1} = -1 + O(N^{-2})\,, \tag{6.5}$$

and the terms involving the combination $\hat{b}_i^+\hat{b}_{i+1}$ in the spin-wave Hamiltonian (3.73) can be neglected to leading order in $1/N$. This approximation is again similar to an adiabatic approximation, since now a local spin deviation follows the direction of the classical ground state as it moves around the ring. The resulting quadratic bosonic Hamiltonian is standard for an antiferromagnetic ring with nearest-neighbor interactions except for the appearance of phase factors in front of the anomalous hopping terms $\hat{b}_i^+\hat{b}_{i+1}^+$,

$$\hat{H}^{(2)}_{\mathrm{AFM}} = \sum_{i=1}^{N}\Big\{\big[2JS + h_s\big]\hat{b}_i^+\hat{b}_i - JS\big[e^{i(\omega_{i\to i+1}+\omega_{i+1\to i})}\hat{b}_i^+\hat{b}_{i+1}^+ + \mathrm{H.c.}\big]\Big\}\,. \tag{6.6}$$

Here, periodic boundary conditions $\hat{b}_{N+1} = \hat{b}_1$ apply, and we have introduced an additional staggered field h_s in the direction of the classical ground-state vectors as an auxiliary tool for the discussion in Sec. 6.4.

The geometrical phase factors are accumulated as a spin deviation is moving around the ring leading to interference effects in its wave function in close analogy

to Aharonov-Bohm interference in charge transport. These phase factors can be eliminated by a gauge transformation with the local rotation angles

$$\alpha_j = \sum_{i=1}^{j-1} (-1)^{j+i} (\omega_{i\to i+1} + \omega_{i+1\to i}) \,. \tag{6.7}$$

This leads to the new boundary condition

$$\hat{b}_{i+N} = e^{\pm i\Omega} \hat{b}_i \,, \quad \Omega = \alpha_{N+1} \,, \tag{6.8}$$

where the upper/lower sign is valid for sublattice A/B (odd/even i). In the gauge with vanishing phase factors in Eq. (6.6) the spin-wave Hamiltonian $\hat{H}^{(2)}_{\rm AFM}$ is diagonalized as usual by first performing Fourier transformations with different signs on the two sublattices:

$$\hat{a}_k = \sqrt{\frac{2}{N}} \sum_{i\in A} e^{-ikl_i} \hat{b}_i \,, \quad \hat{b}_k = \sqrt{\frac{2}{N}} \sum_{i\in B} e^{+ikl_i} \hat{b}_i \,, \tag{6.9}$$

where the quantized wave vectors are given by

$$k_n = \frac{2\pi}{L} \left(n + \frac{\Omega}{2\pi} \right) \,, \quad n = 0, \ldots, \frac{N}{2} - 1 \,. \tag{6.10}$$

The diagonal form of $H_{\rm AFM}$ is then achieved by the Bogoliubov transformation

$$\begin{pmatrix} \hat{a}_k \\ \hat{b}_k^+ \end{pmatrix} = \begin{pmatrix} \cosh\theta_k & \sinh\theta_k \\ \sinh\theta_k & \cosh\theta_k \end{pmatrix} \begin{pmatrix} \hat{\alpha}_k \\ \hat{\beta}_k^+ \end{pmatrix} \,, \tag{6.11}$$

with

$$\tanh(2\theta_k) = \frac{\cos(ka)}{1+\tilde{h}_s} \,, \quad \tilde{h}_s = h_s/2JS \,. \tag{6.12}$$

The diagonal Hamiltonian contains constant terms due to quantum fluctuations,

$$\hat{H}^{(2)}_{\rm AFM} = \sum_k \epsilon_k (\hat{\alpha}_k^+ \hat{\alpha}_k + \hat{\beta}_k^+ \hat{\beta}_k + 1) - NJS(1+\tilde{h}_s) \,, \tag{6.13}$$

where the quasiparticle energies are given by

$$\epsilon_k = 2JS \sqrt{\Delta^2 + \sin^2(ka)} \,, \quad \Delta^2 = \tilde{h}_s(\tilde{h}_s + 2) \,, \tag{6.14}$$

and the free energy is obtained from

$$F_{\rm sw}(\Omega) = 2T \sum_k \ln \left[2 \sinh \frac{\epsilon_k}{2T} \right] - NJS(1+\tilde{h}_s) \,. \tag{6.15}$$

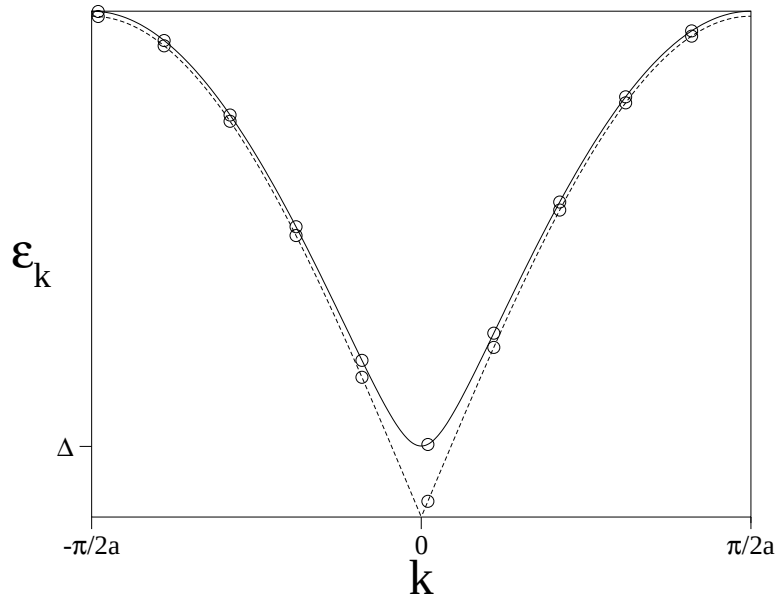

Figure 6.2: Dispersion of antiferromagnetic magnons and allowed wave-numbers in the presence of twisted boundary conditions. The full curve is valid in the presence of a staggered field, whereas for the dotted curve $h_s = 0$.

Thus we have shown that thermodynamic quantities depend on the inhomogeneity of the field only via the single phase Ω. Geometrically, Ω is the anholonomy associated with the parallel transport of a vector orthogonal to the local Néel vector, in analogy to the ferromagnetic case. To see this more clearly, we consider for each bond (ij) two additional sets of local right-handed triads containing the Néel vector $\hat{\boldsymbol{n}}_i$ instead of $\hat{\boldsymbol{m}}_i$. These triads are given by $\{\bar{\boldsymbol{e}}_i^1 = \boldsymbol{e}_i^1, \bar{\boldsymbol{e}}_i^2 = (-1)^{i+1}\boldsymbol{e}_i^2, \hat{\boldsymbol{n}}_i\}$ and $\{\tilde{\bar{\boldsymbol{e}}}_i^1, \tilde{\bar{\boldsymbol{e}}}_i^2 = \hat{\boldsymbol{n}}_i \times \hat{\boldsymbol{n}}_j, \hat{\boldsymbol{n}}_i\}$, and are related by a rotation around $\hat{\boldsymbol{n}}_i$. For the associated spherical vectors this reads

$$\bar{\boldsymbol{e}}_i^{\pm} = e^{\pm i\bar{\omega}_{i\to j}}\tilde{\bar{\boldsymbol{e}}}_i^{\pm}, \tag{6.16}$$

where the rotation angles $\bar{\omega}_{i\to j}$ are given by

$$\bar{\omega}_{i\to j} = i\pi + (-1)^{i+1}\omega_{i\to j} \qquad \text{for} \qquad j = i \pm 1. \tag{6.17}$$

We can now express Ω as

$$\Omega = \sum_{i=1}^{N}(\bar{\omega}_{i\to i+1} - \bar{\omega}_{i+1\to i}) \mod 2\pi\,, \tag{6.18}$$

which is of the same form as the anholonomy for the ferromagnet in Eq. (5.5). Ω is thus the anholonomy of a vector orthogonal to the local Néel vector that is transported around the ring by discrete rotations around $\hat{\boldsymbol{n}}_i \times \hat{\boldsymbol{n}}_{i+1}$. Alternatively,

a continuous parallel transport can be used around a path of geodesics connecting the unit vectors $\hat{\boldsymbol{n}}_i$ on the unit sphere. Ω is therefore equal to the solid angle subtended by this closed path of geodesics.

6.3 Persistent magnetization current

In Sec. 4.3 we have shown that the relevant current operator for magnetization transport is obtained within the spin-wave approximation from a derivative of the Hamiltonian with respect to the gauge field $\omega_{i\to i+1}$. For an antiferromagnet the longitudinal spin current is conveniently defined in the direction of the local Néel vector and can be written as a gauge-invariant derivative of the free energy

$$I_s = \langle \hat{\boldsymbol{n}}_i \cdot \boldsymbol{I}_{i\to i+1} \rangle = -(-1)^{i+1} \left\langle \frac{\partial H_{\rm sw}}{\partial \omega_{i\to i+1}} \right\rangle = -\frac{\partial F_{\rm sw}}{\partial \Omega}\,, \tag{6.19}$$

where $\boldsymbol{I}_{i\to i+1} = J\boldsymbol{S}_i \times \boldsymbol{S}_{i+1}$. This spin current I_s corresponds to a current of magnetic dipoles that are locally oriented in the direction of the Néel vector $\hat{\boldsymbol{n}}_i$, which varies smoothly as we move along the ring. The spin current generates an electric dipole field which has the form discussed in Sec. 4.4. For the magnetization current we obtain

$$I_m = \frac{g\mu_{\rm B}}{\hbar} I_s = -\frac{2g\mu_{\rm B}}{L} \sum_k c_k \Big[n_k + \frac{1}{2} \Big]\,, \tag{6.20}$$

where $c_k = \hbar^{-1}\partial\epsilon_k/\partial k$ is the velocity of a magnon with wave vector k and $n_k = n_B(\epsilon_k/T)$ is the Bose occupation factor. The extra factor of 2 is due to the two degenerate spin-wave modes. Equation (6.20) is the antiferromagnetic spin analog of Eq. (2.12). It clearly shows that the magnetization current is carried by antiferromagnetic magnons, which at this level of approximation are the only quasiparticles available for transport. The current has a finite limit, even for vanishing Bose occupation factors, due to quantum fluctuations.

From Eq. (6.20) the current is clearly seen to be a periodic function of Ω, so that the finite momentum sum can be further evaluated using the Poisson summation formula as described for the ferromagnet in Sec. 5.4. From now on, we will only consider the $T = 0$ limit in more detail. Eq. (6.20) can then be written in the form

$$\frac{I_m}{I_m^0} = \sum_{n=0}^{N/2-1} f\left(\frac{2\pi}{N} \left(n + \frac{\Omega}{2\pi} \right) \right)\,, \tag{6.21}$$

where $f(k) = d/d(ka)(\epsilon_k/2JS)$ is a periodic function of its argument with $f(x + \pi) = f(x) = -f(-x)$, and $I_m^0 = -g\mu_{\rm B}c/L$ is the magnetization current carried by a single magnon with the spin-wave velocity $c = c_{k\to 0^+}$ at the center of the

Brillouin zone. The Fourier coefficients C_ν of the magnetization current are then given by

$$\frac{I_m}{I_m^0} = \sum_{\nu=-\infty}^{\infty} C_\nu e^{i\nu\Omega} \,. \tag{6.22}$$

By appropriate substitutions in the corresponding integral one eliminates the finite momentum sum and obtains

$$C_\nu = -\frac{\nu N^2 \Delta}{2i}\, g_{\nu N}\big(-\Delta^{-2}\big) \,, \tag{6.23}$$

where g_{2l+1} is zero and g_{2l} is given by

$$\begin{aligned} g_{2l}(z) &= \int_0^{2\pi} \frac{d\omega}{2\pi} \sqrt{1 - z\sin^2\omega}\; e^{-i2l\omega} \\ &= \binom{\frac{1}{2}}{l} \left(\frac{z}{4}\right)^l \, {}_2F_1\left(l - \frac{1}{2}, l + \frac{1}{2}; 2l+1; z\right) \\ &= (-1)^l \sqrt{1-z}\, g_{2l}\left(\frac{z}{z-1}\right) \,. \end{aligned} \tag{6.24}$$

The second line follows from expanding the integral in powers of z and identifying the resulting series with the hypergeometric function, whereas the last equality can be derived by elementary manipulations of the integral, or follows from a hypergeometric identity.

For a vanishing staggered field h_s and therefore a vanishing gap Δ in the exitation spectrum, the integral is elementary, and we obtain

$$C_\nu = -\frac{1}{\pi}\frac{i\nu N^2}{1-\nu^2 N^2} \approx -\frac{1}{i\pi}\frac{1}{\nu} \,, \tag{6.25}$$

where the last relation is valid for $N \gg 1$ and $m \neq 0$. For this case, the sum in the Fourier series for the spin current can be performed to yield

$$I_m = I_m^0 \left(1 - \frac{\Omega}{\pi}\right) \,, \quad 0 < \frac{\Omega}{2\pi} < 1 \,. \tag{6.26}$$

The sawtooth shape (see the solid line in Fig. 6.3) of the current in Eq. (6.26) is reminiscent of Eq. (2.13) for charge transport. Indeed, for $T = 0$ Eq. (6.20) is formally equivalent to Eq. (2.12) for charge transport when the Fermi edge is replaced by the lower edge of the magnon band.

6.4 Modified spin-wave theory

The usual spin-wave theory employed so far is inconsistent when zero modes appear. Although the spin current remains finite, the sublattice magnetization

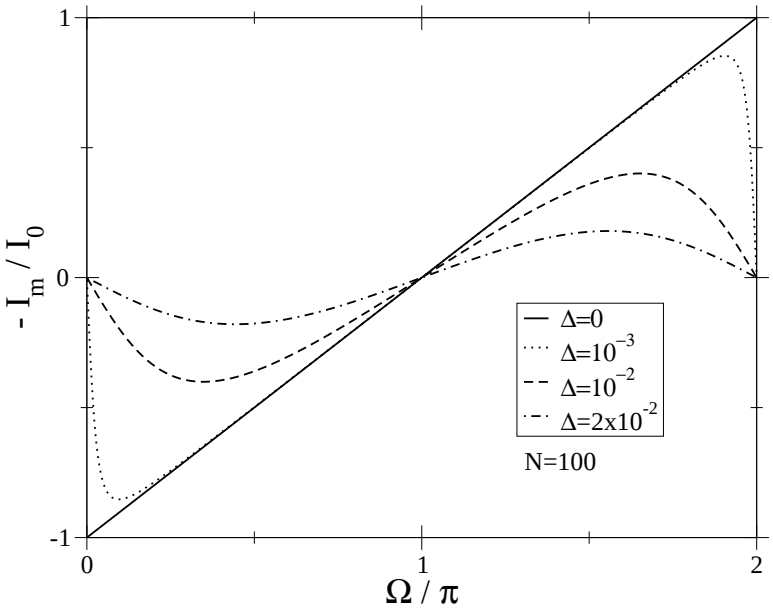

Figure 6.3: Magnetization current in a ring with 100 spins for different values of the energy-gap parameter Δ. The plots are produced by numerically evaluating Eq. (6.20). For $\Delta = 10^{-3}$ the curve is indistinguishable from the approximate expression in Eq. (6.30), and Eq. (6.31) provides a good approximation for $\Delta = 2 \times 10^{-2}$.

diverges in the limit $\Omega \to 0$. This failure is related to the absence of long-range order in one-dimensional systems. It can be resolved by a modified spin-wave theory which was first used by Takahashi for a one-dimensional ferromagnet [Takahashi, 1986, Takahashi, 1987] and then extended to various spin systems without long-range order, including antiferromagnets [Hirsch and Tang, 1989, Takahashi, 1989]. The constraint that is introduced in these theories was recently shown to follow naturally from a calculation at constant order parameter [Kollar *et al.*, 2003]. In the present context, we introduce the additional constraint

$$\sum_i \langle \boldsymbol{S}_i \cdot \hat{\boldsymbol{m}}_i \rangle = 0 \,, \tag{6.27}$$

which suppresses Néel order on average. This constraint is enforced via the staggered field h_s in Eq. (6.6) which acts as a Lagrange multiplier. The expectation value in Eq. (6.27) can be evaluated from $\partial F_{\rm sw}/\partial h_s$, yielding the self-consistency condition

$$\frac{2}{N} \sum_k \frac{\partial \epsilon_k}{\partial h_s} \left[n_k + \frac{1}{2} \right] = S + \frac{1}{2} \,. \tag{6.28}$$

Although the self-consistently determined h_s is itself a periodic function of the geometric flux Ω, the leading order for large N is a constant and can be determined by replacing the sum in Eq. (6.28) by an integral. For $T = 0$ the solution

of Eq. (6.28) yields the Haldane gap $2JS\Delta$, which is inversely proportional to the staggered correlation length ξ [Auerbach, 1994],

$$\Delta = 4\, e^{-\pi(S+1/2)} = \frac{a}{\sqrt{2}\xi}\,. \tag{6.29}$$

The functional form of the magnetization current shows a crossover between the two qualitatively different regimes $\xi \gg L$ and $\xi \ll L$ (see Fig. 6.3). In the former case $\Delta \ll 2\pi/N$ and at most one wave vector can be in the region $-\Delta < k < \Delta$ where the dispersion relation deviates strongly from the dispersion in the limit $\Delta = 0$. When the contribution from this single wave vector is taken into account separately, we obtain

$$\frac{I_m}{I_m^0} = \frac{\sin(2\Omega/N)}{2\sqrt{\Delta^2 + \sin^2(\Omega/N)}} - \frac{\Omega}{\pi}\,, \quad -\pi < \Omega < \pi\,. \tag{6.30}$$

In the case $\Delta = 0$ this reduces to Eq. (6.26), provided $N \gg 1$. Thus, the effect of a finite Δ is to remove the discontinuity at $\Omega = 0, 2\pi$. On the other hand, in the limit $\xi \ll L$ many k values are affected by the energy gap. Using an asymptotic expansion of the hypergeometric function [Watson, 1918] for large l, we derive an expression for the spin current for large system sizes. In particular, the condition that the leading term in the expansion be sufficient can be shown to be equivalent to $L/\xi \gg \mathcal{O}(1)$. After some algebra we obtain

$$\frac{I_m}{I_m^0} = \sqrt{\frac{2}{\pi}} \left(\frac{L}{\sqrt{2}\xi}\right)^{1/2} \exp\left(-\frac{L}{\sqrt{2}\xi}\right) \sin(\Omega)\,, \tag{6.31}$$

implying that the sinusoidal magnetization current is exponentially suppressed in the bulk limit, $L \gg \xi$.

Chapter 7:

Magnetization currents in electric fields

In this chapter, we show that persistent magnetization currents can also be driven by inhomogeneous electric fields. For a ferromagnetic ring in a radial electric field, this was discussed in [Cao *et al.*, 1997]. Here, we will consider the same setup for an antiferromagnetic ring.

Moving magnetic dipoles represent an electric dipole moment [Hirsch, 1999] and are therefore affected by electric fields. Due to this relativistic effect, which is essentially equivalent to spin-orbit coupling, the magnetic moments acquire an Aharonov-Casher phase [Aharonov and Casher, 1984]. For localized spin systems described by a Heisenberg Hamiltonian, the electric field can be taken into account phenomenologically by a substitution in the interaction term,

$$\boldsymbol{S}_i \cdot \boldsymbol{S}_j \longrightarrow \boldsymbol{S}_i \cdot e^{\boldsymbol{\theta}_{ij}\times} \boldsymbol{S}_j \,, \tag{7.1}$$

as long as the electric field varies only weakly on the scale of the lattice spacing. Here,

$$\boldsymbol{\theta}_{ij} = \frac{g\mu_{\mathrm{B}}}{\hbar c^2} \int_{l_i}^{l_j} d\boldsymbol{l} \times \boldsymbol{E}(\boldsymbol{l}) \,, \tag{7.2}$$

and the notation $e^{\boldsymbol{\theta}\times}$ for an SO(3) rotation matrix is defined in Eq. (5.12). For ferromagnetic coupling, inhomogeneous electric fields can lead to persistent magnetization currents [Cao *et al.*, 1997] and a spin analog of the Hall effect was also shown to exist in electric fields [Meier and Loss, 2003].

We now consider the antiferromagnetic ring in an electric field in the x-y plane, e.g. produced by a charged line in the z direction (see Fig. 7.1). The rotation vectors $\boldsymbol{\theta}_{i,i+1} = \theta_{i,i+1}\hat{\boldsymbol{e}}^z$ are then all parallel to the z axis and the Hamiltonian for vanishing magnetic field becomes

$$H = J \sum_i \left[\frac{1}{2} (e^{i\theta_{i,i+1}} S_i^+ S_{i+1}^- + \mathrm{h.c.}) + S_i^z S_{i+1}^z \right] . \tag{7.3}$$

The classical ground state is easily shown to be a doubly degenerate Néel state with $\hat{\boldsymbol{m}}_i = \pm\hat{\boldsymbol{e}}^z$. The spin-wave expansion is thus straightforward. If a gauge transformation is used to eliminate the phase factors, we again obtain the standard bosonic Hamiltonian H_{AFM} of Eq. (6.6) with the boundary condition (6.8), where Ω is replaced by the total Aharonov-Casher phase

$$\Omega_{\mathrm{AC}} = \sum_i \theta_{i,i+1} = \frac{g\mu_{\mathrm{B}}}{\hbar c^2} \oint d\boldsymbol{l} \cdot [\hat{\boldsymbol{e}}^z \times \boldsymbol{E}(\boldsymbol{l})] \,. \tag{7.4}$$

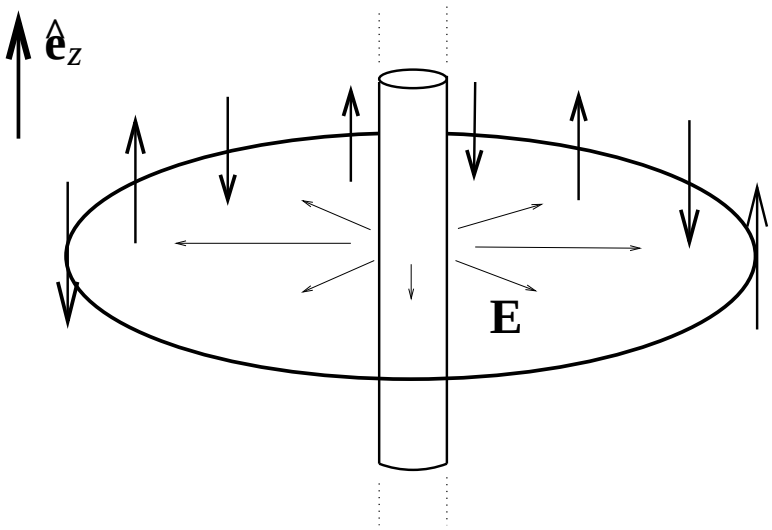

Figure 7.1: Antiferromagnetic Heisenberg ring in the electric field produced by a line charge.

The spin current then only has a z component which can be written as a gauge-invariant derivative of the free energy,

$$I_m = -\frac{\partial F_{\mathrm{AFM}}}{\partial \Omega_{\mathrm{AC}}} \,. \tag{7.5}$$

This leads again to Eq. (6.20) with Ω replaced by Ω_{AC} and all the results derived in the previous sections are also applicable in this context.

It is also interesting to note that the situation of a radial electric field with $\theta_{i,i+1} = \frac{2\pi}{N}$ and an additional homogeneous magnetic field tilted with respect to the z-axis can be formally mapped onto a crown-shaped magnetic field alone via the transformation

$$\boldsymbol{S}_i' = e^{\frac{2\pi}{N}\hat{\boldsymbol{e}}^z \times} \boldsymbol{S}_i \,. \tag{7.6}$$

It would therefore be interesting to further investigate the combined effect of arbitrary inhomogeneous magnetic and electric fields on the produced spin currents to find situations that could be realized more easily in the laboratory for a possible experimental detection of the effect.

Chapter 8:

Conclusions

In this part of the thesis, we have considered mesoscopic Heisenberg rings to predict a new quantum mechanical interference effect which is analogous to persistent charge currents in mesoscopic normal metal rings threaded by a magnetic flux. More precisely, we have shown that inhomogeneous magnetic fields as well as radial electric fields can drive persistent circulating magnetization currents. The current is carried by magnons and endows the ring with an electric dipole moment that might allow for an experimental detection of the effect. For ferromagnetic rings, magnons are only thermally excited and the current is proportional to the temperature T at low temperature. For antiferromagnetic rings, quantum fluctuations lead to ground-state currents, but fluctuations in low dimensions also produce exponential damping when the circumference L of the ring becomes larger than the staggered correlation length ξ. Explicit calculations were performed within leading order spin-wave theory. For antiferromagnetic rings, a modified spin-wave theory has been used that is valid for integer spin S, i.e. for Haldane-gap systems, and accounts for the absence of long-range order in one dimension.

A new definition of the spin-current operator has been proposed that is applicable for non-collinear spin configurations. To further substantiate this proposal for an effective current operator, it would be interesting to look for a more microscopic derivation by starting from a model involving charge degrees of freedom. It would also be instructive to explicitly investigate non-equilibrium situations with time-dependent magnetization.

We have only considered clean systems, i.e., we have focused on the ballistic regime. Since for persistent charge currents disorder is known to be important, it would also be very interesting to consider persistent magnetization currents in the diffusive regime of disordered magnets. In this context, it is interesting to note that also without impurities, a spatially varying magnitude of the effective magnetic field provides an intrinsic impurity potential for magnon excitations.

An experimental detection of the persistent magnetization currents is certainly very challenging. It requires well-characterized rings with a large isotropic Heisenberg coupling J. Furthermore, rather strong magnetic fields with varying directions on the submicron scale have to be created and a potential drop on the order of nanovolts over a length scale comparable to the circumference of the ring has to be detected. Screening of this tiny electric field is also a problem. A detailed estimate of the orders of magnitude was given in Sec. 5.5.

However, the emerging field of spintronics already faces similar challenges. For applications to quantum computing, highly anisotropic magnetic fields are also required for single-qubit operations. Furthermore, a purely electric control of

spin degrees of freedom is being developed using the Rashba spin-orbit coupling in two-dimensional semi-conducting structures. Thus, in view of the rapid development of spintronics, it is not unreasonable to expect that new experimental techniques will be developed in the near future that might overcome the difficulties mentioned above. Persistent magnetization currents could then be used as a quantitative measure for the degree of quantum coherence in mesoscopic spin systems.

Part II

Functional renormalization group with collective fields

Chapter 9:

Introduction

Systems of strongly interacting electrons in one or two spatial dimensions continue to pose interesting challenges to theoretical and experimental condensed matter physicists. The extremely rich phenomenology of these systems includes phases with broken symmetry such as superconductivity and charge or spin density wave states as well as metallic phases with unconventional properties. The high-temperature superconductors [Bednorz and Müller, 1986] provide the most prominent experimental realization for which, despite a tremendous amount of work in the field, eq:any aspects of the phase diagram are still not completely understood. Other well-known examples of strongly correlated systems include highly anisotropic quasi one-dimensional organic and anorganic conductors as well as heavy-fermion systems.

Whereas in three dimensions mean-field theory or a description by quasiparticles of a Landau Fermi liquid is often appropriate [Pines and Nozières, 1989], strong fluctuations invalidate these approaches in low dimensions. Thus, new concepts and calculational tools are needed. For one-dimensional conductors the paradigm of Luttinger liquids was developed [Haldane, 1981] to describe the low energy properties. In this context, bosonization is widely used as a calculational tool and provides solutions for correlation functions. Yet, it relies on assumptions that restrict its validity to the very low energy sector. Relaxing these assumptions to assess the limitations of the Luttinger liquid picture has been notoriously difficult. Experimentally, many signs of non-Fermi liquid behaviour are seen also in (quasi) two-dimensionsal systems. Thus, many workers tried to find a generalization of the Luttinger liquid concept to two spatial dimensions. Yet, except for rather artificial models a consistent theory for Luttinger liquid behavior in two dimension could not be given so far.

Various theoretical approaches are still being developed for strongly correlated electron systems. One promising method is the renormalization group that has already been extensively used to analyze the low-energy behavior of low-dimensional interacting Fermi systems.

9.1 Functional renormalization group

The renormalization group (RG) was designed to deal with problems in which fluctuations on many length scales are important. This usually leads to divergent expressions for Feynman diagrams and diagrammatic perturbation theory breaks down at low energies or long wavelengths. Originally, a renormalization procedure was developed in the field-theoretical context as a device to control these divergencies [Amit, 1984, Zinn-Justin, 2002], and finite results are obtained for renor-

malizable field theories when all parameters are expressed in terms of physically measurable quantities. Later, building on previous work by Kadanoff [Kadanoff *et al.*, 1967], Wilson incorporated the ideas of scaling and transformation of length scales. This led to a thorough understanding of (classical) critical phenomena in terms of renormalization group flows in a large space of possible Hamiltonians and especially the fixed points of this flow [Wilson and Kogut, 1974, Ma, 1976, Fisher, 1998]. Spatial dimensionality plays an important role and leads to well-defined calculational schemes when one uses an expansion about the upper critical dimension above which mean-field theory yields the correct critical behavior [Wilson, 1972, Wilson and Fisher, 1972]. For the standard ϕ^4 theory such an expansion is in powers of ϵ, where the dimension is $D = 4 - \epsilon$. Alternatively, it is sometimes also useful to consider an expansion about the lower critical dimension (using $D = 2 + \epsilon$), below which the order is destroyed by strong fluctuations. The common idea involved in all renormalization group methods is the dependence of physical quantities on the length scale at which they are considered. Scale-dependent coupling constants are introduced and their evolution is analyzed as the scale is changed. Yet, the practical implementation of this idea varies strongly in different versions of the RG.

Formally exact versions of the renormalization group transformation were developed early on [Wilson and Kogut, 1974]. The treatment was formalized by considering infinitesimal RG steps. The first of these infinitesimal generators was introduced by Wegner and Houghton [Wegner and Houghton, 1973]. Problems with the sharp cutoff limit arose that were dealt with by using discrete momenta. A seminal work by Polchinski [Polchinski, 1984] showed the usefulness of continuous flow equations for the Wilsonian effective action to simplify the proof of perturbative renormalizability. This triggered the development of various versions of functional renormalization group (fRG) equations for different generating functionals (for overviews, see e.g. [Bagnuls and Bervillier, 2002, Salmhofer, 1999]). In all of these schemes, the cutoff has a dual interpretation [Morris, 1994]. It acts as an ultraviolett cutoff for the low energy modes, such that the generating functional is the effective actions for the modes that still need to be integrated. At the same time it generates the correlation functions of a theory with an infrared cutoff. The use of the generating functionals for irreducible vertices was made popular by the works by Wetterich and by Morris [Wetterich, 1993, Morris, 1994], although advantages of this scheme were realized earlier [DiCastro *et al.*, 1974, Nicoll *et al.*, 1976, Nicoll and Chang, 1977].

More recently, renormalization group methods were also applied to interacting fermionic systems. Here, the low-energy modes that lead to divergencies are related to gapless excitations in the vicinity of the Fermi surface. For one-dimensional systems, the Fermi 'surface' actually reduces to two separated points in momentum space and the Wilsonian RG can directly be applied [Shankar, 1994]. For a spatial dimension $D > 1$, the Fermi surface is a $D - 1$ dimensional manifold and a full Wilsonian RG including integration of high-energy modes as

well as rescaling of momenta, frequencies and fields is more involved [Shankar, 1994, Kopietz and Busche, 2001]. The functional version of the renormalization group is especially well-suited to deal with the coupling functions that have to be considered for Fermi systems with $D > 1$. Due to its relevance for the high-temperature superconductors, the two-dimensional Hubbard model was extensively studied [Zanchi and Schulz, 1996, Zanchi and Schulz, 1998, Zanchi and Schulz, 2000, Zanchi, 2001, Halboth and Metzner, 2000b, Halboth and Metzner, 2000a, Honerkamp, 2001, Honerkamp and Salmhofer, 2001b, Honerkamp and Salmhofer, 2001a, Honerkamp *et al.*, 2001, Honerkamp *et al.*, 2004, Katanin *et al.*, 2005, Kampf and Katanin, 2003, Katanin and Kampf, 2003, Katanin and Kampf, 2004b, Katanin and Kampf, 2004a, Binz *et al.*, 2002]. Using various versions of the functional RG for different types of vertices and a discretization of the Fermi surface, these authors studied the one-loop flow of the two-particle scattering vertex starting from a model which is weakly coupled at the microscopic scale. The flow is then driven by the competing instabilities of the system. They invariably find a divergence in the flow at some finite cutoff. The nature and the symmetry of the most singular couplings are taken as an indication on the dominant instability, leading to phase diagrams. Yet, since the flow exhibits a divergence, it cannot be continued down to lower energies and the true low-energy theory is not accessible. Furthermore, to obtain a numerically manageable number of coupling constants, power counting arguments are used to project the momenta in the vertex functions onto the Fermi surface. For the same reasons, frequency dependencies are neglected. The runaway flow to strong coupling in these weak-coupling approaches leaves two principal scenarios for the very low-energy behavior. The more conventional view assumes that symmetry breaking occurs in the channel identified as most singular by the one-loop flow equations. Symmetry-breaking terms in the action then regulate the flow at low energies. For the reduced BCS model the flow could indeed be continued into the symmetry-broken regime by introducing some finite symmetry breaking field [Salmhofer *et al.*, 2004]. Another scenario is also possible at least for special Fermi surface geometries. At low energies anomalous exponents can lead to a vanishing quasiparticle weight and thus to non-Fermi liquid behavior. This was indeed found in a two-loop treatment for a Fermi surface with flat parts via the field-theoretical version of the RG [Freire *et al.*, 2005, Ferraz, 2003b, Ferraz, 2003a]. Two-loop calculations within the fRG formalism are extremely challenging and have not yet been performed consistently for fermions in two dimensions. Thus, one might look for alternative methods that are better suited to describe the very low energy physics.

A recently very popular approach to interacting many-fermion systems starts from the vicinity of a quantum critical point [Sachdev, 1999]. This approach was pioneered by Hertz and Millis [Hertz, 1976, Millis, 1993]. Technically, an order parameter is introduced by performing a Hubbard-Stratonovich transformation in the Grassmannian functional integral. Subsequently, the fermionic fields are integrated out and the system is described in terms of the bosonic fluctuating

order parameter alone. A Wilsonian momentum-shell RG is then used to describe the critical behavior of the soft bosonic modes.

In this context, it is also interesting to note that the fRG was successfully applied to weakly interacting bosonic systems [Hasselmann *et al.*, 2004, Ledowski *et al.*, 2004, Blaizot *et al.*, 2004]. In these works, the complete scaling function for the single-particle self-energy could be obtained leading to a result for the shift of the critical temperature.

In the second part of the thesis, we set up a functional renormalization group scheme that is intermediate between the purely fermionic version and a treatment in terms of the order parameter alone. We also use a Hubbard-Stratonovich transformation to introduce collective bosonic fields. However, instead of integrating out the fermions, we derive a hierarchy of flow equations for the irreducible vertices of the coupled Fermi-Bose theory. A closely related method has been developed in [Baier *et al.*, 2004, Baier *et al.*, 2005] to study antiferromagnetic order in the two-dimensional Hubbard model. For the Coulomb gas, similar flow equations were also written down in [Correia *et al.*, 2002]. Nevertheless, due to the freedom in the choice of the cutoff in the mixed theory, our method differs considerably from other approaches. Furthermore, we pay particular attention to Ward identities in forward scattering problems. By choosing a cutoff only in the momentum transfer of the interaction, we can then show how the exact solution for the single-particle Green's function of the Tomonaga-Luttinger model can be obtained entirely within the fRG formalism.

9.2 Electrons in one dimension

Electrons in one spatial dimension provide one of the few examples where exact results for an interacting many-body system may be obtained. Although in the original fermionic language the model seems untractable, an ingenious mapping to bosonic variables related to density fluctuations reduces it to quadratic form. For the ranges of parameters where it is applicable, this bosonization procedure leads to exact solutions for correlation functions. The bosonic degrees of freedom are thus the appropriate variables to describe the system.

The importance of bosonic modes in the low-energy excitation spectrum of one-dimensional electrons was first realized by Bloch [Bloch, 1933] for the case of non-interacting electrons. In a seminal paper, Tomonaga [Tomonaga, 1950] showed how the Hamiltonian of a system of interacting one-dimensional electrons can be approximately diagonalized in bosonic variables when the energy dispersion is linearized and long-range interactions (in real space) are considered. By a complicated treatment using Toeplitz determinants, Luttinger [Luttinger, 1963] discovered that the momentum distribution function no longer has a finite step at the Fermi points, but exhibits a power-law behavior indicative of a breakdown of the Fermi liquid picture. Subsequently, this important result was

confirmed by Mattis and Lieb [Mattis and Lieb, 1965] using a rigorous version of bosonization. They also pointed out a mistake in Luttinger's paper due to an incorrect treatment of anomalous commutators associated with a filled Dirac sea in a model without bandwidth cutoff. Luther and Peschel [Luther and Peschel, 1974] obtained the single-particle spectral function by means of what is now called the 'bosonization of the field operator'. In a seminal paper Haldane [Haldane, 1981] pointed out that the low-energy behaviour found in the exact solution of the Tomonaga-Luttinger model is expected to be a general property of interacting one-dimensional electrons and coined the term 'Luttinger liquid'. From bosonization the single-particle Green's function is obtained in real space, whereas experimental probes such as angle resolved photoemission spectroscopy (ARPES) measure it as a function of frequency and momentum. The Fourier transformation is highly non-trivial, but can be done with the help of an asymptotic analysis [Meden and Schönhammer, 1992]. The resulting spectral function shows spin-charge separation and anomalous scaling at low energies.

A number of reviews [Schönhammer, 1997, Schönhammer, 2003, v. Delft and Schoeller, 1998,Stone, 1994] describe the details of the bosonization method which we will not discuss any further. Nevertheless, we will review briefly certain approximations on which these exact solutions rely, as they will also be necessary in our exact treatment via the functional renormalization group. Starting from a kinetic energy term

$$H_0 = \sum_{k\sigma} \epsilon_k \hat{c}^+_{k\sigma} \hat{c}_{k\sigma} \tag{9.1}$$

with a general dispersion ϵ_k it is assumed that ϵ_k can be linearized in the vicinity of the two Fermi points, i.e.,

$$\epsilon_k \rightarrow \epsilon_{p\alpha} = \alpha v_F p + \epsilon_F \,, \tag{9.2}$$

where $\alpha = \pm$ labels the right ($\alpha = +$) or left ($\alpha = -$) Fermi point, $\epsilon_F = \epsilon_{\pm k_F}$ is the Fermi energy and $p = k - \alpha k_F$ measures the distance from the respective Fermi point. This linearization is shown in Fig. 9.1.

Naturally, Eq. (9.2) is only a valid approximation close to the Fermi points, i.e., for small p. To ensure this, a bandwidth cutoff Λ has to be introduced such that $|p| \leq \Lambda$. Interactions that are sufficiently short ranged in momentum space, i.e., long ranged in real space, will not affect states deep inside the Fermi sea or high above it. For the low-energy physics those states should therefore be irrelevant.

For a general class of models, the electron-electron interaction depends only on the distance in real space. After Fourier transformation it is a function of the transferred momentum and is given by

$$H_{int} = \frac{1}{2V} \sum_{k,k',\bar{k}} \sum_{\sigma\sigma'} v(\bar{k}) \hat{c}^+_{k+\bar{k}\sigma} \hat{c}^+_{k'-\bar{k},\sigma'} \hat{c}_{k'\sigma'} \hat{c}_{k\sigma} \,, \tag{9.3}$$

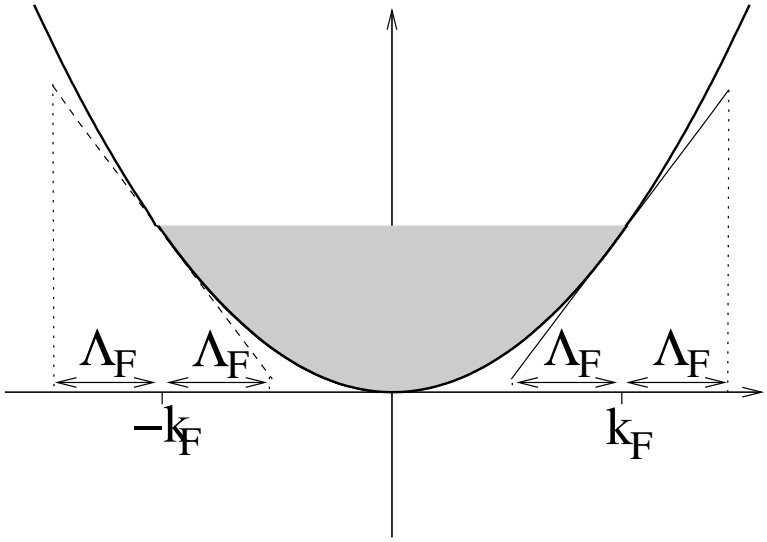

Figure 9.1: Linearization of the dispersion relation for one-dimensional electrons. A bandwidth cutoff Λ_F has to be introduced to restrict the available single particle states to the vicinity of the Fermi points.

where V is the volume of the system and $\bar{k}$ denotes a bosonic momentum, i.e., a difference of two fermionic momenta, as explained in detail in the next chapter. In diagrammatic perturbation theory such an interaction is represented by the vertex

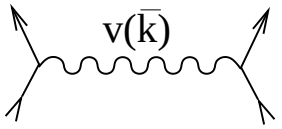

. (9.4)

When the initial and final states are restricted to regions around the two Fermi points, the interaction can be classified according to the different combination of patch labels of incoming and outgoing particles. This gives rise to four different coupling parameters denoted by g_1 to g_4 in the so-called g-ology classification [Solyom, 1979], as shown in Fig. 9.2.

So far, we have started from a microscopic model and simply neglected single particle states far away from the Fermi points. This procedure can be put on firmer grounds by invoking the renormalization group to integrate out the high energy states. In principle, a low-energy Hamiltonian of the g-ology form can be obtained in this way, where now the couplings should be regarded as effective parameters. Compared to the couplings of the microscopic model they contain finite renormalizations due to high-energy states. Once the regime is reached where the g-ology classification is applicable, the change of the coupling parameters as the cutoff is further reduced is easily derived [Solyom, 1979, Shankar, 1994]. As an example, let us consider the one-loop flow in the case of spinless fermions. When

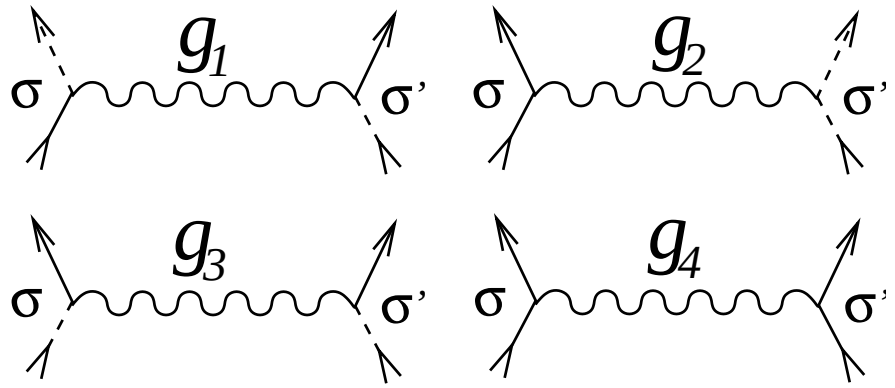

Figure 9.2: Classification of interaction terms according to the g-ology convention. Full and dashed lines represent electrons on different branches of the dispersion. Forward scattering on the same or between different branches is given by g_4 and g_2, respectively. The coupling g_1 describes backward scattering, and g_3 gives the strength of umklapp scattering which is only important in lattice models with special fillings.

coupling *constants* are used, the couplings g_2 and g_4 describe the same physical processes in this case. Since the umklapp term g_3 is only important for lattice models at special filling factors, we will neglect it here. The flow equations for the two remaining couplings are then given by

$$-\Lambda_F \frac{dg_1}{d\Lambda_F} = -\frac{1}{\pi v_F} g_1^2 \,, \qquad -\Lambda_F \frac{dg_2}{d\Lambda_F} = -\frac{1}{2\pi v_F} g_1^2 \,, \tag{9.5}$$

From this one concludes that $2g_2 - g_1$ is an invariant of the flow. For a repulsive initial coupling $g_1 > 0$ the flow eventually reaches the line of fixed points with $g_1 = 0$. Similarly, it can be shown for the full model including spin that the manifold with $g_1 = g_3 = 0$ is fixed under the RG transformation. This conclusion is not altered by higher order corrections in the flow equations and can even be shown to hold to all orders by using Ward identities [DiCastro and Metzner, 1991]. On the fixed-point manifold a pure forward scattering problem remains. Let us slightly change our notation and denote the branch label α and the spin index σ by a single composite index that will also be denoted by σ from now on. The fixed-point interaction can then be written as

$$H_{int} = \frac{1}{2V} \sum_{\bar{k}\sigma\sigma'} f_{\bar{k}}^{\sigma\sigma'} \hat{\rho}_{-\bar{k}\sigma} \hat{\rho}_{\bar{k}\sigma'} \,, \tag{9.6}$$

where we have defined the following matrix of coupling functions (the order of

indices is $(+\uparrow, +\downarrow, -\uparrow, -\downarrow)$):

$$f_{\bar{k}} = \begin{pmatrix} g_{4\parallel}(\bar{k}) & g_{4\perp}(\bar{k}) & g_{2\parallel}(\bar{k}) & g_{2\perp}(\bar{k}) \\ g_{4\perp}(\bar{k}) & g_{4\parallel}(\bar{k}) & g_{2\perp}(\bar{k}) & g_{2\parallel}(\bar{k}) \\ g_{2\parallel}(\bar{k}) & g_{2\perp}(\bar{k}) & g_{4\parallel}(\bar{k}) & g_{4\perp}(\bar{k}) \\ g_{2\perp}(\bar{k}) & g_{2\parallel}(\bar{k}) & g_{4\perp}(\bar{k}) & g_{4\parallel}(\bar{k}) \end{pmatrix}, \tag{9.7}$$

and the density operators in momentum space are given by

$$\hat{\rho}_{\bar{k}\sigma} = \sum_k \hat{c}^+_{k\sigma} \hat{c}_{k+\bar{k},\sigma} \,. \tag{9.8}$$

Bosonization can be used to solve the fixed-point problem. This can only be carried out in a mathematically rigorous way [Mattis and Lieb, 1965] if the bandwidth cutoff is removed, i.e. $\Lambda_F \to \infty$, and if a cutoff in the maximal momentum transfer Λ_B of the interaction is used, i.e., $f_{\bar{k}} \neq 0$ only for $|\bar{k}| < \Lambda_B$. The resulting Hamiltonian has no lower bound in the single-particle energies and a filled Dirac sea of negative energy states has to be imposed as a constraint on the Hilbert space. Meticulous care is required for a proper treatment of the associated anomalous commutators [Mattis and Lieb, 1965].

The fixed-point Hamiltonian that contains only the forward scattering terms g_2 and g_4 is known as the Tomonaga-Luttinger model. Its exact solubility is due to a special symmetry. Namely, the number of electrons with a given spin and branch index is conserved separately by the forward scattering processes g_2 and g_4. It is not surprising that the additional symmetry can also be exploited by other methods. In particular, Dzyaloshinskii and Larkin [Dzyaloshinskii and Larkin, 1974] derived a Ward identity for a vertex function that is directly related to the symmetry. Combining this identity with a skeleton expansion for the self-energy yields a closed integral equation for the single-particle Green's function. Solving this in real space they obtained the exact single-particle Green's function for the first time. A detailed discussion of Ward identities and their relevance for the renormalizability using the field theoretic RG was also given in [DiCastro and Metzner, 1991,Metzner and DiCastro, 1992]. As Ward identities and skeleton diagrams will be derived in detail later on, we will not discuss this approach any further here.

Higher-dimensional generalizations of the forward scattering problem have been considered by many authors (for a review see [Metzner *et al.*, 1998]). The Fermi surface is then devided into different patches within which the dispersion is linearized with respect to the central point [Kopietz, 1997]. When the maximal momentum transfer of the interaction is much smaller than the patch size, "around the corner" scattering processes that take an electron from one patch to another can be neglected. The problem then reduces to Eq. (9.6), however with more than two patch labels. For these higher-dimensional generalizations of bosonization, a formulation in terms of functional integrals is better

suited [Kopietz and Schönhammer, 1996, Kopietz *et al.*, 1995, Kopietz, 1997]. The density-density interaction in Eq. (9.6) is then decoupled by a Hubbard-Stratonovich transformation. Subsequently, the fermions are integrated out as in the Hertz approach. For a linearized energy dispersion, the closed-loop theorem [Bohr, 1981, Kopietz *et al.*, 1995] guarantees that the resulting bosonic action is quadratic. Correlation functions for higher dimensional Luttinger liquids arising from singular interactions where studied with this method in [Bartosch and Kopietz, 1999]. In principle, when the curvature of the dispersion is taken into account, corrections to the non-interacting boson picture can be systematically calculated [Kopietz *et al.*, 1995, Busche and Kopietz, 2000], but the resulting expressions are rather cumbersome and have only been evaluated for a few cases.

Recently, the fermionic version of the functional RG was used to go beyond the flow of a few coupling constants. By an approximate iterative two-loop solution of the hierarchy of flow equations, the single-particle scaling function was calculated [Busche *et al.*, 2002, Busche, 2003]. At the Fermi points, the exact scaling behavior was correctly recovered. For momenta away from the Fermi points, anomalous scaling was found, but with an exponent slightly different from the exact one.

In this context, it is also interesting to note that the functional RG has very successfully been applied to analyze scaling behaviour and transport properties in finite size chains with impurities [Meden *et al.*, 2002, Andergassen *et al.*, 2004].

9.3 Outline

In part II of the thesis, we develop a formulation of the functional renormalization group that includes bosonic modes from the outset. In Chap. 10, we introduce the notation for the action in the functional-integral formalism. An interaction of the density-density type is considered and is decoupled by a Hubbard-Stratonovich transformation. Subsequently, the field-theoretical formalism of generating functionals is reviewed in Chap. 11 and the functional RG equations are derived in a very general notation. In Chap. 12, we analyze symmetries of the action of the coupled Fermi-Bose theories and obtain important identities for the generating functionals. In Chap. 13, we then define physical vertex functions that explicitly respect these symmetry relations. Possible choices of cutoff procedures are discussed and we derive the infinite hierarchy of flow equations for the vertices. We discuss the rescaling of momenta and fields to classify the vertices and propose a truncation that contains only the leading elements of the skeleton expansion. In Chap. 14, we present a flow scheme that takes only the momentum-transfer of the interaction as a running cutoff. For linearized dispersion in a forward scattering problem, the resulting flow equations can be sufficiently simplified to allow for an exact solution by an infinite set of Ward identities. We will then recover the exact solution of the TLM within the functional RG formalism. A summary and outlook is given in Chap. 15.

Most of the material of this part of the thesis is published in [Schütz *et al.*, 2005].

Chapter 10:

Interacting fermions as coupled Fermi-Bose systems

This chapter introduces the notation used in the rest of this work. The action in the functional integral representation is presented in Sec. 10.1 and the normalization of the fields is explained. We consider a density-density interaction and decouple it by a Hubbard-Stratonovich transformation in Sec. 10.2. The interaction is then mediated by an additional bosonic field. To keep track of the different fields and their propagators a shorthand notation is introduced in Sec. 10.3 which will be used throughout the next chapter before going back to more physical variables in Chap. 13.

10.1 Path-integral formulation

We consider a normal fermionic many-body system with two-particle density-density interactions. In the usual Grassmannian functional integral approach [Negele and Orland, 1988] the grand-canonical partition function and all (imaginary)-time-ordered Green's functions can be represented as functional averages involving the following Euclidean action,

$$\begin{aligned} S[\bar{c},c] &= \int_0^\beta d\tau \Big\{ \sum_{\mathbf{k}\sigma} \bar{c}_{\mathbf{k}\sigma}(\tau+0^+)[\partial_\tau + \xi_{\mathbf{k}\sigma}]c_{\mathbf{k}\sigma}(\tau) \\ &+ \frac{1}{2V} \sum_{\mathbf{k},\mathbf{k}',\bar{\mathbf{k}},\sigma,\sigma'} f_{\bar{\mathbf{k}}}^{\sigma\sigma'} \bar{c}_{\mathbf{k}+\bar{\mathbf{k}},\sigma}(\tau+0^+)\bar{c}_{\mathbf{k}'-\bar{\mathbf{k}},\sigma'}(\tau+0^+)c_{\mathbf{k}'\sigma'}(\tau)c_{\mathbf{k}\sigma}(\tau)\Big\}. \quad (10.1) \end{aligned}$$

Here $\beta = 1/T$ denotes the inverse temperature and V is the volume of the system. The Grassmann variables $\bar{c}_{\mathbf{k}\sigma}$ and $c_{\mathbf{k}\sigma}$ are associated with the creation and annihilation operators $\hat{c}^+_{\mathbf{k}\sigma}$ and $\hat{c}_{\mathbf{k}\sigma}$ of a particle with wave vector $\mathbf{k}$ and spin projection σ. The energy dispersion $\xi_{\mathbf{k}\sigma} = \epsilon_{\mathbf{k}\sigma} - \mu$ is measured relative to the chemical potential μ, and $f_{\bar{\mathbf{k}}}^{\sigma\sigma'}$ are the momentum-dependent interaction parameters introduced in the previous chapter. The discrete index σ is formally written as a spin projection, but will later on also serve to distinguish different patches on the Fermi surface. This is why a dependence of the dispersion $\xi_{\mathbf{k}\sigma}$ and the interaction $f_{\bar{\mathbf{k}}}^{\sigma\sigma'}$ on spin indices has been kept. In the case of the Tomonaga-Luttinger model, σ denotes the spin projection as well as the right or left moving character of the field.

With the action in Eq. (10.1) the grand-canonical partition function is given

by the functional integral

$$Z = \int D[\bar{c}, c]\ e^{-S[\bar{c},c]}\,, \tag{10.2}$$

where the functional measure is defined by

$$D[\bar{c}, c] = \prod_{\mathbf{k}\sigma} \prod_{\substack{\tau=0,\Delta\tau,\\ \ldots,\beta-\Delta\tau}} d\bar{c}_{\mathbf{k}\sigma}(\tau) dc_{\mathbf{k}\sigma}(\tau)\,. \tag{10.3}$$

Here, the limit $\Delta\tau \to 0$ has to be taken at the end of the calculation. In this limit, the action is formally given by Eq. (10.1), but in case of doubt the underlying discrete version has to be used [Negele and Orland, 1988]. The notation $\tau + 0^+$ is a reminder that in the discrete case, the Grassmann variables $\bar{c}_{\mathbf{k}\sigma}$ are to be taken at a later time step than $c_{\mathbf{k}\sigma}$. This leads to convergence factors in Hartree and Fock type diagrams, but can otherwise be ignored.

Let us now perform a Fourier transformation to a frequency representation including an appropriate normalization for the thermodynamic ($V \to \infty$) and zero-temperature ($\beta \to \infty$) limits

$$c_{\mathbf{k}\sigma}(\tau) = \frac{1}{\beta\sqrt{V}} \sum_{\omega} e^{-i\omega\tau} \psi_{K\sigma}\,. \tag{10.4}$$

The summation is over fermionic Matsubara frequencies $\omega = (2n+1)\pi T$ ($n = 0, \pm 1, \pm 2, \ldots$) to ensure antiperiodic boundary conditions $c_{\mathbf{k}\sigma}(\beta) = -c_{\mathbf{k}\sigma}(0)$. A composite frequency-momentum index $K = (i\omega, \mathbf{k})$ has been introduced. The inverse transformation is given by

$$\psi_{K\sigma} = \sqrt{V} \int_0^\beta d\tau\, e^{i\omega\tau} c_{\mathbf{k}\sigma}(\tau)\,. \tag{10.5}$$

The transformed action then reads

$$S[\bar{\psi}, \psi] = S_0[\bar{\psi}, \psi] + S_{\rm int}[\bar{\psi}, \psi]\,, \tag{10.6}$$

$$S_0[\bar{\psi}, \psi] = \sum_{\sigma} \int_K \bar{\psi}_{K\sigma} [-i\omega + \xi_{\mathbf{k}\sigma}] \psi_{K\sigma}\,, \tag{10.7}$$

$$S_{\rm int}[\bar{\psi}, \psi] = \frac{1}{2} \sum_{\sigma\sigma'} \int_{\bar{K}} f^{\sigma\sigma'}_{\mathbf{k}}\, \bar{\rho}_{\bar{K}\sigma} \rho_{\bar{K}\sigma'}\,. \tag{10.8}$$

Here, the composite frequency-momentum index $\bar{K} = (i\bar{\omega}, \bar{\mathbf{k}})$ contains a bosonic Matsubara frequency $\bar{\omega} = 2\pi T n$ ($n = 0, \pm 1, \pm 2, \ldots$). Throughout this work we will use the convention of putting a bar over bosonic frequency and momentum labels, while labels without a bar refer to fermionic quantities. With this

normalization of the Grassmann fields $\psi_{K\sigma}$ and $\bar{\psi}_{K\sigma}$ the integration measure in Eq. (10.6) is

$$\int_K = \frac{1}{\beta V} \sum_{\omega,\mathbf{k}} \quad \overset{\beta,V\to\infty}{\longrightarrow} \quad \int \frac{d\omega}{2\pi} \frac{d^D k}{(2\pi)^D} \,, \tag{10.9}$$

The Fourier components of the density are represented by the following composite field

$$\rho_{\bar{K}\sigma} = \int_K \bar{\psi}_{K\sigma} \psi_{K+\bar{K},\sigma} \,, \tag{10.10}$$

which implies $\bar{\rho}_{\bar{K}\sigma} = \rho_{-\bar{K}\sigma}$. In terms of the new variables, the functional measure reads

$$D[\bar{c}, c] = D[\bar{\psi}, \psi] = \prod_{K\sigma} \frac{d\bar{\psi}_{K\sigma} d\psi_{K\sigma}}{\beta V \Delta\tau} \,, \tag{10.11}$$

which is again defined as a limit $\tau \to 0$ of a finite integral with the same number of variables as in the imaginary time formulation in Eq. (10.3). Thus, the product in Eq. (10.11) is only over a finite number $N_t = \beta/\Delta\tau$ of Matsubara frequencies. Strictly speaking, a discrete version of the Fourier transformation has to be used, which in the limit $\Delta\tau \to 0$ turns into Eq. (10.5). In case of need, the discrete version always yields the correct convergence factors.

10.2 Hubbard-Stratonovich transformation

The interaction is bilinear in the densities and can be decoupled by means of a Hubbard-Stratonovich transformation [Stratonovich, 1957, Hubbard, 1959, Kopietz, 1997]. This makes use of standard identities for Gaussian integrals over the components z_i or x_i of a complex vector $\mathbf{z}$ or a real vector $\mathbf{x}$

$$\int \prod_i \frac{dz_i^R dz_i^I}{\pi} e^{-\boldsymbol{z}^+ \mathbf{A} \boldsymbol{z} - i\boldsymbol{a}^+ \boldsymbol{z} - i\boldsymbol{z}^+ \boldsymbol{b}} = [\det(\mathbf{A})]^{-1} e^{-\boldsymbol{a}^+ \mathbf{A}^{-1} \boldsymbol{b}} \,, \tag{10.12}$$

$$\int \prod_i \frac{dx_i}{\sqrt{\pi}} e^{-\frac{1}{2}\boldsymbol{x}^T \mathbf{B} \boldsymbol{x} - i\boldsymbol{y}^T \boldsymbol{x}} = [\det(\mathbf{B})]^{-\frac{1}{2}} e^{-\frac{1}{2}\boldsymbol{y}^T \mathbf{B}^{-1} \boldsymbol{y}} \,. \tag{10.13}$$

Applying these identities, one has to avoid double counting of $\bar{K}$ and $-\bar{K}$. This can be done by writing all sums in terms of just one of them denoted by $\bar{K} > 0$. We treat $\bar{K} = 0$ separately and rewrite the fermionic interaction as

$$S_{\rm int}[\bar{\psi}, \psi] = \sum_{\sigma\sigma'} \int_{\bar{K}>0} f_{\bar{k}}^{\sigma\sigma'} \bar{\rho}_{\bar{K}\sigma} \rho_{\bar{K}\sigma'} + \frac{1}{2} \sum_{\sigma\sigma'} \frac{1}{\beta V} f_0^{\sigma\sigma'} \rho_{0\sigma} \rho_{0\sigma'} \tag{10.14}$$

The first term can be decoupled using Eq. (10.12) once for every value of $\bar{K}$, while for the second term we use the Gaussian integral in Eq. (10.13). The result for both contributions can be recombined in the form

$$e^{-S[\bar{\psi},\psi]} = \frac{1}{\mathcal{Z}_\varphi} \int D\varphi \; e^{-S[\bar{\psi},\psi,\varphi]} \,, \tag{10.15}$$

The interaction is then mediated by a real bosonic field φ and the resulting action reads

$$S[\bar{\psi},\psi,\varphi] = S_0[\bar{\psi},\psi] + S_0[\varphi] + S_1[\bar{\psi},\psi,\varphi] \;, \tag{10.16}$$

where the free bosonic part is given by

$$S_0[\varphi] \;=\; \frac{1}{2}\sum_{\sigma\sigma'}\int_{\bar{K}} [f_{\bar{\mathbf{k}}}^{-1}]^{\sigma\sigma'}\varphi^*_{\bar{K}\sigma}\varphi_{\bar{K}\sigma'} \;, \tag{10.17}$$

and the coupling between Fermi and Bose fields is

$$S_1[\bar{\psi},\psi,\varphi] = i\sum_{\sigma}\int_{\bar{K}}\bar{\rho}_{\bar{K}\sigma}\varphi_{\bar{K}\sigma} = i\sum_{\sigma}\int_{K}\int_{\bar{K}}\bar{\psi}_{K+\bar{K},\sigma}\psi_{K\sigma}\varphi_{\bar{K}\sigma}\,. \tag{10.18}$$

For convenience, we have defined $\varphi_{-\bar{K}\sigma} = \varphi^*_{\bar{K}\sigma}$, such that $\varphi_{\bar{K}\sigma}$ are the Fourier components of a real field. The integration measure in Eq. (10.15) is given by

$$D\varphi = \frac{d\varphi_{0\sigma}}{\sqrt{\pi}}\prod_{\bar{K}>0,\sigma}\frac{d\varphi^R_{\bar{K}\sigma}d\varphi^I_{\bar{K}\sigma}}{\pi}\,. \tag{10.19}$$

Furthermore, the formal free partition function of the φ field is defined as

$$\mathcal{Z}_\varphi = \int D\varphi\; e^{-S_0[\varphi]}\,. \tag{10.20}$$

In a strict sense, the integration for $\mathcal{Z}_\varphi$ does not exist separately in the continuum limit $N_\tau \to \infty$. Only the combination in Eq. (10.15) is finite in this limit, such that $\mathcal{Z}_\varphi$ could also have been incorporated into the functional measure. One might further object that the inverse interaction $f^{-1}_{\bar{\mathbf{k}}}$ is not well defined in all cases. However, our final flow equations below will only depend on the interaction $f_{\bar{\mathbf{k}}}$ itself. For intermediate steps one should then appropriately regularize $f_{\bar{\mathbf{k}}}$ in a way that all inverses exist.

10.3 Compact notation for Fermi and Bose fields

For the manipulations in the next chapter it will prove advantageous to further condense the notation and collect the fields in a vector $\Phi = (\psi, \bar{\psi}, \varphi)$. The quadratic part of the action can then be written in the symmetric form

$$S_0[\Phi] = S_0[\bar{\psi},\psi] + S_0[\varphi] = -\frac{1}{2}\left(\Phi, [\mathbf{G}_0]^{-1}\,\Phi\right) = -\frac{1}{2}\int_\alpha\int_{\alpha'}\Phi_\alpha\,[\mathbf{G}_0]^{-1}_{\alpha\alpha'}\,\Phi_{\alpha'}\;, \tag{10.21}$$

where $\mathbf{G}_0$ is now a matrix in frequency, momentum, spin and field-type indices, and α is a "super label" for all of these indices. The symbol $\int_\alpha$ denotes integration

over the continuous components and summation over the discrete components of α. The matrix $\mathbf{G}_0^{-1}$ has the block structure

$$\mathbf{G}_0^{-1} = \begin{pmatrix} 0 & \zeta[\hat{G}_0^{-1}]^T & 0 \\ \hat{G}_0^{-1} & 0 & 0 \\ 0 & 0 & -\hat{F}_0^{-1} \end{pmatrix} , \tag{10.22}$$

where $\hat{G}_0$ and $\hat{F}_0$ are infinite matrices in frequency, momentum and spin space, with matrix elements

$$[\hat{G}_0]_{K\sigma,K'\sigma'} = \delta_{K,K'}\delta_{\sigma\sigma'}G_{0,\sigma}(K) , \tag{10.23}$$

$$[\hat{F}_0]_{\bar{K}\sigma,\bar{K}'\sigma'} = \delta_{\bar{K}+\bar{K}',0}F_{0,\sigma\sigma'}(\bar{K}) , \tag{10.24}$$

where

$$G_{0,\sigma}(K) = [i\omega - \xi_{\mathbf{k}\sigma}]^{-1} , \tag{10.25}$$

$$F_{0,\sigma\sigma'}(\bar{K}) = f_{\mathbf{k}}^{\sigma\sigma'} . \tag{10.26}$$

To keep the notation general, we have introduced $\zeta = -1$ in Eq. (10.22) appropriate for fermions, which we will exclusively consider in this work. Yet, most of the formulas derived below are also valid for bosons if one sets $\zeta = 1$. The Kronecker $\delta_{K,K'} = \beta V \delta_{\omega,\omega'}\delta_{\mathbf{k},\mathbf{k}'}$ appearing in Eqs. (10.23,10.24) is normalized such that it reduces to Dirac δ-functions

$$\delta_{K,K'} \to (2\pi)^{D+1}\delta(\omega - \omega')\delta^{(D)}(\mathbf{k} - \mathbf{k}') \tag{10.27}$$

in the limit $\beta, V \to \infty$. Note that the bare interaction plays the role of a free bosonic Green's function. For later reference, we note that the inverse of Eq. (10.22) is

$$\mathbf{G}_0 = \begin{pmatrix} 0 & \hat{G}_0 & 0 \\ \zeta\hat{G}_0^T & 0 & 0 \\ 0 & 0 & -\hat{F}_0 \end{pmatrix} , \tag{10.28}$$

and that the transpose of $\mathbf{G}_0$ satisfies

$$\mathbf{G}_0^T = \mathbf{Z}\mathbf{G}_0 = \mathbf{G}_0\mathbf{Z} , \tag{10.29}$$

where the "statistics matrix" $\mathbf{Z}$ is defined by

$$[\mathbf{Z}]_{\alpha\alpha'} = \delta_{\alpha\alpha'}\zeta_\alpha . \tag{10.30}$$

Here, $\zeta_\alpha = -1$ if the super-index α refers to a Fermi field, and $\zeta_\alpha = 1$ if α labels a Bose field. With this compact notation, the partition function can be written as

$$\frac{Z}{Z_0} = \frac{1}{\mathcal{Z}_0}\int D\Phi \; e^{-S[\Phi]} , \tag{10.31}$$

where Z_0 is the free partition function without interaction, given by

$$Z_0 = \mathcal{Z}_\psi = \int D[\bar{\psi}, \psi]\ e^{-S_0[\bar{\psi},\psi]}\,, \tag{10.32}$$

and $\mathcal{Z}_0 = \mathcal{Z}_\psi \mathcal{Z}_\varphi$.

To define generating functionals in the next section, we need to add a source term to the action which in the compact notation reads

$$(J, \Phi) = \int_\alpha J_\alpha \Phi_\alpha\,. \tag{10.33}$$

Functional derivatives with respect to the sources are defined by appropriate normalization of ordinary partial derivatives

$$\frac{\delta}{\delta J_\alpha} = \beta V \frac{\partial}{\partial J_\alpha}\,. \tag{10.34}$$

Conventionally, the source terms for fields of different types are written out explicitly in the form [Negele and Orland, 1988]

$$\begin{aligned}(J, \Phi) &= (\bar{\jmath}, \psi) + (\bar{\psi}, j) + (J^*, \varphi) \\ &= \sum_\sigma \int_K \bar{\jmath}_{K\sigma}\psi_{K\sigma} + \sum_\sigma \int_K \bar{\psi}_{K\sigma} j_{K\sigma} + \sum_\sigma \int_{\bar{K}} J^*_{\bar{K}\sigma}\varphi_{\bar{K}\sigma}\,,\end{aligned} \tag{10.35}$$

A comparison between Eq. (10.33) and Eq. (10.36) shows that the sources in the compact notation are related to the standard ones by $J = (\bar{\jmath}, \zeta j, J^*)$.

It is instructive to undo the Hubbard-Stratonovich transformation after the introduction of sources and integrate out the bosonic fields,

$$\frac{1}{\mathcal{Z}_\varphi}\int D\varphi\ e^{-S[\bar{\psi},\psi,\varphi]+(J^*,\varphi)} = e^{-\frac{1}{2}(J,\hat{F}_0 J)} e^{-S[\bar{\psi},\psi]+i(J,\hat{F}_0\rho)}\,. \tag{10.36}$$

Thus, except for the trivial prefactor, sources for the field φ in the mixed theory are equivalent to sources for the composite density fields in the purely fermionic language.

Finally, note that for purely fermionic systems the notation introduced in this section is identical to the one used in [Salmhofer and Honerkamp, 2001].

Chapter 11:

Field-theoretical formalism in compact notation

We would now like to derive the functional renormalization group flow equations. Before we do this in Sec. 11.2, we review the field-theoretical formalism of generating functionals for various types of vertices and give relations among the different functionals in Sec. 11.1. Throughout this chapter, we use the short-hand notation introduced in Sec. 10.3, but we do not refer to the precise realization in our mixed Fermi-Bose theory. Consequently, our general formalism presented here can be applied to theories containing any combination of fermionic, bosonic, real, or even Majorana fields. The following two chapters will then be concerned with the application of this formalism to our physical situation at hand.

11.1 Generating functionals

The action is assumed to be of the form $S = S_0 + S_1$, where the interaction part S_1 is at least cubic in the fields Φ and the free part is given by

$$S_0[\Phi] = -\frac{1}{2}\left(\Phi, [\mathbf{G}_0]^{-1}\,\Phi\right) , \tag{11.1}$$

as in Sec. 10.3. The free propagator again fulfills the symmetry relation $\mathbf{G}_0^T = \mathbf{Z}\mathbf{G}_0$, with the diagonal statistics matrix $\mathbf{Z}$ defined in Eq. (10.30). However, no reference to the precise block structure of $\mathbf{G}_0$ is necessary in this chapter. Hence, in principle, anomalous (superconducting) propagators or other symmetry breaking terms are also allowed.

11.1.1 Connected Green's functions

To define generating functionals, we introduce source fields J_α which have the same character (fermionic, bosonic, real or Majorana) as the associated fields Φ_α. Green's functions are then generated by the functional

$$\mathcal{G}[J] = e^{\mathcal{G}_c[J]} = \frac{1}{\mathcal{Z}_0}\int D\Phi\; e^{-S_0[\Phi]-S_1[\Phi]+(J,\Phi)} . \tag{11.2}$$

Here, $\mathcal{G}_c[J]$ is the generating functional for *connected* Green's functions and the free partition function $\mathcal{Z}_0$ is given by the Gaussian integral

$$\mathcal{Z}_0 = \int D\Phi\; e^{-S_0[\Phi]} . \tag{11.3}$$

The connected n-line Green's functions $\mathcal{G}^{(n)}_{c,\alpha_1\ldots\alpha_n}$ are defined as coefficients in the functional Taylor expansion of $\mathcal{G}_c[J]$:

$$\mathcal{G}_c[J] = \sum_{n=0}^{\infty} \frac{1}{n!} \int_{\alpha_1} \ldots \int_{\alpha_n} \mathcal{G}^{(n)}_{c,\alpha_1\ldots\alpha_n} J_{\alpha_1} \cdot \ldots \cdot J_{\alpha_n} \,. \tag{11.4}$$

This implies the relation

$$\mathcal{G}^{(n)}_{c,\alpha_1\ldots\alpha_n} = \left. \frac{\delta^{(n)} \mathcal{G}_c[J]}{\delta J_{\alpha_n} \ldots \delta J_{\alpha_1}} \right|_{J=0} \,. \tag{11.5}$$

An analogous functional Taylor expansion for $\mathcal{G}$ generates the n-line Green's functions $\mathcal{G}^{(n)}_{\alpha_1\ldots\alpha_n}$. The functional integration in Eq. (11.2) becomes Gaussian in the non-interacting limit ($S_1 \to 0$) and is easily carried out by completing the square in the exponent. We obtain

$$\mathcal{G}_0[J] = e^{\mathcal{G}_{c,0}[J]} = \frac{1}{\mathcal{Z}_0} \int D\Phi \; e^{\frac{1}{2}\left(\Phi,[\mathbf{G}_0]^{-1}\Phi\right)+(J,\Phi)} = e^{-\frac{1}{2}\left(J,\mathbf{G}_0^T J\right)} \,. \tag{11.6}$$

Therefore, the free propagator can be obtained as a functional derivative of $\mathcal{G}_{c,0}$:

$$[\mathbf{G}_0]_{\alpha\alpha'} = -\frac{\delta^{(2)} \mathcal{G}_{c,0}}{\delta J_\alpha \delta J_{\alpha'}} \,. \tag{11.7}$$

Likewise, the full propagator of the interacting system is defined as

$$[\mathbf{G}]_{\alpha\alpha'} = - \left. \frac{\delta^{(2)} \mathcal{G}_c}{\delta J_\alpha \delta J_{\alpha'}} \right|_{J=0} = -\mathcal{G}^{(2)}_{c,\alpha'\alpha} \,. \tag{11.8}$$

The matrix element $[\mathbf{G}]_{\alpha\alpha'}$ will only be non-zero if α and α' both refer to either fermionic or bosonic fields. The commuting or anti-commuting property of the functional derivative then imply that the full Green's function also fulfills the symmetry relation

$$\mathbf{G}^T = \mathbf{Z}\mathbf{G} = \mathbf{G}\mathbf{Z} \,. \tag{11.9}$$

Interaction corrections to the free propagator can be parameterized by the self-energy matrix $\mathbf{\Sigma}$ which is defined by Dyson's equation

$$\mathbf{G}^{-1} = \mathbf{G}_0^{-1} - \mathbf{\Sigma} \,. \tag{11.10}$$

The Green's functions can be formally expanded in a power series of the interaction. This perturbation theory is derived by replacing $\exp(S_1[\Phi]) \to \exp(S_1[\frac{\delta}{\delta J}])$ in Eq. (11.2), such that the exponential of the interaction can be taken out of the functional integral. The remaining integration is Gaussian and has been carried out in Eq. (11.6). This yields

$$\mathcal{G}[J] = e^{\mathcal{G}_c[J]} = e^{-S_1\left[\frac{\delta}{\delta J}\right]} e^{-\frac{1}{2}\left(J,\mathbf{G}_0^T J\right)} \,. \tag{11.11}$$

Here, one can expand the first exponential in powers of the interaction S_1. Acting with the derivatives on the second exponential creates pairwise contractions with the propagator $\mathbf{G}_0$. It is straightforward to write down diagrammatic representations of the Green's functions. Standard arguments, as for example the replica trick (see [Zinn-Justin, 2002]), show that only connected diagrams contribute to the vertices $\mathcal{G}_c^{(n)}$.

11.1.2 Amputated connected Green's functions

Below, we will need to determine the initial condition for the renormalization group flow of the generating functionals. This initial condition corresponds to the limit $\mathbf{G}_0 \to 0$ of a vanishing propagator. From Eq. (11.11), we see that $\mathcal{G}_c \to 0$ in this case. This is not a sensible starting point for the flow. Instead, it will be useful to consider the generating functional $\mathcal{G}_{\mathrm{ac}}$ of amputated connected Green's functions defined by

$$e^{\mathcal{G}_{ac}[J]} = \frac{1}{\mathcal{Z}_0} \int D\Phi \; e^{-S_0[\Phi]-S_1[\Phi+J]} \,. \tag{11.12}$$

A shift $\Phi \to \Phi - J$ in the integration variables together with the explicit form of the free action allows us to express $\mathcal{G}_c$ in terms of $\mathcal{G}_{ac}$:

$$\mathcal{G}_c[J] = \mathcal{G}_{ac}[-\mathbf{G}_0^T J] - \frac{1}{2}\left(J, \mathbf{G}_0^T J\right) \,. \tag{11.13}$$

Another useful relation is derived by the use of an additional source field in an intermediate step,

$$e^{\mathcal{G}_{ac}[J]} = e^{-S_1[\frac{\delta}{\delta \tilde{J}}]} \frac{1}{Z_0} \int D\Phi \; e^{-S_0[\Phi]+(\tilde{J},\Phi+J)} \Big|_{\tilde{J}=0} = e^{-S_1[\frac{\delta}{\delta \tilde{J}}]} e^{-\frac{1}{2}\left(\mathbf{Z}\frac{\delta}{\delta J}, \mathbf{G}_0^T \mathbf{Z}\frac{\delta}{\delta J}\right)} e^{(\tilde{J},J)} \Big|_{\tilde{J}=0} \,. \tag{11.14}$$

For the second equality, the Gaussian integration over Φ has been carried out and the $\tilde{J}$ has been replaced by derivatives with respect to J. The first two exponential factors can now be interchanged and we finally obtain

$$e^{\mathcal{G}_{\mathrm{ac}}[J]} = e^{-\frac{1}{2}\left(\frac{\delta}{\delta J}, \mathbf{G}_0^T \frac{\delta}{\delta J}\right)} e^{-S_1[J]} \,. \tag{11.15}$$

Similar to Eq. (11.11), this expression can be used to derive perturbative representations for the amputated connected Green's functions generated by $\mathcal{G}_{ac}$. Formally, one obtains a power series in the free propagator. For an interaction which is a monomial in the fields, this is equivalent to a power series in S_1. Since in Eq. (11.15) J appears in the interaction S_1, external lines are attached directly to interaction vertices without a connecting free propagator, whence the name "amputated connected". From Eq. (11.15), we obtain $\mathcal{G}_{ac}[J] = -S_1[J]$ in the limit $\mathbf{G}_0 \to 0$, which is a robust starting point for the renormalization group flow.

11.1.3 One-line irreducible vertices

The perturbative series for the connected Green's functions contains diagrams that can be separated in two parts by cutting a single propagator line. These diagrams will be called one-line reducible. In order to sum infinite subsets of diagrams as well as for renormalization group treatments, it is often advantageous to work with one-line irreducible vertices. To obtain the generating functional of these irreducible vertices we perform a Legendre transformation with respect to all fields. Thus, we introduce the classical field

$$\Phi_\alpha = \frac{\delta \mathcal{G}_c}{\delta J_\alpha} \,. \tag{11.16}$$

For the sake of simplicity, we use the same symbol for the dummy integration field in the definition of the generating functional as well as for the classical field. The latter is technically the expectation value of the former in the presence of the sources. From the context it will always be clear which field is referred to. After inverting the relation (11.16) for $J = J[\Phi]$ we can calculate the Legendre effective action

$$\mathcal{L}[\Phi] = (J[\Phi], \Phi) - \mathcal{G}_c[J[\Phi]] \,. \tag{11.17}$$

From this we obtain

$$J_\alpha = \zeta_\alpha \frac{\delta \mathcal{L}}{\delta \Phi_\alpha} \,, \tag{11.18}$$

which we may write in compact matrix notation as

$$J = \mathbf{Z} \frac{\delta \mathcal{L}}{\delta \Phi} \,. \tag{11.19}$$

In this notation the chain rule simply reads

$$\frac{\delta}{\delta \Phi} = \frac{\delta^{(2)} \mathcal{L}}{\delta \Phi \delta \Phi} \mathbf{Z} \frac{\delta}{\delta J} \,. \tag{11.20}$$

Applying this to both sides of Eq. (11.16) we obtain

$$\mathbf{1} = \frac{\delta \Phi}{\delta \Phi} = \frac{\delta^{(2)} \mathcal{L}}{\delta \Phi \delta \Phi} \mathbf{Z} \frac{\delta^{(2)} \mathcal{G}_c}{\delta J \delta J} \,. \tag{11.21}$$

For vanishing fields Φ and J this yields

$$\left. \frac{\delta^{(2)} \mathcal{L}}{\delta \Phi \delta \Phi} \right|_{\Phi = 0} = -\mathbf{Z} \mathbf{G}^{-1} = -[\mathbf{G}^{-1}]^T \,. \tag{11.22}$$

The advantage of our compact notation is now obvious: the minus signs associated with the Grassmann fields can be neatly collected in the "statistics matrix" $\mathbf{Z}$. If the Grassmann sources are introduced in the conventional way [Negele and

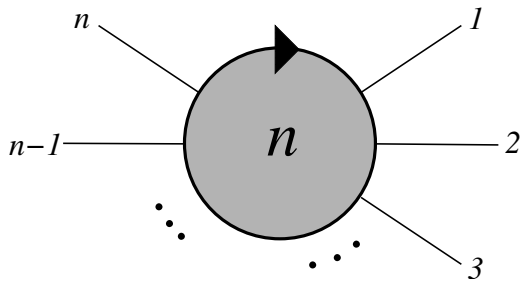

Figure 11.1: Graphical representation of the symmetrized one-line irreducible n-point vertex. Because for fermions the order of the indices is important, the circles representing the irreducible vertices have an arrow that points to the leg corresponding to the first index. Subsequent indices are arranged in the order indicated by the arrow.

Orland, 1988], the minus signs generated by commuting two Grassmann fields are distributed in a more complicated manner in the matrices of second derivatives [Kopietz and Busche, 2001, Correia *et al.*, 2002].

As the irreducible two-point function is nothing but the self-energy $\mathbf{\Sigma}$, it is evident from Eq. (11.22) that $\mathcal{L}[\Phi]$ is not yet the generating functional for irreducible vertex functions. In order to obtain this functional Γ, we need to subtract the free action from $\mathcal{L}[\Phi]$:

$$\Gamma[\Phi] = \mathcal{L}[\Phi] - S_0[\Phi] = \mathcal{L}[\Phi] + \frac{1}{2}(\Phi, [\mathbf{G}_0^{-1}]\Phi)\,. \tag{11.23}$$

Using the Dyson equation (11.10), we obtain

$$\left.\frac{\delta^{(2)}\Gamma}{\delta\Phi\delta\Phi}\right|_{\Phi=0} = \left.\frac{\delta^{(2)}\mathcal{L}}{\delta\Phi\delta\Phi}\right|_{\Phi=0} + [\mathbf{G}_0^{-1}]^T = -[\mathbf{G}^{-1}]^T + [\mathbf{G}_0^{-1}]^T = \mathbf{\Sigma}^T\,. \tag{11.24}$$

In general, the one-line irreducible vertices are defined as coefficients in an expansion of $\Gamma[\Phi]$ in powers of the fields,

$$\Gamma[\Phi] = \sum_{n=0}^{\infty} \frac{1}{n!} \int_{\alpha_1} \cdots \int_{\alpha_n} \Gamma^{(n)}_{\alpha_1,\ldots,\alpha_n} \Phi_{\alpha_1} \cdot \ldots \cdot \Phi_{\alpha_n}\,. \tag{11.25}$$

The vertices $\Gamma^{(n)}$ have the same symmetry with respect to interchange of the indices as the monomial in the fields, i.e., the interchange of two neighboring Fermi fields yields a minus sign. Graphically, we represent the vertices $\Gamma^{(n)}$ by an oriented circle with n external legs, as shown in Fig. 11.1. With the definition (11.25) and Eq. (11.24) we have

$$\Gamma^{(2)}_{\alpha\alpha'} = [\mathbf{\Sigma}]_{\alpha'\alpha}\,. \tag{11.26}$$

The fact that also the higher-order vertices $\Gamma^{(n)}$ defined in Eq. (11.25) are indeed one-line irreducible will be explicitly shown in the next section.

11.1.4 Tree expansion

We now derive explicit relations between the connected and the irreducible vertex functions $G_c^{(n)}$ and $\Gamma^{(n)}$ respectively. It will turn out that the connected Green's functions can be graphically expressed by linking irreducible vertices with full propagator lines. Since no loops occur in these diagrams the expansion of the connected Green's functions in terms of the irreducible ones is called a "tree expansion". The structure of this expansion also provides an explicit proof for the one-line irreducibility of the vertices $\Gamma^{(n)}$.

Usually [Negele and Orland, 1988], the expansion is derived graphically by taking higher-order derivatives of the relation (11.21) between the second functional derivatives of $\mathcal{L}[\Phi]$ and $\mathcal{G}_c[J]$. With the help of our compact notation we can even give the tree expansion in closed form. To do so, it is advantageous to define the functional

$$\mathbf{U} = \left[\frac{\delta^{(2)}\Gamma}{\delta\Phi\delta\Phi} - \frac{\delta^{(2)}\Gamma}{\delta\Phi\delta\Phi}\bigg|_{\Phi=0}\right]^T = \left[\frac{\delta^{(2)}\Gamma}{\delta\Phi\delta\Phi}\right]^T - \mathbf{\Sigma}\,, \tag{11.27}$$

which is a matrix in super-index space. Note that for a mixed Fermi-Bose theory $\mathbf{U}$ can have matrix elements containing an odd number of Grassmann fields, in contrast to the purely fermionic case. With the definition (11.27), we have

$$\frac{\delta^{(2)}\mathcal{L}}{\delta\Phi\delta\Phi} = \mathbf{U}^T - [\mathbf{G}^{-1}]^T\,, \tag{11.28}$$

so that

$$\left[\frac{\delta^{(2)}\mathcal{L}}{\delta\Phi\delta\Phi}\right]^{-1} = -\mathbf{G}^T[\mathbf{1} - \mathbf{U}^T\mathbf{G}^T]^{-1} = -\sum_{l=0}^{\infty}\mathbf{G}^T(\mathbf{U}^T\mathbf{G}^T)^l\,. \tag{11.29}$$

From Eq. (11.21) we obtain

$$\begin{aligned}\frac{\delta^{(2)}\mathcal{G}_c}{\delta J\delta J} &= \mathbf{Z}\left[\frac{\delta^{(2)}\mathcal{L}}{\delta\Phi\delta\Phi}\right]^{-1} = -\mathbf{Z}\mathbf{G}^T[\mathbf{1} - \mathbf{U}^T\mathbf{G}^T]^{-1} \\ &= -\sum_{l=0}^{\infty}\mathbf{Z}\mathbf{G}^T(\mathbf{U}^T\mathbf{G}^T)^l\,.\end{aligned} \tag{11.30}$$

We now expand both sides of Eq. (11.30) in powers of the sources J and compare coefficients. For the matrix on the left-hand side we obtain from Eq. (11.4)

$$\frac{\delta^{(2)}\mathcal{G}_c}{\delta J\delta J} = \sum_{n=0}^{\infty}\frac{1}{n!}\int_{\alpha_1}\ldots\int_{\alpha_n}\left[\mathbf{G}^{(n+2)}_{c,\alpha_1\ldots\alpha_n}\right]^T J_{\alpha_1}\cdot\ldots\cdot J_{\alpha_n}\,, \tag{11.31}$$

where the matrix $\mathbf{G}^{(n+2)}_{c,\alpha_1\ldots\alpha_n}$ is defined by

$$[\mathbf{G}^{(n+2)}_{c,\alpha_1\ldots\alpha_n}]_{\alpha\alpha'} = \mathcal{G}^{(n+2)}_{c,\alpha\alpha'\alpha_1\ldots\alpha_n}\,. \tag{11.32}$$

On the right-hand side we use Eqs. (11.27) and (11.25) to write

$$\mathbf{U} = \sum_{n=1}^{\infty} \frac{1}{n!} \int_{\alpha_1} \dots \int_{\alpha_n} \mathbf{\Gamma}^{(n+2)}_{\alpha_1,\dots,\alpha_n} \Phi_{\alpha_1} \cdot \dots \cdot \Phi_{\alpha_n} \,, \tag{11.33}$$

where

$$[\mathbf{\Gamma}^{(n+2)}_{\alpha_1,\dots,\alpha_n}]_{\alpha\alpha'} = \Gamma^{(n+2)}_{\alpha\alpha'\alpha_1\dots\alpha_n} \,. \tag{11.34}$$

To compare terms with the same powers of the sources J on both sides of Eq. (11.30), we need to express the fields Φ_α on the right-hand side of Eq. (11.33) in terms of the sources, using Eqs. (11.4) and (11.16),

$$\Phi_\alpha = \frac{\delta \mathcal{G}_c}{\delta J_\alpha} = \sum_{m=0}^{\infty} \frac{1}{m!} \int_{\beta_1} \dots \int_{\beta_m} \mathcal{G}^{(m+1)}_{c,\alpha\beta_1\dots\beta_m} J_{\beta_1} \dots J_{\beta_m} \,. \tag{11.35}$$

Substituting Eqs. (11.31), (11.33) and (11.35) into Eq. (11.30) and comparing terms with the same powers of the sources (after symmetrization), we obtain a general relation between the connected and the one-line irreducible correlation functions

$$\begin{aligned}
\mathbf{G}^{(n+2)}_{c,\beta_1,\dots,\beta_n} \;=\; & -\sum_{l=0}^{\infty} \sum_{n_1,\dots,n_l=1}^{\infty} \frac{1}{n_1! \cdot \dots \cdot n_l!} \int_{\alpha^1_1} \dots \int_{\alpha^1_{n_1}} \dots \int_{\alpha^l_1} \dots \int_{\alpha^l_{n_l}} \\
& \times \sum_{m^1_1,\dots,m^1_{n_1}=1}^{\infty} \dots \sum_{m^l_1,\dots,m^l_{n_l}=1}^{\infty} \delta_{n,\sum_{i=1}^{l}\sum_{j=1}^{n_i} m^i_j} \left[\mathbf{Z}\mathbf{G}^T \mathbf{\Gamma}^{(n_1+2)\,T}_{\alpha^1_1,\dots,\alpha^1_{n_1}} \mathbf{G}^T \cdot \dots \cdot \mathbf{G}^T \mathbf{\Gamma}^{(n_l+2)\,T}_{\alpha^l_1,\dots,\alpha^l_{n_l}} \mathbf{G}^T \right]^T \\
& \times \mathcal{S}_{\beta_1,\dots,\beta_{m^1_1};\dots;\beta_{n-m^l_{n_l}+1},\dots,\beta_n} \left\{ \mathcal{G}^{(m^1_1+1)}_{c,\alpha^1_1,\beta_1,\dots,\beta_{m^1_1}} \cdot \dots \cdot \mathcal{G}^{(m^l_{n_l}+1)}_{c,\alpha^l_{n_l},\beta_{n-m^l_{n_l}+1},\dots,\beta_n} \right\} .
\end{aligned} \tag{11.36}$$

On the right-hand side of this rather cumbersome expression, only connected correlation functions with degrees smaller than that of the Green's functions on left-hand side appear. One can therefore recursively express all connected correlation functions via their one-line irreducible counterparts. Only a finite number of terms contribute on the right-hand side. The operator $\mathcal{S}$ symmetrizes the expression in curly brackets with respect to indices on different correlation functions, i.e., it generates all permutations of the indices with appropriate signs, counting expressions only once that are generated by permutations of indices on the same vertex. Thus, it acts on an expression already symmetric in the index groups separated by semi-colons to generate an expression symmetric also with respect to the exchange of indices between different groups. More precisely the action of $\mathcal{S}$ is given by ($m = \sum_{i=1}^{l} m_i$)

$$\mathcal{S}_{\alpha_1,\dots,\alpha_{m_1};\dots;\alpha_{m-m_l+1},\dots,\alpha_m} \{A_{\alpha_1,\dots,\alpha_m}\} = \frac{1}{\prod_i m_i!} \sum_P \mathrm{sgn}_\zeta(P)\, A_{\alpha_{P(1)},\dots,\alpha_{P(m)}} \,, \tag{11.37}$$

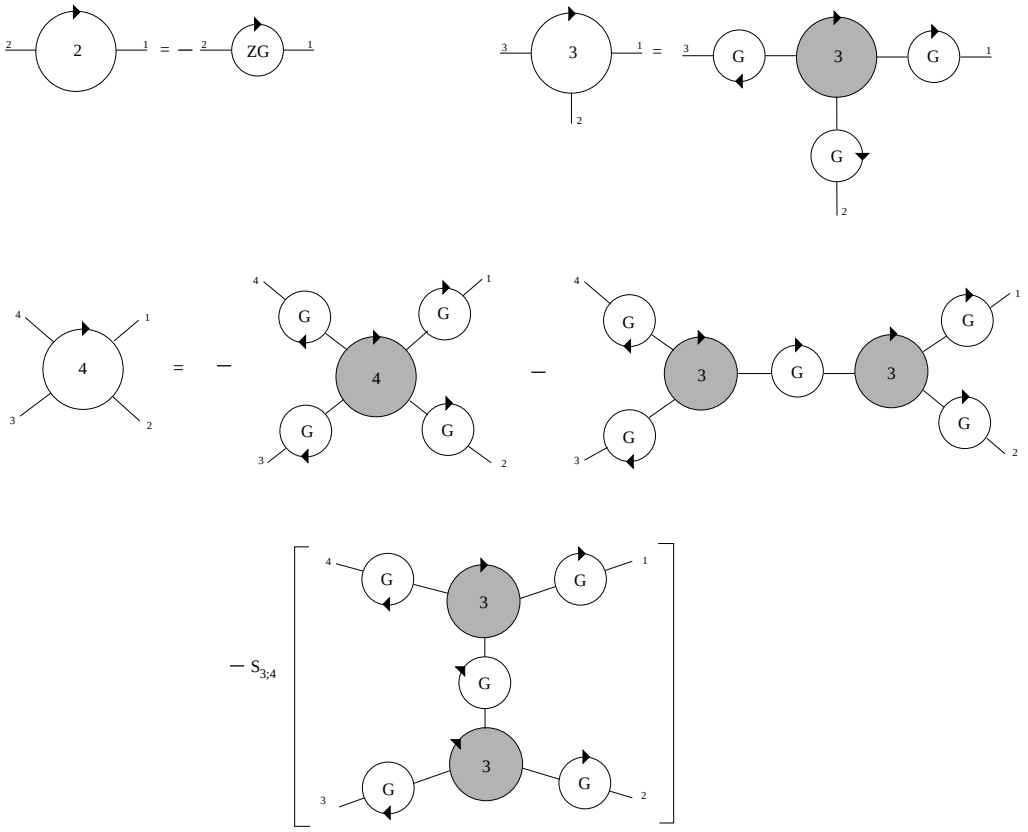

Figure 11.2: Graphical representation of the relation between connected Green's functions and one-line irreducible vertices up to the four-point functions. The irreducible vertices are represented by shaded oriented circles with the appropriate number of legs, see Fig. 11.1. The connected Green's functions are drawn as empty oriented circles with a number indicating the number of external legs.

where P denotes a permutation of $\{1, \ldots, m\}$ and sgn_ζ is the sign created by permuting field variables according to the permutation P, i.e.,

$$\Phi_{\alpha_1} \cdot \ldots \cdot \Phi_{\alpha_m} = \mathrm{sgn}_\zeta(P)\, \Phi_{\alpha_{P(1)}} \cdot \ldots \cdot \Phi_{\alpha_{P(m)}} \; . \tag{11.38}$$

A diagrammatic representation of the first few terms of the tree expansion generated by Eq. (11.36) is given in Fig. 11.2. Note that the right-hand sides contain only irreducible vertices, full Green functions, but no loops. Let us look at the corresponding analytic expressions: If we set $n = 0$ in Eq. (11.36) then only the term with $l = 0$ contributes and we obtain

$$\mathbf{G}_c^{(2)} = -\mathbf{ZG} = -\mathbf{G}^T \; , \tag{11.39}$$

which is the matrix form of Eq. (11.8). For $n = 1$ the single term with $l = 1$, $n_1 = 1$, $m_1^1 = 1$ contributes on the right-hand side of Eq. (11.36). Using $\mathbf{ZG} = \mathbf{G}^T$

the tree expansion of the connected Green's function with three external legs can be written as

$$\mathcal{G}^{(3)}_{c,\beta_1\beta_2\beta_3} = \int_{\alpha_1}\int_{\alpha_2}\int_{\alpha_3} [\mathbf{G}]_{\beta_1\alpha_1}[\mathbf{G}]_{\beta_2\alpha_2}[\mathbf{G}]_{\beta_3\alpha_3}\Gamma^{(3)}_{\alpha_1\alpha_2\alpha_3}\,. \tag{11.40}$$

Finally, consider the connected Green's function with four external legs, corresponding to $n = 2$ in Eq. (11.36). In this case the following three terms contribute,

term	l	n_i	m^i_j
1.)	1	$n_1 = 1$	$m^1_1 = 2$
2.)	1	$n_1 = 2$	$m^1_1 = m^1_2 = 1$
3.)	2	$n_1 = n_2 = 1$	$m^1_1 = m^2_1 = 1$

The corresponding analytic expression is

$$\begin{aligned}\mathcal{G}^{(4)}_{c,\beta_1\beta_2\beta_3\beta_4} = &-\int_{\alpha_1}\ldots\int_{\alpha_4} [\mathbf{G}]_{\beta_1\alpha_1}[\mathbf{G}]_{\beta_2\alpha_2}[\mathbf{G}]_{\beta_3\alpha_3}[\mathbf{G}]_{\beta_4\alpha_4}\Gamma^{(4)}_{\alpha_1\alpha_2\alpha_3\alpha_4} \\ &-\int_{\alpha_1}\ldots\int_{\alpha_6} [\mathbf{G}]_{\beta_1\alpha_1}[\mathbf{G}]_{\beta_2\alpha_2}[\mathbf{G}]_{\beta_3\alpha_3}[\mathbf{G}]_{\beta_4\alpha_4}\Gamma^{(3)}_{\alpha_1\alpha_2\alpha_5}[\mathbf{G}]_{\alpha_5\alpha_6}\Gamma^{(3)}_{\alpha_6\alpha_3\alpha_4} \\ &-\int_{\alpha_1}\ldots\int_{\alpha_6} S_{\beta_3;\beta_4}\Big\{[\mathbf{G}]_{\beta_1\alpha_1}[\mathbf{G}]_{\beta_2\alpha_2}[\mathbf{G}]_{\beta_3\alpha_3}[\mathbf{G}]_{\beta_4\alpha_4}\Gamma^{(3)}_{\alpha_1\alpha_5\alpha_4}[\mathbf{G}]_{\alpha_5\alpha_6}\Gamma^{(3)}_{\alpha_6\alpha_2\alpha_3}\Big\}\,.\end{aligned} \tag{11.41}$$

11.2 Functional RG flow equations

Diagrammatic perturbation theory often suffers from infrared divergencies due to gapless low-energy modes and breaks down at low temperatures. As discussed in the introduction the renormalization group provides a way to treat these divergencies by taking degrees of freedom into account iteratively starting from high-energy modes and proceeding to lower and lower energies. Performing these iterations in infinitesimal steps leads to differential flow equations for the vertices which we derive in this section.

In our compact notation, a cutoff can be formally introduced by the following replacement for the propagator

$$[\mathbf{G}_0]_{\alpha\beta} \longrightarrow \Theta_\alpha(\Lambda)\,[\mathbf{G}_0]_{\alpha\beta} = \Theta_\beta(\Lambda)\,[\mathbf{G}_0]_{\alpha\beta}\,. \tag{11.42}$$

Here, $\Theta_\alpha(\Lambda)$ is a function that suppresses low-energy modes in the bare propagator. It vanishes if α refers to such a low-energy mode whereas it is close to 1 for high energy modes. The cutoff Λ defines the limit between low and high energy modes. For $\Lambda \to 0$, we have $\Theta_\alpha(\Lambda = 0) = 1$ and the theory without an infrared cutoff is recovered. The precise realization depends off course on the physical system and the types of divergencies that occur. For our mixed theory,

possible choices for a cutoff will be discussed in Sec. 13.2. The bare propagator will always be diagonal in the relevant indices that determine the 'energy' so that it does not matter which of the two indices α or β is used in Eq. (11.42) to introduce the cutoff. For the derivation of the flow equations the functions $\theta_\alpha(\Lambda)$ has to be differentiable, i.e., sufficiently smooth. In the final flow equations for the vertices, the limit of a sharp cutoff can be taken as discussed by Morris [Morris, 1994].

Together with the bare propagators all generating functionals depend on the cutoff and we can follow their evolution as we change Λ. Differentiation of Eq. (11.2) with respect to Λ yields for the generating functional of the Green's functions,

$$\partial_\Lambda \mathcal{G} = \left\{ \frac{1}{2} \left(\frac{\delta}{\delta J}, \partial_\Lambda [\mathbf{G}_0^{-1}] \frac{\delta}{\delta J} \right) - \partial_\Lambda \ln \mathcal{Z}_0 \right\} \mathcal{G} \,. \tag{11.43}$$

For the connected version $\mathcal{G}_c[J] = \ln \mathcal{G}[J]$ we obtain

$$\partial_\Lambda \mathcal{G}_c = \frac{1}{2} \left(\frac{\delta \mathcal{G}_c}{\delta J}, \partial_\Lambda [\mathbf{G}_0^{-1}] \frac{\delta \mathcal{G}_c}{\delta J} \right) + \frac{1}{2} \mathrm{Tr} \left(\partial_\Lambda [\mathbf{G}_0^{-1}] \left[\frac{\delta^{(2)} \mathcal{G}_c}{\delta J \delta J} \right]^T \right) - \partial_\Lambda \ln \mathcal{Z}_0 \,. \tag{11.44}$$

In the derivation of flow equations for $\mathcal{L}$ or Γ [see Eqs. (11.17) and (11.23)], we should keep in mind that in these functionals the fields Φ are held constant rather than the sources J. Hence, Eq. (11.17) implies

$$\partial_\Lambda \mathcal{L}[\Phi] = - \left. \partial_\Lambda \mathcal{G}_c[J] \right|_{J = J_\Lambda[\Phi]} \,. \tag{11.45}$$

Using this and Eq. (11.44) we obtain for the functional $\Gamma[\Phi] = \mathcal{L}[\Phi] - S_0[\Phi]$,

$$\partial_\Lambda \Gamma = -\frac{1}{2} \mathrm{Tr} \left(\partial_\Lambda [\mathbf{G}_0^{-1}] \left[\frac{\delta^{(2)} \mathcal{G}_c}{\delta J \delta J} \right]^T \right) + \partial_\Lambda \ln \mathcal{Z}_0 \,. \tag{11.46}$$

To derive a closed equation for Γ, we express the matrix $\frac{\delta^{(2)} \mathcal{G}_c}{\delta J \delta J}$ in terms of derivatives of Γ using Eq. (11.30). After some rearrangements we obtain the exact flow equation for the generating functional $\Gamma[\Phi]$ of the one-line irreducible vertices

$$\begin{aligned} \partial_\Lambda \Gamma \;\; = \;\; & -\frac{1}{2} \mathrm{Tr} \left[\mathbf{Z} \dot{\mathbf{G}}^T \mathbf{U}^T \left\{ \mathbf{1} - \mathbf{G}^T \mathbf{U}^T \right\}^{-1} \right] \\ & -\frac{1}{2} \mathrm{Tr} \left[\mathbf{Z} \dot{\mathbf{G}}_0^T \mathbf{\Sigma}^T \left\{ \mathbf{1} - \mathbf{G}_0^T \mathbf{\Sigma}^T \right\}^{-1} \right] , \end{aligned} \tag{11.47}$$

where the matrix $\mathbf{U}[\Phi]$ is the field-dependent part of the second functional derivative of $\Gamma[\Phi]$, as defined in Eq. (11.27). For convenience we have introduced the single-scale propagator $\dot{\mathbf{G}}$ as

$$\dot{\mathbf{G}} = -\mathbf{G} \partial_\Lambda [\mathbf{G}_0^{-1}] \mathbf{G} = [\mathbf{1} - \mathbf{G}_0 \mathbf{\Sigma}]^{-1} \left(\partial_\Lambda \mathbf{G}_0 \right) [\mathbf{1} - \mathbf{\Sigma} \mathbf{G}_0]^{-1} \,, \tag{11.48}$$

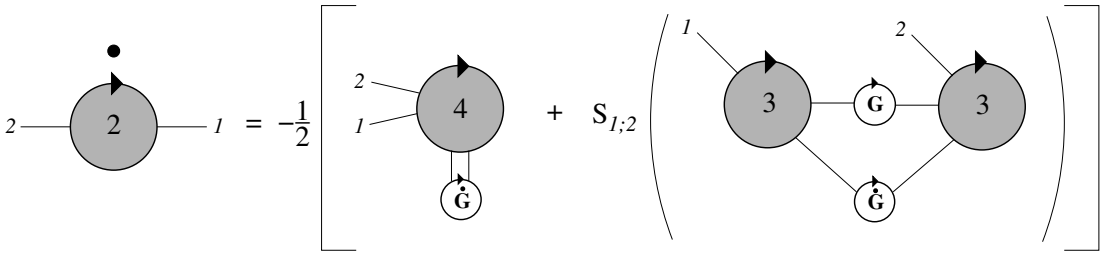

Figure 11.3: Flow of the totally symmetric two-point vertex. Empty circles with $\mathbf{G}$ and $\dot{\mathbf{G}}$ represent the exact matrix propagator $\mathbf{G}$ and the single-scale propagator $\dot{\mathbf{G}}$. The dot on the left-hand side denotes the derivative ∂_Λ.

which reduces to $\dot{\mathbf{G}}_0 = \partial_\Lambda \mathbf{G}_0$ in the absence of interactions.

The second line in Eq. (11.47) does not depend on the fields any longer and therefore represents the flow of the interaction correction $\Gamma^{(0)}$ to the grand-canonical potential,

$$\partial_\Lambda \Gamma^{(0)} = -\frac{1}{2}\mathrm{Tr}\left[\mathbf{Z}\dot{\mathbf{G}}_0^T \mathbf{\Sigma}^T \left\{\mathbf{1} - \mathbf{G}_0^T \mathbf{\Sigma}^T\right\}^{-1}\right] . \tag{11.49}$$

On the other hand, the first line on the right-hand side of Eq. (11.47) gives the flow of one-line irreducible vertices. We can generate their hierarchy of flow equations by expanding both sides in powers of the fields. On the left-hand side, we simply insert the functional Taylor expansion (11.25) of $\Gamma[\Phi]$, while on the right-hand side we substitute the expansion of $\mathbf{U}[\Phi]$ given in Eq. (11.33). For a comparison of the coefficients on both sides, the right-hand side has to be symmetrized with respect to external lines on different vertices. We can write down the resulting infinite system of flow equations for the one-line irreducible vertices $\Gamma^{(n)}$ with $n \geq 1$ in the following closed form,

$$\begin{aligned}
&\partial_\Lambda \Gamma^{(n)}_{\alpha_1,\ldots,\alpha_n} = \qquad\qquad (11.50)\\
&-\frac{1}{2}\sum_{l=1}^{\infty}\sum_{m_1,\ldots,m_l=1}^{\infty} \delta_{n,m_1+\ldots+m_l}\, \mathcal{S}_{\alpha_1,\ldots,\alpha_{m_1};\alpha_{m_1+1},\ldots,\alpha_{m_1+m_2};\ldots;\alpha_{m_1+\ldots+m_{l-1}+1},\ldots,\alpha_n}\Big\{\\
&\qquad \times \mathrm{Tr}\left[\mathbf{Z}\dot{\mathbf{G}}^T \mathbf{\Gamma}^{(m_1+2)\,T}_{\alpha_1,\ldots,\alpha_{m_1}} \mathbf{G}^T \mathbf{\Gamma}^{(m_2+2)\,T}_{\alpha_{m_1+1},\ldots,\alpha_{m_1+m_2}} \mathbf{G}^T \ldots \mathbf{\Gamma}^{(m_l+2)\,T}_{\alpha_{m_1+\ldots+m_{l-1}+1},\ldots,\alpha_n}\right]\Big\} .
\end{aligned}$$

Here the matrices $\mathbf{\Gamma}^{(m+2)}_{\alpha_1\ldots\alpha_m}$ are given in Eq. (11.34) and the symmetrization operator $\mathcal{S}$ is defined in Eq. (11.37).

Figs. 11.3, 11.4, and 11.5 show a graphical representation of the flow of the vertices $\Gamma^{(2)}$, $\Gamma^{(3)}$, and $\Gamma^{(4)}$. Note how a change of the cutoff Λ generates higher-order vertices contracted in a loop by propagators $\mathbf{G}$ and $\dot{\mathbf{G}}$.

With the graphical notation for the totally symmetric vertices introduced in Fig. 11.1 all the signs and combinatorics have a graphical representation. In the

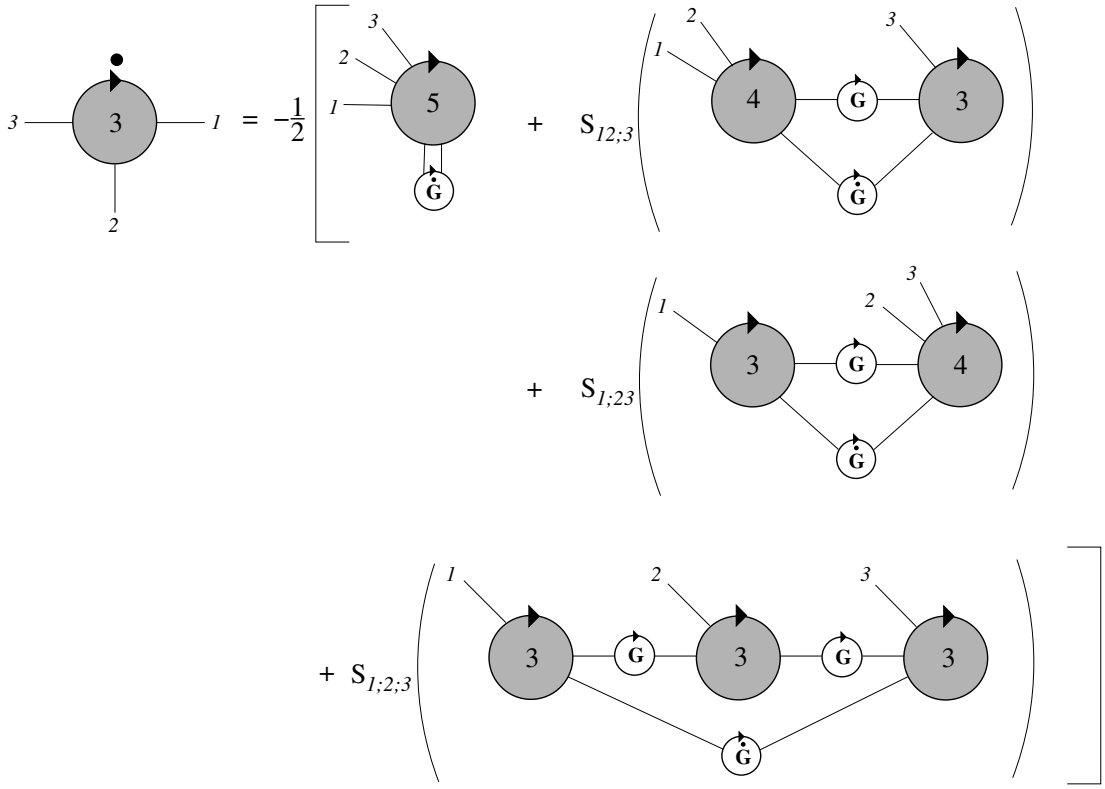

Figure 11.4: Graphical representation of the flow of the totally symmetric three-point vertex.

next two chapters we will leave the shorthand notation and go back to more physical vertices, explicitly exhibiting the different types of fields. All this can be done on a graphical level and involves only straightforward combinatorics. In this sense the derivation of higher flow equations is at the same level of complexity as ordinary Feynman graph expansions.

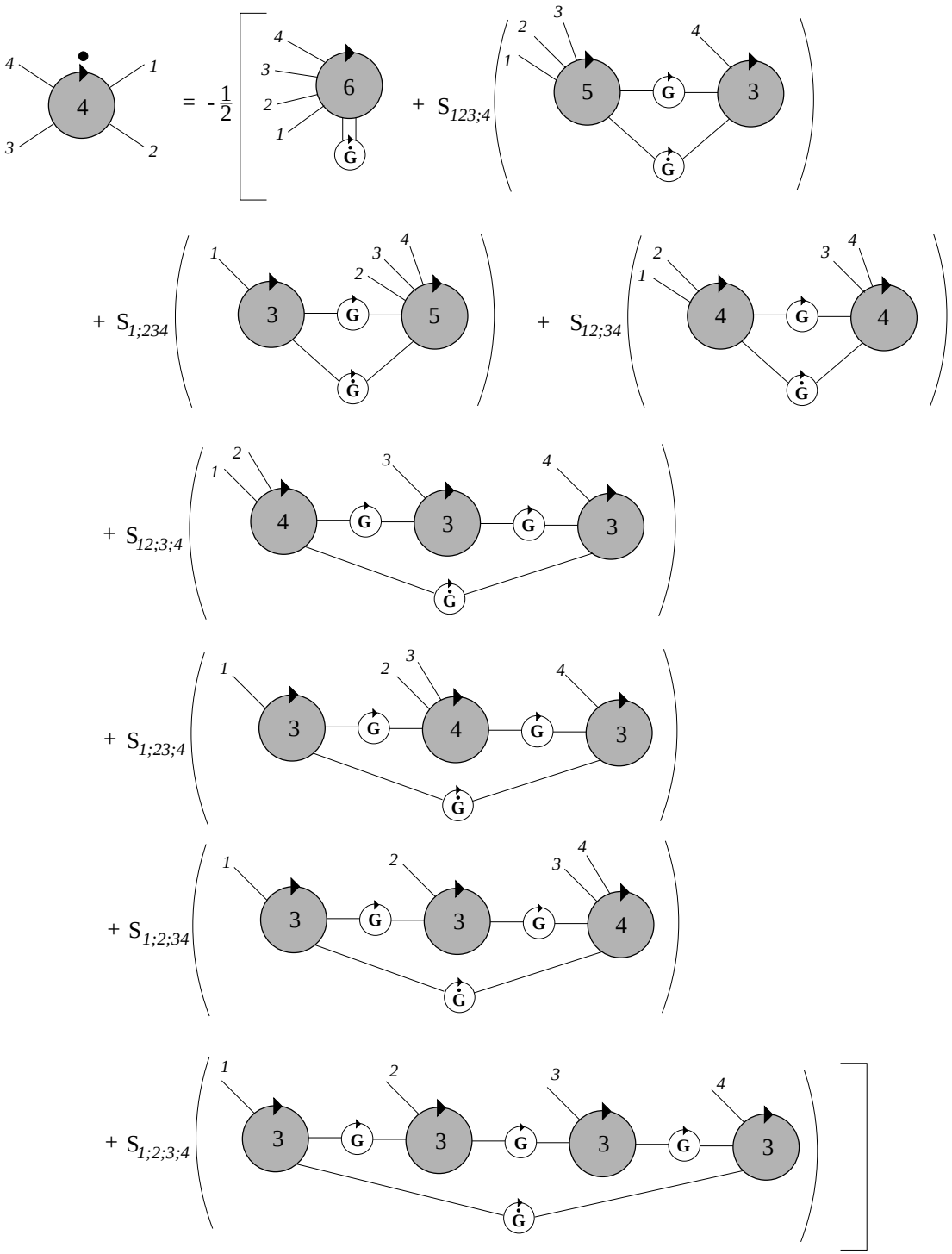

Figure 11.5: Graphical representation of the flow of the totally symmetric four-point vertex.

Chapter 12:

Symmetries of the Fermi-Bose theory

In this chapter, we return to the mixed Fermi-Bose theory which we have derived in Chap. 10 by a Hubbard-Stratonovich transformation and explore the consequences of symmetries of the action. This leads to identities for the generating functionals which are known as Ward identities. When the generating functionals are expanded in powers of the fields, one obtains Ward identities among the vertices. Momentum and particle number conservation is discussed in Secs. 12.1 and 12.2. It will be explicitly used in the next chapter for the definition of the physical vertex functions.

Dyson-Schwinger equations of motion are derived in Sec. 12.3. Although they are not related to a special symmetry of the action, their derivation proceeds along the same line as for the functional Ward identities. Therefore, they are also discussed in this chapter.

In Sec. 12.4, we consider local gauge transformations which lead to Ward identities involving current and charge vertices. When the dispersion can be linearized about a given point on the Fermi surface, current and charge vertices are proportional to each other for small momentum transfers. This can be exploited for a solution of the forward scattering problem [Metzner *et al.*, 1998]. For the Tomonaga-Luttinger model the dispersion is strictly linear and the Ward identities yield exact equalities expressing higher correlation functions in terms of lower ones. Combined with skeleton diagrams this leads to an integral equation for the single-particle Green's function [Dzyaloshinskii and Larkin, 1974]. Yet, in the limit of an infinite bandwidth cutoff Λ_F a linear dispersion is not bounded from below and the theory is not well defined without regularization. The resulting anomaly is briefly discussed.

Here, we only derive symmetry relations that are explicitly used in later chapters. Other symmetries, as, e.g., rotational invariance in spin space could be discussed along the same lines, leading to further constraints on the parametrization of vertex functions.

12.1 Translational invariance

The vertex functions of a system that is translationally invariant in space and time obey momentum and frequency conservation. To show this, we perform a Fourier transformation of the fields of our mixed Fermi-Bose theory to real space

and imaginary time. The transformation reads

$$\psi_\sigma(X) = \int_K \psi_{K\sigma}\, e^{iK\cdot X}\,, \quad \bar\psi_\sigma(X) = \int_K \bar\psi_{K\sigma}\, e^{-iK\cdot X}\,, \quad \varphi_\sigma(X) = \int_{\bar K} \varphi_{\bar K\sigma}\, e^{i\bar K\cdot X}\,, \tag{12.1}$$

where the composite position index is $X = (\tau, \mathbf{r})$, and the scalar product is defined as $K \cdot X = \mathbf{k}\cdot\mathbf{r} - \omega\tau$. The inverse Fourier transformation is given by

$$\psi_{K\sigma} = \int_X \psi_\sigma(X)\, e^{-iK\cdot X}\,, \quad \bar\psi_{K\sigma} = \int_X \bar\psi_\sigma(X)\, e^{iK\cdot X}\,, \quad \varphi_{\bar K\sigma} = \int_X \varphi_\sigma(X)\, e^{-i\bar K\cdot X}\,. \tag{12.2}$$

Remember that $\bar K = (i\bar\omega, \bar{\mathbf{k}})$ contains a bosonic Matsubara frequency. The integration over space and time is given by

$$\int_X = \int d^D r \int_0^\beta d\tau\,. \tag{12.3}$$

We now perform a shift in imaginary time and real space,

$$\psi_\sigma(X) \to \psi_\sigma(X+A)\,, \qquad \bar\psi_\sigma(X) \to \bar\psi_\sigma(X+A)\,, \qquad \varphi_\sigma(X) \to \varphi_\sigma(X+A)\,, \tag{12.4}$$

where the shift vector has time and space components, $A = (a_0, \mathbf{a})$. In Fourier space, this transformation is equivalent to

$$\psi_{K\sigma} \to e^{iA\cdot K}\psi_{K\sigma}\,, \qquad \bar\psi_{K\sigma} \to e^{-iA\cdot K}\bar\psi_{K\sigma}\,, \qquad \varphi_{\bar K\sigma} \to e^{iA\cdot\bar K}\varphi_{\bar K\sigma}\,. \tag{12.5}$$

It is straightforward to check that this transformation does not change the action $S[\bar\psi, \psi, \varphi]$ in Eq. (10.16). To first order in A, the source terms in the functional integral for the generating functional $\mathcal{G}$ transform as

$$\begin{aligned}(\bar\psi, j) + (\bar\jmath, \psi) + (J^*, \varphi) &\to (\bar\psi, j) + (\bar\jmath, \psi) + (J^*, \varphi) \\ &+ iA\cdot\left[-\sum_{K\sigma} K\,\bar\psi_{K\sigma} j_{K\sigma} + \sum_{K\sigma} K\,\bar\jmath_{K\sigma}\psi_{K\sigma} + \sum_{\bar K\sigma} \bar K\, J^*_{\bar K\sigma}\varphi_{\bar K\sigma}\right]\,.\end{aligned} \tag{12.6}$$

Furthermore, the functional measure $D[\bar\psi, \psi, \varphi]$ is also invariant under the transformation (12.5). Expanding the functional integral to first order in A, we obtain

$$\begin{aligned} 0 \;=\; & A\cdot\int D[\bar\psi,\psi,\varphi] e^{-S[\bar\psi,\psi,\varphi]+(\bar\psi,j)+(\bar\jmath,\psi)+(J^*,\varphi)} \\ & \times\left[-\sum_{K\sigma} K\,\bar\psi_{K\sigma} j_{K\sigma} + \sum_{K\sigma} K\,\bar\jmath_{K\sigma}\psi_{K\sigma} + \sum_{\bar K\sigma} \bar K\, J^*_{\bar K\sigma}\varphi_{\bar K\sigma}\right]\,. \end{aligned} \tag{12.7}$$

If the fields ψ and $\bar\psi$ in the square brackets in the lower line are replaced by derivatives with respect to the sources $\bar\jmath$ and j, they can be pulled out of the

functional integral. Remember that in explicit notation the generating functional for Green's functions is given by

$$\mathcal{G}[\bar{\jmath}, j, J] = \frac{1}{\mathcal{Z}_0} \int D[\bar{\psi}, \psi, \varphi] e^{-S[\bar{\psi},\psi,\varphi]+(\bar{\jmath},\psi)+(\bar{\psi},j)+(J^*,\varphi)} \,. \tag{12.8}$$

Since A is arbitrary, Eq. (12.7) leads to a functional identity for $\mathcal{G}$,

$$\left[-\sum_{K\sigma} K\, j_{K\sigma} \frac{\delta}{\delta j_{K\sigma}} + \sum_{K\sigma} K\, \bar{\jmath}_{K\sigma} \frac{\delta}{\delta \bar{\jmath}_{K\sigma}} + \sum_{\bar{K}\sigma} \bar{K}\, J^*_{\bar{K}\sigma} \frac{\delta}{\delta J^*_{\bar{K}\sigma}} \right] \mathcal{G} = 0 \,. \tag{12.9}$$

Note that monomials in the fields are eigenoperators of the differential operator in square brackets. The eigenvalue is the total momentum of all the fields with the appropriate signs. Eq. (12.9) thus states that an expansion of the generating functional in powers of the fields can only contain terms with vanishing total momentum. Thus, the Green's functions which are the coefficients in this expansion obey momentum conservation. Since Eq. (12.9) is linear in the derivatives, the generating functional $\mathcal{G}_c = \ln \mathcal{G}$ fulfills the same relation. Translating this into an expression for the generating functional Γ, we obtain

$$\left[-\sum_{K\sigma} K\, \bar{\psi}_{K\sigma} \frac{\delta}{\delta \bar{\psi}_{K\sigma}} + \sum_{K\sigma} K\, \psi_{K\sigma} \frac{\delta}{\delta \psi_{K\sigma}} + \sum_{\bar{K}\sigma} \bar{K}\, \varphi_{\bar{K}\sigma} \frac{\delta}{\delta \varphi_{\bar{K}\sigma}} \right] \Gamma = 0 \,. \tag{12.10}$$

Thus, connected and irreducible vertices also obey momentum and frequency conservation, as expected.

12.2 Global gauge invariance

When no superconducting symmetry breaking occurs, non-relativistic systems conserve the total particle number. This symmetry is related to the global gauge transformation

$$\psi_{K\sigma} \to e^{i\alpha} \psi_{K\sigma} \,, \qquad \bar{\psi}_{K\sigma} \to e^{-i\alpha} \bar{\psi}_{K\sigma} \,, \tag{12.11}$$

which is easily seen to leave the action $S[\bar{\psi}, \psi, \varphi]$ invariant. Following the same steps as in the last section, we obtain the global Ward identity

$$\left[-\sum_{K\sigma} \bar{\psi}_{K\sigma} \frac{\delta}{\delta \bar{\psi}_{K\sigma}} + \sum_{K\sigma} \psi_{K\sigma} \frac{\delta}{\delta \psi_{K\sigma}} \right] \Gamma = 0 \,. \tag{12.12}$$

The differential operators in the square brackets simply count the numbers of $\bar{\psi}$ and ψ fields in a monomial. Thus, Eq. (12.12) states that an expansion of Γ in powers of the fields only contains terms with an equal number of $\bar{\psi}$ and ψ fields. Naturally, similar relations apply to $\mathcal{G}$ and $\mathcal{G}_c$. Thus, all vertices conserve the particle number.

12.3 Dyson-Schwinger equations

The generating functional $\mathcal{G}$ of the Green's functions is also invariant with respect to infinitesimal shifts in the integration variables Φ_α. In the compact notation, this implies the Dyson-Schwinger equations of motion [Zinn-Justin, 2002]

$$\left(\zeta_\alpha J_\alpha - \frac{\delta S}{\delta \Phi_\alpha}\left[\frac{\delta}{\delta J_\alpha}\right]\right)\mathcal{G}[J_\alpha] = 0\,. \tag{12.13}$$

For our coupled Fermi-Bose system with Euclidean action $S[\bar\psi,\psi,\varphi]$ given by Eq. (10.16) and involving three types of fields, Eq. (12.13) is equivalent to the following three equations,

$$\left(J_{-\bar K\sigma} - \sum_{\sigma'}[f^{-1}_{\bar{\mathbf{k}}}]^{\sigma'\sigma}\frac{\delta}{\delta J_{\bar K\sigma'}}\right)\mathcal{G} \;-\; i\zeta\int_K \frac{\delta^{(2)}\mathcal{G}}{\delta j_{K+\bar K\sigma}\delta\bar\jmath_{K\sigma}} = 0\,, \tag{12.14}$$

$$\left(\zeta\bar\jmath_{K\sigma} + [i\omega - \xi_{\mathbf{k}\sigma}]\frac{\delta}{\delta j_{K\sigma}}\right)\mathcal{G} \;-\; i\int_{\bar K} \frac{\delta^{(2)}\mathcal{G}}{\delta j_{K+\bar K\sigma}\delta J_{-\bar K\sigma}} = 0\,, \tag{12.15}$$

$$\left(j_{K\sigma} + [i\omega - \xi_{\mathbf{k}\sigma}]\frac{\delta}{\delta\bar\jmath_{K\sigma}}\right)\mathcal{G} \;-\; i\int_{\bar K} \frac{\delta^{(2)}\mathcal{G}}{\delta\bar\jmath_{K-\bar K\sigma}\delta J_{-\bar K\sigma}} = 0\,. \tag{12.16}$$

Expressing these equations in terms of the generating functionals $\mathcal{G}_c$ of the connected Green's functions and the generating functional Γ of the irreducible vertices defined in Eq. (11.23), we obtain the Dyson-Schwinger equations of motion in the following form,

$$\frac{\delta\Gamma}{\delta\varphi_{\bar K\sigma}} - i\int_K\left[\bar\psi_{K+\bar K,\sigma}\psi_{K\sigma} \;+\; \frac{\delta^{(2)}\mathcal{G}_c}{\delta\bar\jmath_{K\sigma}\delta j_{K+\bar K,\sigma}}\right] = 0\,, \tag{12.17}$$

$$\frac{\delta\Gamma}{\delta\psi_{K\sigma}} - i\int_{\bar K}\left[\zeta\bar\psi_{K+\bar K,\sigma}\varphi_{\bar K\sigma} + \frac{\delta^{(2)}\mathcal{G}_c}{\delta j_{K+\bar K,\sigma}\delta J_{-\bar K\sigma}}\right] = 0\,, \tag{12.18}$$

$$\frac{\delta\Gamma}{\delta\bar\psi_{K\sigma}} - i\int_{\bar K}\left[\psi_{K-\bar K,\sigma}\varphi_{\bar K\sigma} \;+\; \frac{\delta^{(2)}\mathcal{G}_c}{\delta\bar\jmath_{K-\bar K,\sigma}\delta J_{-\bar K\sigma}}\right] = 0\,. \tag{12.19}$$

The second functional derivatives of $\mathcal{G}_c$ can be expressed in terms of the irreducible vertices using Eq. (11.30) to obtain an equation in terms of Γ only. In Sec. 13.5.1, we will obtain skeleton relations between irreducible vertices from Eqs. (12.17–12.19).

12.4 Local gauge transformations

We now analyze the consequences of gauge transformations that are local in space and time. To do this, we rewrite the parts of the action involving the fermionic

fields $\bar{\psi}$ and ψ in real space and imaginary time using the Fourier transformation in Eq. (12.2). The Euclidean action reads

$$\begin{aligned} S[\bar{\psi},\psi,\varphi] &= S_0[\bar{\psi},\psi] + S_0[\varphi] + S_1[\bar{\psi},\psi,\varphi] \\ S_0[\bar{\psi},\psi] &= \sum_\sigma \int_X \bar{\psi}_\sigma(X)\partial_\tau \psi_\sigma(X) \\ &+ \sum_\sigma \int d\tau \int d^D r \int d^D r'\, \bar{\psi}_\sigma(\tau,\mathbf{r})\xi_\sigma(\mathbf{r}-\mathbf{r}')\psi_\sigma(\tau,\mathbf{r}') \;, \quad (12.20) \\ S_1[\bar{\psi},\psi,\varphi] &= i\sum_\sigma \int_X \bar{\psi}_\sigma(X)\psi_\sigma(X)\varphi_\sigma(X) \;, \quad (12.21) \end{aligned}$$

where we have defined the Fourier transform of the dispersion

$$\xi_\sigma(\mathbf{r}) = \int \frac{d^D k}{(2\pi)^D}\, \xi_{\mathbf{k}\sigma}\, e^{i\mathbf{k}\cdot\mathbf{r}} \;. \quad (12.22)$$

Suppose we perform the following local gauge transformation on the fermion fields,

$$\psi_\sigma(X) \to e^{i\alpha_\sigma(X)}\psi_\sigma(X)\,, \quad \bar{\psi}_\sigma(X) \to e^{-i\alpha_\sigma(X)}\bar{\psi}_\sigma(X)\,, \quad (12.23)$$

where $\alpha_\sigma(X)$ is an arbitrary real function. To linear order in $\alpha_\sigma(X)$, the action (12.21) transforms as

$$\begin{aligned} S[\bar{\psi},\psi,\varphi] \to S[e^{-i\alpha}\bar{\psi}, e^{i\alpha}\psi,\varphi] = S[\bar{\psi},\psi,\varphi] + \; i\sum_\sigma \int_X \bar{\psi}_\sigma(X)[\partial_\tau \alpha_\sigma(X)]\psi_\sigma(X) \\ - i\sum_\sigma \int d\tau \int d^D r \int d^D r'\, \bar{\psi}_\sigma(\tau,\mathbf{r})[\alpha_\sigma(\tau,\mathbf{r}) - \alpha_\sigma(\tau,\mathbf{r}')]\xi_\sigma(\mathbf{r}-\mathbf{r}')\psi_\sigma(\tau,\mathbf{r}') \;. \quad (12.24) \end{aligned}$$

Using this relation and the fact the functional measure is invariant under the transformation (12.23), we obtain

$$\begin{aligned} 0 = \frac{1}{\mathcal{Z}_0}\int D[\bar{\psi},\psi,\varphi] e^{-S[\bar{\psi},\psi,\varphi]+(\bar{\jmath},\psi)+(\bar{\psi},j)+(J,\varphi)} \Bigg\{ \\ + \sum_\sigma \int d\tau \int d^D r \int d^D r'\, \bar{\psi}_\sigma(\tau,\mathbf{r})[\alpha_\sigma(\tau,\mathbf{r}) - \alpha_\sigma(\tau,\mathbf{r}')]\xi_\sigma(\mathbf{r}-\mathbf{r}')\psi_\sigma(\tau,\mathbf{r}') \\ - \sum_\sigma \int_X \bar{\psi}_\sigma(X)[\partial_\tau \alpha_\sigma(X)]\psi_\sigma(X) + (\bar{\jmath},\alpha\psi) - (\bar{\psi}\alpha, j) \Bigg\} \;. \quad (12.25) \end{aligned}$$

Taking the functional derivative of this equation with respect to $\alpha_\sigma(X)$ and transforming back to Fourier space,

$$0 = \int_K \left\{ \left[i\bar{\omega} - \xi_{\mathbf{k}+\bar{\mathbf{k}},\sigma} + \xi_{\mathbf{k}\sigma}\right] \frac{\delta^{(2)}\mathcal{G}}{\delta \bar{\jmath}_{K\sigma}\delta j_{K+\bar{K}\sigma}} + \bar{\jmath}_{K+\bar{K}\sigma}\frac{\delta \mathcal{G}}{\delta \bar{\jmath}_{K\sigma}} - j_{K\sigma}\frac{\delta \mathcal{G}}{\delta j_{K+\bar{K}\sigma}} \right\} \;. \quad (12.26)$$

This equation can also be expressed in terms of the generating functional $\mathcal{G}_c = \ln \mathcal{G}$ of connected Green's functions and the generating functional Γ of irreducible vertices. We obtain the following master Ward identity,

$$0 = \int_K \left\{ \left[i\bar{\omega} - \xi_{\mathbf{k}+\bar{\mathbf{k}},\sigma} + \xi_{\mathbf{k}\sigma} \right] \frac{\delta^{(2)}\mathcal{G}_c}{\delta \bar{\jmath}_{K\sigma} \delta j_{K+\bar{K}\sigma}} + \psi_{K\sigma} \frac{\delta \Gamma}{\delta \psi_{K+\bar{K}\sigma}} - \bar{\psi}_{K+\bar{K}\sigma} \frac{\delta \Gamma}{\delta \bar{\psi}_{K\sigma}} \right\} . \tag{12.27}$$

Alternatively, using the Dyson-Schwinger equation (12.17), we may rewrite this as

$$\begin{aligned} 0 &= i\bar{\omega} \left[\frac{\delta \Gamma}{\delta \varphi_{\bar{K}\sigma}} - i \int_K \bar{\psi}_{K+\bar{K}\sigma} \psi_{K\sigma} \right] - i \int_K (\xi_{\mathbf{k}+\bar{\mathbf{k}},\sigma} - \xi_{\mathbf{k}\sigma}) \frac{\delta^{(2)}\mathcal{G}_c}{\delta \bar{\jmath}_{K\sigma} \delta j_{K+\bar{K}\sigma}} \\ &\quad + i \int_K \left[\psi_{K\sigma} \frac{\delta \Gamma}{\delta \psi_{K+\bar{K}\sigma}} - \bar{\psi}_{K+\bar{K}\sigma} \frac{\delta \Gamma}{\delta \bar{\psi}_{K\sigma}} \right] . \end{aligned} \tag{12.28}$$

If we are interested in vertices involving at least one fermionic momentum and if the momentum transfered by the interaction is small, our master Ward identities (12.27) and (12.28) can be further simplified. Then all fermionic momenta lie close to a given point $\mathbf{k}_{F,\sigma}$ on the Fermi surface so that Eqs. (12.27) and (12.28) become simpler if we assume asymptotic velocity conservation. This means that we replace under the integral sign

$$\xi_{\mathbf{k}+\bar{\mathbf{k}},\sigma} - \xi_{\mathbf{k}\sigma} \to \mathbf{v}_{F,\sigma} \cdot \bar{\mathbf{k}} , \tag{12.29}$$

This approximation amounts to the linearization of the energy dispersion relative to the point $\mathbf{k}_{F,\sigma}$ on the Fermi surface. Using again Eq. (12.17), our master Ward identity becomes

$$\begin{aligned} 0 &= (i\bar{\omega} - \mathbf{v}_{F,\sigma} \cdot \bar{\mathbf{k}}) \left[\frac{\delta \Gamma}{\delta \varphi_{\bar{K}\sigma}} - i \int_K \bar{\psi}_{K+\bar{K}\sigma} \psi_{K\sigma} \right] \\ &\quad + i \int_K \left[\psi_{K\sigma} \frac{\delta \Gamma}{\delta \psi_{K+\bar{K}\sigma}} - \bar{\psi}_{K+\bar{K}\sigma} \frac{\delta \Gamma}{\delta \bar{\psi}_{K\sigma}} \right] . \end{aligned} \tag{12.30}$$

This simplified master Ward identity will be used in Sec. 14.3 to derive Ward identities for irreducible vertices with two external fermion lines and an arbitrary number of boson lines.

For the Tomonaga-Luttinger model (TLM) with an infinite bandwidth cutoff $\Lambda_F \to \infty$, the dispersion is strictly linear and one might expect that Eq. (12.30) becomes exact. Note, however, that Eq. (12.30) then predicts a vanishing polarization $\delta^2\Gamma/\delta\varphi_{\bar{K}\sigma}\delta\varphi_{-\bar{K}\sigma}$. This is a consequence of the well-known anomaly of the TLM due to the fact that the energy dispersion is not bounded from below. Thus, without further regularization, the model does not have a well defined

ground state [Mattis and Lieb, 1965]. In the operator formalism this problem can be resolved by working in a Hilbert space of states with only a finite number of holes with respect to the non-interacting ground state. In other words, there is an infinite Dirac sea of filled states with negative energy. As a consequence, the density operators $\hat{\rho}_{\bar{k}\sigma}$ defined in the introduction no longer commute, but, after proper normalization, they obey canonical commutation relations of bosonic creation and annihilation operators. This fact constitutes the basis of the operator version of bosonization. Alternatively, the anomalous commutators can be obtained by keeping a finite but large bandwidth cutoff Λ_F and by sending $\Lambda_F \to \infty$ only at the very end [Metzner and DiCastro, 1992]. In the functional integral formalism, the anomaly appears through the Jacobian of the transformation (12.23). Although it always vanishes for a finite bandwidth cutoff, it is a priori not well defined in the limit $\Lambda_F \to \infty$. In the field-theoretical literature [Fujikawa, 1980] a method has been developed to regularize the functional integral in a way that allows a correct treatment of the Jacobian for $\Lambda_F \to \infty$. The same anomaly as in the operator formalism is recovered (see [Stone, 1994]). In Chap. 14, we will use Eq. (12.30) to derive Ward identities only for irreducible vertices with two Fermi lines and an arbitrary number of bosonic lines. In these relations the anomaly does not appear. Furthermore, we show that these Ward identities constitute a solution of a hierarchy of flow equations by an inductive argument entirely within the formalism of the fRG. The purely bosonic vertices will be treated by a reference to diagrammatics in the form of the closed-loop theorem which treats the polarization correctly.

Chapter 13:

Functional RG for mixed field theory

Here, the general formalism of Chap. 11 is applied to the coupled Fermi-Bose theory derived in Chap. 10. The physical vertices can be defined in a way that explicitly displays particle number and momentum conservation as discussed in the last chapter. The dependence of connected and one-line-irreducible vertices on indices of different field type is spelled out in detail in Sec. 13.1. Furthermore, we give graphical representations of the first terms of the tree expansion. As a preparation for the functional renormalization group treatment, we discuss different ways of introducing a cutoff in Sec. 13.2. Subsequently, we derive the hierarchy of functional RG equations for the one-line irreducible vertices in Sec. 13.3. Rescaling of momenta, frequencies and fields is performed in Sec. 13.4 in order to classify the vertices according to their scaling dimensions. In the following section, we then propose a new truncation scheme involving the building blocks of the skeleton diagrams for fermionic and bosonic two-point functions. As a preparation, a digression is made to derive skeleton expansions from the Dyson-Schwinger equations obtained in Sec. 12.3.

13.1 Definition of physical vertices

The general vertices defined in Chap. 11 are not suitable for practical calculations. Usually, the generating functionals are rather expanded in terms of correlation functions which respect the symmetries of particle number conservation as well as momentum and frequency conservation discussed in the previous chapter. Additionally, the vertices are conventionally not symmetrized with respect to the exchange of legs involving different types of fields. Particle number conservation implies that in- and outgoing particle fields, ψ and $\bar{\psi}$ respectively, always occur in pairs. If we explicitly display momentum and frequency conservation, the expansion for Γ reads

$$\begin{aligned}\Gamma[\bar{\psi},\psi,\varphi] \;=\; & \sum_{n=0}^{\infty}\sum_{m=0}^{\infty}\frac{1}{(n!)^2 m!}\int_{K_1'\sigma_1'}\cdots\int_{K_n'\sigma_n'}\int_{K_1\sigma_1}\cdots\int_{K_n\sigma_n}\int_{\bar{K}_1\bar{\sigma}_1}\cdots\int_{\bar{K}_m\bar{\sigma}_m} \\ & \times\delta_{K_1'+\ldots+K_n',K_1+\ldots+K_n+\bar{K}_1+\ldots+\bar{K}_m} \\ & \times\Gamma^{(2n,m)}(K_1'\sigma_1',\ldots,K_n'\sigma_n';K_1\sigma_1,\ldots,K_n\sigma_n;\bar{K}_1\bar{\sigma}_1,\ldots,\bar{K}_m\bar{\sigma}_m) \\ & \times\bar{\psi}_{K_1'\sigma_1'}\cdot\ldots\cdot\bar{\psi}_{K_n'\sigma_n'}\psi_{K_1\sigma_1}\cdot\ldots\cdot\psi_{K_n\sigma_n}\varphi_{\bar{K}_1\bar{\sigma}_1}\cdot\ldots\cdot\varphi_{\bar{K}_m\bar{\sigma}_m}\,. \qquad (13.1)\end{aligned}$$

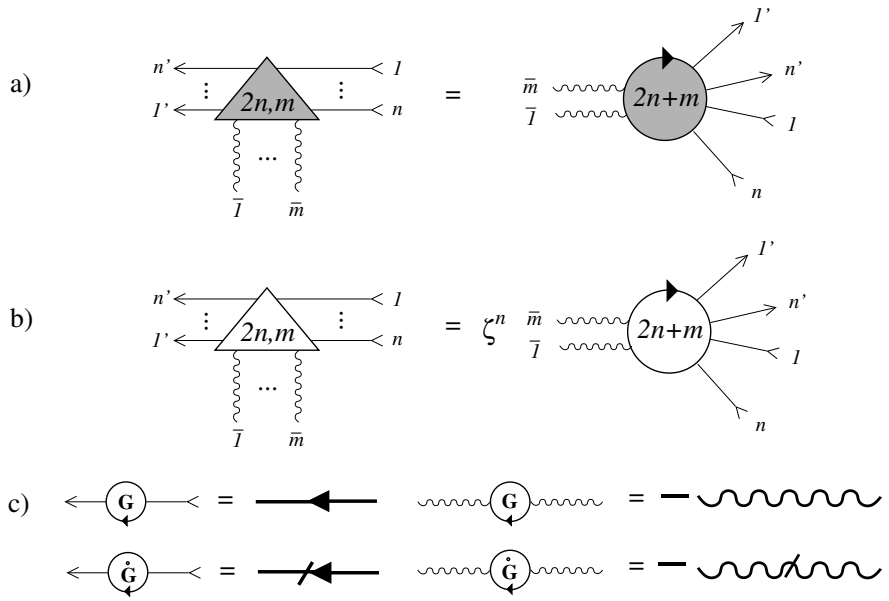

Figure 13.1: Pictorial dictionary to translate graphs involving totally symmetrized vertices to those involving physical vertices, which are only symmetrized within fields of the same type. Relations are given for a) the irreducible vertices, b) the connected Green's functions and c) the full propagators and single scale propagators. The diagrams on the right hand sides in c) represent G, $\dot{G}$, F and $\dot{F}$ respectively. Note the slash on the lines for the single scale propagators.

Naturally, this expansion assumes that the symmetries are not spontaneously broken, and thus anomalous such as superconducting correlation functions are excluded from now on. Diagrammatically, we represent a physical vertex $\Gamma^{(2n,m)}$ involving $2n$ external fermion legs and m external boson legs by a shaded triangle as in Fig. 13.1a. A triangle is used to emphasize that our theory contains three types of fields, and the shading distinguishes it from the diagrams for connected vertices defined below. We represent a leg associated with a $\bar{\psi}$ field by an arrow pointing outwards, a leg for ψ by an arrow pointing inwards, and a leg for φ with a wiggly line without an arrow. Recall that our Bose field is real because it couples to the density, so that it should be represented graphically by an undirected line. Apart from the energy and momentum conserving delta function, the totally symmetric vertices defined by the expansion (11.25) coincide with the non-symmetric ones in Eq. (13.1) for the same order of the indices, i.e.,

$$\Gamma^{(2n+m)}_{(\bar{\psi},K'_1,\sigma'_1),\ldots,(\bar{\psi},K'_n,\sigma'_n),(\psi,K_1,\sigma_1),\ldots,(\psi,K_n,\sigma_n),(\varphi,\bar{K}_1,\bar{\sigma}_1),\ldots,(\varphi,\bar{K}_m,\bar{\sigma}_m)} = \delta_{K'_1+\ldots+K'_n,K_1+\ldots+K_n+\bar{K}_1+\ldots+\bar{K}_m}\Gamma^{(2n,m)}(K'_1\sigma'_1,\ldots,\bar{K}_m\bar{\sigma}_m)\,, \qquad (13.2)$$

where components of the multi-indices are enclosed in brackets and the first (greek) letter indicates the field type. This relation is represented diagrammatically in Fig. 13.1a.

Similarly, the connected Green's functions are defined by the functional expansion of $\mathcal{G}_c$

$$\begin{aligned}\mathcal{G}_c[\bar{\jmath}, j, J] \;=\; & \sum_{n=0}^{\infty}\sum_{m=0}^{\infty}\frac{1}{(n!)^2 m!}\int_{K_1'\sigma_1'}\cdots\int_{K_n'\sigma_n'}\int_{K_1\sigma_1}\cdots\int_{K_n\sigma_n}\int_{\bar{K}_1\bar{\sigma}_1}\cdots\int_{\bar{K}_m\bar{\sigma}_m} \\ & \times\delta_{K_1'+\ldots+K_n',K_1+\ldots+K_n+\bar{K}_1+\ldots+\bar{K}_m} \\ & \times\mathcal{G}_c^{(2n,m)}(K_1'\sigma_1',\ldots,K_n'\sigma_n';K_1\sigma_1,\ldots,K_n\sigma_n;\bar{K}_1\bar{\sigma}_1,\ldots,\bar{K}_m\bar{\sigma}_m) \\ & \times\bar{\jmath}_{K_1'\sigma_1'}\cdot\ldots\cdot\bar{\jmath}_{K_n'\sigma_n'}j_{K_1\sigma_1}\cdot\ldots\cdot j_{K_n\sigma_n}J_{\bar{K}_1\bar{\sigma}_1}\cdot\ldots\cdot J_{\bar{K}_m\bar{\sigma}_m}\,. \end{aligned} \tag{13.3}$$

An analogous expansion for $\mathcal{G}$ defines the (not necessarily connected) Green's functions $\mathcal{G}^{(2n,m)}$. With this definition, the connected correlation function are equivalent to the following connected functional averages with respect to the full action

$$\begin{aligned}&\delta_{K_1'+\ldots+K_n',K_1+\ldots+K_n+\bar{K}_1+\ldots+\bar{K}_m}\mathcal{G}_c^{(2n,m)}(K_1'\sigma_1',\ldots\ldots,\bar{K}_m\bar{\sigma}_m) \\ &= \langle\psi_{K_1'\sigma_1}\cdot\ldots\cdot\psi_{K_n'\sigma_n}\bar{\psi}_{K_1\sigma_1'}\cdot\ldots\cdot\bar{\psi}_{K_n\sigma_n'}\varphi_{-\bar{K}_1\bar{\sigma}_1}\cdot\ldots\cdot\varphi_{-\bar{K}_m\bar{\sigma}_m}\rangle_c \\ &\quad= \zeta^n\mathcal{G}^{(2n+m)}_{c,(\psi,K_1',\sigma_1'),\ldots,(\psi,K_n',\sigma_n'),(\bar{\psi},K_1,\sigma_1),\ldots,(\bar{\psi},K_n,\sigma_n),(\varphi,-\bar{K}_1,\bar{\sigma}_1),\ldots,(\varphi,-\bar{K}_m,\bar{\sigma}_m)}\,, \end{aligned} \tag{13.4}$$

where for the last equality we have explicitly used the relation $J = (\bar{\jmath}, \zeta j, J^*)$ between the sources in the compact notation of the last chapter and the sources in the more explicit notation of this chapter. The definition of the prefactor of the Green's function is arbitrary, but for purely fermionic vertices the convention used here is the same as in the textbook [Negele and Orland, 1988]. Diagrammatically, we represent the Green's functions $\mathcal{G}_c^{(2n,m)}$ by empty triangles as in Fig. 13.1b. The legs associated with a source $\bar{\jmath}$ are represented by an arrow pointing outward, the legs associated with a source j point inwards and J is represented by a wiggly line. Note that the source $\bar{\jmath}$ has a field type index ψ such that when connected and irreducible vertices are linked by a matrix multiplication an outgoing line is linked to an ingoing line and vice versa. Likewise, a leg associated with $J_{\bar{K}\sigma}$ has a multi-index $(\varphi, -\bar{K}, \sigma)$ and is linked to a leg associated with $\varphi_{\bar{K}\sigma}$ with a multi-index $(\varphi, \bar{K}, \sigma)$. The different sign of the composite momentum and frequency index $\bar{K}$ assures that the flow of momentum and frequency can be consistently labeled in a diagram, since an *outgoing* momentum of $\bar{K}$ on one vertex becomes an *ingoing* momentum on the next vertex.

For systems with particle number conservation which are considered here, the full Green's function has the same block structure as the free Green's function

$$\mathbf{G} = -\left.\frac{\delta^{(2)}\mathcal{G}_c}{\delta J\delta J}\right|_{J=0} = \begin{pmatrix} 0 & \hat{G} & 0 \\ \zeta\hat{G}^T & 0 & 0 \\ 0 & 0 & -\hat{F} \end{pmatrix}. \tag{13.5}$$

Likewise, from Dyson's Eq. (11.10) it is evident that the self-energy $\mathbf{\Sigma}$ has the same block structure as the inverse free Green's function. The matrix $\mathbf{\Sigma}$ contains the one-fermion-line irreducible self-energy $\Sigma_\sigma(K)$ and the one-interaction-line irreducible polarization $\Pi_\sigma(\bar{K})$ in the following blocks,

$$\mathbf{\Sigma} = \begin{pmatrix} 0 & \zeta[\hat{\Sigma}]^T & 0 \\ \hat{\Sigma} & 0 & 0 \\ 0 & 0 & \hat{\Pi} \end{pmatrix} , \tag{13.6}$$

where

$$[\hat{\Sigma}]_{K\sigma,K'\sigma'} = \delta_{K,K'}\delta_{\sigma\sigma'}\Sigma_\sigma(K') , \tag{13.7}$$

$$[\hat{\Pi}]_{\bar{K}\sigma,\bar{K}'\sigma'} = \delta_{\bar{K}+\bar{K}',0}\delta_{\sigma\sigma'}\ \Pi_\sigma(\bar{K}') . \tag{13.8}$$

One-interaction line irreducibility implies that the diagrams for $\Pi_\sigma(\bar{K})$ cannot be separated in two parts by cutting a single interaction line, as explain in detail below. These matrices are spin-diagonal because the bare coupling $S_1[\bar{\psi},\psi,\varphi]$ between Fermi and Bose fields in Eq. (10.18) is diagonal in the spin index. The blocks of the full Green's function matrix $\mathbf{G}$ in Eq. (13.5) contain the exact single-particle Green's function and the effective (screened) interaction,

$$[\hat{G}]_{K\sigma,K'\sigma'} = \delta_{K,K'}\delta_{\sigma\sigma'}G_\sigma(K) , \tag{13.9}$$

$$[\hat{F}]_{\bar{K}\sigma,\bar{K}'\sigma'} = \delta_{\bar{K}+\bar{K}',0}\ F_{\sigma\sigma'}(\bar{K}) , \tag{13.10}$$

with

$$G_\sigma(K) = [G_{0,\sigma}^{-1}(K) - \Sigma_\sigma(K)]^{-1} , \tag{13.11}$$

$$F_{\sigma\sigma'}(\bar{K}) = \left[\hat{F}_0^{-1} + \hat{\Pi}\right]^{-1}_{\bar{K}\sigma,-\bar{K}\sigma'} . \tag{13.12}$$

Diagrammatically, the full Green's function $G_\sigma(K)$ and the effective interaction $F_{\sigma\sigma'}$ are represented by bold directed or wiggly lines respectively. This is depicted in Fig. 13.1c. Also shown are the analogous relations for the single-scale propagators. Again, the matrix $\dot{\mathbf{G}}$ has the same block structure as $\mathbf{G}$ in Eq. (13.5). The corresponding blocks are denoted by $\dot{\hat{G}}$ and $\dot{\hat{F}}$ and are given by

$$[\dot{\hat{G}}]_{K\sigma,K'\sigma'} = \delta_{K,K'}\delta_{\sigma\sigma'}\dot{G}_\sigma(K) , \tag{13.13}$$

$$[\dot{\hat{F}}]_{\bar{K}\sigma,\bar{K}'\sigma'} = \delta_{\bar{K}+\bar{K}',0}\ \dot{F}_{\sigma\sigma'}(\bar{K}) . \tag{13.14}$$

Diagrammatic perturbation theory for the mixed theory contains both fermionic and bosonic propagator lines. This can be seen explicitly from the relation (11.11)

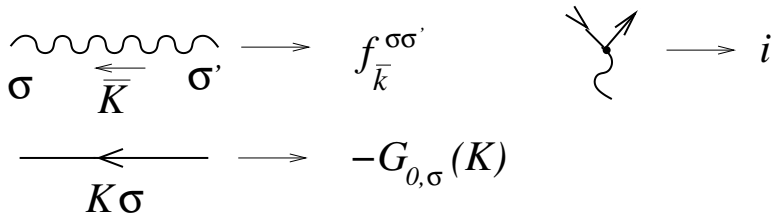

Figure 13.2: Diagrammatic perturbation theory for the physical vertex functions $\mathcal{G}^{(2n,m)}$. In addition to the elements shown here, there is an overall factors of $(-1)^r$ from Eq. (13.15). Moreover, ζ^{L+T} appears, where L is the number of fermion loops in the diagram. Since particle number is conserved, there are n continuous fermion paths connecting ingoing and outgoing particle lines. Here, $T = 0$ or $T = 1$ depending on wether the mapping of ingoing onto outgoing lines defined in this way leads to an even or odd permutation.

applied to our situation. For the Green's functions this yields:

$$\begin{aligned}
&\delta_{K_1'+\ldots+K_n',K_1+\ldots+K_n+\bar{K}_1+\ldots+\bar{K}_m} \\
&\quad\times\mathcal{G}^{(2n,m)}(K_1'\sigma_1',\ldots,K_n'\sigma_n';K_n\sigma_n,\ldots,K_1\sigma_1;\bar{K}_1\bar{\sigma}_1,\ldots,\bar{K}_m\bar{\sigma}_m) \\
&= \zeta^n \frac{\delta^{(2n+m)}}{\delta J_{\bar{K}_m\bar{\sigma}_m}\cdot\ldots\cdot\delta J_{\bar{K}_1\bar{\sigma}_1}\delta\bar{\jmath}_{K_n'\sigma_n'}\delta j_{K_n\sigma_n}\cdot\ldots\cdot\delta\bar{\jmath}_{K_1'\sigma_1'}\delta j_{K_1\sigma_1}} \\
&\quad\times\sum_{r=0}^{\infty}\frac{(-1)^r}{r!}\left[i\sum_\sigma\int_K\int_{\bar{K}}\frac{\delta^{(3)}}{\delta\bar{\jmath}_{K\sigma}\delta j_{K+\bar{K}\sigma}\delta J^*_{\bar{K}\sigma}}\right]^r \\
&\times\exp\left[-\sum_\sigma\int_K\bar{\jmath}_{K\sigma}G_{0,\sigma}(K)j_{K\sigma}+\frac{1}{2}\sum_{\sigma\sigma'}\int_{\bar{K}}f_{\mathbf{k}}^{\sigma\sigma'}J^*_{\bar{K}\sigma}J_{\bar{K}\sigma'}\right]\Bigg|_{\text{sources}=0}
\end{aligned} \tag{13.15}$$

The action of the functional derivatives on the last exponential creates contractions containing the free particle propagator $G_{0,\sigma}(K)$ as well as the bare interaction $f_{\bar{k}}^{\sigma\sigma'}$. The resulting diagrammatic rules are summarized in Fig. 13.2.

One-line irreducibility then implies that the diagrams for the corresponding vertices cannot be split in parts by cutting one of either type of propagator line. One should keep in mind that a boson line represents the two-body electron-electron interaction which is screened by zero-sound bubbles for small momentum transfers. Except for the irreducible polarization itself, our irreducible vertices can thus not be separated in parts by cutting both lines of a zero-sound bubble. In the fermionic language, our vertices are therefore not only one-particle irreducible but are also two-particle irreducible in the zero-sound channel in the sense that particle-hole bubbles are eliminated in favor of the effective bosonic propagator.

With the help of the pictorial dictionary in Fig. 13.1 it is straightforward

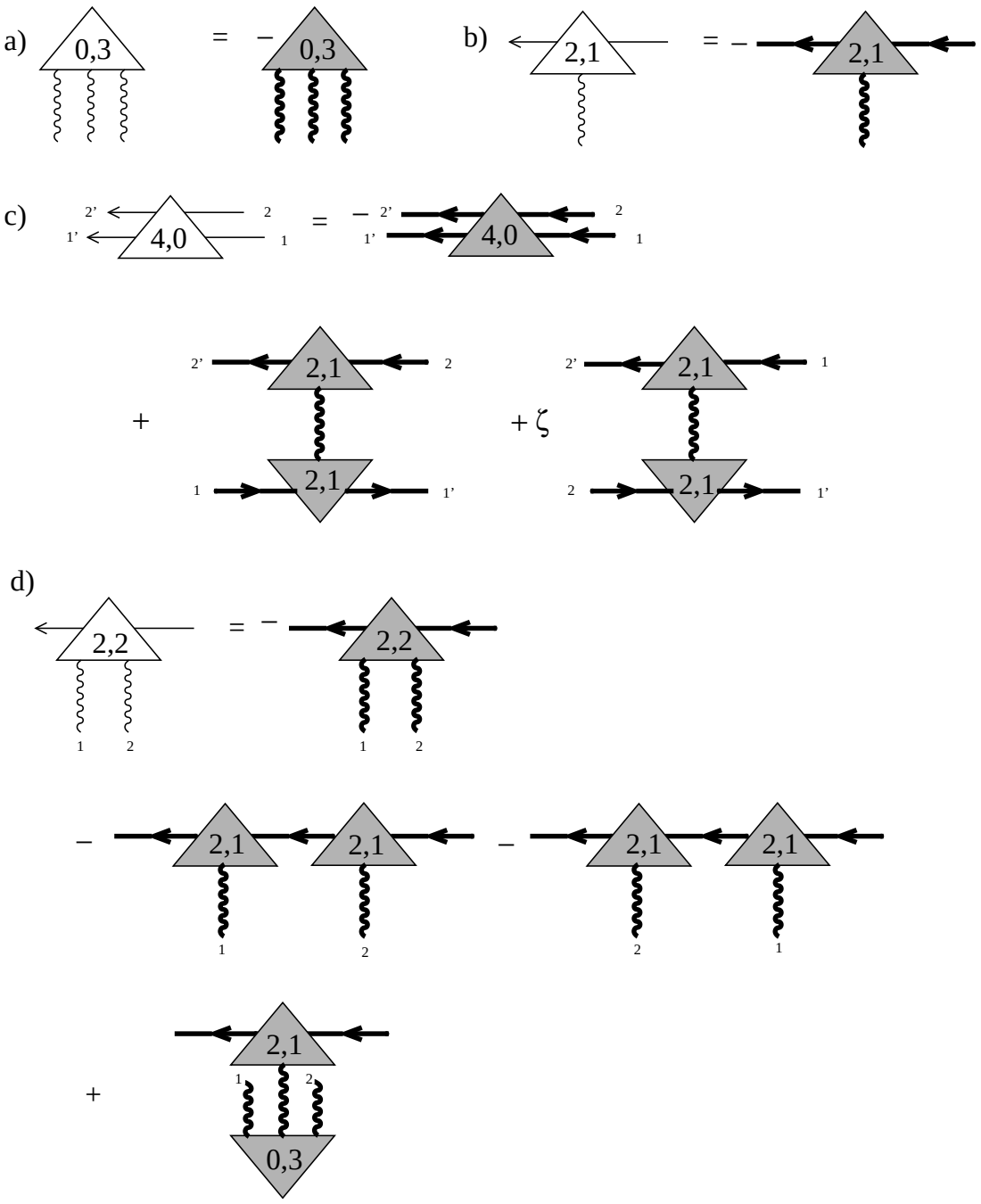

Figure 13.3: Tree expansion for the physical vertices obtained by specializing the general graphs in Fig. 11.2.

to translate the general relations for the symmetrized vertices in Chap. 11 to relations for the physical vertices. First, a definite realization of the external legs has to be chosen. Then the internal sums over the different field species are carried out graphically by replacing the internal lines by lines for the different field types in all possible ways, i.e., by either an oriented solid line (fermions) with two possible orientations or by a wiggly line (bosons). Next, one has to order all the legs on the vertices in an appropriate way keeping track of signs for the interchange of two neighboring fermion legs. Finally, we can use the replacement rules in the pictorial dictionary in Fig. 13.1 to obtain diagrams involving physical correlation functions. By this procedure, we can obtain the leading diagrams of the tree expansion for the physical vertices shown in Fig. 13.3 from the general diagrams in Fig. 11.2. We will derive the RG flow equations for the physical vertices in the same way. Before we do so, we will discuss in more detail the possible choices of the cutoff in the mixed field theory.

13.2 Cutoff schemes

Since the original interaction now appears as a propagator of the field φ, it is possible to introduce a momentum-transfer cutoff in the interaction on the same footing as a bandwidth cutoff. Let us discuss both possibilities in more detail.

A bandwidth cutoff Λ_F restricts the relevant fermionic degrees of freedom to the vicinity of the Fermi surface, and is most natural in the RG approach to fermions in one spatial dimension [Solyom, 1979]. In higher dimensions, the Wilsonian idea of eliminating the degrees of freedom in the vicinity of the Fermi surface is implemented by defining for each momentum $\mathbf{k}$ an associated $\mathbf{k}_F$ by means of a suitable projection onto the Fermi surface [Kopietz and Busche, 2001] and then integrating over fields with momenta in the energy shell $v_0\Lambda_F < |\epsilon_{\mathbf{k}} - \epsilon_{\mathbf{k}_F}| < v_0\Lambda_{F,0}$, where $\epsilon_{\mathbf{k}}$ is the energy dispersion in the absence of interactions. Here v_0 is some suitably defined velocity (for example some average Fermi velocity), which we introduce to give Λ_F units of momentum. Formally, we introduce such a cutoff into our theory by the following substitution for the free fermionic Green's function in Eq. (10.25):

$$\begin{aligned} G_{0,\sigma}(K) \;\longrightarrow\; & \Theta(\Lambda_F < D_K < \Lambda_{F,0})\, G_{0,\sigma}(K) \\ & = \frac{\Theta(\Lambda_F < D_K < \Lambda_{F,0})}{i\omega - \xi_{\mathbf{k}\sigma}} \,, \end{aligned} \tag{13.16}$$

with

$$D_K = |\epsilon_{\mathbf{k}} - \epsilon_{\mathbf{k}_F}|/v_0 \,. \tag{13.17}$$

Here, $\Theta(\Lambda_F < x < \Lambda_{F,0}) = 1$ if the logical expression in the brackets is true, and $\Theta(\Lambda < x < \Lambda_0) = 0$ otherwise. Ambiguities associated with the sharp Θ-function cutoff can be avoided by using smooth versions of the Θ-function and by taking

the sharp cutoff limit at the end of the calculation [Morris, 1994]. In order to construct a consistent scaling theory, the $\mathbf{k}_F$ in Eq. (13.17) should refer to the true Fermi surface of the interacting system, which can be obtained self-consistently from the condition that the RG flows into a fixed point [Kopietz and Busche, 2001, Ledowski and Kopietz, 2003, Ledowski *et al.*, 2005].

The bandwidth cutoff has several disadvantages. On the one hand, for any finite value of the cutoff parameter Λ_F the Ward identities are violated [Katanin, 2004]. Moreover, the RG flow of two-particle response functions probing the response at small momentum transfers (such as the compressibility or the uniform magnetic susceptibility) is artificially suppressed by the bandwidth cutoff. To cure the latter problem, various other parameters have been proposed to serve as flow parameters for the RG, such as temperature [Honerkamp and Salmhofer, 2001b] or even the interaction strength [Honerkamp *et al.*, 2004]. While for practical calculations these new cutoff schemes certainly have advantages, the intuitively appealing RG picture that the coarse-grained parameters of the renormalized theory contain the effect of the degrees of freedom at shorter length scales and higher energies is lost.

To avoid these inconveniences, we can alternatively work with a momentum cutoff Λ_B in the bosonic sector of our theory. This amounts to the replacement

$$\begin{aligned} F_{0,\sigma\sigma'}(\bar{K}) \quad &\longrightarrow \quad \Theta(\Lambda_B < \bar{D}_{\bar{K}} < \Lambda_{B,0})\, F_{0,\sigma\sigma'}(\bar{K}) \\ &= \Theta(\Lambda_B < \bar{D}_{\bar{K}} < \Lambda_{B,0})\, f^{\sigma\sigma'}_{\bar{\mathbf{k}}} \; , \end{aligned} \tag{13.18}$$

where

$$\bar{D}_{\bar{K}} = |\bar{\mathbf{k}}| \; . \tag{13.19}$$

Keeping in mind that the bosonic field mediates the effective interaction, it is clear that Λ_B is a cutoff for the momentum transfer of the interaction. This is the same cutoff scheme employed in the seminal work by Hertz [Hertz, 1976], who discussed also more general frequency-dependent cutoffs for the labels of the bosonic Hubbard-Stratonovich fields, corresponding to more complicated functions $\bar{D}_{\bar{K}}$ than the one given in Eq. (13.19). For one-dimensional electrons, the two possibilities for a cutoff have already been reviewed by Solyom [Solyom, 1979]. Moreover, in the exact solution of the Tomonaga-Luttinger model by means of a careful application of the bosonization method the maximal momentum transfered by the interaction appears as the natural cutoff scale [Schönhammer, 2003].

In our RG approach we have the freedom of keeping both or only one of the two cutoffs: The bandwidth cutoff Λ_F or the momentum-transfer cutoff Λ_B. In particular, we may even get rid of the bandwidth cutoff completely and work with a momentum-transfer cutoff only. We show below that if the interaction transfers only small momenta, then the pure interaction cutoff scheme indeed regularizes all infrared singularities in one dimension. Moreover and most importantly, introducing a cutoff only in the interaction leads to RG flow equations which do not violate the Ward identities responsible for the exact solubility of the TLM.

Given this fact, it is not surprising that we can solve the infinite hierarchy of RG flow equations and obtain the exact single-particle Green's function of the TLM within the framework of the functional RG.

In the limit of a sharp Θ-function cutoff [Morris, 1994] the blocks of the single scale propagator are explicitly given by Eqs. (13.13) and (13.14) with

$$\dot{G}_\sigma(K) = -\frac{\delta(\Lambda - D_K)}{i\omega - \xi_{\mathbf{k}\sigma} - \Sigma_\sigma(K)} , \tag{13.20}$$

$$\dot{F}_{\sigma\sigma'}(\bar{K}) = -\delta(\Lambda - \bar{D}_{\bar{K}}) \left[\hat{F}_0^{-1} + \hat{\Pi}\right]^{-1}_{\bar{K}\sigma,-\bar{K}\sigma'} , \tag{13.21}$$

where on the right-hand side of Eq. (13.21) it is understood that the Θ-function cutoff should be omitted from the matrix elements of $\hat{F}_0$. Furthermore, for the definition of the derivatives in the single scale propagators, we set $\Lambda = \Lambda_F$ in Eq. (13.20), whereas in Eq. (13.21) we set $\Lambda = \Lambda_B$. To derive flow equations for the physical vertices, we formally set $\Lambda = \Lambda_F = \Lambda_B$ from now on. Flow equations for the case that only one of the cutoffs is varied are easily obtained by leaving out terms that do not contain the appropriate single scale propagator $\dot{G}_\sigma(K)$ or $\dot{F}_{\sigma\sigma'}(\bar{K})$, respectively.

13.3 Flow equations for physical vertices

Renormalization group flow equations for the physical vertex functions are obtained from the flow equations in the general notation of Chap. 11 by the graphical procedure outlined at the end of Sec. 13.1. In this way, we obtain from the diagram for the completely symmetric two-point vertex shown in Fig. 11.3 the diagram for the fermionic self-energy in Fig. 13.4 as well as the diagram for the irreducible polarization shown in Fig. 13.5. Moreover, if two of the external legs in the diagram for the completely symmetric three-legged vertex shown in Fig. 11.4 are fermion legs and one is a boson leg, we obtain the flow equation for the three-legged vertex shown in Fig. 13.6.

The flow equation for the vertex correction in Fig. 13.6 looks rather complicated. In Chap. 14, we will work with an interaction cutoff only and all diagrams in Figs. 13.4, 13.5, and 13.6 containing a fermionic single-scale propagator (i.e, a slash on a fermionic line) will vanish. For certain initial conditions this allows for the exact solubility of a whole hierarchy of flow equations. For now we nevertheless proceed without specifying a particular cutoff scheme.

13.4 Rescaling and classification of vertices

For approximate solutions, the infinite hierarchy of flow equations has to be truncated. An analysis of scaling dimensions indicates which terms are most relevant

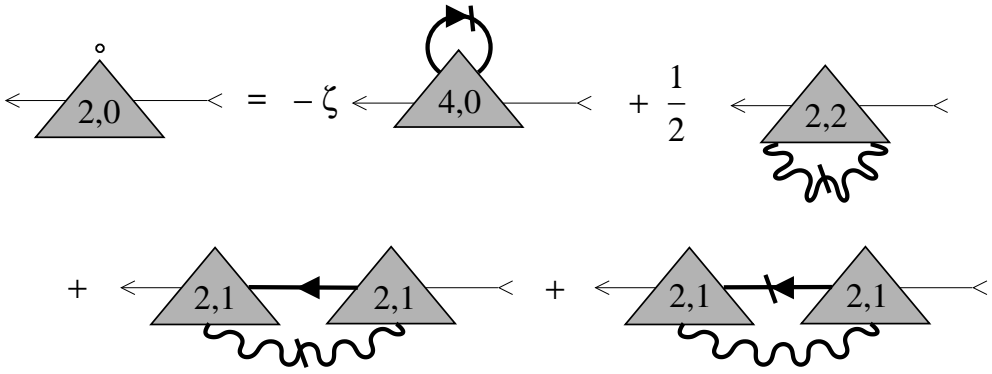

Figure 13.4: Flow of the irreducible fermionic self-energy. The diagrams are obtained from the diagrams shown in Fig. 11.3 by specifying the external legs to be one outgoing and one incoming fermion leg.

in the low-energy limit. Technically, this is performed by rescaling momenta, frequencies and fields at every step of the RG transformation in order to allow for the possibility of fixed points. The rescaling is not unique but depends on the nature of the fixed point we are looking for. Let us be general here and assume that in the bosonic sector the relation between momentum and frequency is characterized by a bosonic dynamic exponent z_φ (this is the exponent z introduced by Hertz [Hertz, 1976]), while in the fermionic sector the corresponding dynamic exponent is z_ψ. Rescaled dimensionless bosonic momenta $\bar{\mathbf{q}}$ and frequencies $\bar{\epsilon}$ are then introduced as usual [Hertz, 1976]

$$\bar{\mathbf{q}} = \bar{\mathbf{k}}/\Lambda \ , \ \bar{\epsilon} = \bar{\omega}/\bar{\Omega}_\Lambda \ , \ \bar{\Omega}_\Lambda \propto \Lambda^{z_\varphi} \ . \tag{13.22}$$

For convenience, we choose the factor $\bar{\Omega}_\Lambda$ such that it has units of energy; $\bar{\epsilon}$ is then dimensionless.

The proper rescaling of the fermionic momenta is not so obvious. Certainly, all momenta should be measured with respect to suitable points $\mathbf{k}_F$ on the Fermi surface. One possibility is to rescale only the component $k_\parallel = (\mathbf{k} - \mathbf{k}_F) \cdot \hat{\mathbf{v}}_F$ of a given momentum that is parallel to the local Fermi velocity $\mathbf{v}_F$ (and hence perpendicular to the Fermi surface) [Shankar, 1994,Kopietz and Busche, 2001]. Unfortunately, in dimensions $D > 1$ this leads to rather complicated geometric constructions, because the component $k_\parallel$ that need to be rescaled is measured in a coordinate systems that varies as one moves along the Fermi surface. Thus, momentum conservation has a cumbersome form in the new variables. However, if the initial momentum-transfer cutoff $\Lambda_{B,0}$ in Eq. (13.18) is small compared with the typical radius of the Fermi surface, the initial and final momenta associated with a scattering process lie both on nearby points on the Fermi surface. It is then natural to use a sectorization of the Fermi surface as depicted in Fig. 13.7. For each patch a fixed reference point $\mathbf{k}_{F,\sigma}$ on the Fermi surface is picked, and all fermionic

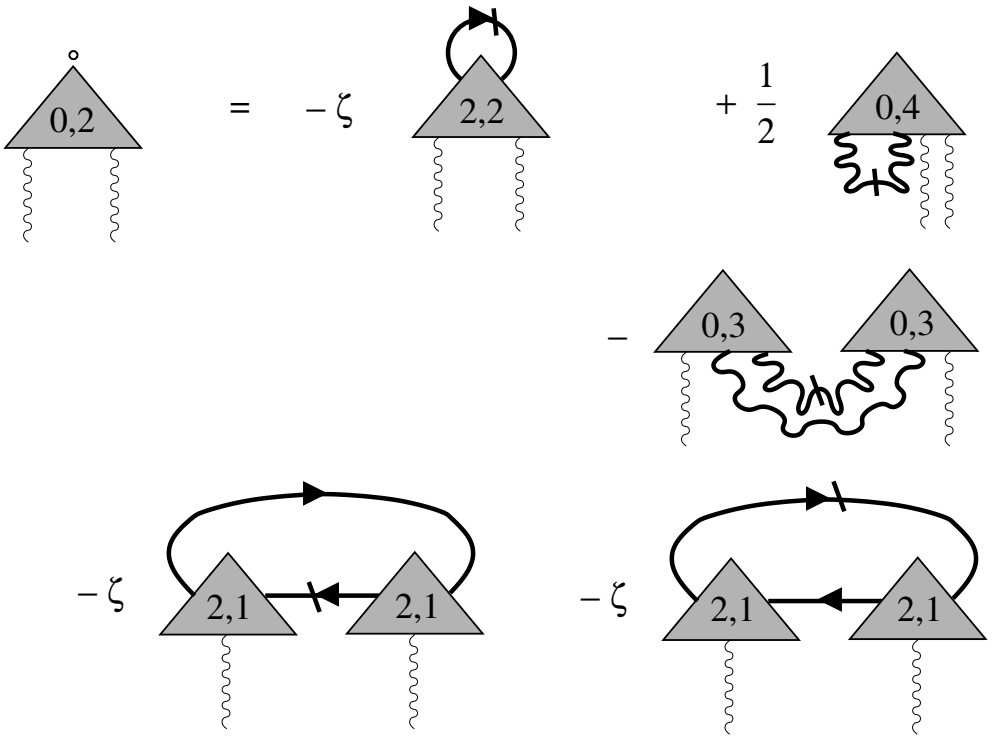

Figure 13.5: Flow of the irreducible polarization, obtained from the totally symmetric diagram in Fig. 11.3 by setting both external legs equal to boson legs. Note that each closed fermion loop gives rise to an additional factor of $\zeta = -1$.

momentum labels $\mathbf{k}_i$ and $\mathbf{k}'_i$ in $\Gamma^{(2n,m)}(K'_1, \ldots, K'_n; K_1, \ldots, K_n; \bar{K}_1, \ldots, \bar{K}_m)$ are measured relative to this $\mathbf{k}_{F,\sigma}$. Here, the index σ labels the different points on the Fermi surface, for example in one dimension $\sigma = \pm 1$, with $k_{F,\pm 1} = \pm k_F$. We then define rescaled fermionic momenta $\mathbf{q}$ and frequencies ϵ as follows

$$\mathbf{q} = (\mathbf{k} - \mathbf{k}_{F,\sigma})/\Lambda \quad , \quad \epsilon = \omega/\Omega_\Lambda \quad , \quad \Omega_\Lambda \propto \Lambda^{z_\psi} \; . \tag{13.23}$$

The factor Ω_Λ should again have units of energy such that ϵ is dimensionless. Iterating the usual RG steps of mode elimination and rescaling, we then coarse grain the degrees of freedom in a sphere around the chosen point $\mathbf{k}_{F,\sigma}$. Because by assumption the maximal momentum transfer mediated by the interaction is small compared with $|\mathbf{k}_{F,\sigma}|$, the fermionic momenta appearing in $\Gamma^{(2n,m)}(K'_1, \ldots, K'_n; K_1, \ldots, K_n; \bar{K}_1, \ldots, \bar{K}_m)$ are all in the vicinity of the chosen $\mathbf{k}_{F,\sigma}$. This property is also responsible for the approximate validity of the *closed loop theorem* for interacting fermions with dominant forward scattering in arbitrary dimensions [Kopietz *et al.*, 1995, Kopietz, 1997, Metzner *et al.*, 1998].

Apart from the rescaling of momenta and frequencies, we have to specify the rescaling of the fields. As usual, we require that the Gaussian part $S_0[\Phi] =$

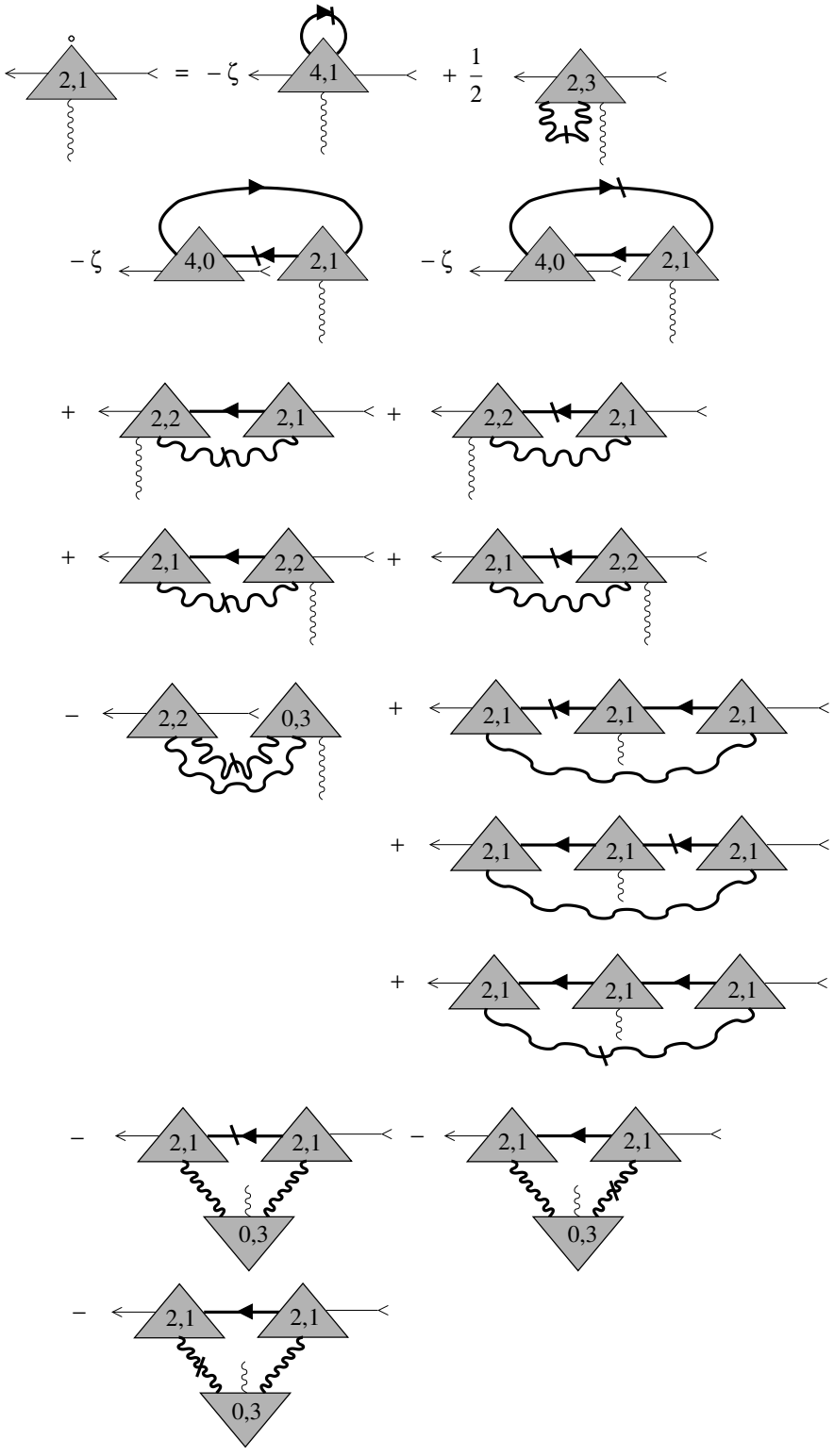

Figure 13.6: Flow of three-legged vertex with two fermion legs and one boson leg, obtained as a special case of the diagram in Fig. 11.4.

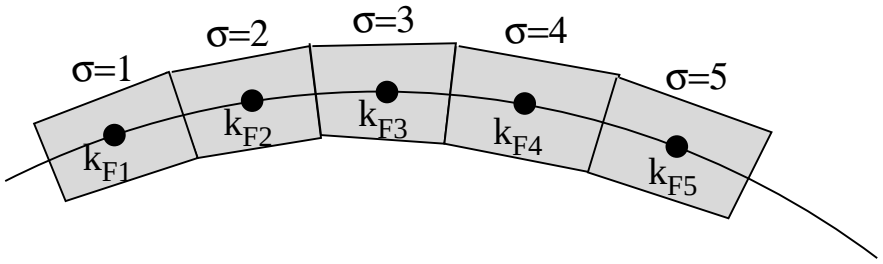

Figure 13.7: Patches on the Fermi surface. Momenta in a given patch σ are measured with respect to central point $\mathbf{k}_{F,\sigma}$.

$S_0[\bar{\psi},\psi] + S_0[\varphi]$ of our effective action is invariant under rescaling. For the fermionic part this is achieved by defining renormalized fields $\tilde{\psi}_{Q\sigma}$ in D dimensions via

$$\psi_{K\sigma} = \left(\frac{Z}{\Lambda^D \Omega_\Lambda^2}\right)^{1/2} \tilde{\psi}_{Q\sigma} \,, \tag{13.24}$$

where Z is the fermionic wave-function renormalization factor and $Q = (\mathbf{q}, i\epsilon)$ denotes the rescaled fermionic momenta and Matsubara frequencies as defined in Eq. (13.23). With this rescaling the wave-function renormalization and the Fermi velocity have a vanishing scaling dimension (corresponding to marginal couplings), while the momentum- and frequency-independent part of the self-energy is relevant with scaling dimension +1, see [Kopietz and Busche, 2001]. Analogously, we find that the bosonic Gaussian part of the action is invariant under rescaling if we express it in terms of the renormalized bosonic field $\tilde{\varphi}_{\bar{Q}\sigma}$ defined by

$$\varphi_{\bar{K}\sigma} = \left(\frac{\bar{Z}}{\Lambda^D \bar{\Omega}_\Lambda \nu_0}\right)^{1/2} \tilde{\varphi}_{\bar{Q}\sigma} \,, \tag{13.25}$$

where $\bar{Z}$ is the bosonic wave-function renormalization factor, $\bar{Q} = (\bar{\mathbf{q}}, i\bar{\epsilon})$ denotes the rescaled bosonic momenta and Matsubara frequencies defined in Eq. (13.22), and ν_0 is the non-interacting density of states at the Fermi surface. We introduce the factor of ν_0 for convenience to make all rescaled vertices dimensionless. By construction Eq. (13.25) assigns vanishing scaling dimensions to the bare interaction parameters $f_{\mathbf{k}}^{\sigma\sigma'}$, corresponding to marginal Landau interaction parameters.

We now express each term in the expansion of the generating functional $\Gamma[\bar{\psi},\psi,\varphi]$ given in Eq. (13.1) in terms of the rescaled variables defined above and use the fact that Γ is dimensionless. The coefficients in an expansion of Γ in terms of the rescaled fields then yield the rescaled vertices. In order to be able to compare coefficients and to express the rescaled vertices in terms of the unrescaled ones, we need to pull the scale factors out of the frequency and momentum conserving δ-function. For $z_\psi \leq z_\varphi$ the bosonic frequencies are not more relevant than the fermionic ones, and we pull out a fermionic scale factor Ω_Λ.

Thus, for $z_\psi \leq z_\varphi$ and omitting the degeneracy label σ, we define the rescaled vertices,

$$\tilde{\Gamma}_l^{(2n,m)}(Q'_1,\ldots,Q'_n;Q_1,\ldots,Q_n;\bar{Q}_1,\ldots,\bar{Q}_m) = \tag{13.26}$$
$$\nu_0^{-m/2}\Lambda^{D(n-1+m/2)}\Omega_\Lambda^{-1}\bar{\Omega}_\Lambda^{m/2}Z^n\bar{Z}^{m/2}\Gamma_\Lambda^{(2n,m)}(K'_1,\ldots,K'_n;K_1,\ldots,K_n;\bar{K}_1,\ldots,\bar{K}_m)\,,$$

On the contrary, for $z_\varphi < z_\psi$ we pull out a bosonic scale factor amounting to the replacement $\Omega_\Lambda^{-1} \to \bar{\Omega}_\Lambda^{-1}$. In Eq. (13.27), we have to exclude the cases of purely bosonic vertices ($n = 0$) as well as the fermionic two-point vertex (i.e., the rescaled irreducible self-energy, corresponding to $n = 1$ and $m = 0$), which both need separate definitions. For the purely bosonic vertices ($n = 0$) we set

$$\tilde{\Gamma}_l^{(0,m)}(\bar{Q}_1,\ldots,\bar{Q}_m) = \nu_0^{-m/2}(\Lambda^D\bar{\Omega}_\Lambda)^{-1+m/2}\bar{Z}^{m/2}\Gamma_\Lambda^{(0,m)}(\bar{K}_1,\ldots,\bar{K}_m)\,,$$

while for the fermionic two-point vertex we should subtract the exact fixed point self-energy $\Sigma_*(\mathbf{k}_{F,\sigma}, i0)$ at the Fermi-surface reference-point $\mathbf{k}_{F,\sigma}$ and vanishing frequency as a counterterm [Kopietz and Busche, 2001, Ledowski and Kopietz, 2003],

$$\tilde{\Gamma}_l^{(2,0)}(Q;Q) \equiv \tilde{\Sigma}_l(Q) = \frac{Z}{\Omega_\Lambda}\left[\Sigma(K) - \Sigma_*(\mathbf{k}_{F,\sigma}, i0)\right]\,. \tag{13.27}$$

If necessary, the counterterm $\Sigma_*(\mathbf{k}_{F,\sigma}, i0)$ can be reconstructed from the condition that the constant part $\tilde{r}_l = \tilde{\Sigma}_l(0)$ of the self-energy flows into an RG fixed point. We consider the rescaled vertices to be functions of the logarithmic flow parameter $l = -\ln(\Lambda/\Lambda_0)$. Introducing the flowing anomalous dimensions associated with the fermionic and bosonic fields,

$$\eta_l = -\partial_l \ln Z \quad , \quad \bar{\eta}_l = -\partial_l \ln \bar{Z}\,, \tag{13.28}$$

we can then write down the flow equations for the rescaled vertices. Omitting the arguments, we obtain for $n \geq 1$ the flow equation

$$\begin{aligned}\partial_l\tilde{\Gamma}_l^{(2n,m)} &= \Big[(1-n)D + z_{\min} - \frac{m}{2}(D+z_\varphi) - n\eta_l - \frac{m}{2}\bar{\eta}_l \\ &\quad - \sum_{i=1}^{n}(Q'_i\cdot\frac{\partial}{\partial Q'_i} + Q_i\cdot\frac{\partial}{\partial Q_i}) - \sum_{i=1}^{m}\bar{Q}_i\cdot\frac{\partial}{\partial\bar{Q}_i}\Big]\tilde{\Gamma}_l^{(2n,m)} \\ &\quad + \dot{\tilde{\Gamma}}_l^{(2n,m)}\,,\end{aligned} \tag{13.29}$$

where $z_{\min} = \min\{z_\varphi, z_\psi\}$. For $n = 0$ we obtain from Eq. (13.27),

$$\partial_l\tilde{\Gamma}_l^{(0,m)} = \left[(1-\frac{m}{2})(D+z_\varphi) - \frac{m}{2}\bar{\eta}_l - \sum_{i=1}^{m}\bar{Q}_i\cdot\frac{\partial}{\partial\bar{Q}_i}\right]\tilde{\Gamma}_l^{(0,m)} + \dot{\tilde{\Gamma}}_l^{(0,m)}\,, \tag{13.30}$$

where we have introduced the notation

$$Q \cdot \frac{\partial}{\partial Q} \equiv \mathbf{q} \cdot \nabla_{\mathbf{q}} + z_\psi \, \epsilon \frac{\partial}{\partial \epsilon} \,, \tag{13.31}$$

$$\bar{Q} \cdot \frac{\partial}{\partial \bar{Q}} \equiv \bar{\mathbf{q}} \cdot \nabla_{\bar{\mathbf{q}}} + z_\varphi \, \bar{\epsilon} \frac{\partial}{\partial \bar{\epsilon}} \,. \tag{13.32}$$

The inhomogeneities in Eqs. (13.29) and (13.30) are given by the rescaled version of the right-hand sides of the flow equations for the unrescaled vertices, i.e., for $n \geq 1$, and $z_\psi \leq z_\varphi$,

$$\dot{\tilde{\Gamma}}_l^{(2n,m)}(Q'_1, \ldots, Q'_n; Q_1, \ldots, Q'_n; \bar{Q}_1, \ldots, \bar{Q}_m) = \nu_0^{-m/2} \Lambda^{D(n-1+m/2)} \Omega_\Lambda^{-1} \bar{\Omega}_\Lambda^{m/2} Z^n \bar{Z}^{m/2} \, [-\Lambda \partial_\Lambda \Gamma_\Lambda^{(2n,m)}(\{K'_i; K_i; \bar{K}_i\})] \,, \tag{13.33}$$

and for $n = 0$,

$$\dot{\tilde{\Gamma}}_l^{(0,m)}(\bar{Q}_1, \ldots, \bar{Q}_m) = \nu_0^{-m/2} (\Lambda^D \bar{\Omega}_\Lambda)^{-1+m/2} \bar{Z}^{m/2} \, [-\Lambda \partial_\Lambda \Gamma_\Lambda^{(0,m)}(\bar{K}_1, \ldots, \bar{K}_m)] \,. \tag{13.34}$$

By properly counting all factors it is then not difficult to see that the explicit expressions for the inhomogeneities in Eqs. (13.33) and (13.34) can be simply obtained from their unrescaled counterparts by replacing all vertices and propagators with their rescaled analogues, where the rescaled propagators are defined by

$$G(K) = \frac{Z}{\Omega_\Lambda} \tilde{G}(Q) \,, \quad F(\bar{K}) = \frac{\bar{Z}}{\nu_0} \tilde{F}(\bar{Q}) \,, \tag{13.35}$$

and the corresponding rescaled single scale propagators are defined via

$$\Lambda \dot{G}(K) = -\frac{Z}{\Omega_\Lambda} \dot{\tilde{G}}(Q) \,, \quad \Lambda \dot{F}(\bar{K}) = -\frac{\bar{Z}}{\nu_0} \dot{\tilde{F}}(\bar{Q}) \,. \tag{13.36}$$

From Eqs. (13.29) and (13.30) we can read off the scaling dimensions of the vertices: the scaling dimension of $\tilde{\Gamma}^{(2n,m)}$ in D dimensions is

$$D^{(2n,m)} = \begin{cases} (1-n)D + z_{\min} - (D + z_\varphi)m/2 & \text{for } n \geq 1 \\ (D + z_\varphi)(1 - m/2) & \text{for } n = 0 \end{cases} \,. \tag{13.37}$$

In the particular case of the Tomonaga-Luttinger model, where $D = 1$ and $z_\psi = z_\varphi = 1$, we have $D^{(2n,m)} = 2 - n - m$. Hence, in this case $\tilde{\Gamma}^{(2,0)}(Q = 0)$ and $\tilde{\Gamma}^{(0,1)}$ are relevant with scaling dimension $+1$, while $\tilde{\Gamma}^{(4,0)}(Q_i = 0)$ and $\tilde{\Gamma}^{(2,1)}(Q_i = \bar{Q}_i = 0)$ are marginal. All other vertices are irrelevant. Of course, the linear terms in the expansion of $\tilde{\Gamma}^{(2,0)}(Q; Q)$ for small Q are also marginal. These terms determine the wave-function renormalization factor Z and the Fermi velocity renormalization

$\tilde{v}_l$, see Eqs. (14.34) and (14.39) below. Note that for short-range interactions the dispersion of the zero-sound mode is linear in any dimension [Kopietz, 1997]. Hence, as long as the density response is dominated by the zero-sound mode, Eq. (13.37) remains valid for $D > 1$ with $z_\psi = z_\psi = 1$. In this case the scaling dimension of the purely fermionic four-point vertex is $D^{(4,0)} = 1 - D$ and the scaling dimension of the three-legged vertex with two fermion legs and one boson leg is $D^{(2,1)} = (1-D)/2$. Both vertices become irrelevant in $D > 1$. As discussed in the following section, this means that the random-phase approximation (RPA) for the effective interaction, as well as the so-called GW-approximation [Hedin, 1965] for the fermionic self-energy, are qualitatively correct in $D > 1$.

13.5 Truncation to skeleton elements of two-point functions

In order to solve the flow equations explicitly, in almost all cases one is forced to truncate the infinite hierarchy of flow equations. In the one-particle irreducible version of the purely fermionic functional RG it is common practice to retain only vertices up to the four-point vertex and set all higher order vertices equal to zero (see references in Sec. 9.1). Our approach offers new possibilities for the choice of truncation schemes. Consider the skeleton graphs [Nozières, 1964] for the one-particle irreducible fermionic self-energy and the one-interaction-line irreducible polarization shown in Fig. 13.8a and b. The skeleton graphs contain three basic elements: the exact fermionic Green's function, the exact bosonic Green's function (i.e., the effective screened interaction), and the three-legged vertex with two fermion legs and one boson leg. Although the skeleton graphs are usually written down directly from topological considerations of the structure of diagrammatic perturbation theory [Nozières, 1964], it is instructive to see how the skeleton expansion of the irreducible vertices can be derived formally within our functional integral approach. Thus, let us make a short digression to show this.

13.5.1 Skeleton graphs

The skeleton diagrams for the two-point functions and the three-legged vertex in Fig. 13.8 can be formally derived from the Dyson-Schwinger equations of motion. Taking derivatives of Eqs. (12.17–12.19) with respect to the fields and then setting the fields equal to zero we obtain the desired skeleton expansions of the irreducible vertices. Let us start with the skeleton diagram for the self-energy shown in Fig. 13.8a. To derive this, we simply differentiate Eq. (12.19) with respect to $\psi_{K'\sigma}$. Using

$$\left.\frac{\delta^{(2)}\Gamma}{\delta\psi_{K'\sigma}\delta\bar{\psi}_{K\sigma}}\right|_{\text{fields}=0} = \delta_{K,K'}\Sigma_\sigma(K)\,, \tag{13.38}$$

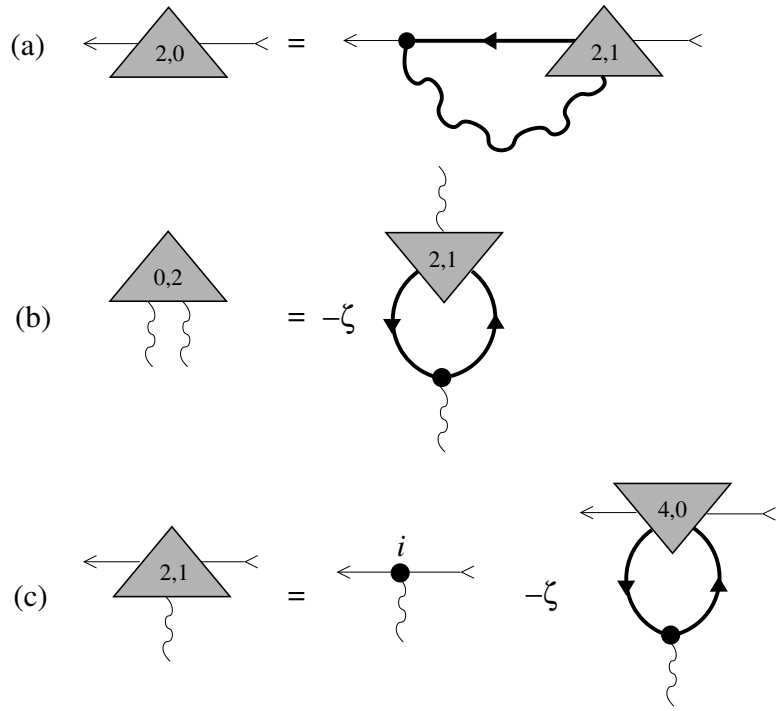

Figure 13.8: Skeleton diagrams for (a) the one-particle irreducible fermionic self-energy; (b) the one-interaction-line irreducible polarization; and (c) the three-legged vertex with two fermion legs and one boson leg. The small black circle denotes the bare three-legged vertex. Thin lines are external legs. The other graphical elements are the same as in Fig. 13.1.

we obtain

$$\delta_{K,K'}\Sigma_\sigma(K) = i\int_{\bar{K}} \frac{\delta^{(3)}\mathcal{G}_c}{\delta\psi_{K'\sigma}\delta\bar{\jmath}_{K-\bar{K},\sigma}\delta J_{-\bar{K}\sigma}}\bigg|_{\text{fields}=0} . \tag{13.39}$$

From the $l = 1$ term in the expansion (11.30) it is easy to show that

$$\frac{\delta^{(3)}\mathcal{G}_c}{\delta\psi_{K'\sigma}\delta\bar{\jmath}_{K-\bar{K},\sigma}\delta J_{-\bar{K}\sigma}}\bigg|_{\text{fields}=0} = \delta_{K,K'}F_{\sigma\sigma}(\bar{K})G_\sigma(K+\bar{K})\Gamma^{(2,1)}(K+\bar{K}\sigma;K\sigma;\bar{K}\sigma) , \tag{13.40}$$

so that

$$\Sigma_\sigma(K) = i\int_{\bar{K}} F_{\sigma\sigma}(\bar{K})G_\sigma(K+\bar{K})\Gamma^{(2,1)}(K+\bar{K}\sigma;K\sigma;\bar{K}\sigma) , \tag{13.41}$$

which is the analytic expression for the skeleton graph shown in Fig. 13.8a. Similarly, we obtain the skeleton expansion of the irreducible polarization by differ-

entiating Eq. (12.17) with respect to $\varphi_{-\bar{K}\sigma}$,

$$\begin{aligned}\Pi_\sigma(\bar{K}) &= i\int_K \frac{\delta^{(3)}\mathcal{G}_c}{\delta\varphi_{-\bar{K}\sigma}\delta\bar{\jmath}_{K,\sigma}\delta j_{K+\bar{K}\sigma}}\bigg|_{\text{fields}=0} \\ &= -i\zeta\int_K G_\sigma(K)G_\sigma(K+\bar{K})\Gamma^{(2,1)}(K+\bar{K}\sigma;K\sigma;\bar{K}\sigma)\ , \quad (13.42)\end{aligned}$$

which is shown diagrammatically in Fig. 13.8b. Finally, applying the operator $\frac{\delta^{(2)}}{\delta\bar{\psi}_{K+\bar{K}\sigma}\delta\psi_{K\sigma}}$ to Eq. (12.17) and subsequently setting the fields equal to zero we obtain the skeleton expansion of the three-legged vertex shown in Fig. 13.8 (c),

$$\begin{aligned}&\Gamma^{(2,1)}(K+\bar{K}\sigma;K\sigma;\bar{K}\sigma) \\ &= i - i\zeta\int_{K'} G_\sigma(K')G_\sigma(K'+\bar{K})\Gamma^{(4,0)}(K+\bar{K}\sigma,K'\sigma;K'+\bar{K}\sigma,K\sigma)\ . \quad (13.43)\end{aligned}$$

Skeleton expansions for higher order vertices can be obtained in an analogous way from the appropriate functional derivatives of Eqs. (12.17–12.19).

13.5.2 Truncation scheme

Let us now go back and analyze the proposed truncation scheme. One advantage of our RG approach (as compared with more conventional methods involving only fermionic fields) is that it yields directly the flow equations for basic elements appearing in the skeleton graphs for the self-energy and the polarization shown in Fig. 13.8. Of course, in principle the three-legged vertex can be obtained from the vertex with four fermion legs with the help of the skeleton graph shown in Fig. 13.8c. However, calculating the three-legged vertex from the four-legged vertex in this way involves an intermediate integration, which requires the knowledge of the momentum and frequency dependence of the four-legged vertex. Unfortunately, in practice the purely fermionic functional RG equations have to be severely truncated so that up to now it was not possible to keep track of the frequency dependence of the four-legged fermion vertex.

To obtain a closed system of RG equations involving only the skeleton elements, let us retain only the vertices $\Sigma_\sigma(K)$, $\Pi_\sigma(\bar{K})$ and $\Gamma^{(2,1)}(K+\bar{K}\sigma;K\sigma;\bar{K}\sigma)$ on the right-hand sides of the exact flow equations for these quantities shown in Figs. 13.4, 13.5, and 13.6, and set all other vertices to zero. The resulting closed system of flow equations is shown graphically in Fig. 13.9. Explicitly, the flow equations are

$$\begin{aligned}\partial_\Lambda\Sigma_\sigma(K) &= \int_{\bar{K}}\Big[\dot{F}_{\sigma\sigma}(\bar{K})G_\sigma(K+\bar{K}) + F_{\sigma\sigma}(\bar{K})\dot{G}_\sigma(K+\bar{K})\Big] \\ &\quad\times\Gamma^{(2,1)}(K+\bar{K}\sigma;K\sigma;\bar{K}\sigma)\Gamma^{(2,1)}(K\sigma;K+\bar{K}\sigma;-\bar{K}\sigma)\ , \quad (13.44)\end{aligned}$$

$$\partial_\Lambda \Pi_\sigma(\bar{K}) = -\zeta \int_K \Big[\dot{G}_\sigma(K) G_\sigma(K+\bar{K}) + G_\sigma(K)\dot{G}_\sigma(K+\bar{K})\Big] \times\Gamma^{(2,1)}(K+\bar{K}\sigma; K\sigma; \bar{K}\sigma)\Gamma^{(2,1)}(K\sigma; K+\bar{K}\sigma; -\bar{K}\sigma) \;, \quad (13.45)$$

$$\begin{aligned}\partial_\Lambda \Gamma^{(2,1)}(K+\bar{K}\sigma; K\sigma; \bar{K}\sigma) = \int_{\bar{K}'} \Big[&\dot{F}_{\sigma\sigma}(\bar{K}') G_\sigma(K+\bar{K}') G_\sigma(K+\bar{K}+\bar{K}') \\ &+ F_{\sigma\sigma}(\bar{K}')\dot{G}_\sigma(K+\bar{K}') G_\sigma(K+\bar{K}+\bar{K}') \\ &+ F_{\sigma\sigma}(\bar{K}') G_\sigma(K+\bar{K}')\dot{G}_\sigma(K+\bar{K}+\bar{K}')\Big] \\ \times\Gamma^{(2,1)}(K+\bar{K}\sigma; K+\bar{K}+\bar{K}'\sigma; -\bar{K}'\sigma)&\Gamma^{(2,1)}(K+\bar{K}+\bar{K}'\sigma; K+\bar{K}'\sigma; \bar{K}\sigma) \\ \times\Gamma^{(2,1)}(K+\bar{K}'\sigma; K\sigma; \bar{K}'\sigma) \;. &\end{aligned} \quad (13.46)$$

These equations form a closed system of integro-differential equations that can in principle be solved numerically. If the initial momentum-transfer cutoff Λ_0 is chosen larger than the maximal momentum transfered by the bare interaction, and if the initial bandwidth cutoff $v_0\Lambda_0$ is larger than the bandwidth of the bare energy dispersion, then the initial conditions are $\Sigma_\sigma(K)_{\Lambda_0} = 0$, $\Pi_\sigma(\bar{K})_{\Lambda_0} = 0$, and $\Gamma^{(2,1)}(K+\bar{K}\sigma; K\sigma; \bar{K}\sigma)_{\Lambda_0} = i$. A numerical solution of these coupled equations seems to be a difficult task, which we shall not attempt in this work. Note, however, that in Sec. 13.4 we have argued that for regular interactions in dimensions $D > 1$ the three-legged vertex is actually irrelevant in the RG sense. Hence, we expect that the qualitatively correct behavior of the fermionic self-energy and of the polarization can be obtained by ignoring the flow of the three-legged vertex, setting $\Gamma^{(2,1)} \to i$. If we further ignore interaction corrections to the internal propagators in the flow equation (13.45) for the polarization, it is easy to see that the solution of this equation is nothing but the non-interacting polarization. This is equivalent with the RPA for the effective interaction. Substituting this into the flow equation (13.44) for the self-energy and ignoring again self-energy corrections to the internal Green's functions, we obtain the non-self-consistent GW approximation [Hedin, 1965] for the fermionic self-energy. For regular interactions in $D > 1$ we therefore expect that the RPA and the GW approximation are qualitatively correct. However, for strong bare interactions quantitatively accurate results can only be expected if the vertex corrections described by Eq. (13.46) are at least approximately taken into account.

We shall consider this problem again in Sec. 14.5, where we discuss truncations of an expansion based on relevance in the RG sense. To lowest order, this approximation will agree with Eqs. (13.44–13.46) when the dependence of the vertex $\Gamma^{(2,1)}$ on momenta and frequencies is ignored. There we use the resulting equations to calculate an approximation to the electronic Green's function of the one-dimensional Tomonaga-Luttinger model. Amazingly, this simple truncation is sufficient to reproduce the correct anomalous dimension known from bosonization even for large values of the bare coupling.

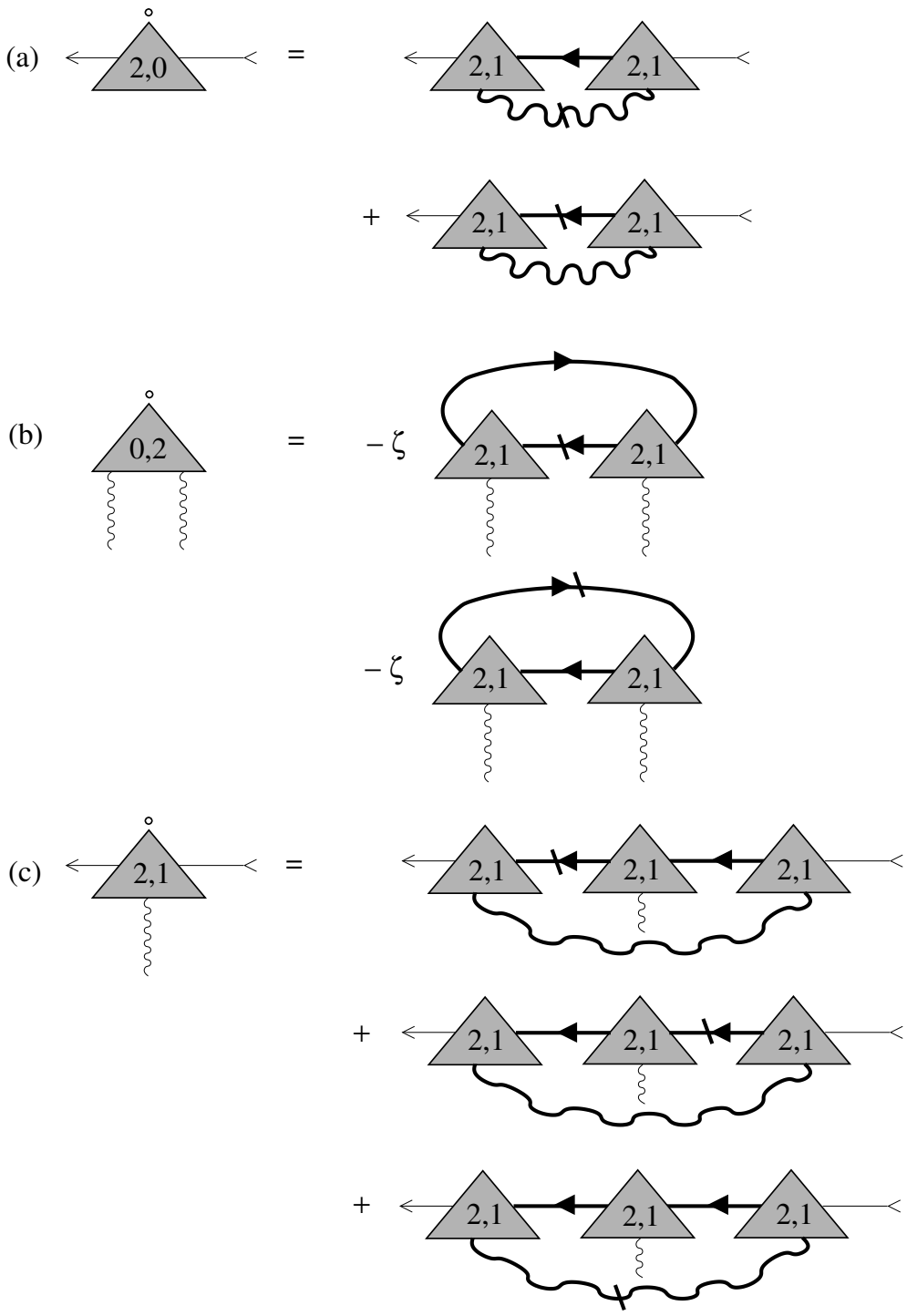

Figure 13.9: Truncation of the flow equations for (a) fermionic self-energy, (b) irreducible polarization, and (c) three-legged vertex which sets all other vertices equal to zero. The internal lines are full propagators, which depend on the self-energies $\Gamma^{(2,0)} = \Sigma$ and $\Gamma^{(0,2)} = \Pi$.

Chapter 14:

Interaction cutoff scheme

A finite bandwidth cutoff Λ_F breaks the gauge symmetry of the action, and Ward identities are generally violated in renormalization group schemes based on Λ_F as the flow parameter [Katanin, 2004, Enss, 2005]. Modified symmetry relations among the vertices can still be derived even in the presence of such a cutoff, but compared to the Ward identities without cutoff they acquire complicated correction terms that are difficult to deal with. Moreover, if the hierarchy of flow equations is truncated, Ward identities are generally only fulfilled to the order of the truncation [Katanin, 2004]. A modified flow scheme that improves this situation was proposed by Katanin [Katanin, 2004] and was important for certain applications [Hedden *et al.*, 2004, Salmhofer *et al.*, 2004]. Alternative flow schemes have been used based on the temperature [Honerkamp and Salmhofer, 2001a] or the strength of the interaction [Honerkamp *et al.*, 2004] as the flow parameter. Although these schemes do not violate the gauge symmetry, the intuitive RG picture of integrating out modes successively in order of decreasing energy is lost.

Here, we show that a new gauge invariant flow scheme is obtained when a cutoff Λ_B in the momentum transfer of the interaction is used as a flow parameter and the bandwidth cutoff Λ_F is removed from the outset. For purely bosonic vertices the resulting infinite hierarchy of flow equations is an exact version of the RG equations analyzed by Hertz [Hertz, 1976]. Thus, the scheme integrates out collective fluctuations in order of decreasing energy. We show that Ward identities are valid at every step of the flow.

The Ward identities and the underlying asymptotic conservation laws are crucial for the exact solubility of the Tomonaga-Luttinger model [Dzyaloshinskii and Larkin, 1974, Bohr, 1981] and its higher-dimensional generalization [Metzner *et al.*, 1998, Kopietz, 1997, Bartosch and Kopietz, 1999]. In the interaction cutoff scheme a solution of an infinite hierarchy of flow equations is provided by Ward identities. Thus, we can derive a closed flow equation for the single-particle Green's function and recover the exact solution of the Tomonaga-Luttinger model.

14.1 Exact flow equations for an interaction cutoff

Let us now derive the hierarchy of flow equations for the interaction cutoff scheme. Thus, we consider only $\Lambda = \Lambda_B$ as a running cutoff and set the bandwidth cutoff to zero, $\Lambda_F = 0$, from the beginning. As a consequence, the fermionic part $\dot{G}_\sigma(K)$ of the single-scale propagator vanishes. As already briefly mentioned at the end

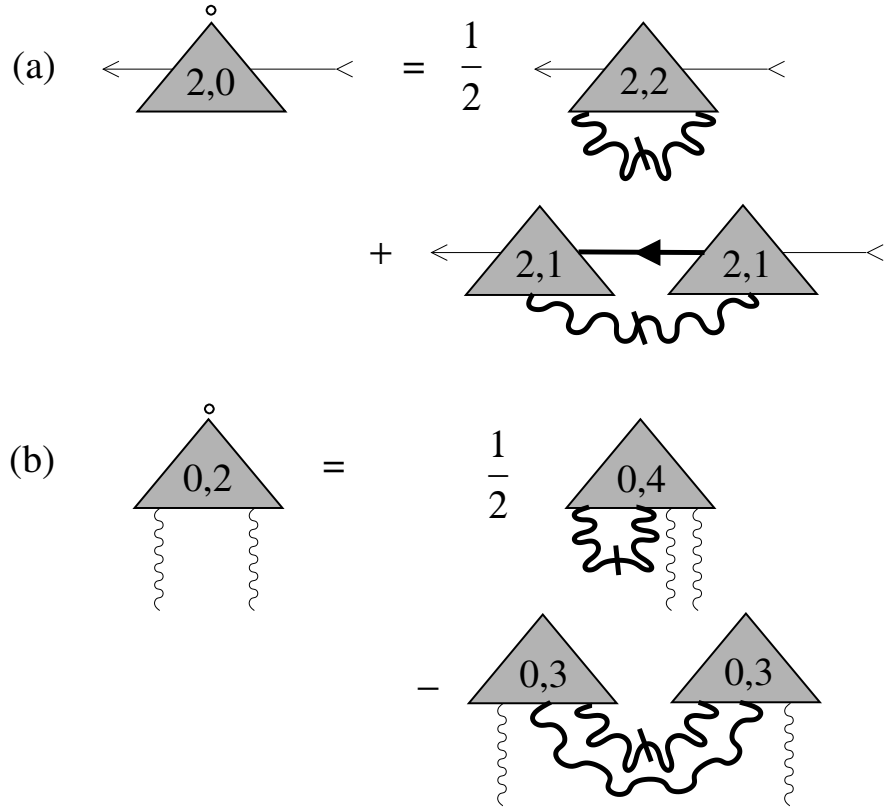

Figure 14.1: Exact flow equations for (a) the fermionic self-energy and (b) the irreducible polarization in the interaction cutoff scheme.

of Sec. 13.3, we should then omit all diagrams with a slash on internal fermionic lines on the right-hand sides of the exact flow equations shown in Figs. 13.4, 13.5, and 13.6. The exact flow equations for the electronic self-energy and the irreducible polarization then reduce to

$$\begin{aligned}\partial_\Lambda \Sigma_\sigma(K) &= \frac{1}{2}\int_{\bar{K}} \dot{F}_{\sigma\sigma}(\bar{K})\Gamma^{(2,2)}(K\sigma; K\sigma; \bar{K}\sigma, -\bar{K}\sigma) \\ &\quad + \int_{\bar{K}} \dot{F}_{\sigma\sigma}(\bar{K}) G_\sigma(K+\bar{K})\Gamma^{(2,1)}(K+\bar{K}\sigma; K\sigma; \bar{K}\sigma) \\ &\qquad \times \Gamma^{(2,1)}(K\sigma; K+\bar{K}\sigma; -\bar{K}\sigma)\,, \end{aligned} \tag{14.1}$$

$$\begin{aligned}\partial_\Lambda \Pi_\sigma(\bar{K}) &= \frac{1}{2}\int_{\bar{K}'} \dot{F}_{\sigma\sigma}(\bar{K})\Gamma^{(0,4)}(\bar{K}'\sigma, -\bar{K}'\sigma, \bar{K}\sigma, -\bar{K}\sigma) \\ &\quad - \int_{\bar{K}'} \dot{F}_{\sigma\sigma}(\bar{K}') F_{\sigma\sigma}(\bar{K}+\bar{K}')\Gamma^{(0,3)}(-\bar{K}\sigma, \bar{K}+\bar{K}'\sigma, -\bar{K}'\sigma) \\ &\qquad \times \Gamma^{(0,3)}(\bar{K}'\sigma, -\bar{K}-\bar{K}'\sigma, \bar{K}\sigma)\,. \end{aligned} \tag{14.2}$$

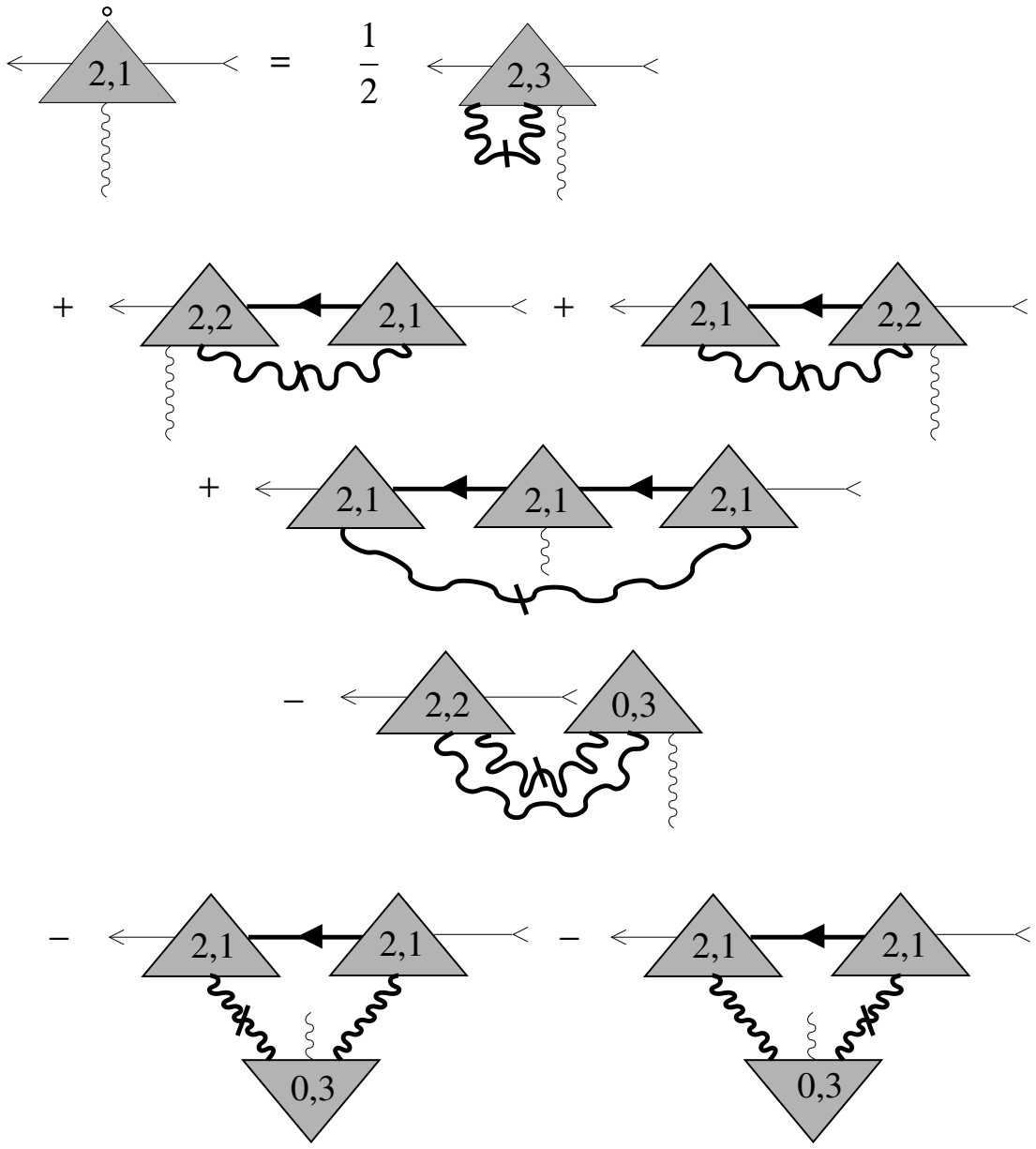

Figure 14.2: Exact flow equations for the three-legged vertex with two fermion legs and one boson leg in the interaction cutoff scheme.

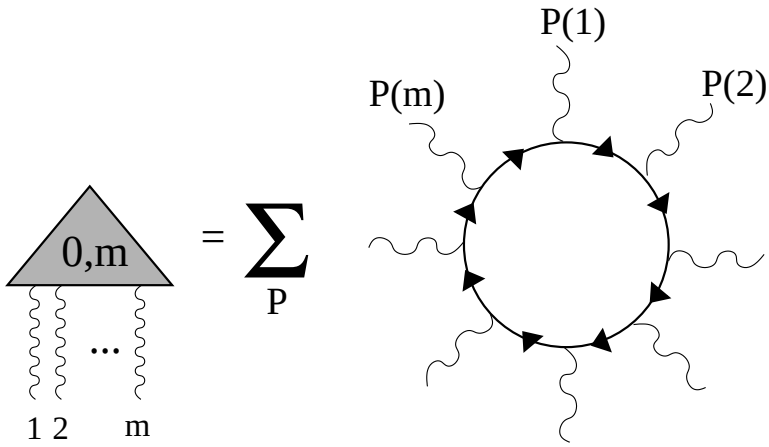

Figure 14.3: Initial condition for the pure boson vertices in the momentum transfer cutoff scheme. The sum is taken over the $m!$ permutations of the labels of the external legs. For linearized energy dispersion all symmetrized closed fermion loops with more than two external legs vanish.

These equations are shown graphically in Fig. 14.1. The diagrams for the corresponding exact flow equation of the three-legged vertex are presented in Fig. 14.2. These flow equations still look deceivingly complicated. They can nevertheless be further simplified for certain cases by specifying the initial condition for the flow. For a linear dispersion and an interaction that transfers only small momenta, we will see in the next section that pure bosonic vertices with more then two external legs vanish and do not contribute to the flow.

14.2 Initial condition

The initial condition for the flow in the interaction-cutoff scheme corresponds to a situation in which interaction lines are turned off while particle propagator lines are fully functional. In addition to the bare three-leg interaction vertex, the only one-line-irreducible diagrams that can be drawn in this case are closed loops of fermionic propagators. These loops have to be symmetrized with respect to the exchange of external bosonic legs in order to obtain the initial condition for the purely bosonic vertices as shown in Fig. 14.3.

A more formal route to the initial condition for Γ follows the procedure outlined in Secs. 11.1.2 and 11.1.3. Yet, since now only the interaction f vanishes initially, it is convenient to define a generating functional for partially amputated-connected Green's functions for which only external interaction lines are amputated,

$$e^{\mathcal{G}_{pac}[\bar{\jmath},j,J]} = \frac{1}{\mathcal{Z}_0}\int D[\bar{\psi},\psi,\varphi]e^{-S_0[\bar{\psi},\psi]-S_0[\varphi]-S_1[\bar{\psi},\psi,\varphi+J]+(\bar{\jmath},\psi)+(\bar{\psi},j)}\,. \tag{14.3}$$

By a manipulation similar to Eq. (11.14) using an additional intermediate source field, we can show the identity

$$e^{\mathcal{G}_{pac}[\bar{\jmath},j,J]} = e^{\frac{1}{2}\left(\frac{\delta}{\delta J},\hat{F}_0\frac{\delta}{\delta J}\right)}\frac{1}{\mathcal{Z}_\psi}\int D[\bar{\psi},\psi]e^{-S_0[\bar{\psi},\psi]-S_1[\bar{\psi},\psi,J]+(\bar{\jmath},\psi)+(\bar{\psi},j)}\,. \tag{14.4}$$

Here, $\hat{F}_0$ is the matrix of the bare interaction defined in Eq. (10.24) and $\mathcal{Z}_\psi$ is the partition function for non-interacting particles. In Eq. (14.4) the limit of a vanishing interaction can readily be taken. The remaining functional integral is Gaussian and yields

$$\mathcal{G}_{pac}^{f\to 0}[J,\bar{\jmath},j] = \mathrm{Tr}\{\ln[\hat{1}-i\hat{G}_0\hat{J}]\} - (\bar{\jmath},[\hat{1}-i\hat{G}_0\hat{J}]^{-1}\hat{G}_0 j)\,, \tag{14.5}$$

where we use a matrix $\hat{J}$ of bosonic sources containing the matrix elements

$$[\hat{J}]_{K\sigma,K'\sigma'} = \delta_{\sigma\sigma'}J_{K-K',\sigma}\,. \tag{14.6}$$

The first term in Eq. (14.5) generates the closed loops of fermion propagators in Fig. 14.3 when expanded in powers of the bosonic sources. The second term generates diagrams that contain a continuous fermionic path linking two external fermionic legs. An arbitrary number of external bosonic legs are then directly attached to this line. The latter diagrams are not one-line-irreducible and will cancel in the expression for Γ. However, before we can perform the Legendre transformation, we first need a relation between $\mathcal{G}_{pac}$ and the generating functional $\mathcal{G}_c$ for connected Green's functions. This is achieved by a shift $\varphi \to \varphi - J$ in the integration variables in Eq. (14.3) and yields

$$\mathcal{G}_c[\bar{\jmath},j,J] = S_0[\tilde{J}] + \mathcal{G}_{pac}[\bar{\jmath},j,\tilde{J}]\,, \tag{14.7}$$

where we have defined $\tilde{J} = \hat{F}_0 J$. The classical field φ is then given by

$$\varphi = \frac{\delta\mathcal{G}_c}{\delta J} = \tilde{J} + \hat{F}_0\frac{\delta\mathcal{G}_{pac}}{\delta\tilde{J}}[\bar{\jmath},j,\tilde{J}] \stackrel{f\to 0}{=} \tilde{J}\,. \tag{14.8}$$

In the limit of a vanishing interaction the classical field φ thus becomes identical to the source field $\tilde{J}$. Since $\mathcal{G}_{pac}^{f\to 0}$ is quadratic in the fermionic sources, the inversion necessary to obtain the sources $\bar{\jmath}$ and j as a function of the classical fields involves just a matrix inversion. The remaining Legendre transformation can then be explicitly performed and we obtain

$$\Gamma^{f\to 0}[\bar{\psi},\psi,\varphi] = i(\bar{\psi},\hat{\varphi}\psi) + \mathrm{Tr}\{\ln[\hat{1}-i\hat{G}_0\hat{\varphi}]\}\,, \tag{14.9}$$

where we have defined a matrix $\hat{\varphi}$ of bosonic fields in analogy to Eq. (14.6). The first term is nothing but the bare interaction S_1 whereas the second generates the closed Fermi loops. To be a little more explicit, we expand Eq. (14.9) in powers

of the fields and symmetrize with respect to interchange of bosonic fields. This yields

$$\begin{aligned}\Gamma^{f\to 0}[\bar\psi,\psi,\varphi] &= i\sum_\sigma \int_K \int_{\bar K} \bar\psi_{K+\bar K,\sigma}\psi_{K\sigma}\varphi_{\bar K\sigma} \\ &+ \sum_{n=1}^{\infty}\frac{1}{n!}\sum_\sigma \int_{\bar K_1}\cdots\int_{\bar K_n} \delta_{\bar K_1+\cdots+\bar K_n,0}\, L_\sigma^{(n)}(\bar K_1,\ldots,\bar K_n)\,, \quad (14.10)\end{aligned}$$

where the symmetrized Fermi loop is defined by

$$\begin{aligned}L_\sigma^{(n)}(\bar K_1,\ldots,\bar K_n) &= \frac{i^n}{n}\sum_P \int_K G_0(K\sigma)G_0(K+\bar K_{P(1)},\sigma)\cdot\ldots \\ &\quad \ldots\cdot G_0(K+\bar K_{P(1)}+\ldots+\bar K_{P(n-1)},\sigma)\,, \quad (14.11)\end{aligned}$$

and the summation is over all permutations P of $\{1,\ldots,n\}$. Comparing Eq. (14.10) to the general Taylor expansion in Eq. (13.1), we can identify the initial condition for the one-line-irreducible vertices as

$$\begin{aligned}\Gamma^{(2,1)}(K+\bar K,\sigma;K\sigma;\bar K\sigma) &= i\,, \quad (14.12)\\ \Gamma^{(0,m)}(\bar K_1,\sigma;\ldots;\bar K_m\sigma) &= L_\sigma^{(m)}(\bar K_1,\ldots,\bar K_m)\,. \quad (14.13)\end{aligned}$$

All other one-line-irreducible vertices vanish initially.

An essential simplification occurs if we linearize the energy dispersion relative to the Fermi surface. If the initial momentum transfer cutoff $\Lambda_0 = \Lambda_{B,0}$ is small compared with the typical Fermi momentum, then we may set all pure boson vertices $\Gamma^{(0,m)}$ with more than two external boson legs ($m \geq 2$) equal to zero. This is nothing but the closed loop theorem [Dzyaloshinskii and Larkin, 1974, Bohr, 1981, Kopietz, 1997, Kopietz *et al.*, 1995, Metzner *et al.*, 1998], which is valid exactly for the one-dimensional TLM (where the energy dispersion is linear by definition). In higher dimensions, the closed loop theorem is valid to a very good approximation as long as the linearization of the energy dispersion is justified within a given sectorization of the Fermi surface and scattering processes that transfer momentum between different sectors of the Fermi surface can be neglected [Kopietz *et al.*, 1995, Kopietz, 1997]. Note that the closed loop theorem is consistent with the momentum-transfer cutoff flow, because pure boson vertices $\Gamma^{(0,m)}$ with $m \geq 3$ are not generated if they vanish initially.

Assuming the validity of the closed loop theorem, the right-hand side of the flow equation (14.2) for the polarization vanishes identically, because it depends only on boson vertices with more than two external legs. Physically, this means that there are no corrections to the non-interacting polarization, so that the RPA for the effective interaction is exact. This is of course well-known since the pioneering work by Dzyaloshinskii and Larkin [Dzyaloshinskii and Larkin, 1974]. Moreover, the last three diagrams in the flow equation for $\Gamma^{(2,1)}$ shown in Fig. 14.2

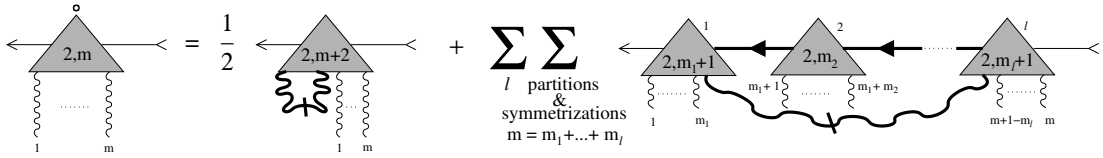

Figure 14.4: Diagrammatic representation of the flow equation (14.14) of vertices with two fermion legs and a general number of boson legs provided the pure boson vertices with more than two external legs vanish, as implied by the closed loop theorem.

also vanish, because they contain the vertex $\Gamma^{(0,3)}$. The remaining diagrams in Fig. 14.1a and Fig. 14.2 are part of an infinite hierarchy of flow equations for vertices with two external fermion legs and an arbitrary number of boson legs. In the next subsection we show that the structure of this infinite system of coupled integro-differential equations is simple enough to be solved exactly.

14.3 Ward identities as solutions of the infinite hierarchy of flow equations

Let us consider the terms on the right-hand sides of the flow equations for the vertices $\Gamma^{(2,m)}$ with two external fermion legs and an arbitrary number of boson legs. Assuming the validity of the closed loop theorem, all pure boson vertices $\Gamma^{(0,m)}$ with $m \geq 2$ vanish. From Fig. 14.1 (a) and Fig. 14.2 it is clear that in general the right-hand side of the flow equation for $\partial_\Lambda \Gamma^{(2,m)}$ depends on $\Gamma^{(2,m+2)}$ and on all $\Gamma^{(2,m')}$ with $m' \leq m$. In fact, from our general expression for the flow of the totally symmetrized vertices given in Eq. (11.51) we can derive the flow equations for the vertices $\Gamma^{(2,m)}$ with arbitrary m in closed form (we omit for simplicity the degeneracy index σ),

$$\begin{aligned}
\partial_\Lambda \Gamma^{(2,m)}(K';K;\bar{K}_1,\ldots,\bar{K}_m) &= \frac{1}{2}\int_{\bar{K}} \dot{F}_{\sigma\sigma}(\bar{K})\Gamma^{(2,m+2)}(K';K;-\bar{K},\bar{K},\bar{K}_1,\ldots,\bar{K}_m) \\
&+\sum_{l=2}^{\infty}\sum_{m_1,\ldots,m_l=1}^{\infty}\frac{\delta_{m,\sum_i m_i}}{\prod_i m_i!}\sum_P \int_{\bar{K}} \dot{F}(\bar{K})\Gamma^{(2,m_1+1)}\left(K';\tilde{K}_1;\bar{K}_{P(1)},\ldots,\bar{K}_{P(m_1)},-\bar{K}\right) \\
&\times G(\tilde{K}_1)\Gamma^{(2,m_2)}\left(\tilde{K}_1;\tilde{K}_2;\bar{K}_{P(m_1+1)},\ldots,\bar{K}_{P(m_1+m_2)}\right) G(\tilde{K}_2)\cdot\ldots\cdot G(\tilde{K}_{l-1}) \\
&\times \Gamma^{(2,m_l+1)}\left(\tilde{K}_{l-1};K;\bar{K},\bar{K}_{P(m-m_l+1)},\ldots,\bar{K}_{P(m)}\right) ,
\end{aligned} \tag{14.14}$$

where we have defined

$$K' = K + \sum_{i=1}^{m}\bar{K}_i\,, \qquad \tilde{K}_i = K' + \bar{K} - \sum_{j=1}^{m_1+\ldots+m_i}\bar{K}_{P(j)}\,, \tag{14.15}$$

and P denotes a permutation of $\{1,\ldots,m\}$. In Fig. 14.4, a graphical representation of Eq. (14.14) is shown. Note that the flow equation (14.1) for the irreducible self-energy is a special case of Eq. (14.14) for $m = 0$.

We are now facing the problem of solving the infinite hierarchy of coupled flow equations given by Eq. (14.14). In view of the fact that these equations are exact and that in one dimension the single-particle Green's function of the TLM can be calculated exactly via bosonization, we expect that this infinite hierarchy of flow equations can also be solved exactly. Indeed, the solutions of these equations are nothing but infinitely many Ward identities relating the vertex $\Gamma^{(2,m)}$ with two fermion legs and m boson legs to the vertex $\Gamma^{(2,m-1)}$ with one fewer boson leg.

These Ward identities for the vertex functions can be obtained from the "master Ward identities" in Eqs. (12.27) and (12.28) by functional differentiation. For example, taking the derivative $\frac{\delta}{\delta\varphi_{-\bar{K}\sigma}}$ of Eq. (12.28) we obtain

$$i\bar{\omega}\Pi_\sigma(\bar{K}) - \Pi^c_\sigma(\bar{K}) = 0 \;, \tag{14.16}$$

where we have defined

$$\Pi^c_\sigma(\bar{K}) = -i\zeta \int_K (\xi_{\mathbf{k}+\bar{\mathbf{k}},\sigma} - \xi_{\mathbf{k}\sigma}) G_\sigma(K) G_\sigma(K+\bar{K}) \Gamma^{(2,1)}(K+\bar{K}\sigma; K\sigma; \bar{K}\sigma) \;. \tag{14.17}$$

Eq. (14.16) is a relation between response functions, which follows more directly from the equation of continuity.

The simplified "master Ward identitiy" in Eq. (12.30) can be used if at least one fermionic momentum is involved. Differention with respect to the fields using the relation (13.38) as well as

$$\left.\frac{\delta^{(3)}\Gamma}{\delta\varphi_{\bar{K}\sigma}\delta\psi_{K\sigma}\delta\bar{\psi}_{K+\bar{K}\sigma}}\right|_{\text{fields}=0} = \Gamma^{(2,1)}(K+\bar{K}\sigma; K\sigma; \bar{K}\sigma) \;, \tag{14.18}$$

$$\left.\frac{\delta^{(4)}\Gamma}{\delta\varphi_{\bar{K}_1\sigma}\delta\varphi_{\bar{K}_2\sigma}\delta\psi_{K\sigma}\delta\bar{\psi}_{K+\bar{K}_1+\bar{K}_2\sigma}}\right|_{\text{fields}=0} = \Gamma^{(2,2)}(K+\bar{K}_1+\bar{K}_2\sigma; K\sigma; \bar{K}_1\sigma, \bar{K}_2\sigma) \;, \tag{14.19}$$

and so on, we obtain Ward identities for the irreducible vertices. For $m = 1$ the Ward identity is well known [Dzyaloshinskii and Larkin, 1974,Bohr, 1981,Metzner *et al.*, 1998, Kopietz, 1997]

$$G(K+\bar{K})\Gamma^{(2,1)}(K+\bar{K}; K; \bar{K})G(K) = \frac{-i}{i\bar{\omega} - \mathbf{v}_{F,\sigma}\cdot\bar{\mathbf{k}}}\Big[G(K+\bar{K}) - G(K)\Big] \;. \tag{14.20}$$

Here $\mathbf{v}_{F,\sigma}$ is the Fermi velocity associated with the independent fermionic label $K = (\mathbf{k}, i\omega)$, where $|\mathbf{k} - \mathbf{k}_{F,\sigma}| \ll |\mathbf{k}_{F,\sigma}|$. The Ward identity (14.20) has been used in [Dzyaloshinskii and Larkin, 1974] and [Metzner *et al.*, 1998] to close the skeleton equation for the self-energy and thus obtain the exact Green's function

of the TLM without invoking the machinery of bosonization. A Ward identity for $\Gamma^{(4,1)}$ has also been used to prove the vanishing of the renormalization group β function for the TLM [DiCastro and Metzner, 1991]. However, for solving the TLM within the framework of the functional RG, we need the Ward identities for all vertices $\Gamma^{(2,m)}$ with $m \geq 1$. For these, we obtain

$$\Gamma^{(2,m)}\Big(K'; K; \bar{K}_1, \ldots, \bar{K}_m\Big) = \frac{-i}{i\bar{\omega}_l - \mathbf{v}_{F,\sigma}\cdot\bar{\mathbf{k}}_l}\Bigg[\Gamma^{(2,m-1)}\Big(K'; K+\bar{K}_l; \bar{K}_1, \ldots, \bar{K}_{l-1}, \bar{K}_{l+1}, \ldots, \bar{K}_m\Big) - \Gamma^{(2,m-1)}\Big(K'-\bar{K}_l; K; \bar{K}_1, \ldots, \bar{K}_{l-1}, \bar{K}_{l+1}, \ldots, \bar{K}_m\Big)\Bigg], \quad (14.21)$$

where $1 \leq l \leq m$. For clarity let us write down here the special case $m = 2$,

$$\begin{aligned}\Gamma^{(2,2)}&\Big(K+\bar{K}_1+\bar{K}_2; K; \bar{K}_1, \bar{K}_2\Big) \qquad (14.22)\\ &= \frac{-i}{i\bar{\omega}_1 - \mathbf{v}_{F,\sigma}\cdot\bar{\mathbf{k}}_1}\Big[\Gamma^{(2,1)}\Big(K+\bar{K}_1+\bar{K}_2; K+\bar{K}_1; \bar{K}_2\Big) - \Gamma^{(2,1)}\Big(K+\bar{K}_2; K; \bar{K}_2\Big)\Big]\\ &= \frac{-i}{i\bar{\omega}_2 - \mathbf{v}_{F,\sigma}\cdot\bar{\mathbf{k}}_2}\Big[\Gamma^{(2,1)}\Big(K+\bar{K}_1+\bar{K}_2; K+\bar{K}_2; \bar{K}_1\Big) - \Gamma^{(2,1)}\Big(K+\bar{K}_1; K; \bar{K}_1\Big)\Big].\end{aligned}$$

Diagrammatic representations of the Ward identities given in Eqs. (14.20) and (14.21) are shown in Fig. 14.5. Although the Ward identity (14.20) for the three-legged vertex is well-known [Dzyaloshinskii and Larkin, 1974,Bohr, 1981,Metzner *et al.*, 1998, Kopietz, 1997], it seems that the higher order Ward identities given in Eqs. (14.21) and (14.23) cannot be found anywhere in the literature.

Of course, other Ward identities, e.g., the Ward identity for $\Gamma^{(4,1)}$ discussed in [Benfatto and Mastropietro, 2005], can also be obtained from Eq. (12.30). If the dispersion is not linearized as in Eq. (12.29), the master Ward identity (12.30) should be replaced by the more general master Ward identity (12.28), so that the Ward identities (14.20,14.21,14.23) for the vertices acquire correction terms. The effect of these correction terms on the Ward identities for $\Gamma^{(2,1)}$ and $\Gamma^{(4,1)}$ has very recently been studied in a mathematically rigorous way by Benfatto and Mastropietro [Benfatto and Mastropietro, 2005]

Once the form of the higher Ward identities is known, we can also show by induction that they provide a solution of the infinite hierarchy of flow equations in Eqs. (14.1) and (14.14). This can be done entirely within the fRG formalism without referring to the derivation via local gauge transformations. In the initial condition, i.e., for $\Lambda_B = \Lambda_{B,0}$, the Ward identities are almost trivially fulfilled. More precisely, vertices $\Gamma^{(2,m)}$ with $m > 1$ vanish, whereas a difference of inverse free propagators for a linearized dispersion cancels the denominator in Eq. (14.20) and this Ward identity is also fulfilled. To show that the flow equations respect

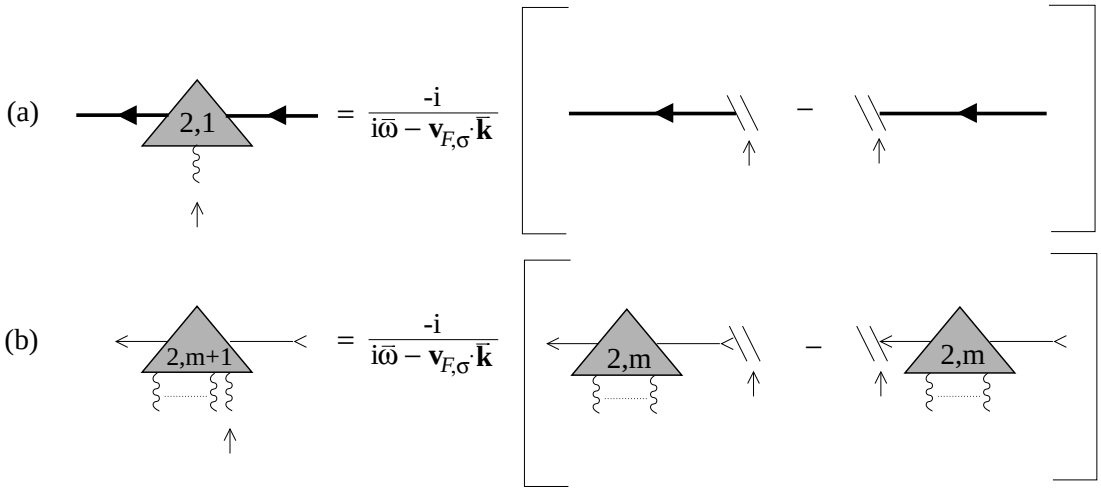

Figure 14.5: (a) Diagrammatic representation of the Ward identity (14.20) for the three-legged vertex and (b) of the Ward identity (14.21) for the vertex with two fermion legs and $m > 1$ boson legs. The small arrow indicates the place in the diagram where the external bosonic energy-momentum enters. A double-slash to the right of an arrow means that the bosonic momentum is added before the corresponding Green's function, while a double-slash to the left of an arrow means that the momentum is added after the Green's function.

the Ward identities, we then substitute them on the right hand side of the exact flow equation for $\Gamma^{(2,m+1)}$. Graphically, we indicate the place where the bosonic momentum enters the vertex by a double-slash, as shown in Fig. 14.5. The important point is now that all diagrams with double-slashes attached to intermediate Green's functions cancel due to the fact that all vertices $\Gamma^{(2,m')}$ can be expressed in terms of a difference of vertices $\Gamma^{(2,m'-1)}$, with a same prefactor that is independent of m'. Graphically, only the diagrams with a double-slash attached to the leftmost or rightmost Green's function survive. We end up with diagrams that are present on the right hand side of the flow equations for $\Gamma^{(2,m)}$. In this way, we can show from the fRG flow equations that the derivative of the Ward identities with respect to Λ is fulfilled. This completes the inductive proof, since if the Ward identities are fulfilled initially and the flow respects them, they hold at all stages of the RG flow.

14.4 Exact fRG solution of the Tomonaga-Luttinger model

Given the cascade of Ward identities (14.20) and (14.21) we can close the integro-differential equation (14.1) for the irreducible self-energy. Note that this equation

involves both the three-legged vertex and the four-legged vertex with two fermion legs and two boson legs, so that the Ward identity (14.20) is not sufficient to close the flow equation. Of course, if one is only interested in calculating the Green's function of the TLM, it is simpler to start from the skeleton equation for the self-energy shown in Fig. 13.8, which can be closed by means of the Ward identity (14.20) for the three-legged vertex only. Nevertheless, it is instructive to see how the exact solution emerges within the framework of the functional RG. Substituting Eqs. (14.20) and (14.23) into Eq. (14.1), we obtain the following integrodifferential equation for the electronic self-energy,

$$\partial_\Lambda \Sigma_\sigma(K) = G_\sigma^{-2}(K) \int_{\bar{K}} \frac{\dot{F}_{\sigma\sigma}(\bar{K})}{(i\bar{\omega} - \mathbf{v}_{F,\sigma}\cdot\bar{\mathbf{k}})^2} \left[G_\sigma(K) - G_\sigma(K+\bar{K})\right] . \tag{14.23}$$

Remember that the index σ labels not only the different spin species, but also the different patches of the sectorized Fermi surface. For example, for the spinless case $\sigma = \pm k_F$. Using the fact that in the momentum-transfer cutoff scheme $G^2\partial_\Lambda \Sigma = \partial_\Lambda G$ we can alternatively write Eq. (14.23) as a *linear* integro-differential equation for the fermionic Green's function,

$$\partial_\Lambda G_\sigma(K) = \int_{\bar{K}} \frac{\dot{F}_{\sigma\sigma}(\bar{K})}{(i\bar{\omega} - \mathbf{v}_{F,\sigma}\cdot\bar{\mathbf{k}})^2} \left[G_\sigma(K) - G_\sigma(K+\bar{K})\right] .$$

If we had simply set the vertex $\Gamma^{(2,2)}$ equal to zero in Eq (14.1) and had then closed this equation by means of the Ward identity (14.20), we would have obtained a non-linear equation. Thus, the linearity of Eq. (14.24) is the result of a cancellation of non-linear terms arising from both Ward identities (14.20) and (14.23). Because the second term on the right hand side of Eq. (14.24) is a convolution, we can easily solve this equation by a Fourier transformation to imaginary time and real space. Defining

$$G_\sigma(X) = \int_K e^{i(\mathbf{k}\cdot\mathbf{r} - \omega\tau)} G_\sigma(K) , \tag{14.24}$$

$$H_{\Lambda,\sigma}(X) = \int_{\bar{K}} e^{i(\bar{\mathbf{k}}\cdot\mathbf{r} - \bar{\omega}\tau)} \frac{\dot{F}_{\sigma\sigma}(\bar{K})}{(i\bar{\omega} - \mathbf{v}_{F,\sigma}\cdot\bar{\mathbf{k}})^2} , \tag{14.25}$$

where $X = (\tau, \mathbf{r})$, the flow equation (14.24) is transformed to

$$\Big[\partial_\Lambda + H_{\Lambda,\sigma}(X) - H_{\Lambda,\sigma}(0)\Big] G_\sigma(X) = 0 . \tag{14.26}$$

This implies the conservation law

$$\partial_\Lambda \left[\exp\left\{\int_0^\Lambda d\Lambda' \left[H_{\Lambda',\sigma}(X) - H_{\Lambda',\sigma}(0)\right]\right\} G_\sigma(X)\right] = 0 . \tag{14.27}$$

Integrating from $\Lambda = 0$ to $\Lambda = \Lambda_0$, we obtain

$$G_\sigma(X) = G_{0,\sigma}(X)\, \exp\left[Q_\sigma(X)\right] , \tag{14.28}$$

with

$$Q_\sigma(X) = S_\sigma(0) - S_\sigma(X) , \tag{14.29}$$

and

$$S_\sigma(X) = -\int_0^{\Lambda_0} d\Lambda' H_{\Lambda',\sigma}(X) = \int_{\bar{K}} \frac{\Theta(\Lambda_0 - |\bar{\mathbf{k}}|) F_{\sigma\sigma}(\bar{K})}{(i\bar{\omega} - \mathbf{v}_{F,\sigma}\cdot\bar{\mathbf{k}})^2} \cos(\bar{\mathbf{k}}\cdot\mathbf{r} - \bar{\omega}\tau) , \tag{14.30}$$

where we have used the invariance of the RPA interaction $F(\bar{K})$ under $\bar{K} \to -\bar{K}$. The solution in Eqs. (14.28)–(14.30) is well known from the functional integral approach to bosonization [Kopietz, 1997, Kopietz *et al.*, 1995, Fogedby, 1976, Lee and Chen, 1988] where $Q_\sigma(X)$ arises as a Debye-Waller factor from Gaussian averaging over the distribution of the Hubbard-Stratonovich field. In one dimension, Eqs. (14.28)–(14.30) can be shown [Kopietz, 1997] to be equivalent to the exact solution for the Green's function of the Tomonaga-Luttinger model obtained via conventional bosonization. We have thus succeeded to calculate the single-particle Green's function of the TLM entirely within the framework of the functional RG.

14.5 Truncation scheme based on relevance

The structure of the exact Green's function of the TLM and the corresponding spectral function $A(k,\omega) = -\pi^{-1}\mathrm{Im}\, G(k,\omega + i0)$ depend crucially on the Ward identities discussed above, which in turn are only valid if the energy dispersion is strictly linear. In order to assess the validity of the linearization of the energy dispersion, it is important to develop truncations of the exact hierarchy of flow equations which do not explicitly make use of Ward identities. We now propose such a truncation scheme.

The coefficients generated in the expansion of a given vertex $\Gamma^{(2n,m)}$ in powers of frequencies and momenta have decreasing scaling dimensions, so that the most relevant part of any vertex is obtained by setting all momenta and frequencies equal to zero. This classification leads to a simple truncation scheme: We retain only those vertices whose leading (momentum- and frequency-independent) part has a positive or vanishing scaling dimension, corresponding to relevant or marginal couplings in the usual RG jargon. In the context of calculating the critical temperature of the weakly interacting Bose gas in three dimensions, such a truncation procedure has recently been shown to give very accurate results [Ledowski *et al.*, 2004].

To begin with, let us classify all couplings according to their relevance. With the rescaling defined in Sec. 13.4, for $D = z_\psi = z_\varphi = 1$, the scaling dimensions of

the vertices $\tilde{\Gamma}^{(2n,m)}$ are $D^{(2n,m)} = 2 - n - m$, see Eq. (13.37). Hence the vertex $\tilde{\Gamma}^{(2,2)}$ as well as the vertices $\tilde{\Gamma}^{(0,3)}$ and $\tilde{\Gamma}^{(0,4)}$, whose unrescaled versions appear on the right-hand sides of Eqs. (14.1) and (14.2), are irrelevant in the RG sense. In contrast, the momentum- and frequency-independent part of the three-legged vertex,

$$\tilde{\gamma}_l = \tilde{\Gamma}^{(2,1)}(0;0;0) = \left(\frac{\Lambda}{\nu_0 \Omega_\Lambda}\right)^{1/2} Z_l \Gamma^{(2,1)}(K_F; K_F; 0) \;, \tag{14.31}$$

is marginal [Ueda and Rice, 1984]. Here $K_F = (\pm k_F, \omega = 0)$. From the general flow equations (13.29) and (13.33) for the rescaled vertices we obtain the following exact flow equation for the rescaled self-energy defined in Eq. (13.27),

$$\partial_l \tilde{\Sigma}_l(Q) = \left(1 - \eta_l + Q \cdot \frac{\partial}{\partial Q}\right) \tilde{\Sigma}_l(Q) + \dot{\tilde{\Gamma}}_l^{(2,0)}(Q) \;, \tag{14.32}$$

with [see Eq. (13.33)]

$$\dot{\tilde{\Gamma}}_l^{(2,0)}(Q) = -\frac{Z_l}{\Omega_\Lambda} \Lambda \partial_\Lambda \Gamma_\Lambda^{(2,0)}(K) \;. \tag{14.33}$$

We restrict ourselves to spinless fermions here and choose $\Omega_\Lambda = \bar{\Omega}_\Lambda = v_F \Lambda$, so that with $\nu_0 = (\pi v_F)^{-1}$ the prefactor in Eq. (14.31) turns out to be $(\frac{\Lambda}{\nu_0 \Omega_\Lambda})^{1/2} = \pi^{1/2}$. As usual, the fermionic wave-function renormalization factor Z_l is defined via

$$Z_l = \left[1 - \left.\frac{\partial \Sigma(K)}{\partial(i\omega)}\right|_{K=0}\right]^{-1} = 1 + \left.\frac{\partial \tilde{\Sigma}_l(Q)}{\partial(i\epsilon)}\right|_{Q=0} \;. \tag{14.34}$$

According to Eq. (13.28) the wave-function renormalization Z_l satisfies the flow equation

$$\partial_l Z_l = -\eta_l Z_l \;, \tag{14.35}$$

where the flowing anomalous dimension of the fermion fields is given by

$$\eta_l = -\left.\frac{\partial \dot{\tilde{\Gamma}}_l^{(2,0)}(Q)}{\partial(i\epsilon)}\right|_{Q=0} \;. \tag{14.36}$$

According to Eq. (14.32) the constant part of the self-energy,

$$\tilde{r}_l = \tilde{\Sigma}_l(0) \;, \tag{14.37}$$

is relevant and satisfies

$$\partial_l \tilde{r}_l = (1 - \eta_l)\, \tilde{r}_l + \dot{\tilde{\Gamma}}_l^{(2,0)}(0) \;. \tag{14.38}$$

In general, $\tilde{r}_l$ will only flow into the fixed point if the initial coupling $\tilde{r}_0$ is properly fine-tuned. Apart from Z_l, there are two more marginal couplings. The first is the Fermi velocity renormalization factor [Busche *et al.*, 2002]

$$\tilde{v}_l = Z_l + \left. \frac{\partial \tilde{\Sigma}_l(Q)}{\partial q} \right|_{Q=0} , \tag{14.39}$$

and the second marginal coupling is the momentum- and frequency-independent part $\tilde{\gamma}_l$ of the rescaled three-legged vertex given in Eq. (14.31). The exact flow equations for $\tilde{v}_l$ and $\tilde{\gamma}_l$ are

$$\partial_l \tilde{v}_l = -\eta_l \tilde{v}_l + \left. \frac{\partial \dot{\tilde{\Gamma}}_l^{(2,0)}(Q)}{\partial q} \right|_{Q=0} , \tag{14.40}$$

and

$$\partial_l \tilde{\gamma}_l = -\eta_l \tilde{\gamma}_l + \dot{\tilde{\Gamma}}_l^{(2,1)}(0;0;0) . \tag{14.41}$$

If we retain only relevant and marginal couplings, then in the momentum-transfer cutoff scheme the rescaled fermionic Green's function defined in Eq. (13.35) is in $D = 1$ simply approximated by

$$\tilde{G}(Q) \approx \frac{1}{i\epsilon - \tilde{v}_l q - \tilde{r}_l} . \tag{14.42}$$

In order to make progress, we have to approximate the inhomogeneities $\dot{\tilde{\Gamma}}_l^{(2,0)}(Q)$ and $\dot{\tilde{\Gamma}}_l^{(2,1)}(0;0;0)$. In Sec. 13.5 we have proposed an approximation scheme which retains only the skeleton elements of the two-point functions. In the momentum-transfer cutoff scheme, the corresponding flow equations (13.44,13.45, 13.46) further simplify because we should omit all terms involving the fermionic single-scale propagator. Unfortunately, the resulting non-linear integro-differential equations still cannot be solved analytically. In order to simplify these equations further, let us replace the three-legged vertex on the right-hand sides of these equations by its marginal part. In this approximation we obtain from Eq. (13.44)

$$\dot{\tilde{\Gamma}}_l^{(2,0)}(Q) \approx \tilde{\gamma}_l^2 \int_{\bar{Q}} \dot{\tilde{F}}(\bar{Q}) \tilde{G}(Q + \bar{Q}) , \tag{14.43}$$

and from Eq. (13.46)

$$\dot{\tilde{\Gamma}}_l^{(2,1)}(0;0;0) \approx \tilde{\gamma}_l^3 \int_{\bar{Q}} \dot{\tilde{F}}(\bar{Q}) \tilde{G}^2(\bar{Q}) . \tag{14.44}$$

In order to be consistent, we should approximate $\tilde{G}(Q)$ in Eqs. (14.43) and (14.44) by Eq. (14.42). Then it is easy to see that the second term on the right-hand

sides of the flow equations (14.40) and (14.41) exactly cancels the contribution from the anomalous dimension, so that

$$\partial_l \tilde{\gamma}_l = 0 \ , \ \ \partial_l \tilde{v}_l = 0 \ . \tag{14.45}$$

For explicit calculations, let us assume that the coupling parameters of the TLM defined in the introduction are $g_2 = g_4 = f_0$, so that

$$\dot{\tilde{F}}(\bar{Q}) = \delta(1-|\bar{q}|)\frac{\tilde{f}_0(\bar{q}^2+\bar{\epsilon}^2)}{(1+\tilde{f}_0)\bar{q}^2+\bar{\epsilon}^2} \ , \tag{14.46}$$

where $\tilde{f}_0 = \nu_0 f_0$. From Eqs. (14.36) and (14.43) we then find that the anomalous dimension $\eta = \eta_l$ does not flow and is given by

$$\eta = \frac{\tilde{f}_0^2}{2\sqrt{1+\tilde{f}_0}\left[\sqrt{1+\tilde{f}_0}+1\right]^2} \ , \tag{14.47}$$

which agrees exactly with the bosonization result [Kopietz, 1997]. We emphasize that Eq. (14.47) is the correct anomalous dimension of the TLM even for $\tilde{f}_0 \gg 1$, so that, at least as far as the calculation of η is concerned, the validity of our simple truncation is not restricted to the weak coupling regime. Recall that the restriction to weak coupling is one of the shortcomings of the conventional fermionic functional RG, which was implemented for the TLM in Ref. [Busche *et al.*, 2002]. Because η is finite, the running vertex $\Gamma^{(2,1)}(K_F;K_F;0)$ without wave-function renormalization actually diverges for $\Lambda \to 0$. However, the properly renormalized vertex $\tilde{\gamma}_l \propto Z_l \Gamma^{(2,1)}(K_F;K_F;0)$ remains finite due to the vanishing wave-function renormalization

$$Z_l = e^{-\eta l} = \left(\frac{\Lambda}{\Lambda_0}\right)^{\eta} \tag{14.48}$$

for $l \to \infty$. Integrating the flow equation (14.32) for the self-energy with the inhomogeneity approximated by Eqs. (14.43) and (14.42), we obtain, after going back to physical variables

$$\Sigma(k_F+k,i\omega) = \\ -\int_{-\Lambda_0}^{\Lambda_0}\frac{d\bar{k}}{2\pi}\int_{-\infty}^{\infty}\frac{d\bar{\omega}}{2\pi}\left(\frac{\Lambda_0}{|\bar{k}|}\right)^{\eta}\frac{f^{\rm RPA}(\bar{k},i\bar{\omega})}{i(\omega+\bar{\omega})-v_F(k+\bar{k})} \ , \tag{14.49}$$

where the RPA screened interaction is

$$f^{\rm RPA}(\bar{k},i\bar{\omega}) = f_0\frac{v_F^2\bar{k}^2+\bar{\omega}^2}{v_c^2\bar{k}^2+\bar{\omega}^2} \ . \tag{14.50}$$

Here $v_c = v_F\sqrt{1+\tilde{f}_0}$ is the velocity of collective charge excitations. Eq. (14.49) resembles the GW approximation, [Hedin, 1965] but with the RPA interaction multiplied by an additional singular vertex correction $(\Lambda_0/|\bar{k}|)^\eta$. The explicit evaluation of Eq. (14.49) is rather tedious and will not be further discussed in this work. The resulting spectral function $A(k,\omega)$ agrees at $k = k_F$ with the bosonization result (even at strong coupling), but has the wrong threshold singularities for $|\omega| \to v_c|(k \pm k_F)|$. So far we have not been able to find a reasonably simple truncation of the exact flow equations which completely produces the spectral line shape of $A(k,\omega)$, as predicted by bosonization or by our exact solution presented in the previous section. Whether a self-consistent numerical solution of the truncation discussed in Sec. 13.5 [see Eqs. (13.44)-(13.46)] would reproduce the correct spectral line-shape or not remains an open problem. The numerical solution of these equations seems to be rather difficult and is beyond the scope of this work.

Chapter 15:

Summary and outlook

In the second part of this thesis we have developed a new formulation of the functional renormalization group (fRG) for interacting fermions, which is based on the explicit introduction of collective bosonic degrees of freedom via a suitable Hubbard-Stratonovich transformation. Our method unifies two well-known approaches to interacting Fermi systems. On the one hand, the purely fermionic version of the fRG has been used by many authors during the last decade to analyze the phase diagram of the two-dimensional Hubbard model and its extensions. On the other hand, a renormalization group treatment of a theory containing only a fluctuating order parameter is often appropriate in the vicinity of a quantum critical point. In the latter approach the fermionic degrees of freedom are integrated out after introducing a bosonic order parameter via a Hubbard-Stratonovich transformation. In contrast, we explicitly kept the fermionic variables and derived a hierarchy of flow equations for the vertex functions of the coupled theory containing fermionic as well as bosonic fields. In this formulation, the interaction of the purely fermionic model appears as a propagator of the bosonic fields, and a cutoff in the momentum transfer of the interaction can be introduced on the same footing as a bandwidth cutoff. It is then quite natural to work with vertices which are one-line-irreducible and cannot be split in half by cutting either a particle propagator line or a line representing the interaction. Irreducibility with respect to the interaction line is closely related to two-particle irreducibility in the zero-sound channel, and an extension of our approach to other interaction channels would bring us closer to full two-particle irreducibility. A similar strategy has been used previously in Refs. [Correia *et al.*, 2002], [Wetterich, 2004] and [Baier *et al.*, 2004]. However, on a technical level the practical implementation of the method presented here differs considerably from previous works.

We have presented the theoretical foundation of our approach and developed an efficient method to keep track of all terms. As an important application, we have considered interactions that are dominated by small momentum transfers. In these forward scattering problems Ward identities play a crucial role. We have presented a fRG scheme that uses only a cutoff in the momentum transfer of the interaction. Within this scheme, we have shown that the RG flow does not violate the Ward identities. In fact, Ward identities emerged as the solution of the infinite hierarchy of coupled RG flow equations for the one-line irreducible vertices involving two external fermion legs and an arbitrary number of boson legs. We could obtain a closed linear integro-differential equation for the single-particle Green's function which was solved by a Fourier transformation to real space and imaginary time. The solution has the form familiar from the functional

version of bosonization [Kopietz, 1997]. In one dimension, this form is known to be equivalent to the solution obtained from the operator version of bosonization. Hence, the Tomonaga-Luttinger model (TLM) has been solved exactly within the fRG formalism.

In addition, a truncation scheme of the infinite hierarchy of flow equations has been developed based on the leading terms in an expansion in relevance. This rather simple truncation was sufficient to obtain the exact anomalous dimension of the spinless TLM for arbitrary strength of the interaction. Note that in the purely fermionic RG, a two loop calculation is necessary to obtain the leading perturbative contribution to the anomalous dimension. Also, frequency dependencies of the fermionic four point vertex have to be taken into account, which is quite intractable in numerical solutions of the flow equations. In our approach, the effective interaction acquires a frequency dependence even within the lowest-order approximation. In fact, if we ignore vertex corrections, the effective interaction is simply given by the RPA. Hence, strong coupling fixed points might be accessible within our approach. Furthermore, the truncation lead to the correct scaling behavior of the single particle Green's function for momenta $k = \pm k_F$ at the Fermi points. On the other hand, the threshold singularities for $k \neq \pm k_F$ are not correctly reproduced within this approximation. Nevertheless, the result for the anomalous dimension is quite promising and more elaborate truncation schemes should therefore be analyzed to obtain accurate results for the spectral properties. Such truncations would be extremely valuable for situations where Ward identities are not valid.

The development of a reliable truncation could for example lead to an understanding of non-universal effects in one-dimensional metals. If the energy dispersion is not linearized, there should be a finite momentum scale k_c (depending on the interaction and the band curvature) below which typical scaling behavior predicted by the TLM emerges. The calculation of k_c as well as the non-universal spectral line-shape are difficult within bosonization [Busche and Kopietz, 2000]. On the other hand, within the framework of the functional RG the inclusion of irrelevant coupling parameters should be possible. Note that an entire crossover scaling function between the critical regime and the short-wavelength regime of interacting bosons in $D = 3$ was recently calculated within the fRG formalism [Ledowski *et al.*, 2004, Hasselmann *et al.*, 2004].

Our approach might also be useful for the treatment of quantum phase transitions in situations where the fermions cannot be completely integrated out. The traditional Landau-Ginzburg-Wilson approach in terms of the order parameter alone breaks down when generic non-critical soft modes are present [Belitz *et al.*, 2004, Belitz *et al.*, 2001a, Belitz *et al.*, 2001b]. In the purely fermionic fRG symmetry breaking manifests itself via the divergence of the relevant order-parameter susceptibility. The symmetry broken phase itself is difficult to describe within this approach, although for the simplified case of the reduced BCS model the flow could recently be continued into the symmetry broken phase [Salmhofer *et al.*,

2004]. On the other hand, in our approach the order parameter can be introduced explicitly as a bosonic field, which acquires a vacuum expectation value in the symmetry broken phase. Previously, a similar approach has been developed in Ref. [Baier *et al.*, 2004] to study antiferromagnetism in the two-dimensional Hubbard model.

In summary, we believe that the new formalism presented in this part of the thesis and possible extensions will be useful for various physical situations.

Bibliography

[Affleck, 1989] I. Affleck, *Quantum spin chains and the Haldane gap*, J. Phys.: Condens. Matter **1**, 3047 (1989).

[Aharonov and Bohm, 1956] Y. Aharonov and D. Bohm, *Significance of Electromagnetic Potentials in the Quantum Theory*, Phys. Rev. **115**, 485 (1956).

[Aharonov and Casher, 1984] Y. Aharonov and A. Casher, *Topological Quantum Effects for Neutral Particles*, Phys. Rev. Lett. **53**, 319 (1984).

[Ambegaokar and Eckern, 1990] V. Ambegaokar and U. Eckern, *Coherence and Persistent Currents in Mesoscopic Rings*, Phys. Rev. Lett. **65**, 381 (1990).

[Amit, 1984] D. J. Amit, *Field theory, the renormalization group, and critical phenomena* (World Scientific, 1984).

[Andergassen *et al.*, 2004] S. Andergassen, T. Enss, V. Meden, W. Metzner, U. Schollwöck, and K. Schöhammer, *Functional renormalization group for Luttinger liquids with impurities*, Phys. Rev. B **70**, 075102 (2004).

[Anderson, 1952] P. W. Anderson, *An Approximate Quantum Theory of the Antiferromagnetic Ground State*, Phys. Rev. **86**, 694 (1952).

[Auerbach, 1994] A. Auerbach, *Interacting Electrons and Quantum Magnetism* (Springer, New York, 1994).

[Awschalom *et al.*, 2002] D. D. Awschalom, D. Loss, and N. Samarth, eds., *Semiconductor Spintronics and Quantum Computation* (Springer, Berlin, 2002).

[Bagnuls and Bervillier, 2002] C. Bagnuls and C. Bervillier, *Exact Renormalization Group equations. An introductory Review*, Phys. Rept. **348**, 91 (2002).

[Baier *et al.*, 2004] T. Baier, E. Bick, and C. Wetterich, *Temperature dependence of antiferromagnetic order in the Hubbard model*, Phys. Rev. B **70**, 125111 (2004).

[Baier *et al.*, 2005] T. Baier, E. Bick, and C. Wetterich, *Antiferromagnetic gap in the Hubbard model*, Phys. Lett. B **605**, 144 (2005).

[Bartosch and Kopietz, 1999] L. Bartosch and P. Kopietz, *Correlation functions of higher-dimensional Luttinger liquids*, Phys. Rev. B **59**, 5377 (1999).

[Bednorz and Müller, 1986] J. G. Bednorz and K. A. Müller, *Possible high Tc superconductivity in the Ba-La-Cu-O system*, Z. Phys. B **64**, 189 (1986).

[Belitz *et al.*, 2001a] D. Belitz, T. R. Kirkpatrick, M. T. Mercaldo, and S. L. Sessions, *Local field theory for disordered itinerant quantum ferromagnets*, Phys. Rev. B **63**, 174427 (2001a).

[Belitz *et al.*, 2001b] D. Belitz, T. R. Kirkpatrick, M. T. Mercaldo, and S. L. Sessions, *Quantum critical behavior in disordered itinerant ferromagnets: Logarithmic corrections to scaling*, Phys. Rev. B **63**, 174428 (2001b).

[Belitz *et al.*, 2004] D. Belitz, T. R. Kirkpatrick, and J. Rollbühler, *Breakdown of the Perturbative Renormalization Group at Certain Quantum Critical Points*, Phys. Rev. Lett. **93**, 155701 (2004).

[Benfatto and Mastropietro, 2005] G. Benfatto and V. Mastropietro, *Ward identities and Chiral anomaly in the Luttinger liquid*, Commun. Math. Phys. **258**, 609 (2005).

[Binz *et al.*, 2002] B. Binz, D. Baeriswyl, and B. Douçot, *Wilson's renormalization group applied to 2D lattice electrons in the presence of van Hove singularities*, Eur. Phys. J. B **25**, 69 (2002).

[Blaizot *et al.*, 2004] J.-P. Blaizot, R. M. Galain, and N. Wschebor, *Non Perturbative Renormalization Group, momentum dependence of n-point functions and the transition temperature of the weakly interacting Bose gas*, cond-mat/0412481 (2004).

[Bloch, 1930] F. Bloch, *Zur Theorie des Ferromagnetismus*, Z. Physik **61**, 206 (1930).

[Bloch, 1933] F. Bloch, ZS. Physik **81**, 363 (1933).

[Bohr, 1981] T. Bohr, *Lectures on the Luttinger Model* (Nordita preprint 81/4 (unpublished), 1981).

[Busche, 2003] T. Busche, *Renormalization-group approach to the spectral function of the Tomonaga-Luttinger model*, Ph.D. thesis, Universität Frankfurt (2003).

[Busche and Kopietz, 2000] T. Busche and P. Kopietz, *How does a quadratic term in the energy dispersion modify the single-particle Green's function of the Tomonaga-Luttinger model?*, Int. J. Mod. Phys. B **14**, 1481 (2000).

[Busche *et al.*, 2002] T. Busche, L. Bartosch, and P. Kopietz, *Dynamic scaling in the vicinity of the Luttinger liquid fixed point*, J. Phys.: Cond. Mat. **14**, 8513 (2002).

[Büttiker *et al.*, 1983] M. Büttiker, Y. Imry, and R. Landauer, *Josephson behaviour in small normal one-dimensional rings*, Phys. Lett. **96A**, 365 (1983).

[Canali *et al.*, 1992] C. M. Canali, S. M. Girvin, and M. Wallin, *Spin-wave velocity renormalization in the two-dimensional Heisenberg antiferromagnet at zero temperature*, Phys. Rev. B **45**, 10131 (1992).

[Cao *et al.*, 1997] Z. Cao, X. Yu, and R. Han, *Quantum phase and persistent magnetic moment current and Aharonov-Casher effect in a S=1/2 mesoscopic ferromagnetic ring*, Phys. Rev. B **56**, 5077 (1997).

[Castilla and Chakravarty, 1991] G. E. Castilla and S. Chakravarty, *Spin-wave expansion of the staggered magnetization of a square-lattice Heisenberg antiferromagnet at T=0*, Phys. Rev. B **43**, 13687 (1991).

[Cerletti *et al.*, 2005] V. Cerletti, W. A. Coish, O. Gywat, and D. Loss, *Recipes for spin-based quantum computing*, Nanotechnology **16**, R27 (2005).

[Chakravarty *et al.*, 1988a] S. Chakravarty, B. I. Halperin, and D. R. Nelson, *Low-temperature behavior of two-dimensional quantum antiferromagnets*, Phys. Rev. Lett. **60**, 1057 (1988a).

[Chakravarty *et al.*, 1988b] S. Chakravarty, B. I. Halperin, and D. R. Nelson, *Two-dimensional quantum Heisenberg antiferromagnet at low temperatures*, Phys. Rev. B **39**, 2344 (1988b).

[Chandra *et al.*, 1990] P. Chandra, P. Coleman, and A. I. Larkin, *A quantum fluids approach to frustrated Heisenberg models*, J. Phys.: Condens. Matter **2**, 7933 (1990).

[Chandrasekhar *et al.*, 1991] V. Chandrasekhar, R. A. Webb, M. J. Brady, M. B. Ketchen, W. J. Gallagher, and A. Kleinsasser, *Magnetic response of a single, isolated gold loop*, Phys. Rev. Lett. **67**, 3578 (1991).

[Chau and Kopietz, 2004] L. P. Chau and P. Kopietz, *Linear magnetic response of disordered metallic rings: Large contribution from forward-scattering interactions*, Phys. Rev. B **70**, 155317 (2004).

[Cheung *et al.*, 1988] H.-F. Cheung, Y. Gefen, and E. K. Riedel, *Isolated rings of mesoscopic dimensions. Quantum coherence and persistent currents*, IBM Res. Develop. **32**, 359 (1988).

[Correia *et al.*, 2002] S. Correia, J. Polonyi, and J. Richert, *The Functional Callan-Symanzik Equation for the Coulom Gas*, Annals Phys. **296**, 214 (2002).

[DiCastro and Metzner, 1991] C. DiCastro and W. Metzner, *Ward identities and the beta function in the Luttinger liquid*, Phys. Rev. Lett. **67**, 3852 (1991).

[DiCastro *et al.*, 1974] C. DiCastro, G. Jona-Lasinio, and L. Peliti, *Variational Principles, Renormalization Group, and Kadanoff's Universality*, Annals of Physics **87**, 327 (1974).

[DiVincenzo, 2000] D. P. DiVincenzo, *The Physical Implementation of Quantum Computation*, Fortschr. Phys. **48**, 771 (2000).

[Dyson, 1956a] F. J. Dyson, *General Theory of Spin-Wave Interactions*, Phys. Rev. **102**, 1217 (1956a).

[Dyson, 1956b] F. J. Dyson, *Thermodynamic Behavior of an Ideal Ferromagnet*, Phys. Rev. **102**, 1230 (1956b).

[Dzyaloshinskii and Larkin, 1974] I. E. Dzyaloshinskii and A. I. Larkin, *Correlation functions of a one-dimensional Fermi system with long-range interaction (Tomonaga model)*, Zh. Eksp. Teor. Fiz. **65**, 411 (1973) [Sov. Phys. JETP **38**, 202 (1974)] (1974).

[Eckern and Schwab, 2002] U. Eckern and P. Schwab, *Persistent Currents Versus Phase Breaking in Mesoscopic Metallic Samples*, J. of Low Temp. Phys, **126**, 1291 (2002).

[Enss, 2005] T. Enss, *Renormalization, Conservation Laws and Transport in Correlated Electron Systems*, Ph.D. thesis, Max-Planck-Institut für Festkörperforschung, Stuttgart (2005).

[Ferraz, 2003a] A. Ferraz, *Fermi surface renormalization in two spatial dimensions*, Europhys. Lett. **61**, 228 (2003a).

[Ferraz, 2003b] A. Ferraz, *Non-Fermi liquid in a truncated two-dimensional Fermi surface*, Phys. Rev. B **68**, 075115 (2003b).

[Feynman, 1982] R. P. Feynman, *Simulating Physics with Computers*, Int. J. Theor. Phys. **21**, 467 (1982).

[Fisher, 1998] M. E. Fisher, *Renormalization group theory: Its basis and formulation in statistical physics*, Rev. Mod. Phys. **70**, 653 (1998).

[Fogedby, 1976] H. C. Fogedby, *Correlation functions for the Tomonaga model*, J. Phys. C **9**, 3757 (1976).

[Freire *et al.*, 2005] H. Freire, E. Correa, and A. Ferraz, *Field-theoretical renormalization group for a flat two-dimensional Fermi surface*, Phys. Rev. B **71**, 165113 (2005).

[Fujikawa, 1980] K. Fujikawa, *Path integral for gauge theories with fermions*, Phys. Rev. D **21**, 2848 (1980).

[Gao and Qian, 1993] X.-C. Gao and T.-Z. Qian, *Aharonov-Anadan phase and persistent currents in a mesoscopic ring*, Phys. Rev. B **47**, 7128 (1993).

[Gorelik *et al.*, 2003] L. Y. Gorelik, R. I. Shekhter, V. Vinokur, D. Feldman, V. Kozub, and M. Jonson, *Electrical manipulation of nanomagnets*, Phys. Rev. Lett. **91**, 088301 (2003).

[Halboth and Metzner, 2000a] C. J. Halboth and W. Metzner, *d-Wave Superconductivity and Pomeranchuk Instability in the Two-Dimensional Hubbard Model*, Phys. Rev. Lett. **85**, 5162 (2000a).

[Halboth and Metzner, 2000b] C. J. Halboth and W. Metzner, *Renormalization-group analysis of the two-dimensional Hubbard model*, Phys. Rev. B **61**, 7364 (2000b).

[Haldane, 1981] F. D. M. Haldane, *'Luttinger liquid theory' of one-dimensional quantum fluids. I. Properties of the Luttinger model and their extension to the general 1D interacting spinless Fermi gas*, J. Phys. C: Solid State Phys. **14**, 2585 (1981).

[Haldane, 1983a] F. D. M. Haldane, *Continuum dynamics of the 1-D Heisenberg antiferromagnet: Identification with the O(3) nonlinear sigma model*, Phys. Lett. **93A**, 464 (1983a).

[Haldane, 1983b] F. D. M. Haldane, *Nonlinear Field Theory of Large-Spin Heisenberg Antiferromagnets: Semiclassically Quantized Solitons of the One-Dimensional Easy-Axis Néel State*, Phys. Rev. Lett. **50**, 1153 (1983b).

[Harris *et al.*, 1971] A. B. Harris, D. Kumar, B. I. Halperin, and P. C. Hohenberg, *Dynamics of an Antiferromagnet at Low Temperatures: Spin-Wave Damping and Hydrodynamics*, Phys. Rev. B **3**, 961 (1971).

[Hasselmann *et al.*, 2004] N. Hasselmann, S. Ledowski, and P. Kopietz, *Critical behavior of weakly interacting bosons: A functional renormalization-group approach*, Phys. Rev. A **70**, 063621 (2004).

[Hedden *et al.*, 2004] R. Hedden, V. Meden, T. Pruschke, and K. Schönhammer, *Functional renormalization group approach to zero-dimensional interacting systems*, J. Phys.: Condensed Matter **16**, 5279 (2004).

[Hedin, 1965] L. Hedin, *New Method for Calculating the One-Particle Green's Function with Application to the Electron-Gas Problem*, Phys. Rev. **139**, A796 (1965).

[Hertz, 1976] J. A. Hertz, *Quantum critical phenomena*, Phys. Rev. B **14**, 1165 (1976).

[Hirsch, 1999] J. E. Hirsch, *Overlooked contribution to the Hall effect in ferromagnetic metals*, Phys. Rev. B **60**, 14787 (1999).

[Hirsch and Tang, 1989] J. E. Hirsch and S. Tang, *Spin-wave theory of the quantum antiferromagnet with unbroken sublattice symmetry*, Phys. Rev. B **40**, 4769 (1989).

[Holstein and Primakoff, 1940] T. Holstein and H. Primakoff, *Field Dependence of the Intrinsic Domain Magnetization of a Ferromagnet*, Phys. Rev. **58**, 1908 (1940).

[Honerkamp, 2001] C. Honerkamp, *Electron-doping versus hole-doping in the 2D t-t' Hubbard model*, Euro. Phys. J. B **21**, 81 (2001).

[Honerkamp and Salmhofer, 2001a] C. Honerkamp and M. Salmhofer, *Magnetic and Superconducting Instabilities of the Hubbard Model at the Van Hove Filling*, Phys. Rev. Lett. **87**, 187004 (2001a).

[Honerkamp and Salmhofer, 2001b] C. Honerkamp and M. Salmhofer, *Temperature-flow renormalization group and the competition between superconductivity and ferromagnetism*, Phys. Rev. B **64**, 184516 (2001b).

[Honerkamp *et al.*, 2001] C. Honerkamp, M. Salmhofer, N. Furukawa, and T. M. Rice, *Breakdown of the Landau-Fermi liquid in two dimensions due to umklapp scattering*, Phys. Rev. B **63**, 35109 (2001).

[Honerkamp *et al.*, 2004] C. Honerkamp, D. Rohe, S. Andergassen, and T. Enss, *Interaction flow method for many-fermion systems*, Phys. Rev. B **70**, 235115 (2004).

[Hubbard, 1959] J. Hubbard, *Calculation of partition functions*, Phys. Rev. Lett. **3**, 77 (1959).

[Hund, 1938] F. Hund, Ann. Phys. (Leipzig) **32**, 102 (1938).

[Igarashi, 1992] J. Igarashi, *1/S expansion for thermodynamic quantities in a two-dimensional Heisenberg antiferromagnet at zero temperature*, Phys. Rev. B **46**, 10763 (1992).

[Imry, 1997] Y. Imry, *Introduction to Mesoscopic Physics* (Oxford University Press, Oxford, 1997).

[Jariwala *et al.*, 2001] E. M. Q. Jariwala, P. Mohanty, M. B. Ketchen, and R. A. Webb, *Diamagnetic Persistent Current in Diffusive Normal-Metal Rings*, Phys. Rev. Lett. **86**, 1594 (2001).

[Kadanoff *et al.*, 1967] L. P. Kadanoff, W. Götze, D. Hamblen, R. Hecht, E. A. S. Lewis, V. V. Palciauskas, M. Rayk, J. Swift, D. Aspnes, and J. Kane, *Static Phenomena Near Critical Points: Theory and Experiment*, Rev. Mod. Phys. **39**, 395 (1967).

[Kampf and Katanin, 2003] A. P. Kampf and A. A. Katanin, *Competing phases in the extended U-V-J Hubbard model near the Van Hove fillings*, Phys. Rev. B **67**, 125104 (2003).

[Katanin, 2004] A. A. Katanin, *Fulfillment of Ward identities in the functional renormalization group approach*, Phys. Rev. B **70**, 115109 (2004).

[Katanin and Kampf, 2003] A. A. Katanin and A. P. Kampf, *Renormalization group analysis of magnetic and superconducting instabilities near van Hove band fillings*, Phys. Rev. B **68**, 195101 (2003).

[Katanin and Kampf, 2004a] A. A. Katanin and A. P. Kampf, *Order parameter symmetries for magnetic and superconducting instabilities: Bethe-Salpeter analysis of functional renormalization-group solutions*, cond-mat/0408246 (2004a).

[Katanin and Kampf, 2004b] A. A. Katanin and A. P. Kampf, *Quasiparticle Anisotropy and Pseudogap Formation from the Weak-Coupling Renormalization Group Point of View*, Phys. Rev. Lett. **93**, 106406 (2004b).

[Katanin *et al.*, 2005] A. A. Katanin, A. P. Kampf, and V. Y. Irkhin, *Anomalous self-energy and Fermi surface quasisplitting in the vicinity of a ferromagnetic instability*, Phys. Rev. B **71**, 085105 (2005).

[Kollar *et al.*, 2003] M. Kollar, I. Spremo, and P. Kopietz, *Spin-wave theory at constant order parameter*, Phys. Rev. B **67**, 104427 (2003).

[König *et al.*, 2001] J. König, M. C. Bonsager, and A. H. MacDonald, *Dissipationless Spin Transport in Thin Film Ferromagnets*, Phys. Rev. Lett. **87**, 187202 (2001).

[Kopietz, 1990] P. Kopietz, *Magnon damping in the two-dimensional quantum Heisenberg antiferromagnet at short wavelengths*, Phys. Rev. B **41**, 9228 (1990).

[Kopietz, 1997] P. Kopietz, *Bosonization of Interacting Fermions in Arbitrary Dimensions* (Springer, 1997).

[Kopietz and Busche, 2001] P. Kopietz and T. Busche, *Exact renormalization group flow equations for nonrelativistic fermions: Scaling toward the Fermi surface*, Phys. Rev. B **64**, 155101 (2001).

[Kopietz and Castilla, 1991] P. Kopietz and G. E. Castilla, *Magnon damping, spin stiffness, and dynamic scaling in the two-dimensional quantum Heisenberg ferromagnet at low temperatures*, Phys. Rev. B **43**, 11100 (1991).

[Kopietz and Schönhammer, 1996] P. Kopietz and K. Schönhammer, *Functional bosonization of interacting fermions in arbitrary dimensions*, Z. Phys. B **100**, 259 (1996).

[Kopietz *et al.*, 1995] P. Kopietz, J. Hermisson, and K. Schönhammer, *Bosonization of interacting fermions in arbitrary dimension beyond the Gaussian approximation*, Phys. Rev. B **52**, 10877 (1995).

[Kubo, 1952] R. Kubo, *The Spin-wave Theory of Antiferromagnetics*, Phys. Rev. **87**, 568 (1952).

[Ledowski and Kopietz, 2003] S. Ledowski and P. Kopietz, *An exact integral equation for the renormalized Fermi surface*, J. Phys.: Cond. Mat. **15**, 4779 (2003).

[Ledowski *et al.*, 2004] S. Ledowski, N. Hasselmann, and P. Kopietz, *Self-energy and critical temperature of weakly interacting bosons*, Phys. Rev. A **69**, 061601(R) (2004).

[Ledowski *et al.*, 2005] S. Ledowski, P. Kopietz, and A. Ferraz, *Self-consistent Fermi surface renormalization of two coupled Luttinger liquids*, Phys. Rev. B **71**, 235106 (2005).

[Lee and Chen, 1988] D. K. K. Lee and Y. Chen, *Functional bosonisation of the Tomonaga-Luttinger model*, J. Phys. A **21**, 4155 (1988).

[Leuenberger and Loss, 2001] M. N. Leuenberger and D. Loss, *Quantum computing in molecular magnets*, Nature **410**, 789 (2001).

[Lévy *et al.*, 1990] L. P. Lévy, G. Dolan, J. Dunsmuir, and H. Bouchiat, *Magnetization of mesoscopic copper rings: Evidence for persistent currents*, Phys. Rev. Lett. **64**, 2074 (1990).

[Loss and DiVincenzo, 1998] D. Loss and P. DiVincenzo, *Quantum computation with quantum dots*, Phys. Rev. A **57**, 120 (1998).

[Loss *et al.*, 1990] D. Loss, P. Goldbart, and A. V. Balatsky, *Berry's phase and persistent charge and spin currents in textured mesoscopic rings*, Phys. Rev. Lett. **65**, 1655 (1990).

[Luther and Peschel, 1974] A. Luther and I. Peschel, *Single-particle states, Kohn anomaly, and pairing fluctuations in one dimension*, Phys. Rev. B **9**, 2911 (1974).

[Luttinger, 1963] J. M. Luttinger, *An exactly suluble model of a many-fermion system*, J. Math. Phys. **4**, 1154 (1963).

[Ma, 1976] S. K. Ma, *Modern Theory of Critical Phenomena* (Benjamin/Cummings, Reading, MA, 1976).

[Mailly *et al.*, 1993] D. Mailly, C. Chapelier, and A. Benoit, *Experimental observation of persistent currents in GaAs-AlGaAs single loop*, Phys. Rev. Lett. **70**, 2020 (1993).

[Maleyev, 1957] S. V. Maleyev, *Scattering of slow neutrons in ferromagnets*, Sov. Phys.-JETP **6**, 776 [Zh. Eksp. Teor. Fiz **30**, 1010] (1957).

[Maleyev, 2000] S. V. Maleyev, *Spin-Wave Interaction and Renormalization of Magnetic Anisotropy in 2D Antiferromagnets*, Phys. Rev. Lett. **85**, 3281 (2000).

[Mal'shukov *et al.*, 2003] A. G. Mal'shukov, C. S. Tang, C. S. Chu, and K. A. Chao, *Spin-current generation and detection in the presence of an ac gate*, Phys. Rev. B **68**, 233307 (2003).

[Manousakis, 1991] E. Manousakis, *The spin-1/2 Heisenberg antiferromagnet on a square lattice and its application to the cuprous oxides*, Rev. Mod. Phys. **63**, 1 (1991).

[Mattis and Lieb, 1965] D. C. Mattis and E. L. Lieb, *Exact Solution of a Many-Fermion System and Its Associated Boson Field*, J. of Math. Phys. **6**, 304 (1965).

[Meden and Schönhammer, 1992] V. Meden and K. Schönhammer, *Spectral functions for the Tomonaga-Luttinger model*, Phys. Rev. B **46**, 15753 (1992).

[Meden *et al.*, 2002] V. Meden, W. Metzner, U. Schollwöck, and K. Schönhammer, *Scaling behavior of impurities in mesoscopic Luttinger liquids*, Phys. Rev. B **65**, 045318 (2002).

[Meier and Loss, 2003] F. Meier and D. Loss, *Magnetization Transport and Quantized Spin Conductance*, Phys. Rev. Lett. **90**, 167204 (2003).

[Meier *et al.*, 2003] F. Meier, J. Levy, and D. Loss, *Quantum Computing with Spin Cluster Qubits*, Phys. Rev. Lett. **90**, 47901 (2003).

[Metzner and DiCastro, 1992] W. Metzner and C. DiCastro, *Conservation laws and correlation functions in the Luttinger liquid*, Phys. Rev. B **47**, 16107 (1992).

[Metzner *et al.*, 1998] W. Metzner, C. Castellani, and C. DiCastro, *Fermi Systems with Strong Forward Scattering*, Adv. Phys. **47**, 317 (1998).

[Millis, 1993] A. J. Millis, *Effect of a nonzero temperature on quantum critical points in itinerant fermion systems*, Phys. Rev. B **48**, 7183 (1993).

[Moore, 1965] G. E. Moore, *Cramming more components onto integrated circuits*, Electronics **3** (1965).

[Morris, 1994] T. R. Morris, *The exact renormalization group and approximate solutions*, Int. J. Mod. Phys. A **9**, 2411 (1994).

[Negele and Orland, 1988] J. W. Negele and H. Orland, *Quantum Many-Particle Systems* (Addison-Wesley, Redwood City, CA, 1988).

[Nicoll and Chang, 1977] J. F. Nicoll and T. S. Chang, *An exact one-particle-irreducible renormalization-group generator for critical phenomena*, Phys. Lett. A **62**, 287 (1977).

[Nicoll *et al.*, 1976] J. F. Nicoll, T. S. Chang, and H. E. Stanley, *A Differential Generator for the Free Energy and the Magnetization Equation of State*, Phys. Lett. A **57**, 7 (1976).

[Nozières, 1964] P. Nozières, *Theory of Interacting Fermi Systems* (Benjamin, New York, 1964).

[Oguchi, 1960] T. Oguchi, *Theory of Spin-Wave Interactions in Ferro- and Antiferromagnetism*, Phys. Rev. **117**, 117 (1960).

[Pines and Nozières, 1989] D. Pines and P. Nozières, *The Theory of Quantum Liquids*, vol. I (Addison-Wesley Advanced Book Classics, Redwook City, CA, 1989).

[Polchinski, 1984] J. Polchinski, *Renormalization and effective Lagrangians*, Nucl. Phys. B **231**, 269 (1984).

[Rabaud *et al.*, 2001] W. Rabaud, L. Sminadayer, D. Mailly, K. Hasselbach, A. Benoît, and B. Etienne, *Persistent Currents in Mesoscopic Connected Rings*, Phys. Rev. Lett. **86**, 3124 (2001).

[Rashba, 2003] E. I. Rashba, *Spin currents in thermodynamic equilibrium: The challenge of discerning transport currents*, Phys. Rev. B **68**, 241315 (2003).

[Reulet *et al.*, 1995] B. Reulet, M. Ramin, H. Bouchiat, and D. Mailly, *Dynamic Response of Isolated Aharonov-Bohm Rings Coupled to an Electromangetic Reservoir*, Phys. Rev. Lett. **75**, 124 (1995).

[Sachdev, 1999] S. Sachdev, *Quantum Phase transitions* (Cambridge University Press, Cambridge, 1999).

[Salmhofer, 1999] M. Salmhofer, *Renormalization: An introduction* (Springer, 1999).

[Salmhofer and Honerkamp, 2001] M. Salmhofer and C. Honerkamp, *Fermionic Renormalization Group Flows – Technique and Theory*, Prog. Theor. Physics **105**, 1 (2001).

[Salmhofer *et al.*, 2004] M. Salmhofer, C. Honerkamp, W. Metzner, and O. Lauscher, *Renormalization group flows into phases with broken symmetry*, Progr. Theor. Phys. **112**, 943 (2004).

[Schechter *et al.*, 2003] M. Schechter, Y. Oreg, Y. Imry, and Y. Levinson, *Magnetic Response of Disordered Metallic Rings: Large contribution of Far Levels*, Phys. Rev. Lett. **90**, 26805 (2003).

[Schmeltzer *et al.*, 2004] D. Schmeltzer, A. Saxena, A. R. Bishop, and D. L. Smith, *Persistent spin currents induced by a spatially-dependent magnetic field in a spin-1/2 Heisenberg antiferromagnetic ring*, cond-mat/0405659 (2004).

[Schönhammer, 1997] K. Schönhammer, *Interacting fermions in one dimension: The Tomonaga-Luttinger model*, cond-mat/9710330 (1997).

[Schönhammer, 2003] K. Schönhammer, *in: Strong Interactions in Low Dimensions* (Dordrecht, Kluwer, 2003).

[Schütz *et al.*, 2003] F. Schütz, M. Kollar, and P. Kopietz, *Persistent spin currents in mesoscopic Heisenberg rings*, Phys. Rev. Lett. **91**, 017205 (2003).

[Schütz *et al.*, 2004a] F. Schütz, M. Kollar, and P. Kopietz, *Persistent spin currents in mesoscopic Haldane gap spin rings*, Phys. Rev. B **69**, 035313 (2004a).

[Schütz *et al.*, 2004b] F. Schütz, M. Kollar, and P. Kopietz, *What are spin currents in Heisenberg magnets?*, Eur. Phys. J. B **41**, 557 (2004b).

[Schütz *et al.*, 2005] F. Schütz, L. Bartosch, and P. Kopietz, *Collective fields in the functional renormalization group for fermions, Ward identities, and the exact solution of the Tomonaga-Luttinger model*, Phys. Rev. B **72**, 035107 (2005).

[Shankar, 1994] R. Shankar, *Renormalization-group approach to interacting fermions*, Rev. Mod. Phys. **66**, 129 (1994).

[Shapere and Wilczek, 1989] A. Shapere and F. Wilczek, *Geometric Phases in Physics* (World Scientific, Singapore, 1989).

[Shen and Xie, 2003] S.-Q. Shen and X. C. Xie, *Spin current in the Kondo lattice model*, Phys. Rev. B **67**, 144423 (2003).

[Shor, 1994] P. W. Shor, *Algorithms for quantum computation: Discrete logrithms and factoring*, Proceedings of the 35th Annual Symposium on Foundations of Computer Science, pp. 124-134 (1994).

[Singh and Huse, 1989] R. R. P. Singh and D. Huse, *Microscopic calculation of the spin-stiffness constant for the spin-1/2 square-lattice Heisenberg antiferromagnet*, Phys. Rev. B **40**, 7247 (1989).

[Solyom, 1979] J. Solyom, *The Fermi gas model of one-dimensional conductors*, Adv. Phys. **28**, 201 (1979).

[Spremo *et al.*, 2005] I. Spremo, F. Schütz, P. Kopietz, V. Pashchenko, B. Wolf, M. Lang, J. W. Bats, C. Hu, and M. U. Schmidt, *Magnetic properties of a metal-organic antiferromagnet on a distorted honeycomb lattice*, cond-mat/0505425 (to appear in Phys. Rev. B) (2005).

[Stern, 1992] A. Stern, *Berry's phase, motive forces, and mesoscopic conductivity*, Phys. Rev. Lett. **68**, 1022 (1992).

[Stone, 1994] M. Stone, *Bosonization* (World Scientific, Singapore, 1994).

[Stratonovich, 1957] R. L. Stratonovich, *On a method of calculating quantum distribution functions*, Doklady Akad. Nauk S.S.S.R. **115**, 1097 [Sov. Phys. Doklady **2**, 416 (1958)] (1957).

[Syromyatnikov and Maleyev, 2002] A. V. Syromyatnikov and S. V. Maleyev, *Spin-wave interaction in two- and three-dimensional antiferromagnets in a weak magnetic field*, Phys. Rev. B **65**, 12401 (2002).

[Takahashi, 1986] M. Takahashi, *Quantum Heisenberg Ferromagnet in One and Two Dimensions at Low Temperature*, Prog. Theor. Phys. Suppl. **87**, 233 (1986).

[Takahashi, 1987] M. Takahashi, *Few-dimensional Heisenberg ferromagnets at low temperature*, Phys. Rev. Lett. **58**, 168 (1987).

[Takahashi, 1989] M. Takahashi, *Modified spin-wave theory of a square-lattice antiferromagnet*, Phys. Rev. B **40**, 2494 (1989).

[Tatara and Kohno, 2003] G. Tatara and H. Kohno, *Permanent current from noncommutative spin algebra*, Phys. Rev. B **67**, 113316 (2003).

[Tomonaga, 1950] S. Tomonaga, *Remarks on Bloch's Method of Sound Waves applied to Many-Fermion Problems*, Prog. Theor. Phys. **5**, 544 (1950).

[Ueda and Rice, 1984] Ueda and Rice, $1+\epsilon$ *expansion for interacting fermions*, Phys. Rev. B **29**, 1514 (1984).

[v. Delft and Schoeller, 1998] J. v. Delft and H. Schoeller, *Bosonization for Beginners - Refermionization for Experts*, Annalen Phys. **7**, 225 (1998).

[Volovik, 1987] G. E. Volovik, *Linear momentum in ferromagnets*, J. Phys. C **20**, L83 (1987).

[Watson, 1918] G. N. Watson, *Asymptotic expansions of hypergeometric functions*, Trans. Cambr. Phil. Soc. **22**, 36 (1918).

[Wegner and Houghton, 1973] F. J. Wegner and A. Houghton, *Renormalization Group Equation for Critical Phenomena*, Phys. Rev. A **8**, 401 (1973).

[Wetterich, 1993] C. Wetterich, *Exact evolution equation for the effective potential*, Phys. Lett. B **301**, 90 (1993).

[Wetterich, 2004] C. Wetterich, *Bosonic effective action for interacting fermions*, cond-mat/0208361v3 (2004).

[Wilson, 1972] K. G. Wilson, *Feynman-Graph Expansion for Critical Exponents*, Phys. Rev. Lett. **28**, 548 (1972).

[Wilson and Fisher, 1972] K. G. Wilson and M. E. Fisher, *Critical Exponents in 3.99 Dimensions*, Phys. Rev. Lett. **28**, 240 (1972).

[Wilson and Kogut, 1974] K. G. Wilson and J. Kogut, *The Renormalization group and the epsilon Expansion*, Phys. Reports **12C**, 75 (1974).

[Wolf *et al.*, 2001] S. A. Wolf, D. D. Awschalom, R. A. Buhrman, J. M. Daughton, S. von Molnar, M. L. Roukes, A. Y. Chtchelkanova, and D. M. Treger, *Spintronics: A Spin-Based Electronics Vision for the Future*, Science **294**, 1488 (2001).

[Zanchi, 2001] D. Zanchi, *Angle-resolved loss of Landau quasiparticles in the 2D Hubbard model*, Europhys. Lett. **55**, 376 (2001).

[Zanchi and Schulz, 1996] D. Zanchi and H. J. Schulz, *Superconducting instabilities of the non-half-filled Hubbard model in two dimensions*, Phys. Rev. B **54**, 9509 (1996).

[Zanchi and Schulz, 1998] D. Zanchi and H. J. Schulz, *Weakly correlated electrons on a square lattice: A renormalization group theory*, Europhys. Lett. **44**, 235 (1998).

[Zanchi and Schulz, 2000] D. Zanchi and H. J. Schulz, *Weakly correlated electrons on a square lattice: Renormalization-group theory*, Phys. Rev. B **61**, 13609 (2000).

[Zhitomirsky and Chernyshev, 1999] M. E. Zhitomirsky and A. L. Chernyshev, *Instability of Antiferromagnetic Magnons in Strong Fields*, Phys. Rev. Lett. **82**, 4536 (1999).

[Zhitomirsky and Nikuni, 1998] M. E. Zhitomirsky and T. Nikuni, *Magnetization curve of a square-lattice Heisenberg antiferromagnet*, Phys. Rev. B **57**, 5013 (1998).

[Zinn-Justin, 2002] J. Zinn-Justin, *Quantum Field Theory and Critical Phenomena* (Claredon Press, Oxford, 2002), 4th edn.

Deutsche Zusammenfassung

Diese Dissertation diskutiert in zwei Teilen unterschiedliche Aspekte stark korrelierter Elektronensysteme. Neben der Untersuchung physikalischer Fragestellungen werden dabei Vielteilchenmethoden neu entwickelt und angepasst.

Im ersten Teil behandeln wir Magnetisierungstransport in eindimensionalen Spinringen, die durch ein Heisenbergmodell in einem inhomogenen Magnetfeld beschrieben werden. In Analogie zu Ladungsdauerströmen in mesoskopischen normalleitenden Metallringen können in einer solchen Geometrie aufgrund quantenmechanischer Interferenz der Magnon-Wellenfunktionen Spindauerströme auftreten.

Der zweite Teil der Arbeit beschäftigt sich mit neuen Aspekten der funktionalen Renormierungsgruppe für Fermionen. Durch eine Entkopplung der Wechselwirkung mittels einer geeigneten Hubbard-Stratonovich-Transformation führen wir kollektive bosonische Felder ein und analysieren die Hierarchie von Flussgleichungen für die gekoppelte Feldtheorie. Die Möglichkeit eines Cutoffs im Impulsübertrag der Wechselwirkung führt zu einer neuen Technik, die wir als "Wechselwirkungs-Fluss" bezeichnen. In diesem Zugang sind Ward-Identitäten für Vorwärtsstreuung zu jedem Zeitpunkt des Renormierungsgruppenflusses gültig, und liefern eine exakte Lösung für eine komplette Hierarchie von Flussgleichungen. Auf diese Weise erhalten wir das bekannte exakte Ergebnis für die Einteilchen Greensche Funktion des Tomonaga-Luttinger Modells.

I. Spindauerströme in Heisenberg-Ringen

Die fortschreitende Miniaturisierung mikroelektronischer Bauelemente wird in naher Zukunft an die fundamentale Grenze atomarer Dimensionen stoßen. Jenseits von traditionellem Chipdesign gewinnen quantenmechanische Interferenzeffekte für Systeme an Bedeutung, die kleiner sind als die stark temperaturabhängige Kohärenzlänge L_ϕ. Das Fernziel eines Quantencomputers, basierend auf der kohärenten Zeitentwicklung einer grossen Zahl von Quanten-Bits (Qubits), verspricht eine exponentielle Leistungssteigerung für spezielle Problemklassen. Ein wichtiges Hindernis bei der Realisierung eines Quantencomputers in Festkörpersystemen ist die Dekohärenz durch den Einfluss der Umgebung. Dekohärenzzeiten sind in der Regel für Spin- größer als für Ladungsfreiheitsgerade. Daher gelten isolierte Spins auf Quantenpunkten sowie Spinzustände von molekularen Magneten als vielversprechende Kandidaten für Qubits. Zudem umfasst das neuentstandende Gebiet der Spintronik (Spin-Elektronik) auch die Nutzung von Spinfreiheitsgraden in konventionelleren Bauelementen. Die Untersuchung von Magnetisierungstransport erfährt allgemein in letzter Zeit große Aufmerksamkeit, insbesondere in Systemen in denen Spin-Ströme durch itinerante Elektronen getragen

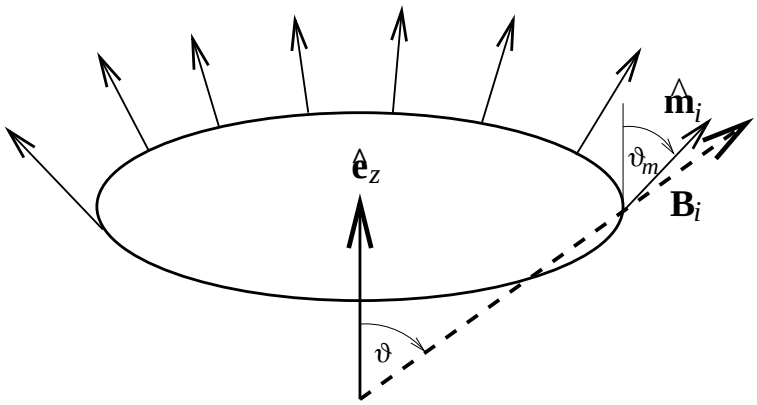

Abbildung 1: Klassischer Grundzustand eines ferromagnetischen Heisenbergrings in einem radialen Magnetfeld.

werden. Darüber hinaus zeigen auch auch magnetische Isolatoren interessante Spin-Transport-Phänomene. So berechneten Meier und Loss kürzlich die Spin-Leitfähigkeit für Heisenberg-Systeme in einer Zwei-Terminal Geometrie [Meier and Loss, 2003].

Mesoskopische Systeme besitzen noch keine atomaren Dimensionen, sind aber klein genug, dass sie durch kohärente Wellenfunktionen beschrieben werden müssen, die sich über das gesamte System erstrecken. Ein wichtiges mesoskopisches Phänomen ist der Dauerstrom in normalleitenden Metallringen, die von einem magnetischen Fluss durchsetzt sind. Dieses Phänomen basiert auf dem Aharonov-Bohm Effekt [Aharonov and Bohm, 1956] und wurde bereits vor langer Zeit theoretisch vorhergesagt [Hund, 1938,Büttiker *et al.*, 1983]. Die experimentellen Schwierigkeiten wurden erst zu Beginn der 1990er Jahre überwunden, als ein oszillierendes magnetisches Moment als Funktion des angelegten Flusses nachgewiesen werden konnte. Trotz vieler theoretischer Arbeiten konnte die Amplitude des experimentell gemessenen Stroms in diffusiven Leitern nicht befriedigend erklärt werden. Im ballistischen Regime genügt jedoch schon ein einfaches Modell freier Elektronen, um die Größenordnung des beobachteten Stroms zu erklären.

In Analogie zu Ladungsdauerströmen in normalleitenden Metallringen zeigen wir, dass Spindauerströme in Heisenberg-Ringen auftreten können. Dazu betrachten wir mesoskopische Heisenberg-Ringe in Magnetfeldern, die räumlich derart inhomogen sind, dass das lokale Feld einen endlichen Raumwinkel bei Umlaufen des Ringes aufspannt. Das einfachste Beispiel ist ein radiales Feld wie in Abb. 1 gezeigt. Analog zum magnetischen Fluss für Ladungs-Dauerströme kann der Raumwinkel Ω als geometrischer Fluss fungieren und Magnetisierungs-Dauerströme hervorrufen. Zur theoretischen Beschreibung dieses Phänomens passen wir die Formulierung der Spinwellentheorie an diese Situation an. Startpunkt ist der sogenannte klassische Grundzustand, d.h. die Spinkonfiguration, die die klassi-

sche Energie minimiert. Für den Fall eines räumlich inhomogenen Magnetfeld ist dieser klassische Grundzustand in der Regel auch inhomogen (siehe Abb. 1). In einer semi-klassischen Entwicklung werden nun lokale Quantisierungsachsen so gewählt, dass die lokale z-Achse in Richtung des klassischen Grundzustandes zeigt. Die Spinoperatoren werden in dieser Basis durch bosonische Erzeugungs- und Vernichtungsoperatoren dargestellt [Holstein and Primakoff, 1940, Maleyev, 1957]. Im Gegensatz zur lokalen z-Achse sind die transversalen Quantisierungsachsen durch den klassischen Grundzustand nicht eindeutig festgelegt. Vielmehr führt eine beliebe Rotation um die lokale z-Achse zu einer ebenso akzeptablen transversalen Basis. Dies führt zu einer Eichfreiheit im Spinwellen-Hamilton-Operator. Eine spezielle Eichung wird durch ein Eichfeld beschrieben, das den Winkel der transversalen Quantisierungsachsen zu einer festen Referenzrichtung angibt.

Die Definition des Spinstrom-Operators in Heisenberg-Magneten in inhomogenen Magnetfelder erfordert besondere Sorgfalt. Wir zeigen, dass nur die Komponente des naiven "Strom-Operators" $J_{ij}\boldsymbol{S}_i \times \boldsymbol{S}_j$ in der Ebene, die durch die lokalen Ordnungsparameter $\langle \boldsymbol{S}_i \rangle$ und $\langle \boldsymbol{S}_j \rangle$ aufgespannt wird, mit dem Transport von Magnetisierung verbunden ist. Spinströme sind somit ein direkter Ausdruck von Quantenkorrelationen und verschwinden in einer Molekularfeldnäherung oder im klassischen Grundzustand. In führender Ordnung der Spinwellentheorie kann der Spinstrom-Operator als Ableitung des Hamilton-Operators nach dem Eichfeld berechnet werden. Für die elektrischen Dipolfelder, die durch einen stationären Fluss von magnetischen Dipolen erzeugt werden, leiten wir ein Biot-Savart-artiges Gesetz her.

Für einen mesoskopischen ferromagnetischen Ring bei tiefen Temperaturen T in einem inhomogenen Magnetfeld der Stärke B berechnen wir den Spin-Strom in führender Ordnung der Spinwellen-Theorie. Unter optimalen Bedingungen kann dieser den Wert $g\mu_{\mathrm{B}}(T/\hbar)\exp[-2\pi(g\mu_{\mathrm{B}}B/\Delta)^{1/2}]$ erreichen, wobei g das gyromagnetische Verhältnis, μ_{B} das Bohrsche Magneton und Δ die Energielücke zwischen dem Grundzustand und der ersten Spinwellenanregung ist. Zur Bewertung der experimentellen Detektierbarkeit des beschriebenen Effekts liefern wir eine Abschätzung der Größenordnung der generierten elektrischen Dipolfelder. So kommen wir zu dem Schluss, dass die Messung eines Potenzialabfalls in der Größenordnung eines Nanovolts über die Grösse des mesoskopischen Ringes erforderlich ist.

Antiferromagnetische Ringe können ebenfalls Spin-Dauerströme tragen. Wir zeigen dies für sogenannte Haldane-Gap Systeme, d.h. für Spinsysteme mit ganzzahligem Spin S, mittels einer modifizierten Spinwellentheorie. Aufgrund von Quantenfluktuationen hat der Strom einen endlichen Grenzwert von der Größenordnung $(-g\mu_{\mathrm{N}})c/L$ bei verschwindender Temperatur, in enger Analogie zu ballistischen Strömen in mesoskopischen normalleitenden Ringen. Hierbei ist c die Spinwellen-Geschwindigkeit, g das gyromagnetische Verhältnis und μ_{B} das Bohrsche Magneton. Dieses Ergebnis setzt voraus, dass die antiferromagne-

tische Korrelationslänge ξ größer ist als der Umfang L des Ringes. Für $\xi \ll L$ ist der Strom exponentiell unterdrückt. Spindauerströme treten auch in inhomogenen elektrischen Feldern auf und können mit denselben Methoden wie für inhomogene Magnetfelder berechnet werden.

Eine experimentelle Bestätigung des Effekt von Spindauerströmen in mesoskopischen Heisenberg-Ringen stellt eine große Herausforderung dar. Neben der Messung eines Potentialabfalls in der Größenordnung eines Nanovolts über die Grösse des Rings ist die Generierung eines verhältnismäßig starken Magnetfeldes mit Inhomogenitäten auf mesoskopischer Skala erforderlich. Ausserdem sind wohlcharakterisierte Ringe mit großer Austauschkopplung J nötig. Angesichts der schnellen Entwicklung im Bereich der Spintronik erscheint es aber nicht unrealistisch, dass in naher Zukunft Techniken zur Verfügung stehen, die den Nachweis des hier vorhergesagten Effekts ermöglichen werden.

II. Funktionale Renormierungsgruppe mit kollektiven Feldern

Stark korrelierte Elektronensysteme stellen große Herausforderungen an die theoretische wie auch experimentelle Festkörperphysik. Die experimentellen Systeme umfassen z.B. die Hochtemperatur Supraleiter, organische und anorganische anisotrope (quasi-) eindimensionale Leiter, sowie Schwerfermionensysteme, und zeigen eine extrem reichhaltige Phänomelogie verschiedener Phasen.

Wohlbewährte Konzepte in drei Dimensionen, wie die Molekularfeldtheorie oder die Landausche Theorie der Fermiflüssigkeiten, versagen in niedrigen Dimensionen aufgrund von starken Fluktuationen. Für eindimensionale Leiter wurde das Konzept einer Luttinger-Flüssigkeit entwickelt um die Niedrigenergie-Eigenschaften zu beschreiben. Die Technik der Bosonisierung liefert Ergebnisse für Korrelationsfunktionen, basiert jedoch auf Annahmen, die die Gültigkeit auf extrem kleine Energieskalen beschränken. Eine Lockerung dieser Annahmen zur Beschreibung der Grenzen des Luttinger-Flüssigkeits-Konzepts ist notorisch schwierig. Experimentell werden viele Anzeichen für Nicht-Fermi-Flüssigkeitsverhalten auch in (quasi-) zweidimensionalen Systemen beobachtet. Viele Autoren haben somit versucht das Konzept der Luttinger-Flüssigkeit auf zwei Raumdimensionen zu erweitern. Bis auf recht künstliche Modelle ist die Entwicklung einer konsistenten Theorie für Luttinger-Flüssigkeiten in zwei Dimensionen jedoch bisher nicht gelungen.

Zur theoretischen Modellierung stark korrelierter Systeme werden weiterhin verschiedenartige Zugänge entwickelt. Ein vielversprechendes Verfahren zur Untersuchung der Niedrigenergie-Eigenschaften wechselwirkender niedrigdimensionaler Systeme ist die Renormierungsgruppe (RG). Ursprünglich wurden Renormierungsgruppen-Methoden als formales Werkzeug in der Quantenfeldtheo-

rie entwickelt, um Divergenzen in der diagrammatischen Störungstheorie zu kontrollieren. Der Zusammenhang mit dem Verhalten der Theorien unter der Transformation von Längenskalen wurde später von Wilson ausgearbeitet und führte zu einem detailierten Verständnis von (klassischen) kritischen Phänomenen durch RG-Flüsse in einem großen Raum möglicher Hamilton-Operatoren. Formal exakte Versionen von RG-Transformationen wurden schon früh hergeleitet und später elegant in der sogenannten funktionalle Renormierungsgruppe (fRG) formuliert, die auf kontinuierlichen Flussgleichungen für verschiedene erzeugende Funktionale basiert.

In den letzten zehn Jahren wurde die Renormierungsgruppe verstärkt auch auf fermionische Systeme angewandt. Die Niedrigenergie-Moden, die in Störungstheorie zu Divergenzen führen, sind hierbei mit lückenlosen Anregungen in der Nähe der Fermi-Fläche vebunden, die in Raumdimensionen $D > 1$ eine $D - 1$ dimensionale Manigfaltigkeit bildet. Die funktionale Version der Renormierungsgruppe ist besonders geeignet, um die Kopplungsfunktionen zu behandeln, die für $D > 1$ betrachtet werden müssen. Mit der fRG-Technik wurde das zweidimensionale Hubbard-Modell intensiv studiert. In allen Rechnungen wird eine Divergenz der fließenden Kopplungen bei niedrigen Energien beobachtet. Die Art und Symmetrie der singulärsten Kopplungen werden als Hinweis auf die dominante Instabilität interpretiert, und so können Phasendiagramme gewonnen werden. Aufgrund des divergenten Flusses ist die tatsächliche Niedrigenergie-Physik jedoch nicht direkt zugänglich. Neben dem Szenario der Symmetriebrechung besteht zumindest für spezielle Geometrien der Fermi-Fläche auch die Möglichkeit von Nicht-Fermi-Flüssigkeits-Verhalten mit verschwindenden Quasiteilchen-Gewichten an der Fermifläche. Es stellt sich somit die Frage, ob nicht alternative Methoden zur Beschreibung der Physik bei sehr niedrigen Energien entwickelt werden können.

Ein weiterer Zugang zu wechselwirkenden Fermi-Systemen beschreibt die Umgebung eines quantenkritischen Punktes. In diesem von Hertz und Millis initiierten Zugang [Hertz, 1976, Millis, 1993] wird das System allein durch einen bosonischen fluktuierenden Ordnungsparameter beschrieben, nachdem die fermionischen Freiheitsgrade ausintegriert wurden. Eine Wilsonsche Impulsschalen-RG wird anschließend benutzt, um das kritische Verhalten der weichen bosonischen Moden zu beschreiben.

Bosonische kollektive Moden sind von besonderer Bedeutung in eindimensionalen Systemen, in denen sie die natürlichen Quasiteilchen-Anregungen darstellen. Wird die Dispersion in der Nähe der Fermipunkte linearisiert, so liefert die Technik der Bosonisierung exakte Lösungen für Korrelationsfunktionen. Neben der weit verbreiteten Operator-Variante kann die Bosonisierung auch in der Sprache der Funktionalintegrale formuliert werden, und so auch auf höhere Dimensionen verallgemeinert werden [Kopietz, 1997]. In dieser Formulierung wird die Dichte-Dichte-Wechselwirkung mittels einer Hubbard-Stratonovich-Transformation entkoppelt und die Fermionen anschließend, wie im Hertz-

Zugang, ausintegriert. Für eine linearisierte Dispersion garantiert dann das sogenannte Closed-Loop-Theorem, dass die generierte bosonische Wirkung quadratisch ist.

Im zweiten Teil dieser Arbeit entwickeln wir eine neue Formulierung der funktionalen Renormierungsgruppe für wechselwirkende Fermionen, die auf der expliziten Einführung kollektiver bosonischer Freiheitsgrade durch eine geeignete Hubbard-Stratonovich-Transformation beruht. Unser Zugang vereint die rein fermionische Formulierung mittels Grassmannscher Funktionalintegrale mit dem Hertz-Zugang. Im Gegensatz zum Hertz-Zugang eliminieren wir jedoch nicht die Fermionen, sondern leiten eine exakte Hierarchie von RG Flussgleichungen für die Vertizes der so entstandenen gekoppelten Feldtheorie her, die sowohl fermionische als auch bosonische Felder enthält. In dieser Formulierung erscheint die Wechselwirkung des rein fermionischen Modells als Propagator des bosonischen Feldes. Ein Cutoff im Impulsübertrag der Wechselwirkung kann somit gleichberechtig zum üblichen Band-Cutoff eingeführt werde. In unserer Formulierung werden Vertizes zu benutzen, die sowohl irreduzibel bzgl. des Teilchen-Propator als auch der Wechselwirkungslinie sind. Irreduzibilität bzgl. der Wechselwirkungslinie is eng verbunden mit Irreduzibilität im Zero-Sound-Kanal und eine Erweiterung unseres Zugang auf andere Kanäle der Wechselwirkung könnte uns näher an eine vollständige Zweiteilchen-Irreduzibilität bringen. Ein ähnliche Strategie wurde zuvor schon in [Correia *et al.*, 2002], [Wetterich, 2004] und [Baier *et al.*, 2004] vorgeschlagen. Auf der technischen Ebene unterscheidet sich die praktische Implementierung der hier vorgestellten Methode jedoch beträchtlich von verhergehenden Arbeiten.

Wir behandeln hauptsächlich das theoretische Fundament unseres Zugangs und entwickeln eine effiziente Methode zur übersichtlichen Darstellung aller auftretenden Terme. Als eine wichtige Anwendung betrachten wir Wechselwirkungen, die durch kleine Impulsüberträge dominiert werden und für die Ward-Identitäten eine entscheidende Rolle. Wir stellen eine fRG-Methode vor, die nur einen Cutoff im Impulsübertrag der Wechselwirkung verwendet. Im Rahmen dieser Methode zeigen wir, dass der RG-Fluss die Ward-Identitäten nicht verletzt. Vielmehr treten Ward-Identitäten als Lösung einer unendlichen Hierarchie von gekoppelten RG-Flussgleichungen für einlinien-irreduzible Vertizes auf, die zwei externe Fermi-Beinchen und eine beliebige Anzahl von Bose-Beinchen besitzen. Wir erhalten eine geschlossene Integro-Differenzial-Gleichung für die Einteilchen Greensche Funktion, die durch eine Fourier-Transformation in den Realraum und zu imaginärer Zeit gelöst werden kann. Die Lösung hat die aus funktionalen Bosonisierung bekannte Form [Kopietz, 1997]. Es ist weiterhin bekannt, dass diese Form in einer Dimension äquivalent zum Ergebnis der Operator-Version der Bosonisierung ist. Somit ist es gelungen, das Tomonaga-Luttinger-Modell (TLM) im Rahmen der fRG exakt zu lösen.

Außerdem entwickeln wir ein Trunkierungsschema für die unendliche Hier-

archie von Flussgleichungen basierend auf den führenden Termen einer Entwicklung nach Relevanz. Diese vergleichsweise einfache Trunkierung ist schon ausreichend, um die exakte anomale Dimension des spinlosen TLM für beliebige Wechselwirkungsstärken zu erhalten. Dies sollte mit der rein fermionischen Formulierung der RG verglichen werden, im Rahmen derer eine Zweischleifen-Rechnung nötig ist, um den führenden störungstheoretischen Beitrag zur anomalen Dimension zu erhalten. Weiterhin müssen Frequenzabhängigkeiten des fermionischen Vierpunkt-Vertex bestimmt werden, was in numerischen Lösungen der Flussgleichungen derzeit nicht möglich ist. In unserem Zugang entstehen Frequenzabhängigkeiten schon in der führenden Näherung. Wenn Vertexkorrekturen vernachlässigt werden, ist die effektive Wechselwirkung durch die RPA-Näherung gegeben. Daher sind Starkkopplungs-Fixpunkte mit unserem Verfahren möglicherweise zugänglich. Weiterhin führte die Trunkierung zum korrekten Skalenverhalten für die die Einteilchen Greensche Funktion für Impulse $k = \pm k_F$ an den Fermi-Punkten. Allerding werden in dieser Näherung die algebraischen Singulariatäten für $k \neq \pm k_F$ nicht korrekt reproduziert. Trotzdem ist das Ergebnis für die anomale Dimension vielversprechend und erweiterte Trunkierungsschemata sollten untersucht werden, um bessere Ergebnisse für spektrale Eigenschaften zu erhalten. Derartige Trunkierungen wären extrem wertvoll in Situationen in denen Ward Identitäten nicht gelten.

Die Entwicklung verlässlicher Trunkierungen könnte zum Beispiel zu einem Verständnis von nicht-universellen Effekten in eindimensionalen Metallen führen. Wenn die Energiedispersion nicht linearisiert wird, sollte eine endliche Impulsskala k_c, abhängig von der Wechselwirkung und der Bandkrümmung, existieren unterhalb derer das Skalenverhalten des TLM auftritt. Die Berechnung von k_c sowie der nicht-universelle spektralen Linienform ist im Rahmen der Bosonisierung schwierig [Busche and Kopietz, 2000]. Im Rahmen der funktionalen RG sollte eine Einbeziehung irrelevanter Kopplungen jedoch möglich sein. In diesem Zusammenhang verweisen wir darauf, dass eine komplette Crossover-Skalenfunktion zwischen dem kritischen Regime und dem Regime kurzer Wellenlängen kürzlich für wechselwirkende Bosonen in $D = 3$ mit dem fRG-Formalismus gelungen ist [Ledowski *et al.*, 2004, Hasselmann *et al.*, 2004].

Unser Zugang könnte auch nützlich zur Beschreibung von quantenkritischen Phänomenen in Situationen werden, die ein Ausintegrieren der Fermionen nicht erlauben. Der traditionelle Landau-Wilson-Ginzburg Zugang allein über einen Ordnungsparameter bricht zusammen, wenn generische, nicht-kritische weiche Moden existieren [Belitz *et al.*, 2004, Belitz *et al.*, 2001a, Belitz *et al.*, 2001b]. In der rein fermionischen fRG tritt Symmetriebrechung durch die Divergenz der relevanten Suszeptibilität für den Ordnungsparameter in Erscheinung. Die symmetriegebrochene Phase selbst ist in diesem Zugang schwer zu beschreiben, obwohl es für den einfacheren Fall des reduzierten BCS-Modells kürzlich gelungen ist, den Fluss in die symmetriegebrochene Phase fortzusetzen [Salmhofer *et al.*, 2004]. Andererseits kann in unserem Zugang der Ordnungsparameter explizit als

bosonisches Feld eingeführt werden. Dieser erhält dann einen Vakuumerwartungswert in der symmetriegebrochenen Phase. Ein ähnlicher Zugang wurde kürzlich in Ref. [Baier *et al.*, 2004] entwickelt, um Antiferromagnetismus im zweidimensionalen Hubbard-Modell zu untersuchen.

Zusammenfassend glauben wir, dass der im zweiten Teil der Arbeit vorgestellte neue Formalismus und seine möglichen Erweiterungen für eine Vielzahl physikalischer Situationen nützlich sein werden.

Veröffentlichungen

1. Florian Schütz, Marcus Kollar, and Peter Kopietz,
   Persistent Spin Currents in Mesoscopic Heisenberg Rings,
   Phys. Rev. Lett. **91**, 017205 (2003).

2. Florian Schütz, Marcus Kollar, and Peter Kopietz,
   Persistent spin currents in mesoscopic Haldane gap spin rings,
   Phys. Rev. B **69**, 035313 (2004).

3. V. Pashchenko, B. Brendel, B. Wolf, M. Lang, M. Kollar, F. Schütz, P. Kopietz, Y. Molodtsova, O. Shchegolikhina, N. Auner, and J. Bats,
   Structural and magnetic investigations on a new molecular quantum magnet,
   J. Mag. Magn. Mat. **272-276**, e755 (2004).

4. Florian Schütz, Peter Kopietz, Marcus Kollar,
   What are spin currents in Heisenberg magnets?
   Eur. Phys. J. B **41**, 557-560 (2004).

5. Florian Schütz, Lorenz Bartosch, Peter Kopietz,
   Collective fields in the functional renormalization group for fermions, Ward identities, and the exact solution of the Tomonaga-Luttinger model,
   Phys. Rev. B **72**, 035107 (2005).

6. I. Spremo, F. Schütz, P. Kopietz, V. Pashchenko, B. Wolf, M. Lang, J. W. Bats, C. Hu, M. U. Schmidt,
   Magnetic properties of a metal-organic antiferromagnet on a distorted honeycomb lattice,
   cond-mat/0505425 (to appear in Phys. Rev. B).

7. V. Pashchenko, B. Brendel, B. Wolf, M.Lang, K. Lyssenko, O. Shchegolikhina, Y. Molodtsova, L. Zherlitsyna, N. Auner, F. Schütz, M. Kollar, P. Kopietz, N. Harrison
   Synthesis, Structure and Magnetic Properties of a novel linear Cu(II)-trimer Complex,
   (to appear in Eur. J. Inorg. Chem.).

Lebenslauf

Angaben zur Person

Name:	Florian Schütz
Geburtsdatum:	12. April 1976
Geburtsort:	Göttingen
Staatsangehörigkeit:	Deutsch

Bildungsgang

September 2005	Promotion mit Auszeichnung
2002-2005	Doktorand am Institut für Theoretische Physik an der Johann Wolfgang Goethe-Universität Frankfurt Betreuer: Prof. Dr. P. Kopietz
Juli 2002	Diplom im Studiengang Physik an der Georg-August-Universität Göttingen
2000-2002	Diplomarbeit am Institut für Theoretische Physik in Göttingen Betreuer: Prof. Dr. K. Schönhammer Thema: "Elektronische Eigenschaften von Kondo-Dimeren"
1999-2000	Auslandsstudium an der University of California in San Diego mit einem Stipendium des Education Abroad Program (EAP).
1996	Aufnahme des Diplomstudiengangs Physik an der Georg August-Universität in Göttingen
1995-1996	Zivildienst bei der Selbsthilfe Körperbehinderter e.V., Göttingen
1995	Abitur am Otto-Hahn-Gymnasium in Göttingen

Danksagung

Am Ende dieser Arbeit verbleibt die angenehme Aufgabe all denjenigen Menschen zu danken, ohne deren Unterstützung diese Arbeit wohl nie zustande gekommen wäre.

Meinem Betreuer Prof. Dr. Peter Kopietz danke ich für die Möglichkeit, diese interessanten Themen in seiner Gruppe bearbeiten zu können. Er hatte stets ein offenes Ohr für Fragen und Probleme. Einerseits ist es wohl kaum möglich mit seinem Rechentempo Schritt zu halten, anderseits half seine physikalische Intuition und Begeisterung, den Blick für die wesentliche Physik nicht zu verlieren.

Prof. Dr. Roser Valenti danke ich für interessante Diskussionen und die bereitwillige Übernahme der Begutachtung.

An den Veröffentlichungen des ersten Teils dieser Arbeit war Marcus Kollar wesentlich beteiligt. Für die enge Zusammenarbeit während der gemeinsamen Zeit in Frankfurt und die vielen Diskussionen danke ich ihm herzlich. Ebenfalls zu Dank verpflichtet bin ich ihm für ein sehr gründliches und zügiges Korrekturelesen der gesamten Arbeit.

Meinem Büropartner Nils Hasselmann danke ich ebenfalls für viele Diskussionen über Physik und auch private Themen. Die feste Institution unserer Kaffeerunde bereicherte er unter anderem mit interessanten Berichten über das Kloster Eberbach und den Karneval in Barranquilla. Auch ihm danke ich für das gründliche Korrekturelesen der kompletten Arbeit.

Ivan Spremo begleitet meine Universitätslaufbahn nun schon seit unserer Diplomzeit in Göttingen. Für viele interessante Gespräche, seine kompetente Beratung in allen Computer-Fragen, sowie das Korrekturlesen der Arbeit bin ich ihm sehr dankbar.

Für die Zusammenarbeit im zweiten Teil der Arbeit bin ich Lorenz Bartosch zu herzlichem Dank verpflichtet.

Frau Edda Vogel half mir mit ihrer einzigartigen Art immer wieder kompetent die Hürden der Universitätsbürokratie zu umschiffen. Einen ganz herzlichen Dank dafür.

Weiterhin danke ich allen noch nicht erwähnten Mitgliedern der Theoretischen Festkörperphysik in Frankfurt. Von Gesprächen und Diskussionen mit ihnen habe ich auf die eine oder andere Art profitiert.

Die oben erwähnte Kafferunde wurde neben den schon erwähnten Personen in wechselnder Besetzung auch durch Long Phi, Peyman, Francesca, Philipp und Andrea bereichert. Vielen Dank dafür. Für Inneneinsichten der “russischen Schule” sowie viele weitere einprägsame Statements über Physik danke ich Dr. Miodrag Kulic.

Interessante Diskussionen über Physik ergaben sich auch im Rahmen von Zusammenarbeiten in der Forschergruppe in Frankfurt, sowie während einer Win-

terschule im International Center for Condensed Matter Physics in Brasília. Für die Gastfreundschaft dort bin ich sehr dankbar.

Meiner Familie danke ich für ihre stetige mentale, sowie gelegentlich auch finanzielle Unterstützung.

Zu guter Letzt bedanke ich mich bei Wencke, dem wichtigsten Menschen in meinem Leben, für ihre Geduld und permanente Unterstützung. Einen gestressten Physiker zu ertragen ist manchmal eine heroische Leistung, ich gelobe Besserung.